



UNIVERSIDADE ESTADUAL DE CAMPINAS
Faculdade de Engenharia de Alimentos

VICTOR COELHO GERALDO

**MODELING, SIMULATION AND OPTIMIZATION OF
THE SUGARCANE JUICE EXTRACTION BY
DIFFUSION/LIXIVIATION PROCESSES**

**MODELAGEM, SIMULAÇÃO E OTIMIZAÇÃO DA
EXTRAÇÃO DO CALDO DE CANA-DE-AÇÚCAR POR
PROCESSOS DE DIFUSÃO/LIXIVIAÇÃO**

CAMPINAS - SP
2019

VICTOR COELHO GERALDO

MODELING, SIMULATION AND OPTIMIZATION OF THE SUGARCANE
JUICE EXTRACTION BY DIFFUSION/LIXIVIATION PROCESSES

MODELAGEM, SIMULAÇÃO E OTIMIZAÇÃO DA EXTRAÇÃO DO
CALDO DE CANA-DE-AÇÚCAR POR PROCESSOS DE
DIFUSÃO/LIXIVIAÇÃO

*Thesis presented to the Faculty of Food Engineering of the
University of Campinas in partial fulfillment of the require-
ments for the degree of Doctor in Science.*

*Tese apresentada à Faculdade de Engenharia de Alimen-
tos da Universidade Estadual de Campinas como parte dos
requisitos exigidos para a obtenção do título de Doutor em
Ciências.*

Advisor/Orientador: Dr. Edvaldo Rodrigo de Moraes

Este trabalho corresponde à versão final da tese de doutorado defendida pelo aluno Victor Coelho Geraldo e orientada pelo Dr. Edvaldo Rodrigo de Moraes.

CAMPINAS - SP
2019

Ficha catalográfica
Universidade Estadual de Campinas
Biblioteca da Faculdade de Engenharia de Alimentos
Claudia Aparecida Romano - CRB 8/5816

G311m Geraldo, Victor Coelho, 1990-
Modeling, simulation and optimization of the sugarcane juice extraction by diffusion/lixiviation processes / Victor Coelho Geraldo. – Campinas, SP : [s.n.], 2019.

Orientador: Edvaldo Rodrigo de Moraes.
Tese (doutorado) – Universidade Estadual de Campinas, Faculdade de Engenharia de Alimentos.

1. Difusores. 2. Modelagem matemática. 3. Simulação. 4. Lixiviação. 5. Difusão. I. Moraes, Edvaldo Rodrigo. II. Universidade Estadual de Campinas. Faculdade de Engenharia de Alimentos. III. Título.

Informações para Biblioteca Digital

Título em outro idioma: Modelagem, simulação e otimização da extração do caldo de cana-de-açúcar por processos de difusão/lixiviação

Palavras-chave em inglês:

Diffusers

Mathematical modeling

Simulation

Lixiviation

Diffusion

Área de concentração: Bioenergia

Titulação: Doutor em Ciências

Banca examinadora:

Edvaldo Rodrigo de Moraes [Orientador]

João Frederico da Costa Azevedo Meyer

José Antonio Rabi

Reinaldo Giudici

Paulo Seleglim Junior

Data de defesa: 18-07-2019

Programa de Pós-Graduação: Bioenergia

Identificação e informações acadêmicas do(a) aluno(a)

- ORCID do autor: <http://orcid.org/0000-0003-0539-6668>

- Currículo Lattes do autor: <http://lattes.cnpq.br/6631075893416678>

Examination committee

Dr. Edvaldo Rodrigo de Moraes - Orientador
Universidade Estadual de Campinas

Dr. João Frederico da Costa Azevedo Meyer
Universidade Estadual de Campinas

Dr. José Antonio Rabi
Universidade de São Paulo

Dr. Paulo Selegim Junior
Universidade de São Paulo

Dr. Reinaldo Giudici
Universidade de São Paulo

Ata da defesa com as respectivas assinaturas dos membros encontra-se no SIGA/Sistema de Fluxo de Dissertação/Tese e na Secretaria do Programa da Unidade.

To my parents, Dolores e
Nivaldo, by the limitless
love.

Aos meus pais, Dolores
e Nivaldo, pelo amor sem
limites.

Acknowledgments

Principalmente aos meus pais, **Nivaldo e Dolores**, pelo o amor, paciência, compreensão e dedicação. Obrigado por serem minha fortaleza, meu porto seguro e por terem feito de tudo para que eu pudesse ter todas as oportunidades do mundo. Vocês são meus melhores amigos, levarei os ensinamentos de vocês para o resto da vida. Gostaria de frisar que esta tese não seria realidade se não fosse pela ajuda destes dois anjos.

Aos meus **familiares**, por terem me ensinado o significado de amor e carinho sem limites. Obrigado por todos os momentos maravilhosos que passamos (e passaremos) juntos. A presença destas pessoas maravilhosas na minha vida é meu combustível para continuar em frente e batalhar pelos meus sonhos.

Ao meu filho de quatro patas **Aquiles Francisco**, pelo carinho e pelo companheirismo. Aprendi com este serzinho um novo tipo de amor; sou muito feliz por saber que tal sentimento existe dentro de mim. Agradeço ele por ter tornado o processo de escrita mais leve e desculpe me por não ter jogado a bolinha todas as vezes que você pediu.

Ao meu grande irmão **Henrique**, por ter ensinado me o significado de uma grande amizade. Obrigado pelo companheirismo e pelo apoio incondicional. Não vejo a hora de você comprar sua armadura metálica que cospe doce ou mesmo, caso tudo dê errado, tornar-se papa por indicação direta de Deus.

Às minhas amigas **Beatriz, Jéssica e Regiane** pelas risadas e pelos momentos felizes. A amizade de vocês foi essencial ao longo de todo o doutorado.

Ao meu amigo e orientador **Edvaldo**, pelo apoio e amparo ao longo destes anos de doutorado. Sou muito sortudo por ter encontrado na figura do orientador um amigo que levarei para toda a vida. Abrigado pelo constante incentivo. Esta tese em sua essência deve muito à você por ter se tornado real. Por último, mas não menos importante, obrigado por ter me apresentado ao maravilhoso mundo do Linux.

Ao **Antônio Bonomi**, por ter recebido me de braços abertos em sua equipe. Sou muito grato pela amizade e, principalmente, pela inspiração. Espero um dia ser um profissional tão bom e capaz quanto este grande pesquisador.

Ao professor **Rubens**, pelo apoio e incentivo. Agradeço muito a ele pelo exemplo e por ter dado vazão à minha criatividade. Espero trabalhar ainda por muitos anos com este grande profissional.

Ao grande **Eduardo Coselli**, mais conhecido pela alcunha de **Urso**, pela contribuição fundamental dada a este trabalho. Sou muito grato ao doutorado por ter me dado a oportunidade de conhecer este ser humano impar. Espero que nossas conversas filosóficas tornem se mais frequentes no futuro.

Aos meus amigos de CTBE, **Bruno, Isabele, Mateus, Tássia, Alexandre, Marcos, Lucas, Terezinha, Raquel, Danilo, Otávio, Charles, Milene, Elmer e Celina**. Agradeço pelas risadas, pelo café e por toda ajuda a mim dada. Ter estas pessoas nos meus dias foi sem dúvida um grande privilégio.

O presente trabalho foi realizado com apoio da Coordenação de Aperfeiçoamento de Pessoal de Nível Superior - Brasil (CAPES) - Código de Financiamento 024/2013. Agradeço, pois, a ajuda financeira recebida por essa instituição.

Por fim, a todos que direta ou indiretamente contribuíram para a realização deste trabalho.

Obrigado!

"The world is what exists and what happens, but we gain enormous insight by talking about it - telling its story - in different ways. (...) [Therefore, the poetic naturalism] can be summarized in three points:

- There are many ways of talking about the world;
- All good ways of talking must be consistent with one another and with the world;
- Our purposes in the moment determine the best way of talking."

Sean Carroll, excerpted from the book
The Big Picture: On the Origins of Life, Meaning, and
the Universe Itself.

Abstract

In the ethanol industry, extraction is the unit operation in charge of recovering as much sucrose as possible from sugarcane. Guaranteeing the quality of this operation is crucial, since ethanol production has sucrose as raw material and bagasse can be used to cogenerate electricity and/or to produce second-generation ethanol. Although crushing mills are the more widespread extraction method around the world, the importance of diffusers should not be neglected, especially regarding its advantages over the crushing mills (*e.g.*, higher sucrose extraction, lower mechanical power consumption, lower maintenance costs). For many mills, extraction via diffusers is a “black-box” process in which the operation procedure of this equipment is often based on heuristic knowledge. In these cases, extraction becomes a subjective procedure, lacking reliable predictive methodologies. In order to provide a robust and reliable approach to fulfill this predictive requirement, this thesis proposes a two-dimensional phenomenological model for sugar extraction in industrial moving-bed diffusers, both at steady and transient states. The mathematical formulation of the model is based on the theories of transport phenomena in porous media, which is an original and formal theoretical approach to describe sugar extraction in sugarcane beds. Averaging techniques were applied to convert the model equations into macroscopic mass balances over continuous volumes. The model was discretized by the finite volume method (FVM). The discretized model at steady-state is solved by a supernodal LU factorization routine and the dynamic simulations are performed using a 4th order Runge-kutta method. In order to make the model and the solution procedures user-friendly, a computer-aided simulation framework was developed in *Python* programming language. The outputs of this framework are extraction degree, °Brix curve, and °Brix distribution in the bed. This last output is unprecedented in literature. Moreover, the simulation framework also has an optimization module, in which a genetic algorithm is implemented to seek improvements in the extraction performance. A real industrial moving-bed diffuser was used as a case study to demonstrate the capabilities of the simulation framework. Simulated results both at steady and transient states are in good agreement with the expected behavior of the real equipment. Moreover, °Brix distribution in the bed emerges as a new approach to assess the operation of a moving-bed diffuser. Regarding the optimization module, the optimum results demonstrate the potential of the Simulation Framework to improve the extraction performance via diffusers. In a final analysis, the developed simulation framework arises as a reliable predictive tool, which has the potential to assist design, operation, and optimization of moving-bed diffuser in the ethanol production industry.

Resumo

Na indústria alcooleira, extração é a operação unitária responsável por recuperar o máximo possível de sacarose da cana-de-ácúcar. Garantir a qualidade desta operação é crucial, uma vez que a produção de etanol usa a sacarose como matéria-prima e o bagaço pode ser usado para cogear eletricidade e/ou produzir etanol de segunda geração. Apesar de as moendas serem o método de extração mais utilizado ao redor do mundo, a importância dos difusores não deve ser negligenciada, especialmente em relação a suas vantagens sobre as moendas (*e.g.*, maior extração de sacarose, menor consumo mecânico, menor custos de manutenção). Para muitas usinas, extração via difusores é um processo em “caixa-preta”, na qual o procedimento de operação é baseado em conhecimentos heurísticos. Nestes casos, a extração torna-se um procedimento subjetivo, carecendo de uma metodologia preditiva confiável. Com a intenção de prover uma abordagem robusta e confiável para suprir esta carência, esta tese propõe um modelo fenomenológico bidimensional para a extração em difusores de leito móvel industriais, tanto em estado estacionário quanto em estado transiente. A formulação matemática do modelo é baseada nas teorias de fenômenos de transporte em meios porosos, o que é uma abordagem original e formal para descrever a extração de açúcar em leitos de cana-de-açúcar. Técnicas de média foram aplicadas para converter as equações do modelo em balanços macroscópicos em torno de volumes contínuos. O modelo foi discretizado usando o método dos volumes finitos. O modelo discretizado em estado estacionário é resolvido usando uma rotina de fatoração LU super-nodal e as simulações dinâmicas são realizadas usando um método de Runge-Kutta de quarta ordem. Com a intenção de tornar o modelo e os procedimentos de solução “*user-friendly*”, uma plataforma de simulação auxiliada por computador foi desenvolvida na linguagem de programação *Python*. As saídas da plataforma são o grau de extração, a curva °Brix e a distribuição °Brix no leito. Esta última saída não possui precedentes na literatura. Além disto, a plataforma de simulação também possui um módulo de otimização, na qual um algoritmo genético é implementado para buscar melhorias na performance da extração. Um difusor de leito móvel real foi usado como caso de estudo para demonstrar as capacidades da plataforma de simulação. Os resultados simulados, tanto em estado estacionário quanto transiente, estão de bom acordo com o comportamento esperado de um equipamento real. Além do mais, a distribuição °Brix no leito surge como uma abordagem nova para avaliar a operação de difusores de leito móvel. Em relação ao módulo de otimização, os resultados ótimos demonstraram o potencial da plataforma de simulação em melhorar a performance da extração via difusores. Numa análise final, a plataforma de simulação desenvolvida surge como uma ferramenta confiável de predição, que possui o po-

tencial de assistir o designe, a operação e a otimização de difusores de leito móvel na indústria alcooleira.

List of Figures

2.1	Scheme of the extraction process in a moving-bed diffuser with 14 stages. . .	42
2.2	(a)Structures of the plant cell wall; (b) micro-fibrils conformation in a primary wall and (c) in a secondary wall. Adapted from: RYTIOJA <i>et al.</i> , 2014. . . .	45
2.3	(a)Sugarcane structures. (b) Anatomical tissues present in an internode of a sugarcane culm viewed by Scanning Electron Microscopy (<i>SEM</i>). (c) Details of the vascular bundles surrounded by the sclerenchyma tissues, viewed by SEM. Adapted from SANT'ANNA <i>et al.</i> , 2013	47
2.4	(a) Sugar beet structures. (b) A transversal cut of a sugar beet root and the tissues present in this structure. (c) A magnified view of a portion of the root (red dashed rectangle) showing the distribution of the vascular and parenchyma bands. Adapted from MILFORD, 2006	49
2.5	Lateral view of a sugarcane bed inside an industrial moving-bed diffuser under operation. Sugarcane fibers arranged in a complex conformation inside the bed. Extracting liquid moving through the network of void spaces formed by the fibers.	52
2.6	Liquid distribution inside a simplified representation of a sugarcane bed. Liquid pattern in the bed divided into three zones: motion, stagnant, and isolated regions. Region I^1 is a separated region from the network of voids; I^2 is a zone not accessed by the flowing liquid.	54
2.7	Liquid velocity in a sugarcane bed in relation to stage N of a diffuser. (a) Liquid percolating a motionless bed. (b) A moving bed with liquid moving to the target stage. (c) Deviations from the counter-current arrangement due to recirculation and (d) by-passing.	56

2.8	Lateral view of moving-bed diffuser under operation. Liquid building up at the top of the sugarcane due to the occurrence of flooding.	57
2.9	Schematic representation of the sub-processes present in the sucrose extraction via moving-bed diffusers.	59
2.10	Schematic representation of the relations among the operational variables and the impacts of this relations on the extraction performance.	65
2.11	Schematic representation of the extraction model proposed by REIN (1972). Adapted from REIN, 1972	68
2.12	Schematic representation of a part-flooded bed. Adapted from PICARO and WHITE, 1993	70
3.1	A section of a sugarcane bed represented as a fractured porous media. White and yellow regions represent, respectively, the void space and the sugarcane fibers.	74
3.2	Schematic representation of the proposed extraction process. The volumetric fraction of the void spaces and fibers are represented by θ_v and θ_f , respectively. The fraction of the void space comprising the percolating liquid is accounted for the α term. The β term is the fraction of the fibers extracted by lixiviation.	75
3.3	Velocity components for each bed section following an Eulerian approach and a static referential.	76
3.4	A generic infinitesimal volume U along with its sucrose fluxes. General form of the sucrose balance equation.	77
3.5	Continuum hypothesis applied to an illustrative scenario. (a) Region of a sugarcane bed described by a generic system property Φ^γ . Red dashed square represents the macroscopic subdivisions where the continuum hypothesis is assumed valid. (b) Continuous volume described by the average of a generic system property $\bar{\Phi}^\gamma$. (c) Sugarcane bed as union of continuous volumes.	80
3.6	Average concentration of sugar in the cane bed as a function of the volume element size	82
3.7	Schematic representation of a frontier between two portions of the sugarcane bed	85

3.8	Boundary conditions for the four bed sections in each border of the diffuser.	89
4.1	(a) Grid representation for a stage of a moving-bed diffuser. The highlighted volumes show the applied index rule for a generic volume centered in “ i, j ” and its nearest neighbors. North boundary divided into aspersion and non-aspersion regions. Number of volumes per stage presented and size of the aspersion zone are illustrative. (b) Generic volume of the grid along with its faces nomenclature as common used in the finite volumes method literature. Integration sense for both x and z directions.	93
4.2	Schematic representation of the variation in the bed height promoted by an increase in the bed velocity. (a) A diffuser initially operating with a bed velocity V_1 and a bed height H_1 . (b) Bed velocity is increased to V_2 , but keeping the same amount of sugarcane fed into the equipment. It is formed three distinct regions in the bed: new and old height zones surrounding a transient region that propagates in the same sense of the bed velocity. (c) A new steady-state operational condition with bed height H_2 and bed velocity V_2 .	100
4.3	Transient behavior of the increase of the bed height.	101
4.4	Schematic representation of the grid for two generic stages. (a) Solution grid in Cartesian coordinates presenting a non-regular grid in the transient regions. (b) Solution grid in the new coordinate system, in which the regularity of the volumes is always preserved. The blue equations are the transformation functions used to convert the Cartesian system into the new coordinates, and vice-versa.	102
4.5	Proof for the zero value of the red terms in the Eq 4.36.	108
4.6	Approach used in this thesis to compute z_τ in the model equations.	111
4.7	Boundary conditions for the four bed sections in the new coordinates system.	115
4.8	Section of a grid at three distinct times (<i>i.e.</i> , $t_1 < t_2 < t_3$). (a) Initial period when a propagation front (PF) enters in the section. (b) As PF penetrates the grid, the initial percolating velocity in the volumes is replaced by the new value. (c) Each volume in the given section presenting the new percolating velocity. It is important to highlight that this abstraction is assumed valid whatever coordinate system is considered.	116

4.9	Main features of the moving-bed diffuser simulation framework.	118
4.10	Schematic representation of the fitting procedure. Gray colored boxes are inputs provided by the end users.	120
4.11	Schematic representation of the optimization procedure. Gray colored boxes are either an input (top of the scheme) or an output (bottom of the scheme) of the optimization procedure.	121
5.1	°Brix curves from the moving-bed diffuser simulation framework as a function of the resolution grid size. Labels represent the size of the grid per stage (<i>e.g.</i> , 6X6 means 6 vertical volumes and 6 horizontal volumes per stage).	126
5.2	Time in minutes to perform a simulation as function grid size per stage. . . .	126
5.3	Ideal °Brix curve used and fitted results of one hundred bootstrap iterations.	127
5.4	°Brix curve simulated using the average of parameters fitted through the bootstrap iteration.	128
5.5	°Brix curves simulated for different number of stages.	131
5.6	Simulated °Brix distribution for moving-bed diffusers with 10, 14, and 18 stages, respectively. Regions of same °Brix value are represented by dashed lines (isolines).	132
5.7	°Brix curve as function of the width of the diffuser.	133
5.8	Simulated °Brix distribution as function of the width of the diffuser. Regions of the same °Brix value are represented by dash lines (isolines).	134
5.9	Simulated °Brix curves regarding two °Brix values in the raw material: 18.0 and 14.0 °Brix.	135
5.10	Simulated °Brix distribution for two °Brix values in the raw material: 18.0 and 14.0 °Brix. Regions of the same °Brix value are represented by dash lines (isolines).	135
5.11	Simulated °Brix distribution for bed velocities of 0.85 and 0.95 <i>m/min</i> . Regions of the same °Brix value are represented by dash lines (isolines).	137
5.12	°Brix curve for bed velocities of 0.85 and 0.95 <i>m/min</i>	137

5.13	Resultant trajectory of the percolating liquid inside the bed for two bed velocities: v_b and v_b +increment.	138
5.14	°Brix curves simulated considering two different amounts of imbibition water: 2.8 and 3.5 kg_{water}/kg_{fiber}	139
5.15	°Brix gradation for two amounts of imbibition water: 2.8 and 3.5 kg_{water}/kg_{fiber} . Regions of the same °Brix value are represented by dash lines (isolines).	140
5.16	°Brix curve simulated considering distinct positions of the imbibition. The position 51 m is the current configuration of the diffuser. The four remaining positions (<i>i.e.</i> , 15, 30, 45, and 60 m) relate to each quarter of a diffuser with 60 m long.	141
5.17	Simulated °Brix gradation concerning distinct positions of the imbibition. The position 51 m is the current configuration of the diffuser. The four remaining positions (<i>i.e.</i> , 15, 30, 45, and 60 m) relate to each quarter of a diffuser with 60 m long. Regions of the same °Brix value are represented by dash lines (isolines).	142
5.18	Simulated °Brix curves concerning two distinct sugar concentrations of the imbibition water.	144
5.19	Simulated °Brix gradation concerning two distinct sugar concentrations of the imbibition water. Regions of the same °Brix value are represented by dash lines (isolines).	144
5.20	Simulated °Brix distribution inside the sugar cane for percolating velocities of 0.4 and 0.5 m/min . Regions of the same °Brix value are represented by dash lines (isolines)	146
5.21	°Brix curve for percolating velocities of 0.4 and 0.5 m/min	147
5.22	Resultant trajectory of the percolating liquid inside the bed for two percolating velocities: v_p and v_p +increment.	148
5.23	Percolating velocity profiles regarding the cases 1 to 4.	149
5.24	Simulated °Brix curves for the cases 1 to 4. The °Brix curves of the two constant v_p scenarios are also displayed in this figure (base 0.4 and 0.5 m/min).	150
5.25	Simulated °Brix distribution regarding the cases 1 to 4. Regions of the same °Brix value are represented by dash lines (isolines).	151

5.26	Percolating velocity profile regarding the case 5.	152
5.27	Simulated °Brix curves for case 5 in comparison with case 4 and base case of constant v_p at 0.5 m/min	153
5.28	Simulated °Brix distribution for case 5. Regions of the same °Brix value are represented by dash lines (isolines).	153
5.29	Evolution of the average of the estimated local error over the first hour of the transient process. Figure generated using a time step of 0.5 s . Such errors concerns the transient state promoted by a variation in the °Brix of the raw material from 18 to 14 °Brix.	156
5.30	Evolution of the °Brix curve as function of time promoted by a variation in the °Brix of the raw material from 18 to 14 °Brix (YouTube). URL: https://youtu.be/bvxyZX9h3hc	158
5.31	Evolution of the °Brix distribution as function of time promoted by a variation in the °Brix of the raw material from 18 to 14 °Brix (YouTube). URL: https://youtu.be/IpbjiYEZEwo	159
5.32	Evolution of the average of the estimated local error over (a) the initial 10 s of the transient process and (b) from 10.0 s to 1.0 hour of the same dynamic procedure. Figure generated using a time step of 0.5 s . These errors concerns the transient state promoted by a change in the aspersion position of the imbibition water from 51 to 15 m	161
5.33	Variation in the °Brix curve as function of time promoted by a change in the aspersion position of the imbibition water from 51 to 15 m (YouTube). URL: https://youtu.be/93sYuNQry3A	162
5.34	Variation in the °Brix distribution as function of time promoted by a change in the aspersion position of the imbibition water from 51 to 15 m (YouTube). URL: https://youtu.be/yqIMbLWtVSc	163

5.35	Evolution of the average of the estimated local error over the time promoted by a variation of the percolating velocity from 0.4 to 0.5 <i>m/min</i> , without propagation (frames a and b) and with propagation (frames c and d). Frame (a) regards the first simulated minute and frame (b) presents the average of the estimated local errors from 1 <i>min</i> to 1 hour. In their turn, frame (c) is the initial 6 minutes of simulation and frame (d) shows the the average of the estimated local errors from 6 <i>min</i> to 1 hour.	166
5.36	Evolution of the °Brix curve as function of time promoted by a variation of the percolating velocity, without propagation , from 0.4 to 0.5 <i>m/min</i> (YouTube). URL: https://youtu.be/1kWPWhI2OV8	168
5.37	Evolution of the °Brix distribution as function of time promoted by a variation of the percolating velocity, without propagation , from 0.4 to 0.5 <i>m/min</i> (YouTube). URL: https://youtu.be/Z6YezFR4iOI	169
5.38	Evolution of the °Brix curve as function of time promoted by a variation of the percolating velocity, with propagation , from 0.4 to 0.5 <i>m/min</i> (YouTube). URL: https://youtu.be/57zytbI7_KY	170
5.39	Evolution of the °Brix distribution as function of time promoted by a variation of the percolating velocity, with propagation , from 0.4 to 0.5 <i>m/min</i> (YouTube). URL: https://youtu.be/suBdLLroGrc	171
5.40	Average of the estimated local errors acquired during the transient simulation of a system facing a change in the bed velocity from 0.85 (base case) to 0.95 <i>m/min</i> , with instantaneous variation in the bed height. Frame (a) presents the first two minutes of the transient process and frame (b) displays the evolution of the average of the local errors up to the end of the first simulated hour. Errors acquired using a time step of 0.5 s.	174
5.41	°Brix curve, as function of time, of a system facing a change in the extraction characteristics promoted by a variation in the bed velocity from 0.85 (base case) to 0.95 <i>m/min</i> , with instantaneous modification of the bed height. The two motionless curves displayed in the frames of this Figure are the old and the new steady-state conditions (YouTube). URL: https://youtu.be/nLAOyvi2tKE	175

5.42	°Brix distribution, as function of time, of a system facing a change in the extraction characteristics promoted by a variation in the bed velocity from 0.85 (base case) to 0.95 <i>m/min</i> , with instantaneous modification of the bed height (YouTube). URL: https://youtu.be/O63LOvRgPEA	176
5.43	Simulated °Brix distribution for bed velocities of 0.85 and 0.95 <i>m/min</i> in the new coordinates system.	177
5.44	Average of the estimated local errors acquired during the transient simulation of a system facing a change in the bed velocity from 0.85 (base case) to 0.95 <i>m/min</i> , with gradual variation in the bed height. Errors acquired using a time step of 0.5 s.	180
5.45	Evolution of the °Brix distribution, over the course of the transient process, for a change in the bed velocity from 0.85 to 0.95 <i>m/min</i> , with gradual variation in the bed height. Size of the transient region (<i>STR</i>) is equal to 10 m. Vertical dashed lines depict the frontiers of the transient regions (YouTube). URL: https://youtu.be/5OCr8ZJ5At8	181
5.46	Evolution of the °Brix distribution, over the course of the transient process, for a change in the bed velocity from 0.85 to 0.95 <i>m/min</i> , with gradual variation in the bed height. Size of the transient region (<i>STR</i>) is equal to 15 m. Vertical dashed lines depict the frontiers of the transient regions (YouTube). URL: https://youtu.be/pYKwtQ4lrBE	182
5.47	Evolution of the °Brix distribution, over the course of the transient process, for a change in the bed velocity from 0.85 to 0.95 <i>m/min</i> , with gradual variation in the bed height. Size of the transient region (<i>STR</i>) is equal to 20 m. Vertical dashed lines depict the frontiers of the transient regions (YouTube). URL: https://youtu.be/EShZZ05p5y8	183
5.48	Convective fluxes of the sucrose balance of the percolating liquid regarding a generic volume of the grid (i,j) in the new coordinates sytem.	184
5.49	Schematic representation of a thought experiment in which two generic isolines are interpreted as real entities of a sugarcane bed. During the experiment, it is analyzed the transient behavior of the isolines promoted by a variation in the bed velocity with gradual change in the bed height.	185

5.50	°Brix curve evolution as function of time for a variation in the bed velocity from 0.85 (base case) to 0.95 m/min , with gradual modification of the bed height. Size of the transient region (STR) is equal to 10 m . Vertical dashed lines depict the frontiers of the transient regions (YouTube). URL: https://youtu.be/k6m95zJwwyc	187
5.51	°Brix curve evolution as function of time for a variation in the bed velocity from 0.85 (base case) to 0.95 m/min , with gradual modification of the bed height. Size of the transient region (STR) is equal to 15 m . Vertical dashed lines depict the frontiers of the transient regions (YouTube). URL: https://youtu.be/aMh2eZ3JOEc	188
5.52	°Brix curve evolution as function of time for a variation in the bed velocity from 0.85 (base case) to 0.95 m/min , with gradual modification of the bed height. Size of the transient region (STR) is equal to 20 m . Vertical dashed lines depict the frontiers of the transient regions (YouTube). URL: https://youtu.be/-cgK8HDE0dY	189
5.53	Schematic representation of the variation in the aspersion position.	193
5.54	Results of the optimization procedure that aims to improve the extraction performance of the base case by changing the aspersion positions as a conjunct. (a) Fitness evolution (<i>i.e.</i> , objective function) over the course of the optimization procedure. (b) °Brix curve for the base case in comparison with the °Brix curve for the optimized scenario.	195
5.55	°Brix distribution for the base case and for the optimized scenario concerning an optimization procedure that aims to improve the extraction performance by changing the aspersion positions as a conjunct.	196
5.56	Results of the optimization procedure in which the main goal was to improve the extraction performance of a scenario in which the bed velocity is 0.95 m/min . (a) Fitness evolution (<i>i.e.</i> , objective function) over the course of the optimization procedure. (b) °Brix curves for the base case and the scenario with $v_b = 0.95 m/min$ in comparison with the °Brix curve for the optimized scenario.	197
5.57	°Brix distributions regarding the scenarios with $v_b = 0.95 m/min$ with and without optimization.	198

5.58	Optimization results regarding the procedure to seek improvements in the extraction performance by changing the imbibition rate. (a) Fitness evolution (<i>i.e.</i> , objective function) over the course of the optimization procedure. (b) °Brix curves for the base case with and without optimization.	199
5.59	°Brix distribution simulated considering the optimum value of the Imbibition rate (<i>i.e.</i> , $4.0 \text{ kg}_{water}/\text{kg}_{fiber}$).	200
5.60	Optimization results regarding the procedure to seek improvements in the extraction performance by changing the imbibition rate, with cost assumption. (a) Fitness evolution (<i>i.e.</i> , objective function) over the course of the optimization procedure. (b) °Brix curves for the base case in comparison with the optimized scenario assuming a cost assumption.	202
5.61	°Brix distribution regarding the procedure to seek improvements in the extraction performance by changing the imbibition rate, with cost assumption.	202
5.62	Schematic representation of the implemented mixed-integer optimization routine.	204
5.63	Details of the optimization procedure concerning the sub-scenario with the best optimum solution ($N_{st} = 18$). (a) Fitness evolution over the course of the optimization procedure. (b) °Brix curves regarding the extraction process performed in a diffuser with 18 stages, both optimized and non-optimized, in comparison with the °Brix curve of the base case.	205
5.64	°Brix Curves for a 12 stage diffuser, with and without optimization, in comparison with the base case and the scenario regarding a optimized 18 stage diffuser.	207
7.1	Spatial configurations of water and air in an unsaturated porous medium. Adapted from SZYMKIEWICZ, 2013	211
7.2	Simulated flux in a 2-D section of a sugarcane bed using the Lattice Boltzmann method. (a) Picture of a sugarcane bed used as base to perform the liquid flux simulation. (b) Velocity profile at steady-state condition within the region of the picture surrounded by the red rectangle (in the “a” panel).	213

List of Tables

1.1	Thesis organization and a brief description of the chapter's contents.	40
2.1	Vegetable tissues along their characteristics and functionalities.	46
5.1	Characteristics and operational conditions of the equipment from a full-scale moving-bed diffuser located in a mill in Central-Western Brazil.	124
5.2	Configurations of the computer used to perform all the simulations	125
5.3	Averages and standard deviations of the fitted parameters in bootstrap iterations.	128
5.4	Extraction degree according to the number of stages in a moving-bed diffuser.	130
5.5	Extraction degree as function of the width of the diffuser	132
5.6	Extraction degree as function of the °Brix value in the raw material	134
5.7	Simulated sugar extraction degree as a function of the bed velocity.	136
5.8	Extraction degree as function of the amount of imbibition water	138
5.9	Extraction degree concerning distinct imbibition positions	140
5.10	Extraction degree values for three sugar concentrations in the imbibition water	143
5.11	Simulated extraction degree values for two percolating velocities. Each velocity is assumed valid in the whole equipment.	145
5.12	Simulated extraction degrees regarding the cases 1 to 4.	150
5.13	Simulation time, as function of the integration step, required to simulate 10 <i>min</i> of a transient process promoted by a variation in the °Brix of the raw material from 18 to 14 °Brix.	157

5.14	Simulation time, as function of the integration step, required to simulate 10 <i>min</i> of a transient process promoted by a variation of the percolating velocity from 0.4 to 0.5 <i>m/min</i> , with propagation.	167
5.15	Optimization results concerning each sub-scenario describe in Figure 5.62	204
5.16	Values of the objective function considering cost assumption of the diffuser's size.	206

Nomenclature

Acronyms and Abbreviations

CTBE Brazilian Bioethanol Science and Technology Laboratory

DEAP Distributed Evolutionary Algorithm in Python

FVM Finite Volume Method

GA Genetic Algorithm

LBM Lattice Boltzmann Methodology

N Generic stage

ODE Ordinary Differential Equation

REV Representative Elementary Volumes

SEM Scanning Electron Microscopy

VSF Virtual Sugarcane Biorefinery

Greek Symbols

α Fraction of the void region representing the percolating liquid (%)

β Fraction of fibers representing the portion extracted by lixiviation (%)

$\Delta\eta$ Vertical size of a continuous volume in the grid for the new coordinates system

$\Delta\psi$ Horizontal size of a continuous volume in the grid for the new coordinates system

ΔP_{sup} Pressure drop in the support screen (Pa)

Δx	Horizontal size of a continuous volume in the grid for the Cartesian coordinates (m)
Δz	Vertical size of a continuous volume in the grid for a Cartesian coordinates (m)
η	Vertical direction in the new coordinate system
η_x	Conversion metric: Relation between η and x
η_z	Conversion metric: Relation between η and z
$\Lambda_{\gamma,\xi}$	Specific area of the surface separating ξ and γ sections (m^2)
μ	Percolating liquid viscosity ($Pa.s$)
μ_φ	Viscosity of a generic fluid phase φ ($Pa.s$)
ν	Unitary vector normal to S , pointing outward U
Ω	Dispersive coefficient (m^2/min or m^2/s)
Ω_x	Dispersive coefficient on the horizontal direction (m^2/min or m^2/s)
Ω_z	Dispersive coefficient on the vertical direction (m^2/min or m^2/s)
$\overline{\Phi}^\gamma$	Average of a generic system property in a γ section
Φ^γ	Generic system property in a γ section
ψ	Horizontal direction in the new coordinate system
ψ_x	Conversion metric: Relation between ψ and x
ψ_z	Conversion metric: Relation between ψ and z
ρ	Percolating liquid density (kg/m^3)
ρ_φ	Density of a generic fluid phase φ (kg/m^3)
θ_γ	Volume fraction of a γ section (%)
θ_f	Volume fraction of the fibers (%)
θ_v	Volume fraction of the void regions (%)
Υ	Generic parameter of the model

Symbols

∇ Gradient operator

$\overline{\dot{C}V}^\gamma$ Average dispersion effect within the fibrous medium ($kg/m^2.s$)

\overline{C}^γ Average sugar concentration of γ section (kg/m^3)

$\overline{C}_{\circ Brix}^\gamma$ Average soluble solid content in the γ section ($^\circ Brix$)

\overline{C}^ξ Average sugar concentration of ξ section (kg/m^3)

\overline{C}^e Average sugar concentration of the stagnant liquid (kg/m^3)

\overline{C}^{fd} Average sugar concentration of the fiber section extracted by diffusion (kg/m^3)

\overline{C}^{fl} Average sugar concentration of the fiber section extracted by lixiviation (kg/m^3)

\overline{C}^p Average sugar concentration of the percolating liquid (kg/m^3)

\overline{j}^γ Average diffusive flux of sugar in a γ section ($kg/m^2.s$)

\overline{Puri} Average purity of a sucrose solution ($kg_{sucrose}/kg_{solublesolids}$)

\overline{V}^γ Average velocity of the γ section (m/s or m/min)

\overline{V}_x^γ Generic average velocity in the x direction (m/s or m/min)

\overline{V}_z^γ Generic average velocity in the z direction (m/s or m/min)

B Generic macroscopic continuous volume (m^3)

B_\circ Generic Representative elementary volume (m^3)

C^γ Sugar concentration of a γ section within U (kg/m^3)

$C_{\circ Brix,rm}^{in}$ Sugar concentration in the raw material entering the equipment ($^\circ Brix$)

C_{rm}^{in} Sugar concentration in the raw material entering the equipment (kg/m^3)

$C_{\circ Brix,n}^{model}$ Soluble solid content in the n stage, calculated by the model

C_{asp}^n Sugar concentration in the aspersion point over stage n (kg/m^3)

$C_{\circ Brix,n}^{real}$ Soluble solid content in the n stage, collected a real equipment

C_{asp}	Sugar concentration in an aspersion point (kg/m^3)
D	Diffusive coefficient (m^2/min or m^2/s)
DPF	Fiber packing density (kg_{fiber}/m_{bed}^3)
Ext	Extraction degree (%)
F_c	Fiber content in the raw material (kg_{fiber}/kg_{cane})
G	Number of new data sets constructed by the bootstrap method
g	Gravitational acceleration (m/s^2)
H	Bed height (m)
$H(x)$	Bed height as function of the x positions (m)
HU_t	Total liquid hold-up of the fibrous bed (kg_{liquid}/kg_{fiber})
j^γ	Diffusive flux of sugar in a γ section ($kg/m^2.s$)
j^{SC}	Flux of sugar content in a infinitesimal area ($kg/m^2.s$)
k_1	Mass transfer rate for the lixiviation mechanism ($1/s$)
k_2	Mass transfer rate for the diffusion mechanism ($1/s$)
K_p	Permeability of the medium (m^2)
K_s	Laminar resistance of the support screen (m^{-1})
$larg$	Bed width (m)
N_{st}	Total number of stages
P	Pressure (Pa)
P_φ	Pressure of a generic fluid phase φ (Pa)
P_e	Grid Peclet number
$Prod$	Amount of processed sugarcane (kg/s or ton/s)
Q	Set containing each bed sections

S	Surface of a generic infinitesimal volume U (m^2)
s_Υ	Standard deviation of a generic parameter of the model Υ
SC	Sucrose content within U (kg)
SC^γ	Sucrose content within γ (kg)
SQ_{rm}^{in}	Sugar quantity in raw material (kg)
$SQ_{f_d}^{out}$	Sugar quantity in the f_d bed section leaving the diffuser (kg)
$SQ_{f_l}^{out}$	Sugar quantity in the f_l bed section leaving the diffuser (kg)
STR	Size of transient region (m)
t	Time (s or min)
U	Generic infinitesimal volume (m^3)
V^γ	Velocity of the γ section (m/s or m/min)
V^ξ	Velocity of the ξ section (m/s or m/min)
v_φ	Velocity of a fluid in a generic phase φ (m/s or m/min)
v_b	Bed velocity (m/s or m/min)
v_p	Percolating velocity (m/s or m/min)
x	Horizontal direction in the Cartesian coordinates (m)
z	Vertical direction in the Cartesian coordinates (m)

Superscripts and subscripts

γ	Generic bed section
φ	Generic fluid phase in a multi-phase flow inside a porous medium
ξ	Generic bed section, where $\xi \neq \gamma$
e	<i>As a superscript:</i> Stagnant liquid / <i>As a subscript:</i> East face of a volume in the grid
f_d	Fiber portion extracted by diffusion

f_l	Fiber portion extracted by lixiviation
i	Index of the grid's volumes in relation to the horizontal direction
j	Index of the grid's volumes in relation to the vertical direction
n	North face of a volume in the grid or a generic stage
p	Percolating Liquid
s	South face of a volume in the grid
w	West face of a volume in the grid

Summary

1	Introduction	35
1.1	Sugar Extraction by Diffusers	37
1.2	Objective of the thesis	38
1.3	Thesis Organization	40
2	Moving-Bed Diffusers: an Overview	41
2.1	Operation of a Moving-bed Diffuser	41
2.2	Extraction Mechanism	43
2.2.1	A cellular view of the extraction	43
2.2.1.1	Cell wall and plant tissues	43
2.2.1.2	Sugarcane and sugar beet: an anatomical comparison.	45
2.2.2	Fluid-dynamic of extraction	51
2.2.2.1	Liquid-solid contact in sugarcane beds	51
2.2.2.2	Aspersion configuration	54
2.2.3	Concluding remarks about Extraction	57
2.3	Operational Variables	58
2.3.1	Sugarcane preparation	58
2.3.2	Percolating velocity	60
2.3.3	Retention time and Diffuser size	62
2.3.4	Temperature	63

2.3.5	pH	64
2.3.6	Concluding remarks about the operational variables	64
2.4	Mathematical modeling	65
2.4.1	POL (1957)	66
2.4.2	REIN (1972)	67
2.4.3	LOVE and REIN (1980)	68
2.4.4	RODRIGUEZ (1990)	69
2.4.5	PICARO and WHITE (1993)	70
2.4.6	Concluding remarks about Mathematical modeling	72
3	Mathematical formulation	73
3.1	Phenomenological abstraction	73
3.2	Concerning the moving nature of sugarcane bed	75
3.3	General assumptions	75
3.4	Model equations in infinitesimal scale	76
3.4.1	Accumulation of sucrose within U	78
3.4.2	Net influx of sucrose into U	78
3.4.3	Production or degradation of sucrose within U	79
3.5	On the path to a macroscopic scale model	80
3.5.1	Continuum hypothesis	80
3.5.2	Representative elementary volumes	81
3.5.3	Averaging rules	82
3.6	Model equations in macroscopic scale	82
3.6.1	Sugar content in the percolating liquid	86
3.6.2	Sugar content in the stagnant liquid	88
3.6.3	Sugar content in the fibers	88
3.7	Boundary conditions	88

3.8	Auxiliary equations	90
3.8.1	Bed height	90
3.8.2	Volume fractions in the bed portions	90
3.8.3	Converting concentration into °Brix	90
3.8.4	Extraction degree	91
3.9	Concluding remarks	91
4	Numerical Solution	92
4.1	Discretization procedure	92
4.1.1	Discretization of the convective terms	94
4.1.2	Discretization of the dispersion terms	95
4.1.3	Discretization of the extraction terms	96
4.1.4	Time derivatives	97
4.1.5	Mathematical model in the discretized form	97
4.2	Bed height at transient state	99
4.2.1	Modifying the coordinate system	101
4.2.2	An invariant model	103
4.2.3	Invariant mathematical model in the discretized form	110
4.3	Percolating velocity at the transient state	115
4.4	Simulation framework	117
4.4.1	Fitting model parameters	118
4.4.2	Optimization procedure	119
4.5	Concluding remarks	121
5	Performance of the Simulation Framework	123
5.1	Case Study	123
5.2	Steady state simulations	125

5.2.1	Solution procedure	125
5.2.2	Fitted parameters	126
5.2.3	Dimensions of the diffuser	130
5.2.4	°Brix in the raw material	133
5.2.5	Bed velocity	135
5.2.6	Imbibition characteristics	137
5.2.7	Percolating velocity	144
	5.2.7.1 Percolating velocity constant in the bed	145
	5.2.7.2 Percolating velocity variation in the bed	147
5.2.8	Concluding remarks about the steady-state simulations	153
5.3	Dynamic simulations	154
	5.3.1 °Brix in the raw material	155
	5.3.2 Imbibition position	158
	5.3.3 Percolating velocity	164
	5.3.4 Bed velocity	171
	5.3.4.1 Instantaneous variation of the bed height	172
	5.3.4.2 Gradual variation of the bed height	175
	5.3.5 Concluding remarks about the dynamic simulations	191
5.4	Optimization analyses	191
	5.4.1 Aspersion positions	192
	5.4.1.1 Optimizing the base case	193
	5.4.1.2 Optimizing a scenario with bed velocity equal to 0.95 m/min	195
	5.4.2 Imbibition rate	198
	5.4.3 Size of the moving-bed diffuser	203
	5.4.4 Concluding remarks about the optimization analyses	206

7 Recommendations for future work	210
Bibliography	214
A Averaging rules	223

Chapter 1

Introduction

Global energy demand in 2017 was 14 050 million tonnes of oil equivalent, with fossil fuels representing 85% of this energy requirement (IEA, 2017). It is projected an increase of 40% in this demand in 2035 (IEA, 2013), along with a reduction on the availability of fossil energy sources (GOLDEMBERG, 2007). In this scenario, global awareness regarding energy security issues and environmental changes explain the current interest on biofuels (SENDICH and DALE, 2009), in which the present and future uses of oil play a constant stress factor. Fluctuations in the oil prices works toward increasing economic and politic instabilities around the world. From a environmental point of view, the consolidation of an alternative and renewable fuel can help the world to satisfy the goal of reducing greenhouse gas emissions, thus limiting the extent of future extreme climate impacts (ELLABBAN *et al.*, 2014).

In this urge for renewable energy sources, the area of society with greatest vulnerability is the one of liquid transportation fuels (DALE, 2008). Bioethanol is one of the most promising alternatives for liquid fossil fuels (ZABED *et al.*, 2017). The large-scale production from renewable sources (*e.g.*, sugarcane and corn), the fact of being less pollutant than oil (GOLDEMBERG, 2007) and the lower impact on greenhouse effect and ozone depletion than its fossil counterparts (CAVALETT *et al.*, 2013) are just a few reasons that make bioethanol an important player to be fostered in the current energy matrix. Indeed, bioethanol can be a renewable alternative for transportation fuels over a short-term horizon, promoting both economic and environmental benefits, as well as security in energy supply (ZAMBONI *et al.*, 2009).

Brazil is the second largest ethanol producer in the world (USA is the leader),

with an annual production of around 26 000 million liters, representing 26% of the global ethanol production (RFA, 2017). Ethanol is produced in Brazil mainly from sugarcane. This crop gives to the country an advantageous position, since few nations have large amounts of renewable energy source without jeopardizing food production (CERQUEIRA LEITE *et al.*, 2009). Moreover, Brazilian ethanol is, in principle, competitive with gasoline without the government support (GOLDEMBERG, 2007; CERQUEIRA LEITE and LEAL, 2007 *apud* SALLES-FILHO *et al.*, 2017;). This favorable national scenario, along with the aforementioned ethanol environmental benefits, places Brazil as one of the prominent leaders in the development of a future renewable and eco-friendly economy.

A biorefinery is an industrial facility that converts biomass to produce fuels, power and value-added chemicals (DEMIRBAS, 2010). Sugarcane processing facilities in Brazil are considered a sort of biorefinery (CAVALETT *et al.*, 2012), where this raw material is used to produce three large-scale products: ethanol, sugar and electricity. This already-established biorefinery structure may provide a starting pointing to develop a high-tech industrial configuration, thus understanding sugarcane not only as an energy carrier, but also as a source of carbon (BONOMI *et al.*, 2016). Indeed, an abundant renewable source of carbon would be the building block for a green chemistry market in Brazil. In this bio-based economy, goods would be produced in a sustainable way, avoiding the current strong dependency on fossil fuels.

The foundations of a bio-based economy in Brazil must be well-planned, considering different technological routes and establishing a fully integrated view of the existing industries (BONOMI *et al.*, 2016). The quality of this planning requires detailed technological assessments, which can point crucial bottlenecks and throw light on new technologies. For the assessment of new technologies, which there are no full-scale commercial examples, modeling tools are required to check viability and improvements (SENDICH and DALE, 2009). In this context, the *Brazilian Bioethanol Science and Technology Laboratory* (CTBE) is developing the *Virtual Sugarcane Biorefinery* (VSB), which is a novel framework that integrates economic, social and environmental evaluation tools with computer simulation platforms (CAVALETT *et al.*, 2012). VSB main goal is to assess technical and sustainability indicators of different sugarcane biorefinery routes and/or alternatives.

A essential aspect of the VSB development is the constant improvement of the modeling capacities of the framework. By constructing new mathematical models or making the existing ones more detailed give a flexible nature to VSB, which permit the simulations to incorporate different technological scenarios to answer emerging new questions. In fact,

the very subject of this Ph.D project is an example of this constant improvement of the VSB framework. Before the development of this thesis, sugar extraction by diffusers was modeled in VSB as a “block-box” operation. This type of model limits the range of the analysis that VSB could perform to understand and improve the extraction process by diffusers. Therefore, this Ph.D project was proposed to answer this modeling limitation, incorporating a phenomenological model of a diffuser into the VSB framework.

1.1 Sugar Extraction by Diffusers

On the ethanol industry, extraction is the unity operation in charge of recovering as much juice (sucrose-water solution) as possible from sugarcane (PELLEGRINI and DE OLIVEIRA, 2011). Guarantee the quality of this operation is important, since the succeeding stages of ethanol production have sucrose as the principal raw material (PALACIOS-BERECHÉ *et al.*, 2014). Moreover, the solid structure of sugarcane after extraction, so called bagasse, can be used to co-generate electricity (STANMORE, 2010; CAVALETT *et al.*, 2012) and/or to produce second generation ethanol (DIAS *et al.*, 2012). At industrial scale, extraction can be performed using crushing mills or diffusers. Crushing mills are constituted by sets of three or five rolls where sugarcane stalks are pressed, separating juice from bagasse (DIAS *et al.*, 2015). Alternatively, diffusers are solid-liquid extraction devices, operating on stage basis (REIN, 1995).

So far crushing mills are the traditional and more widespread extraction method around the world (REIN, 2013). However, the presence and the importance of diffusers in the sugarcane industry must not be neglected. A remarkable example of successful use of diffusers is South Africa, where nowadays 90 % of the produced sugarcane (around 15,07 million tons of cane in the 2016/17 season (SINGELS *et al.*, 2017)) is processed through diffusers (REIN, 2013). Diffusers in Brazil appeared in 2.3 % of the sugarcane processing units during 2005/2006 season (OLIVERIO *et al.*, 2013). This share increases to around 8.0 % in 2016/2017 season. This growing tendency has its roots in economical and environmental trends in Brazil toward energy-efficient factories and sale of electricity (VOIGT, 2010), especially in greenfield projects. Other notable experiences using diffusers can be found in USA, India, Thailand (VOIGT and HULLEY, 2014), Egypt (HEMAIDA *et al.*, 1989) and Australia (MCGINN *et al.*, 1981).

Several studies in the literature compare diffusers and crushing mills (PALACIOS-

BERECHE *et al.*, 2014; HOEKSTRA, 1995; KOSTER, 1995; REIN, 1995). These studies present the advantages related to the operation of diffusers, such as higher sucrose extraction, lower mechanical power consumption (about 10 kWh/t of cane for diffusers compared to 15 kWh/t of cane for crushing mills), and lower maintenance costs (between 70% and 80% higher for crushing mills). Moreover, diffusers could have an important role in the second generation ethanol production chain, since crushing mills show lower efficiency when it comes to handle energy crops with high fiber content (*e.g.*, energy cane).

It is a common practice at industrial scale to operate diffusers following heuristic knowledge, based on expertises acquired in the daily routine. For many mills, extraction using diffusers is a “black-box” process in which sugar distribution inside the bed is not accessible. In these cases, extraction performance relies only on subjective relations of causality among inputs and outputs, lacking reliable predictive methodologies. In fact, such methodologies allows for the exploration of the whole potential of diffusers, so they can work in a more efficient way when compared to crushing mills. Mathematical modeling with a suitable solution procedure and computer-aided simulation tools are robust and reliable approaches to fulfill this predictive requirement.

A mathematical model describing the extraction process is an important, useful tool to project new diffusers and optimize operational aspects of existing ones (REIN, 1972). Embedding this mathematical description in a simulation framework makes the model readily available to be used in daily routine of ethanol factories and research institutions (GERALDO *et al.*, 2016). There are few recent works on mathematical modeling of the sugar extraction in full-scale diffusers and no experiences on development of computer-aided simulation frameworks for this equipment (GERALDO *et al.*, 2018).

1.2 Objective of the thesis

The overall objective of this PhD project may be divided into two complementary contributions. The first contribution encompass the proposition of a phenomenological model to describe the extraction process in industrial moving-bed diffusers. Such model must represent the diffuser operation both at steady and transient states. In its final version, the developed model must be a formal mathematical description of the main physical mechanisms/phenomena behind the sucrose extraction from the sugarcane fibers. In its turn, the second contribution is the development of a computer-aided Simulation Framework with the

intention to make the model and its solution procedure readily available and user-friendly. It is desired that the synergy of this two contributions leads to a reliable simulation tool with the potential to assist diffusers' design, operation, and optimization; thus making sucrose extraction via diffusers a less subjective procedure.

1.3 Thesis Organization

Table 1.1 presents the following chapters of the thesis along with a brief description of their respective contents.

Table 1.1: Thesis organization and a brief description of the chapter's contents.

Chapter	Main contents
Chapter 2: Moving-Bed Diffusers: an Overview	To present the main characteristics of moving-bed diffuser operation as well as the phenomenological behavior of the extraction process in this very equipment. It is also discussed past studies concerning the mathematical modeling of diffusers.
Chapter 3: Mathematical formulation	To introduce the phenomenological interpretation of the sugar extraction in diffusers and the mathematical formulation of the model equations.
Chapter 4: Numerical Solution	To describe the numerical solution of the model and to introduce the main features of the simulation framework. It is also presented the strategies to fit the model's parameters, as well as to perform the optimization analysis.
Chapter 5: Performance of the Simulation Framework	To explore the features and potentialities of the developed framework using data collected in a real equipment. This exploration is divided into three categories: Steady-state simulations, Dynamic simulations, and optimization analyses.
Chapter 6: Conclusion	To summarize the main conclusions of this study.
Chapter 7: Recommendations for future work	To present some suggestions and guidelines for future works.

Chapter 2

Moving-Bed Diffusers: an Overview

This chapter introduces the main characteristics of the moving-bed diffuser operation as well as the phenomenological behavior of the extraction process in this very equipment. The intention here is to give an overview to those interested in better understand a moving-bed diffuser over a phenomenological point-of-view, providing theoretical bases to the discussions in the succeeding chapters. Moreover, at the end of this chapter, it is presented past studies concerning the mathematical modeling of diffusers.

2.1 Operation of a Moving-bed Diffuser

Moving-bed diffusers are stage based equipments. Figure 2.1 represents a scheme of a moving-bed diffuser along with a quick reference of the whole extraction process. The first part of the explanation of the moving-bed diffuser operation focus on the cane pathway. Sugarcane before entering the equipment goes through a preparation step (Figure 2.1-[1]), which is performed by sets of knives and shredders. This preparation step has the intention to open the cells and exposes the fibrous content of the sugarcane. As presented in some cases reported in the literature, it is also possible to place a set of mills before the diffuser. After this initial step, the raw material is fed into the moving-bed diffuser (Figure 2.1-[2]), forming a bed of prepared sugarcane that is conveyed along the equipment (Figure 2.1-[3]). The cane bed is sprinkled with liquid in the aspersion points. The sugar content of the cane is extracted by the sprinkled liquid (Figure 2.1-[4]). As a result of the aspersion process, the bed suffers a compaction, which jeopardizes the extraction. To overcome this problem, there are two sets of screws that are responsible to lift the fibrous bed. After passing through each

stage of the diffuser, the cane bed leaves the equipment with high moisture content. The material leaving the equipment, called as *megasse*, is sent to a set of two dewatering mills in order to reduce its moisture (Figure 2.1-[5]).

The second part of the explanation presents the extraction liquid pathway. Imbibition water is added in the equipment rear and percolates through the sugarcane bed (Figure 2.1-[6]). Another point of liquid insertion in the equipment is the return of the *weak-juice* (Figure 2.1-[7]). The *weak-juice* is the liquid extracted from the *megasse* by the dewatering mills. The percolating liquid is collected in trays at the equipment bottom. At any stage, the liquid is pumped and then sprinkled onto the bed to again percolates through it and be collected by the next stage. This process repeats until the percolation liquid reaches the equipment front (Figure 2.1-[8]), extracting in this process the sugar from the cane fibers. Percolating liquid in the second and third stages is pumped to a set of heating exchangers in order to increase its temperature (Figure 2.1-[9]). This heating process has the intention to guarantee that the cane entering in the diffuser achieves as faster as possible the operation temperature. The percolating liquid collected in the front of the equipment has the higher sugar content and is transported to the ethanol/sugar production (Figure 2.1-[10]).

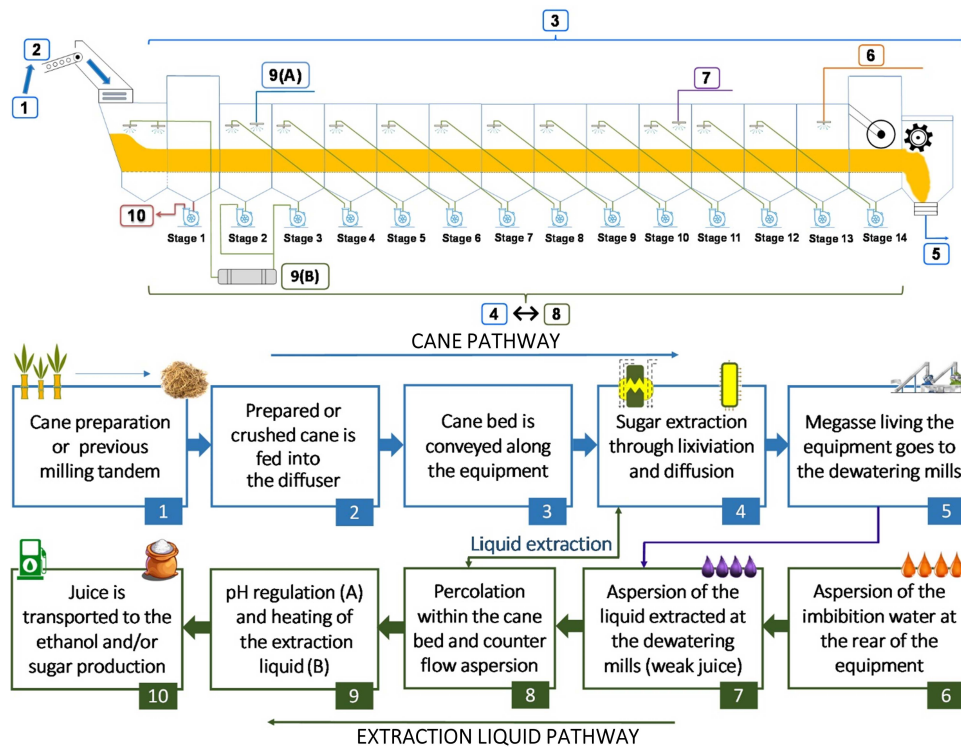


Figure 2.1: Scheme of the extraction process in a moving-bed diffuser with 14 stages.

2.2 Extraction Mechanism

Extraction in a sugarcane bed is influenced by two levels of effects ([REIN,1971](#)). In a cellular level, anatomy and morphology of the vegetable tissues regulate sugar withdrawn from the interior of the storage cells. Size and shape of the fibers, as well as their conformation in the bed, determine the fluid-dynamic level. Fluid-dynamic effects determine the liquid patterns inside the bed and control the access to the sugar extracted from the cells. The extraction phenomenon is the result of the interaction among the effects taking place in the two levels. Therefore, to understand the extraction process by diffusers is necessary to comprehend the levels both separated and linked. The following subsections are devoted to describe these levels, their particularities and synergies.

2.2.1 A cellular view of the extraction

The name “diffuser” is an historical heritage from the sugar beet industry. The equality of the name can evoke a false similarity between sugarcane and beet, especially concerning the anatomical features of both plants. Indeed, the structural particularities of these two raw materials lead to important differences on the respective extraction mechanisms, in which the name “diffuser” may sound inaccurate for the sugarcane processing. Comparing these two raw materials opens room to present the particularities of the sugarcane structures, thus highlighting the importance of plant anatomy to understand the extraction process. To explore sugarcane and sugar beet plant anatomies in a more coherent way, some points concerning the plant cell structure and the vegetable tissues properties must be introduced.

2.2.1.1 Cell wall and plant tissues

The specialized abilities of plants to a certain practical purpose emerges from the cells structures, as well as from the macroscopic organization of these cells into tissues. In fact, cells and their organizations determine many important aspects of the plant life, from physiological reactions to the morphology of the plant ([BUONAFINA and COSGROVE, 2014](#); [NOBEL, 2009](#)). The vegetable cells is going to be presented first, in order to make more understandable the differences of the tissues. It is not the intention to provide a thorough discussion about organelles and their functions. In fact, the following paragraphs focus on the cellular wall, once this structure is fundamental to explain the differences between sugarcane and beet in the sucrose storage regions.

An unique feature of the vegetable cells is the presence of a cell wall. The molecular architecture of the cell wall regulates many functions and mechanical properties of the vegetable cells (LEE *et al.*, 2011; SANT'ANNA *et al.*, 2013). For instance, the rigidity of this wall provides protection, strength, and resistance to the plant structures (RAVEN *et al.*, 1996). The major organic component of the cell wall is cellulose, which is a linear polysaccharide (NOBEL, 2009). Van der Waals and hydrogen bonds combine multiple cellulosic chains into fibrils, which aggregate themselves into larger and stiff micro-fibrils (MOON *et al.*, 2011). In a cell wall, the fibrils structures are placed in a complex matrix of hemicellulose and pectins, forming resilient and load-bearing arrangements (BUONAFINA and COSGROVE, 2014). In some structures of the cell wall (*i.e.*, secondary cell wall), lignin binds the fibrils by the hemicellulose components, providing extra strength and resistance to the cell.

A cell wall may be made up of three distinct layers, so called middle lamella, primary wall and secondary wall (Figure 2.2-(a)). The middle lamella surrounds the cell wall and is responsible for the adhesion among neighboring cells. Primary cell wall is always present in the vegetable tissues, being formed in the development phase of the cells (NOBEL, 2009). This primary layer is composed by fibrils structures arranged in a less organized way, without the presence of lignin (Figure 2.2-(b)) (BUONAFINA and COSGROVE, 2014). Therefore, such cell wall is more flexible, permitting the cell growth and division (RAVEN *et al.*, 1996). Ceasing the formation of the primary wall, cells present in some specialized tissues start to produce a secondary layer. Fibrils are arranged in a parallel conformation and entangled by lignin in the secondary wall (Figure 2.2-(c)) (SANT'ANNA *et al.*, 2013). Lignin is a hydrophobic phenolic polymer, which provides extra strength and protection to cells. The inclusion of this component makes the wall more rigid and less permeable to water (BUONAFINA and COSGROVE, 2014). It is common to observe three distinct layers in the secondary wall (*e.g.*, S_1 , S_2 and S_3), each of them with a distinct orientation of the cellulosic fibrils.

The vegetable cells can be organized in tissues, following their structural and/or functional distinctions (RAVEN *et al.*, 1996). Table 2.1 summarizes the vegetable tissues relevant for the present discussion. As a general tendency, cells of tissues with some metabolic role have just primary wall (RAVEN *et al.*, 1996). On the other hand, cells with secondary wall are presented in tissues with required mechanical strength, such as those specialized in supporting, conduction and protection. For instance, parenchyma cells are specialized in important metabolic/physiologic functions, such as sucrose storage and short distance transport of solutes. Thus, cells in parenchyma tissues should be alive and thin-walled, which is

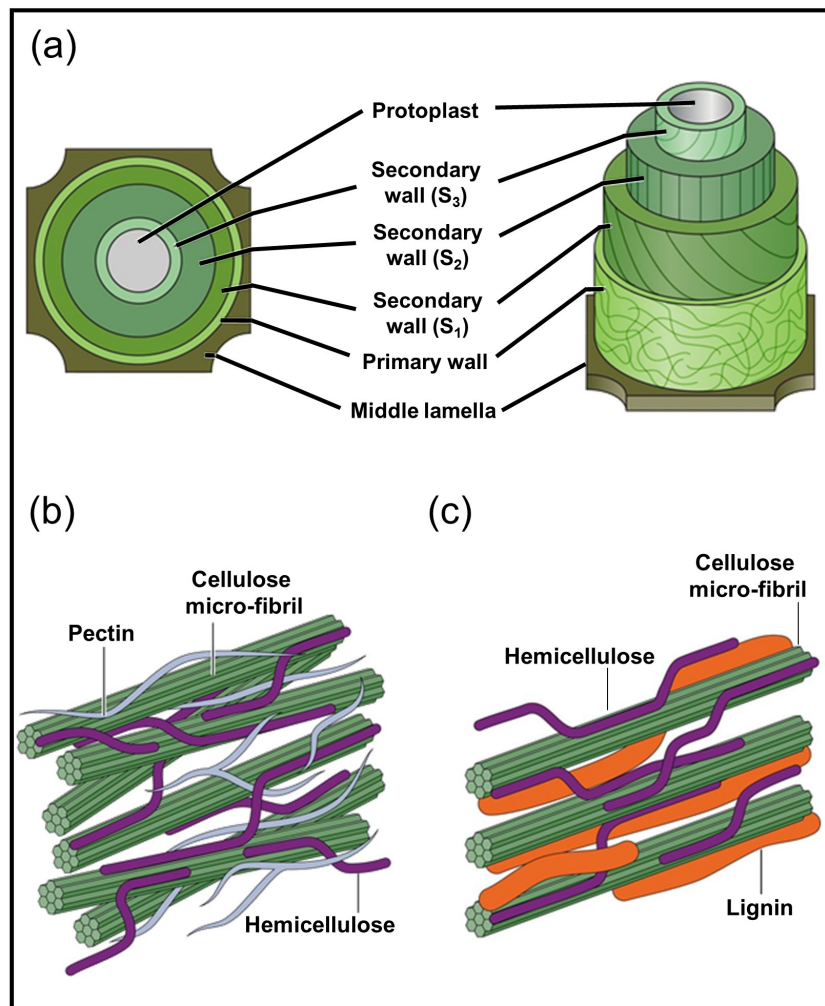


Figure 2.2: (a) Structures of the plant cell wall; (b) micro-fibrils conformation in a primary wall and (c) in a secondary wall. Adapted from: [RYTIOJA *et al.*, 2014](#).

accomplished with the absence of a secondary cell wall. As a counter example, Sclerenchyma tissues are responsible for support and protection, thus requiring the mechanical strength provided by a lignified secondary cell wall.

2.2.1.2 Sugarcane and sugar beet: an anatomical comparison.

So far, the tissues properties were related with the cell wall architecture over a generalist point of view. In the following paragraphs, the above discussion is particularize to sugarcane and sugar beet. The final intention of this comparison is to explore the influence of tissues anatomy on the extraction mechanism of these two vegetables.

Sugarcane structures are presented in Figure 2.3-(a). Culm is the vegetable re-

Table 2.1: Vegetable tissues along their characteristics and functionalities.

Tissue	Cells Characteristics	Function
Cambium	Undifferentiated living cells, without secondary cell wall.	Meristematic tissue in charge of originate parallel layers of new cells.
Parenchyma	Living cells in the mature phase; usually, just the primary cell wall is present. Some plant structures can have parenchyma with secondary wall.	Activities requiring living cells, such as storage, photosynthesis and secretion. Water and solute transport among cells.
Sclerenchyma	Dead cells in the mature phase with high lignified secondary cell wall. Long cells forming fibers.	Mechanical support and resistance of mature tissues
Colenchyma	Living cells with just primary cell wall.	Mechanical support of growing organs and tissues.
Xylem	Usually dead cells in the mature phase.	Water and nutrients transport; plant support.
Phloem	Living cells in mature phase; Presence of just primary wall	Transport of metabolized components (<i>e.g.</i> , sucrose).

Adapted from: [BUONAFINA and COSGROVE, 2014](#); [SANT'ANNA *et al.*, 2013](#); [NOBEL, 2009](#); [RAVEN *et al.*, 1996](#).

gion processed in the extraction operation, since it contains the higher concentration of sucrose. A transversal cut of the internode (Figure 2.3-(b)) shows vascular bundles surrounded by parenchyma tissues. Parenchyma cells represent 70% of the sugarcane volume, being the principal tissue in charge of sucrose storage ([REIN, 1971](#)). Before the mature phase, parenchyma tissues present thin and elongated cells, with just primary cell wall. However, as the internode mature, the parenchyma cell wall becomes lignified and suberized, especially in the cells near the vascular bundles ([RAE *et al.*, 2014](#)). Although the presence of these hydrophobic components (*i.e.*, lignin and suberin) limits the water movement across the cell wall, the parenchyma cells are connected by microscopic channels called plasmodesma ([RAE *et al.*, 2014](#)). Through these channels, the cells change water and solutes such as sucrose.

Vascular bundles comprises two different types of tissues, xylem and phloem. Along with the transport duties of xylem, this tissue has also an important role in the support of sugarcane in an upright position. This mechanical support is possible due to the presence of a rigid secondary wall in the mature xylem cells ([RAE *et al.*, 2014](#)). Phloem often does not have a secondary wall in mature phase, being a living cell responsible to transport the

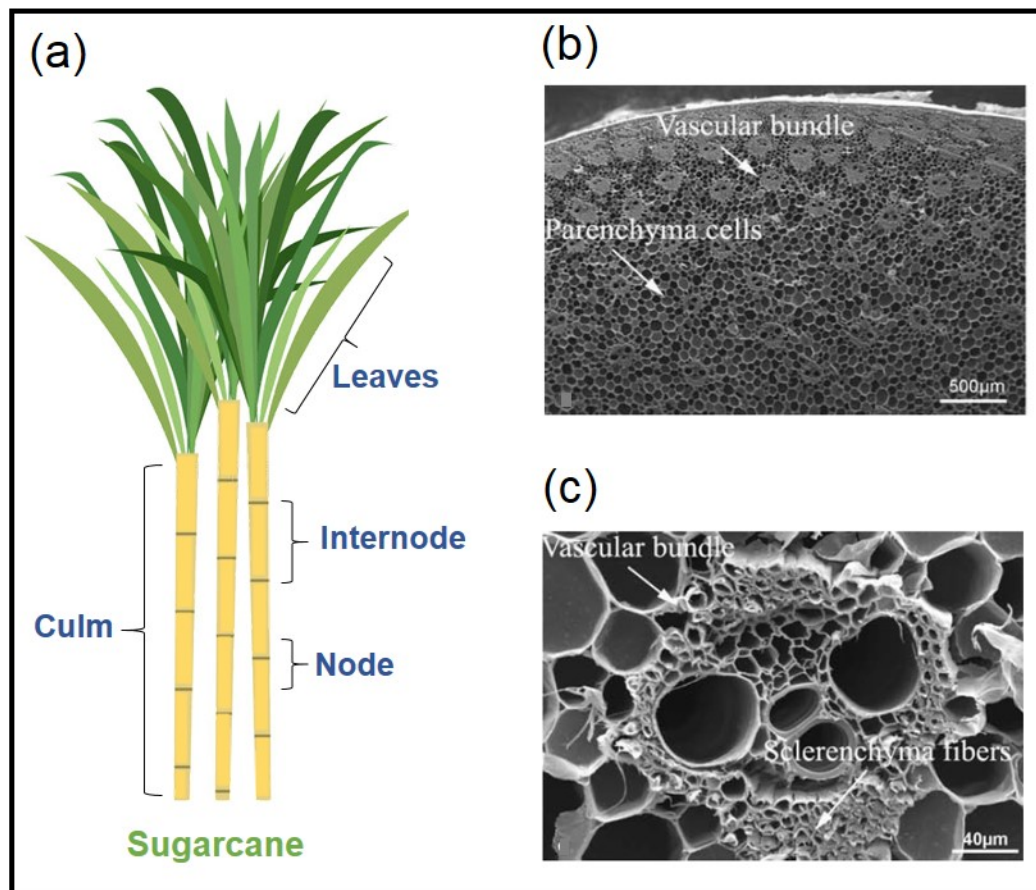


Figure 2.3: (a) Sugarcane structures. (b) Anatomical tissues present in an internode of a sugarcane culm viewed by Scanning Electron Microscopy (SEM). (c) Details of the vascular bundles surrounded by the sclerenchyma tissues, viewed by SEM. Adapted from [SANT'ANNA et al., 2013](#)

metabolized components ([RAVEN et al., 1996](#)). An important feature of the culm anatomy is the presence of sclerenchyma tissue surrounding the vascular bundles (Figure 2.3-(c)) ([SANT'ANNA et al., 2013](#)). Besides the mechanical strengthening, sclerenchyma tissue acts as a barrier, providing protection to the cells, but also blocking water transport among the tissues inside the sugarcane culm ([RAE et al., 2014](#)). It is worth to stress that the “waterproof” capacity is not a particularity of the sclerenchyma tissue, since it emerges from the secondary wall characteristics, specially the higher content of lignin ([BUONAFINA and COSGROVE, 2014](#)).

From the central region to the peripheral zone of the sugarcane culm, the size of the vascular elements decrease, but the number of bundles raise ([REIN, 1971](#)). In the central region, one to two layers of sclerenchyma cells surround larger and widely spaced vascular bundles. Otherwise, the peripheral zone presents small xylem and phloem tissues and larger

sclerenchyma sheaths, thus the vascular bundles merge to form a thick rind (RAE *et al.*, 2014). As a consequence, lignin has a higher concentration in the rind than in the central region of the culm (SANT'ANNA *et al.*, 2013). The epidermis is one of the outermost layers of the sugarcane culm. The cells in this layer secrete cutin and waxes (RAE *et al.*, 2014). These secretions give to the epidermis its barrier function against dehydration and predators attack.

The evolutionary result of the sugarcane selection, either by natural or artificial means, is a vegetable structure with the ability to store higher amounts of sucrose and to provide protection to the plant. The storage capacity is evident in the great number of parenchyma cells present in the sugarcane culm. Protection against exogenous events (*e.g.*, drought, pathogens) is accomplished by the higher recalcitrance of the culm structures. The principal character of this structural recalcitrance is the presence of tissues with highly lignified secondary cell wall (*i.e.*, sclerenchyma and xylem). Moreover, other features also play important roles in culm recalcitrance, such as the thick rind and the secretion of cutin and waxes by the epidermis. In this scenario, sugarcane is an economical valuable raw material with the capacity to provide high amounts of sucrose. However, the recalcitrance imposes a technological challenge to the extraction process.

Sugar extraction from beets is less affected by recalcitrant structures. The sugar beet structure (Figure 2.4-(a)) stores sugar in the underground root, which is an organ with unlimited capacity of growth (ELLIOTT and WESTON, 1993). This unlimited growth ability is an evidence of the lower recalcitrance issues of beet processing, since such behavior is incompatible with a highly lignified storage structure. A transversal cut of a beet root (Figure 2.4-(b)) shows a ringed structure with successive layers. This ringed pattern is also observed in a longitudinal cut of the root. Each annular layer grows simultaneously (*i.e.*, not successively) by a continuum cell production and enlargement (MILFORD, 2006). The annular layers are constituted of a narrow ring of vascular tissues followed by a broad band of parenchyma cells (Figure 2.4-(c)) (ARTSCHWAGER, 1926).

The narrow ring of vascular elements are made up of xylem and phloem bundles, separated by layers of cambium cells (ELLIOTT and WESTON, 1993). Instead of the lignified sclerenchyma tissue, the xylem bundles have collenchyma cells in their structure (ARTSCHWAGER, 1926), which is coherent with an uninterrupted growing root. The cambium is a meristematic tissue with the ability to continuously produce new parenchyma cells in a parallel arrangement (RAVEN *et al.*, 1996). Equally sugarcane, the parenchyma tissue is responsible for the sucrose storage. As new cells are produced by the cambium, the

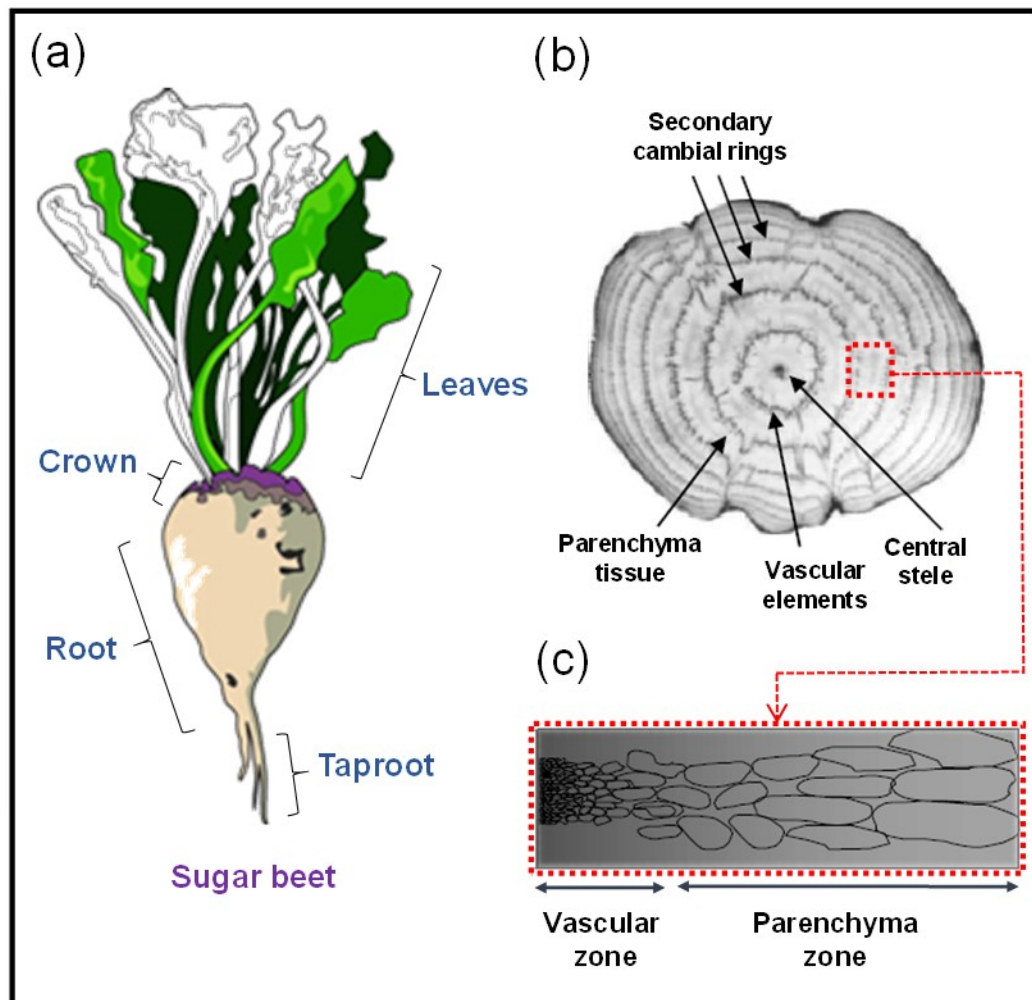


Figure 2.4: (a) Sugar beet structures. (b) A transversal cut of a sugar beet root and the tissues present in this structure. (c) A magnified view of a portion of the root (red dashed rectangle) showing the distribution of the vascular and parenchyma bands. Adapted from MILFORD, 2006

older parenchyma layers elongate (Figure 2.4-(c)), thus forming the aforementioned band of parenchyma cells (MILFORD, 2006). The end of a parenchyma band is in next ring of vascular tissues, which marks the beginning of the follow annular layer of growth. A mature beet at the harvesting period can have up to 15 concentric layers of growth (ELLIOTT and WESTON, 1993).

Sugarcane and beet have differences in the types of cells and tissues patterns in the structures with high content of sucrose. Sugarcane culm stands out as a highly recalcitrant structure, with hydrophobic lignified tissues that restrict the free access to the storage cells. Moreover, even the thin walled parenchyma cells can develop lignified structures, representing an extra obstacle to extraction. On the other hand, the lower recalcitrance of the beet root

allows a more straight access to the storage cells. During beet processing, this straight access makes possible a more intimate contact between the extraction liquid and the beet tissues. As a consequence, extraction exclusively by a diffusional mechanism is feasible, especially over a technological and practical points of view. For sugarcane, though, the lignified tissues restrict the diffusional extraction, making it a slow process and impracticable for commercial purposes.

In order to enhance extraction by the diffusional mechanism, beets undergo a preparation process in which the storage root is sliced into small strips. The slicing procedure improves the surface area for mass transfer (CLARKE and SINGH, 2017), making the contact among the beet cells and the extracting liquid better. As a thought experiment, imagine the same preparation procedure applied to sugarcane. Certainly, sugarcane prepared into slices has higher surface area for mass transfer, which would improve the diffusional extraction. However, slicing does not directly mean a reduction in the sugarcane recalcitrance. Even in small strips, sugarcane remains with many storage cells surrounded by highly lignified tissues. Therefore, a substantial amount of sucrose is still inaccessible to the extracting liquid or at least is extracted in a slow rate by diffusion. Sugarcane requires a preparation procedure that breaks the recalcitrant barriers, thus promoting a parallel extraction mechanism faster than the diffusional one.

Diffusers became a feasible unit operation to process sugarcane just with the development of a suitable preparation procedure (REIN, 2013). Instead of slicing, sugarcane culm requires a more drastic preparation than beet, commonly composed by shredders and knives. The main purpose of this drastic preparation is to break the wall of the storage cells and to surpass the barriers imposed by the recalcitrant tissues organization. A suitable preparation must break as many cell walls as possible (REIN and WOODBURN, 1974), exposing the intracellular sucrose to the exterior medium. In contact with the extracting liquid, a washing-displacement mechanism, called lixiviation, extracts the exposed sucrose from the open cells on the surfaces of the sugarcane fibers (REIN, 1971). Lixiviation extraction rate is around 50 times higher than diffusion in a moving-bed diffuser under operation (REIN, 2013). To guarantee the predominance of the lixiviation mechanism over the diffusional one is a crucial condition to make diffusers a commercially feasible operation. Indeed, around 97% of sucrose is extracted by lixiviation in an industrial scale diffuser processing sugarcane (HUGOT, 1986).

The previously comparison exercise showed that the anatomical features of the vegetables lead to differences in the extraction mechanisms. Sucrose extraction from beet

is accomplished mainly by a pure diffusional mechanism due to the absence of recalcitrant tissues. Moreover, it is probable that the slicing procedure breaks some storage cells, which implies in a lixiviation mechanism extracting a smaller fraction of the beet sucrose content. In relation to sugarcane, an opposite extraction process occurs inside a diffuser. The presence of high lignified tissues in the sugarcane culm imposes a great importance on the rupture of the storage cells. In this scenario, lixiviation acts as the principal mechanism for sucrose extraction, followed by a less pronounced diffusional process.

2.2.2 Fluid-dynamic of extraction

Another level regulating extraction is the interaction among the sugarcane fibers and the extracting liquid. Such interaction is crucial for extraction, once it promotes lixiviation and diffusion mechanisms, and controls the removal of sucrose out of the diffuser. Therefore, the following discussion will analyze the fluid dynamic level of extraction by focusing on two aspects: characteristics of liquid-solid contact and aspersion configuration in a moving-bed diffuser. Presenting the importance of liquid-solid interaction to sucrose extraction is the underlying intention of the fluid dynamic discussion.

2.2.2.1 Liquid-solid contact in sugarcane beds

Sugarcane bed is an heterogeneous structure. To a great extent, such heterogeneity is due to the fibrous nature of sugarcane. Inside a diffuser, sugarcane fibers are arranged in a complex conformation (Figure 2.5), which generates tortuous networks of void space. Such networks are surrounded by fibers with the potential to take part in the extraction process. Extracting liquid penetrates the sugarcane bed through these networks. In this sense, size and shape of such networks regulates the accessibility of extracting liquid to the fibers. Moreover, the void space promotes the connectivity between upper and bottom faces of the bed, thus defining the pathways through which the liquid moves.

Restricted or blocked accessibility to the fibers promotes a deficient contact among liquid and fibers. Sucrose extraction is partial in regions of the bed in which the access to fibers is restricted. In its turn, blocked fibers do not take part in the extraction process. In fact, extraction by either lixiviation or diffusion requires the interaction between liquid and solid phases. Therefore, deficient liquid-solid contact decreases the efficiency of extraction (POL, 1957). As a general rule, improving liquid-solid contact is essential to achieve high

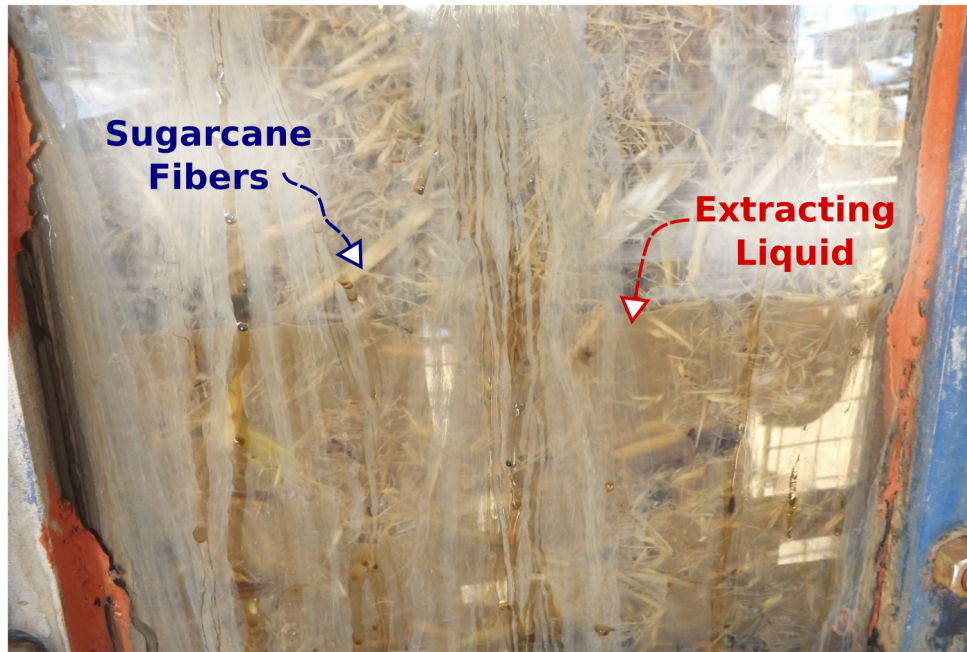


Figure 2.5: Lateral view of a sugarcane bed inside an industrial moving-bed diffuser under operation. Sugarcane fibers arranged in a complex conformation inside the bed. Extracting liquid moving through the network of void spaces formed by the fibers.

extraction levels in a moving-bed diffuser (MUNSAMY and BACHAN, 2006).

Liquid motion inside a diffuser is also important for the extraction performance. Extraction is not efficient if liquid remains motionless within the sugarcane bed. Liquid flux throughout the networks of void spaces improves the liquid-solid contact by increasing the wetting of the fibers (REIN and WOODBURN, 1974). In this sense, higher liquid fluxes promote more wetting of the fibers, thus leading to a positive impact on extraction (LIONNET *et al.*, 2005; REIN and INGHAM, 1992; LOVE and REIN, 1980). Moreover, liquid renewal in the bed is another contribution of the liquid motion, once it increases the extraction rate by improving the concentration difference among liquid and fibers. Last but not least, liquid motion is necessary to guarantee the drainage of the liquid out of the diffuser. With a poor drainage, extracting liquid is not recovered efficiently after the extraction process. An efficient drainage is a consequence of the connectivity of the networks of void space, which defines the permeability of bed to the extracting liquid.

From the exposed in the previous three paragraphs, quality of extraction is dependent on the liquid pattern inside a sugarcane bed (REIN, 1971). Liquid flux throughout the network of void spaces and conformation/shapes of the fibers in the bed change such liquid

pattern. These two effects regulates the interaction among liquid and fibers, which defines the liquid distribution within the bed. During operation, liquid distribution in a sugarcane bed may be divided into dynamic and static hold-ups (LOVE and REIN, 1980; REIN and WOODBURN, 1974). Dynamic hold-up represents the amount of liquid that moves inside the bed. Ceasing liquid aspersion, dynamic liquid drains freely out of the sugarcane bed. On the other hand, static hold-up is the amount of liquid trapped by the fibers, thus forming pockets of stagnant liquid. Static liquid remains in the bed and does not drain freely out of the sugarcane fibers.

For the sake of illustration, Figure 2.6 presents the liquid distribution inside a simplified representation of a sugarcane bed. Liquid penetrates this bed with downward flux and occupies the network of void spaces. Inside the bed, liquid pattern forms tree distinct regions. In the “motion region”, liquid flows freely through an interconnected network of void spaces. The amount of liquid flowing in this region is the dynamic hold-up. Frequently, liquid moving in the bed may enters into a dead-end branch of the network. Such branches form a “stagnant region” in which liquid remains motionless inside it. The amount of liquid trapped in a “stagnant region” represents the static liquid hold-up in the bed. Lastly, “isolated regions” accounts for void spaces in which fibers are not in contact with the liquid. Such regions may be either separated from the network of voids or not accessed by the flowing liquid (isolated regions I¹ and I² in Figure 2.6, respectively).

Lixiviation is directly related with the motion regions of the sugarcane bed (*i.e.*, dynamic hold-up). As a consequence of the liquid motion (red arrows in Figure 2.6), such mechanism extracts the exposed cellular content from the fibers surface by a piston-like washing-displacement process (LOUBSER and BARKER, 2011; PAYNE, 1969). Moreover, the rate in which liquid pass through the fibers has a directly proportional relation with the magnitude of the lixiviation extraction (REIN and INGHAM, 1992). Therefore, lixiviation mechanism requires liquid movement to perform the extraction process. Absence of liquid motion (*i.e.*, static hold-up) restricts lixiviation extraction in the stagnant regions. Inside such regions, extraction is accomplish by the diffusion mechanism (green arrows in Figure 2.6). Diffusion extracts sucrose either from the intact cells or from exposed cellular content trapped by the fibers. Provided that continuity of the trapped liquid with the movement region is preserved, sucrose extracted in the stagnant region may be transferred to the flowing liquid also through a diffusion mechanism (REIN and WOODBURN, 1974).

Sugarcane processing via moving-bed diffusers requires the predominance of the lixiviation extraction over the diffusion mechanism. Therefore, along with high amounts of

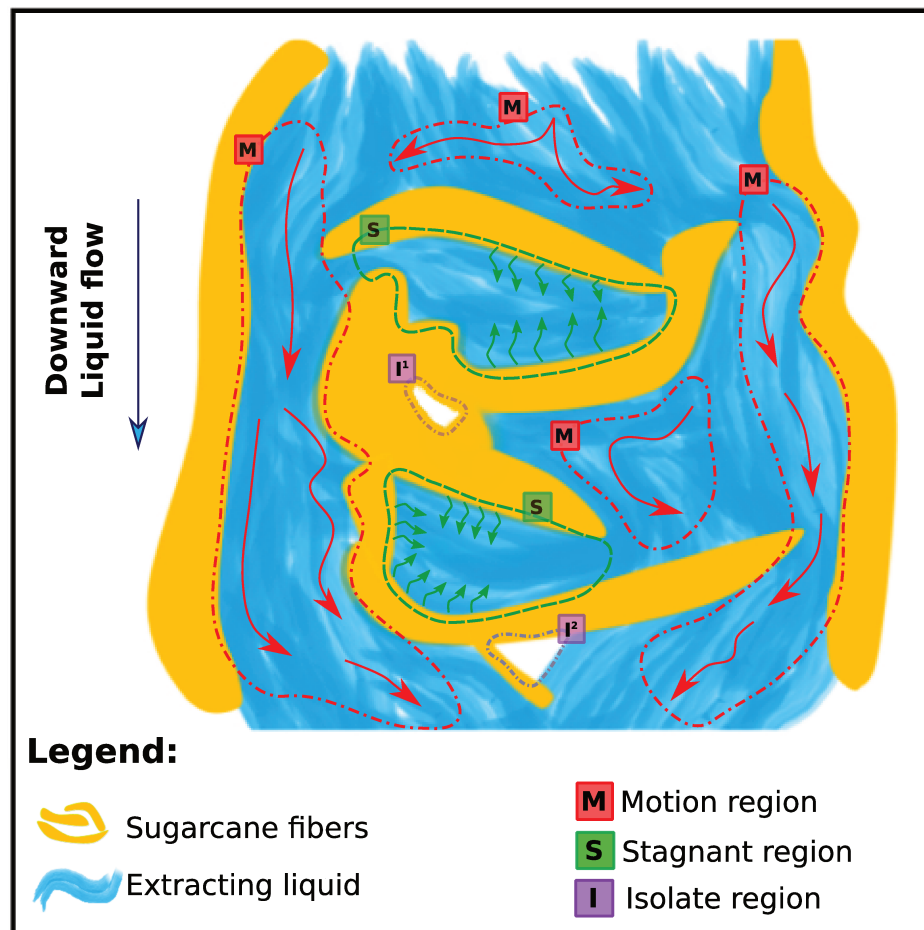


Figure 2.6: Liquid distribution inside a simplified representation of a sugarcane bed. Liquid pattern in the bed divided into three zones: motion, stagnant, and isolated regions. Region I^1 is a separated region from the network of voids; I^2 is a zone not accessed by the flowing liquid.

broken cells, feasible extraction processes need motion regions as extensive as possible in the sugarcane bed (REIN, 1971). Such requirement is fulfilled by manipulating the liquid pattern inside the bed in order to diminish the extent of stagnant and isolated regions. As aforementioned, such manipulation may be accomplished by changing either the liquid flux in the network of voids or the conformation and shapes of the fibers in the sugarcane bed.

2.2.2.2 Aspersation configuration

The driving force for extraction is the sucrose concentration difference between liquid and solid. A counter-current arrangement between these two phases fosters extraction, once it promotes higher concentration differences than a co-current interaction (POL, 1957). Aspersation positions and the stage-based configuration of a diffuser are responsible to guar-

antee the counter-current operation during the extraction process. Moreover, the stage-base configuration requires that liquid flowing in the bed (*i.e.*, dynamic hold-up) leaves it on the right stages (PAYNE, 1969). For instance, liquid from stage $N + 1$ must be sprinkled over the bed in a position that guarantees its collection in stage N , thus preserving the counter-current arrangement in the equipment. Deviations of this arrangement may decrease the sucrose gradient along the equipment, which promotes negative impacts on extraction levels.

Aspersion positions and bed movement affect the liquid motion in relation to the stages of the diffuser. Understanding such influence in the liquid motion is important either to seek or to maintain a pure counter-current liquid-solid interaction. In a motionless bed (Figure 2.7-(a)), liquid moves in relation to the stages (*i.e.*, a static referential) only with a vertical downward velocity, so called from now on percolating velocity V_p . In this case, aspersion may be placed right above the target stage, once the liquid does not deviate horizontally from the desired destination. On the other hand, liquid percolating a moving bed has an horizontal component in its velocity (Figure 2.7-(b)). In relation to the stages, liquid presents a diagonal resultant V_r velocity made up for V_p and the bed velocity V_b . Therefore, aspersion position must be placed before the target stage in order to guarantee that the sprinkled liquid leaves the bed in the right position.

Provided that the aspersion positions are fixed, two deviations of the counter-current arrangement may occur in a diffuser under operation: Recirculation and by-passing (REIN and INGHAM, 1992). Recirculation happens when the liquid leaves the bed after the right position (stage N), thus returning to the previous stage (Figure 2.7-(c)). As a consequence of the recirculation, the amount of liquid sprinkled over a stage N increases, which may lead to liquid flooding. In turn, by-passing is a condition in which liquid leaves the bed before the target stage (Figure 2.7-(d)). The amount of liquid sprinkled over the target stage N decreases under by-passing conditions, which leads to an inefficient contact among liquid and fibers (REIN and INGHAM, 1992).

The ideal aspersion point is the one that maintain a pure counter-current arrangement among liquid and fibers (PAYNE, 1969). In other words, the ideal aspersion point prevents the occurrence of recirculation and by-pass. It is important to highlight that the right aspersion point is not fixed, but changes as function of V_p and V_b . Therefore, adjustments in the aspersion positions are necessary when V_p and V_b variate, which happens in face of changes in the feedstock properties or in the operational conditions. Due to the heterogeneity of the fibers conformation and changes in the bed characteristics along the equipment (*e.g.*, bed hight, porosity), V_p may have different values in distinct positions of the bed. As

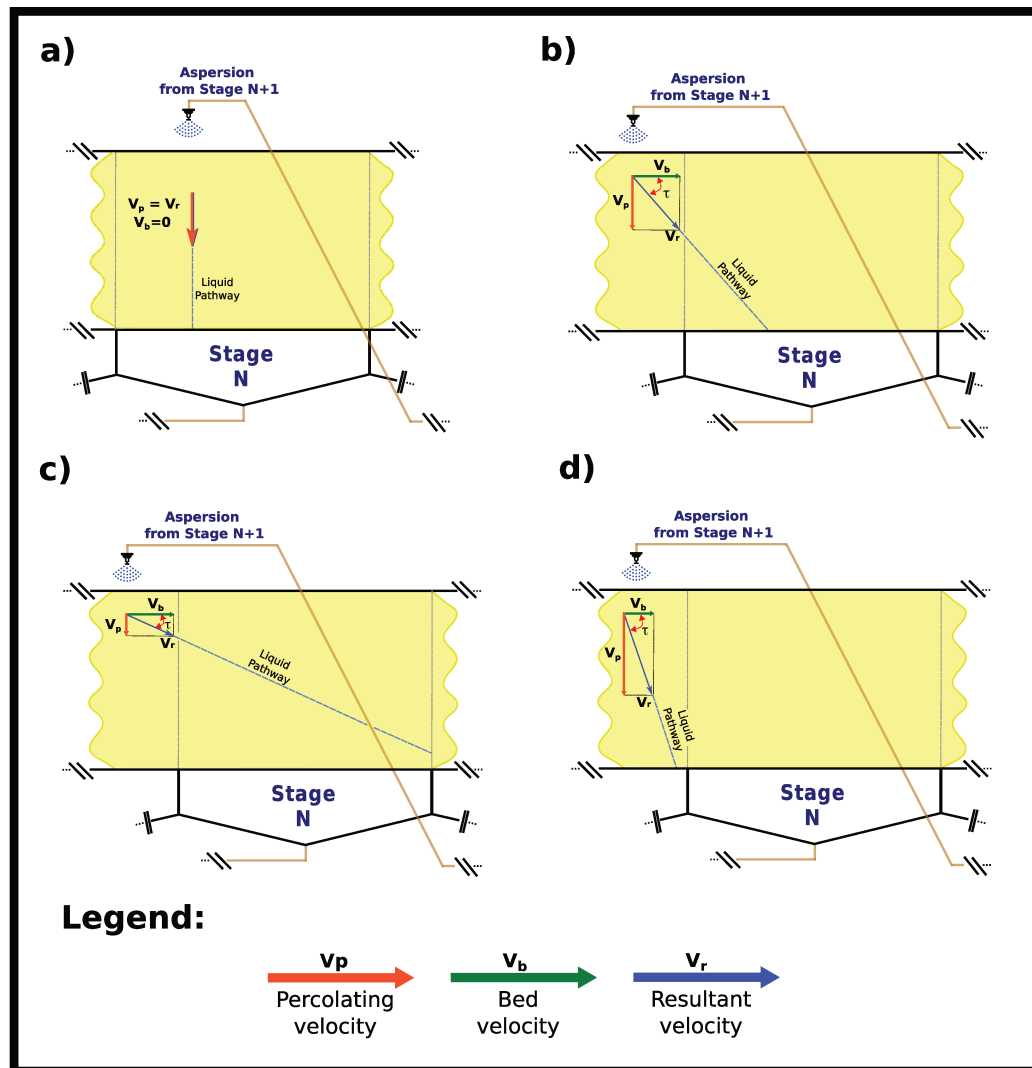


Figure 2.7: Liquid velocity in a sugarcane bed in relation to stage N of a diffuser. (a) Liquid percolating a motionless bed. (b) A moving bed with liquid moving to the target stage. (c) Deviations from the counter-current arrangement due to recirculation and (d) by-passing.

a result, the ideal aspersor points must be defined individually in order to respect the local characteristics of the bed in the vicinity of the stages. Changes in bed velocity acts equally in the whole sugarcane bed, thus shifting the ideal aspersor positions in the same direction and magnitude.

Recirculation and by-passing may be used judiciously to control the retention time of liquid inside the bed and to solve some operational problems, such as flooding and few liquid content in a stage. The discussion about the retention time will be performed elsewhere (see section 2.3). Flooding is the most serious problem that may occur during the operation of a moving bed diffuser (LOVE and REIN, 1980). Such condition happens when the

quantity of liquid sprinkled over the bed exceeds the amount of liquid that is able to percolate downward through the sugarcane fibers. As a consequence, liquid starts to build up at the top of the bed (Figure 2.8). Flooding occurrence causes a decrease in the extraction levels, as the counter-current arrangement is destroyed (LIONNET *et al.*, 2005; LOVE and REIN, 1980). By-passing may be used to stop a flooding condition, once it reduces the amount of liquid in a given stage. In turn, few liquid content in a stage leads to a poor liquid-solid contact. It is possible to solve this problem by promoting recirculation in the stage, which leads to an increase in the amount of liquid in this very stage.

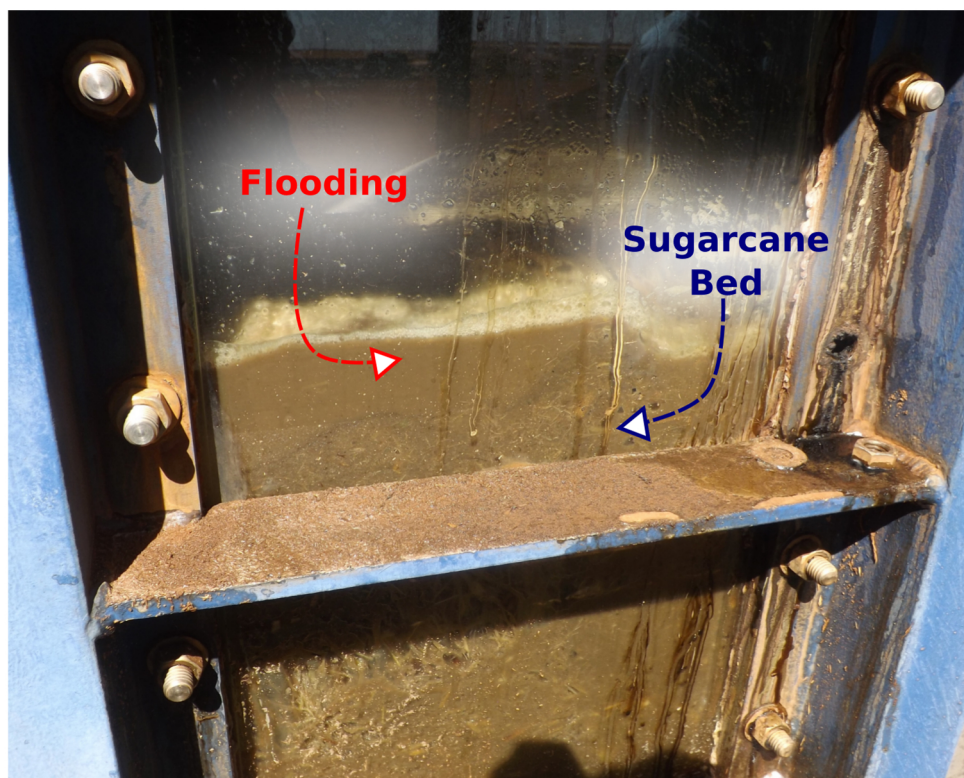


Figure 2.8: Lateral view of moving-bed diffuser under operation. Liquid building up at the top of the sugarcane due to the occurrence of flooding.

2.2.3 Concluding remarks about Extraction

It is not possible to describe sucrose extraction via moving-bed diffusers as a single process, self contained in its mechanisms and not influenced by external process or systems. On the contrary, extraction is a phenomenon which may be divided into sub-processes, all of them interacting with each other in order to promote sucrose removal from the sugarcane bed. The quality of the extraction process is a result of the quality of each

sub-process individually. Therefore, if one of these sub-process fails for any reason, extraction level decreases. Figure 2.9 summarizes the interaction of the sub-processes described along section 2.2 (dashed lines in this very figure).

Two processes performed in the cellular level of extraction should be highlighted: rupture of the cell wall and the reduction of the sugarcane recalcitrance. These processes work towards the improvement of the accessibility of the extracting liquid to the sucrose inside the cells. During the extraction process, this improved accessibility leads to a faster extraction by the lixiviation mechanism and to a better liquid-solid contact. The contact among liquid and fibers is the central issue of the fluid-dynamic level. Fibers conformation define the pathways through which the liquid moves inside the bed. At last, motion of the liquid in these pathways accomplishes the interaction of the liquid with the fibers. Liquid-solid contact is essential for lixiviation and diffusion extraction mechanisms. Moreover, such contact have an important role to define the ideal aspersion positions to preserve a pure counter-current arrangement. Liquid movement also controls the drainage of the liquid out of the bed.

2.3 Operational Variables

This section presents the main operational variables of a moving-bed diffuser and their influence on the extraction process. The following discussion will focus on the sugarcane preparation, liquid fluxes inside the bed, retention times inside the diffuser, temperature, and pH.

2.3.1 Sugarcane preparation

Sugarcane preparation is considered the most important operational variable in the extraction process via moving-bed diffusers (REIN, 2013; REIN and INGHAM, 1992; PAYNE, 1969). As discussed in the previous section, preparation is responsible to reduce the recalcitrance of the sugarcane culm and broke as many storage cells as possible. The rupture of the cells is essential to the lixiviation extraction, which makes diffusers a feasible equipment to process sugarcane. In fact, the rupture of the cells is so important for a diffuser operation that the quality of the preparation process is defined by the amount of open cells in the prepared sugarcane. Diffusion extraction is also improved by the sugarcane preparation,

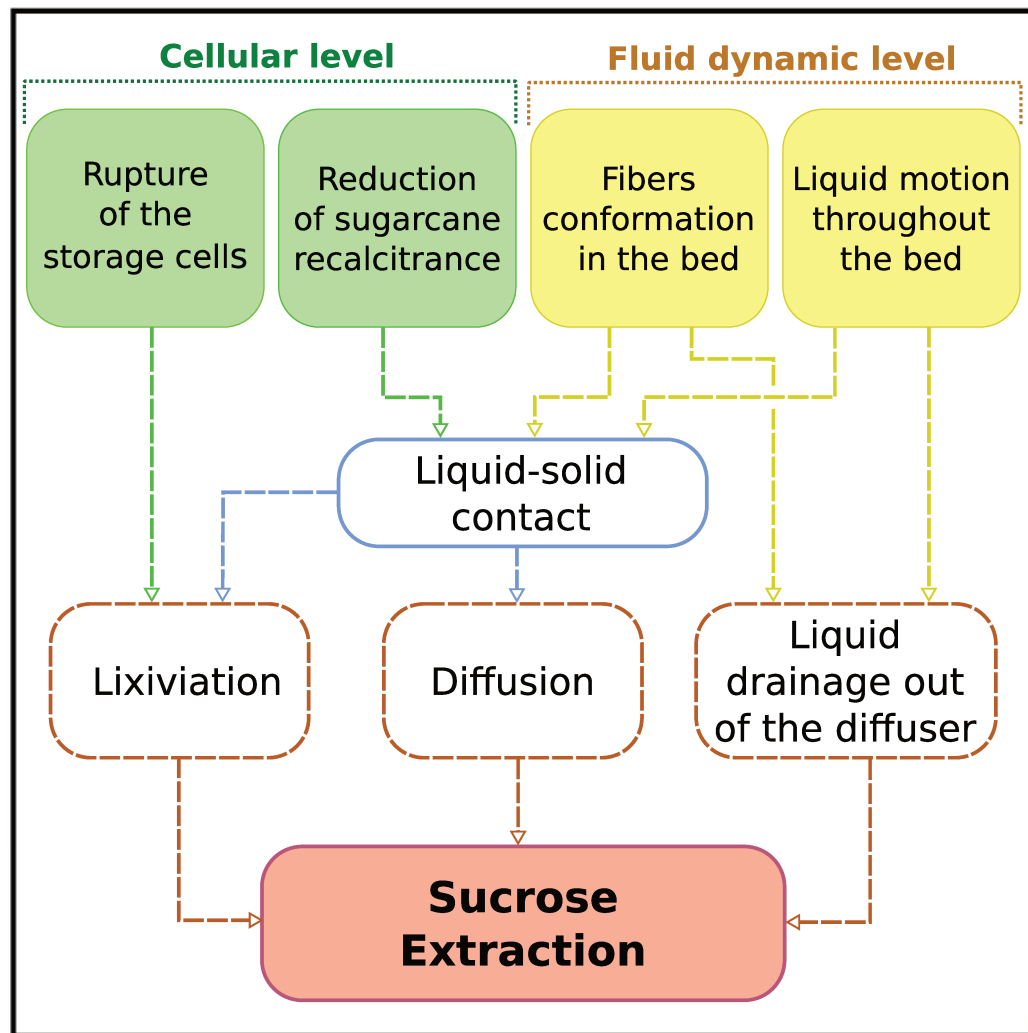


Figure 2.9: Schematic representation of the sub-processes present in the sucrose extraction via moving-bed diffusers.

once such process shorten the path through which sucrose has to diffuse (DELAVIER and SHOKRANI, 1974; REIN, 1971; POL, 1957). As a consequence of the previous facts, preparation process has the potential to impact positively the extraction process occurring inside diffusers (BRUNICHE-OLSEN and BUNDGAARD, 1971; PAYNE, 1969).

The preparation process is frequently performed by knives and shredders (REIN, 2013; KENT and LEWINSKI, 2007). Knives are used to cut the culm into small pieces and shredders act toward the exposition and separation of the sugarcane fibers. In order to achieve high extraction levels in a moving-bed diffuser, it is necessary a preparation process that leads to at least 92% of open cells in the prepared sugarcane (REIN, 2013; RIVIERE, 1989). Therefore, a finer preparation is beneficial for sucrose removal from the interior of

the cells. In relation to a fluid-dynamic perspective, however, a finer preparation (*i.e.*, short and small fibers) leads to a compact bed in which the mobility of the liquid is reduced (LOUBSER and BARKER, 2011). With a poor mobility of the liquid, liquid-solid contact is not accomplished efficiently, thus preventing the access of the extracting liquid to the sucrose content of sugarcane. Moreover, a finer preparation generates a bed more prone to flooding conditions (REIN and WOODBURN, 1974).

Both extraction and fluid-dynamic issues must be taken into account during the preparation process. Knives and shredders, or wherever specific equipment used in the preparation step, have to be set to guarantee the maximum rupture of the cells and to promote a permeable bed. The preparation process must preserve the fibers intact and evident in order to generate a permeable bed (LOVE and REIN, 1980). It may be accomplished by breaking as many stored cells as possible, but keeping intact the vascular bundles, especially the lignified cells in the xylem tissue. As a consequence, a prepared cane with evident fibers leads to a more stable bed, which is less affected by compaction problems (REIN, 2013).

Compaction of the sugarcane bed may be characterized by the fiber packing density (*FPD*). *FPD* may be interpreted as the bulk density of the sugarcane fibers inside the diffuser. The fiber content of the raw material (*i.e.*, sugarcane) as well as the dimensions of the fibers after the preparation step impact *FPD*. Fiber content and *FPD* have a directly proportional relation (LOVE and REIN, 1980). Fiber dimension after preparation may be characterized by their mean particle size. A finer preparation (*i.e.*, lower mean particle sizes) leads to higher packing densities (REIN and INGHAM, 1992), which means more compact beds during operation. In this sense, *FPD* holds an inversely proportional relation with the mean particle size (LOVE and REIN, 1980). Moreover, a wide mean particle distribution promotes a higher *FPD* value (REIN (2013), REIN (2013)).

2.3.2 Percolating velocity

In the previous discussion about the fluid-dynamic level of extraction, it was presented the importance of the liquid motion to the extraction process. Liquid moving through the fibers promotes the necessary liquid-solid contact that enables the removal of sucrose from the sugarcane. Moreover, high fluxes of liquid in the bed improve the extraction rate by fostering the lixiviation mechanism (REIN and INGHAM, 1992) and by reducing the extent of the stagnant and isolated regions. Therefore, a desired operation condition is the one that promotes the highest liquid velocity as possible through the fibers and prevents

the occurrence of flooding conditions (LOVE and REIN, 1980). In fact, percolating velocity inside the bed is considered the second most important variable to the operation of moving-bed diffusers, behind only the preparation process (REIN, 2013; LIONNET *et al.*, 2005). Percolating velocity in a diffuser is determined by the aspersion characteristics and by the properties of the sugarcane bed during the operation process (PAYNE, 1969).

Concerning the aspersion characteristics, modifying the aspersion rate of liquid and the aspersion positions are the most common approaches to control the percolating velocity. The rate in which liquid is sprinkled over the bed in each aspersion point has a directly proportional relation with the velocity achieved by the liquid inside the network of void spaces formed by the sugarcane fibers. Among the aspersion points, the imbibition rate is considered the control variable that impacts more the extraction performance during the operation of a diffuser (MUNSAMY and BACHAN, 2006). Along with the raising of the percolating velocity, increasing the imbibition rate also leads to higher sucrose gradients inside the bed, thus fostering the extraction rate (REIN, 2013). However, increasing the imbibition rate is not a limitless procedure, once it may increase the energy consumption of the mill (RIVIERE, 1989) and promote flooding conditions. As aforementioned, the aspersion rate may also be controlled by changing the aspersion positions and judiciously promoting recirculation and by-passing.

Shape, size and conformation of the fibers in the bed controls the influence of the bed properties in the percolating velocities. These three aspects of the bed properties determine the permeability of the bed to the flowing liquid. In a more permeable bed, liquid may achieve a higher percolating velocity and flooding conditions is less prone to happen (LOUBSER and BARKER, 2011). Shape and size of the fibers is a result of the preparation process, in which a finer preparation leads to less permeable beds. Fibers conformation is directly related with the packing density of the fibers, which defines, in the limit, the compaction of the system and the morphology of the network of void spaces. Low packing density promotes higher percolating velocities (MUNSAMY and BACHAN, 2006; LIONNET *et al.*, 2005; LOVE and REIN, 1980). Another aspect controlling the permeability of the bed is the presence of elements that block the void spaces, such as impurities (PAYNE, 1969) and sugarcane fines.

The percolating velocity presents different values in distinct positions of the bed. Moreover, such velocity distribution changes during the extraction process due to the deformable nature of the fibrous bed. Liquid aspersion over the bed compacts the fibers, thus reducing the percolating velocity along the length of the equipment (LOUBSER and BARKER,

2011). Percolating velocity may likewise decrease along the height of the bed, once the weight of the liquid surrounding the fibers promotes higher packing densities at the bottom of the bed. The presence of the two sets of lifting screws also promotes variations of the percolating liquid velocity.

2.3.3 Retention time and Diffuser size

Retention time is the period in which liquid and fibers remain inside a moving-bed diffuser, interacting with each other. Due to the aspersion configuration and to the bed motion, liquid and fibers have different retention times. A liquid portion stays in contact with fibers a period 1.5 to 2.0 times higher than fibers interact with the liquid content inside a diffuser (REIN, 2013). As a general rule of thumb, increasing the period in which liquid interacts with fibers has a positive impact on extraction (MUNSAMY and BACHAN, 2006). However, extending too much the retention time inside the diffuser promotes reduction of sucrose and bagasse production rate, which may decrease the overall productivity of the sugarcane mill. Therefore, the retention time has to guarantee an effective liquid-solid contact for extraction purpose and to meet the demand for sucrose and bagasse of the succeeding operations of the mill.

Fibers are conveyed along the diffuser by the motion of the bed. In this sense, bed velocity is the more straightforward approach to control the retention time of fibers inside a diffuser. Such operational variable and the retention time of the fibers hold an inversely relation. In turn, the most common and practical approaches to control the retention time of liquid manipulate either the recirculation or the by-passing of liquid inside the bed. Retention time raises if liquid is recirculated backward in the diffuser. On the other hand, by-passing liquid reduces the period in which liquid remains inside a diffuser. In this sense, bed velocity is also a possible approach to modify the retention time of the liquid (see Figure 2.7). Following the same logic, modifying the aspersion positions is another suitable approach to control the retention period of the liquid.

Retention time of the liquid may also be changed by varying the height of the sugarcane bed. Assuming a constant percolating velocity, different bed heights mean a different extension of the pathway through which liquid has to move in order to leave the bed in each aspersion-percolation cycle. Provided that the aspersion positions remain fixed, variations in the extension of such pathways represent, in the limit, distinct degrees of recirculation or by-passing of the liquid. Bed height may be controlled by varying either

the amount of prepared sugarcane fed into the diffuser (*i.e.*, sugarcane throughput), the bed velocity or the fiber packing density. Sugarcane throughput inside a diffuser and bed height have a directly proportional relation. Assuming a constant sugarcane throughput, bed velocity holds an inversely relation with the bed height (REIN, 2013). Increasing the packing density leads to shallow beds (REIN and INGHAM, 1992). Moreover, another effect of *FPD* on the retention time of the liquid is promoted by its influence on the percolating velocity, which decreases for more compact bed.

The retention time is one of the most important variables for the project of a new moving-bed diffuser. The size of a diffuser is defined by the screen area of the moving bed. Length and width of the screen are specified to achieve the required retention time and hence the desired extraction level. The relation between length and width does not affect the extraction performance, but is an important parameter to define the capital required to build a new diffuser (REIN, 2013). As aforementioned, diffusers are divided into stages to allow a counter-current interaction among liquid and fibers. Increasing the number of stages, the extraction process comes closer to a pure counter-current arrangement, thus improving the sucrose concentration difference between liquid and solid. Moreover, operating moving-bed diffusers with multiple stages is an alternative to compensates the inefficiencies of the extraction process (RIVIERE, 1989; PAYNE, 1969). However, above a given number of stages, extraction gain becomes only incremental, and does not justify the increase in the investment required to build a longer diffuser (REIN, 2013).

2.3.4 Temperature

Temperature is controlled inside a moving-bed diffuser by direct injection of vapor in some points spread along the equipment. Operating temperature of a diffuser is kept around 80-85 °C. Performing extraction at high temperatures makes the unbroken cells more permeable to sucrose, thus increasing the diffusion extraction rate (RIVIERE, 1989; HUGOT, 1986; DELAVIER and SHOKRANI, 1974). Moreover, viscosity of the extracting liquid decreases as temperature raises (REIN, 2013). A less viscous liquid has a better mobility inside the bed, which improves the liquid accessibility to the sucrose present in the fibers and, as a consequence, enhance the liquid-solid contact. As a general tendency, higher temperatures promote an increase in the extraction level (REIN, 1971).

Increasing the extraction level, however, is not the main reason to operating a diffuser at high temperatures, once this variable has a feeble influence on extraction. For

instance, REIN (1974) reports an increase of 0.2% in the extraction level for a temperature change from 75 to 80 °C. Reduction of the microbial activities, indeed, is the main reason to keep diffusers at high temperatures during the extraction process (KENT and LEWINSKI, 2007; MUNSAMY and BACHAN, 2006). Sucrose inversion promoted by several species of microorganisms is substantial in a sugarcane bed for temperatures below 70 °C (PAYNE, 1969). At the operating temperature (80-85 °C), such diversity of microorganisms is drastically reduced and only few thermophile species survive (RAVNO, 2001). Moreover, operating a diffuser at high temperature is cheaper than the use of biocides for microbial control (REIN, 2013). Therefore, temperature control is considered the most efficient way to reduce sucrose losses by microbial activities inside a diffuser (RAVNO, 2001).

2.3.5 pH

The pH of a diffuser is commonly controlled by adding lime at the front of the equipment (Figure 2.1-[9]). An old practice on diffusers operation prescribes that pH control is necessary to reduce sucrose losses by microbial activities (MUNSAMY and BACHAN, 2006; POL, 1957). However, this old prescription does not hold anymore, once recent publications argue that, within normal operational conditions, pH influence on sucrose inversion is minimal inside a diffuser (REIN, 2013; KENT and LEWINSKI, 2007; MUNSAMY and BACHAN, 2006). Such publications also agree that pH control is still necessary during the extraction process to reduce corrosion inside the diffuser.

2.3.6 Concluding remarks about the operational variables

From the exposed above, it is evident the complexity in which the operational variables influence the extraction process in a moving-bed diffuser. With the intention to summarize the information presented in the present section, it is proposed in Figure 2.10 a visual representation of the main operational variables, their interactions, and their ultimate impact on the extraction performance. The maze-like structure of this schematic representation is a visual confirmation of the complexity of this extraction operation.

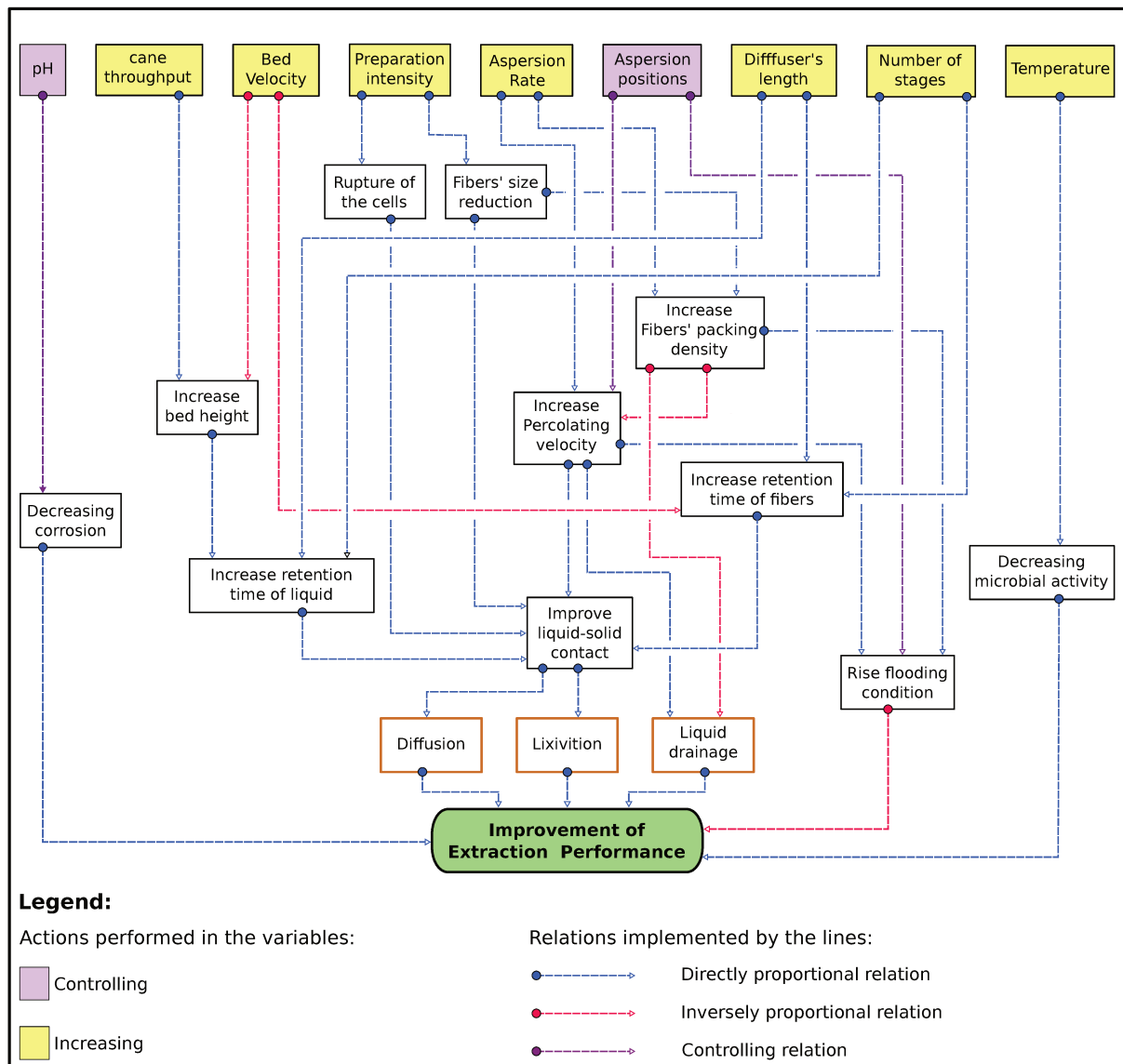


Figure 2.10: Schematic representation of the relations among the operational variables and the impacts of this relations on the extraction performance.

2.4 Mathematical modeling

Since the initial efforts to implement diffusers in the sugarcane sector, it is evident the importance of a mathematical model to describe the sucrose extraction and the fluid-dynamic in this equipment. According to REIN (1972), one of the most important seminal works of sugarcane processing via diffusers, a mathematical model is a necessary requisite for two important investigations:

1. In the design of a new diffuser installation in order to find optimum size, configuration

and operation conditions for a given sugarcane throughput and extraction level;

2. In the formulation of optimum operating policy for an existing diffuser in order to predict the extraction level as a function of the control variables.

Despite the relevance of a model to these two important investigations, the number of studies concerning mathematical modeling of diffusers is small. One possible cause for this fact is the common practice to operate diffusers following heuristic knowledges acquired in the daily routine of the mills. Such practice is evident in the large number of published studies with focus on reporting the daily routine of the extraction process via diffusers. In this section, it is going to be presented the previous studies about mathematical modeling of diffusers. The objective of such presentation is to delineate the state-of-art of the mathematical interpretation of the extraction process by diffusers.

2.4.1 Pol (1957)

The beet industry is the background to the early studies on mathematical modeling of diffusers processing sugarcane. The phenomenological interpretation of the sucrose extraction from beet were extended to sugarcane sector. Therefore, sucrose extraction from sugarcane was initially interpreted as a pure diffusional mechanism, thus being described by the Fick's fundamental law.

POL (1957) performed laboratory and pilot plant experiments in order to assess the validity of a pure diffusional mechanism to depict the sucrose extraction from sugarcane. In this sense, POL (1957) proposed a mathematical model in which extraction is performed only by a diffusion mechanism (Eq 2.1). In this equation, $d W_{sac.}$ is the weight of sucrose diffusing in the time interval dt across an area A ; D is the diffusion coefficient, T is the absolute temperature of the system, and μ is the viscosity of the extracting liquid; the spatial derivative represents the difference in concentration between liquid and fiber across a diffusion path of length dx . The validity of the pure diffusional mechanism was assessed by evaluating the ability of this model to represent the data collect in the experiments.

$$\frac{d W_{sac.}}{dt} = \frac{D \cdot T}{\mu} \cdot A \cdot \frac{d(C_{liquid} - C_{fibers})}{dx} \quad (2.1)$$

As a final result, the proposed model was not able to represent the experimental data. The main reason for such result is the omission of the lixiviation mechanism in the

mathematical model. According to POL (1957), “the equation was developed for diffusion from killed but unruptured cells”. Moreover, lixiviation extraction does not “need to obey the same equation” of the diffusion mechanism. In other words, lixiviation and diffusion are different extraction mechanism, and must be treated individually by the mathematical models.

2.4.2 Rein (1972)

REIN (1972) is one of the most important studies concerning diffusers in the sugarcane sector. In this study, it was performed an extensive investigation about the phenomenology of the sucrose extraction from sugarcane. As a result, REIN (1972) established the now widely accepted extraction mechanism for sugarcane processing in diffusers, (SCHRODER *et al.*, 2007), which is, as aforementioned, lixiviation in parallel with diffusion. Figure 2.11 presents a scheme of the phenomenological interpretation of the extraction process proposed by REIN (1972). In this interpretation, the sugarcane bed is divided into a region occupied by the fibers and a region in which the percolating liquid flows. Fiber in their turn are separated into two fractions, one in which sucrose is extracted by lixiviation and other that extraction happens by means of diffusion. Such separation of the fibers is performed by the parameter α , which is the fraction of sucrose in the fibers extracted by the lixiviation mechanism. Unlike POL (1957), REIN (1972) considered two different mass transfer rates to account for the extraction by lixiviation, K_1 , and diffusion, K_2 .

The proposed phenomenological abstraction was formalized in a mathematical model (Eqs 2.2 to 2.4). Liquid motion is describe by a plug-flow model, in which L stands for the liquid mass flow rate. C_j is the sucrose concentration in the percolating liquid; Sucrose concentration in the fractions of fibers is accounted for C_{b1} , for lixiviation extraction, and C_{b2} , for diffusion extraction. H is the total liquid hold-up of the bed (*i.e.*, dynamic plus static), h_d is the dynamic hold-up and ρ is the density of the extracting liquid. The underling intention of REIN (1972) is to assess the validity of the proposed extraction mechanism by testing the ability of the model to describe the experimental data collected in a pilot column diffuser processing bagasse. As a conclusion of this study, the model was able to describe satisfactorily the experimental data, thus legitimating the proposed extraction mechanism. According to REIN (1972), the mathematical model “can be used to provide a valid description of the extraction behavior” in diffuser. At the end of this study and in a paper released two years later (REIN, 1974), Rein satisfactory applied his model to assess the extraction in a full-scale

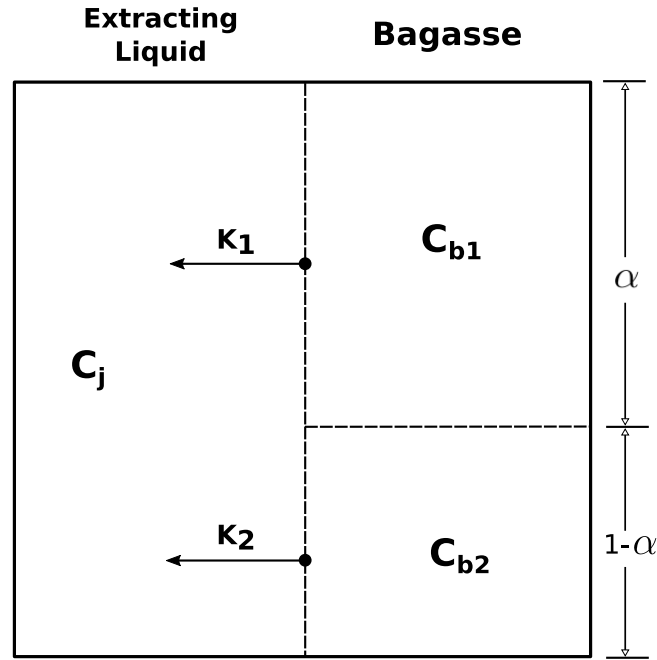


Figure 2.11: Schematic representation of the extraction model proposed by [REIN \(1972\)](#). Adapted from [REIN, 1972](#)

moving-bed diffuser.

$$-L \frac{\partial C_j}{\partial z} + K_1 (C_{b1} - C_j) + K_2 (C_{b2} - C_j) = \rho h_d \frac{\partial C_j}{\partial t} \quad (2.2)$$

$$-\alpha H \frac{\partial C_{b1}}{\partial t} = K_1 (C_{b1} - C_j) \quad (2.3)$$

$$-(1 - \alpha) H \frac{\partial C_{b2}}{\partial t} = K_2 (C_{b2} - C_j) \quad (2.4)$$

2.4.3 Love and Rein (1980)

[LOVE and REIN \(1980\)](#) investigated the percolation behavior in a sugarcane bed. This study assessed the influence of some important operational variables (*e.g.*, preparation intensity, temperature, fibers packing density) in the percolating velocity achieved by the liquid inside the bed of a pilot column diffuser. The majority of the results of such assessment were already presented in the section 2.3. [LOVE and REIN \(1980\)](#) also performed tracer tests to evaluate the liquid dispersion inside a sugarcane bed for both pilot and full-scale diffusers.

The flow pattern in the pilot diffuser were represented by a plug-flow model coupled with axial dispersion (Eq 2.5). Ω_z is the dispersion coefficient in the vertical direction and C is the concentration of the tracer used in the tests. This model represents the tracer data better than a model without the dispersion effect, such as the plug-flow model proposed by REIN (1972).

$$\Omega_z \frac{\partial^2 C}{\partial z^2} - V_p \frac{\partial C}{\partial z} = \frac{\partial C}{\partial t} \quad (2.5)$$

In relation to the full-scale moving-bed diffuser, it was included in the model a lateral dispersion (Eq 2.6), which is accounted for by the horizontal dispersion coefficient Ω_x . The proposed model was able to represent satisfactorily the tracer tests performed in a diffuser with 13 stages. From the results of the tracer tests, the authors concluded that dispersion effects in a sugarcane are high. Indeed, according to LOVE and REIN (1980), these tests “indicate that the degree of dispersion occurring (in a diffuser) was very larger than that found in beds of more conventional packing materials”.

$$\Omega_x \frac{\partial^2 C}{\partial x^2} + \Omega_z \frac{\partial^2 C}{\partial z^2} - V_p \frac{\partial C}{\partial z} = \frac{\partial C}{\partial t} \quad (2.6)$$

2.4.4 Rodriguez (1990)

In his PhD thesis, RODRIGUEZ (1990) projected a continuous diffuser to be used in mini sugarcane mills. In order to understand the sucrose extraction via diffusers, the author performed several batch extraction experiments. Classical mathematical models of solid-liquid extraction were used to analyzed the data collected in those batch experiments. Among the assessed models, the one that achieved better results is the Fick’s second law. RODRIGUEZ (1990) fitted the parameter of this law in two distinct periods of the extraction processes. Therefore, the whole extraction process was characterized by two fitted parameters: one describing a faster extraction rate at the beginning of the process, and the other depicting a slower rate at the end of the sucrose withdraw from sugarcane.

By applying the Fick’s second law separately to each step of the extraction, RODRIGUEZ (1990) acknowledged the sucrose extraction from sugarcane as constituted by two distinct mechanism. The first mechanism accounts for the extraction of sucrose from the open, broken cells. The second mechanism is the slowest one, which represents the extraction from unbroken cells. Such dual-mechanism is in accordance with the extraction phenomenology

proposed by REIN (1972). Also in RODRIGUEZ (1990), extraction charts were used to assess the continuous extraction.

2.4.5 Picaro and White (1993)

In this study, PICARO and WHITE (1993) proposed a model to evaluate the height of a liquid inside a column filled with sugarcane fibers. The authors included this study beneath the scope of what they called “fluid mechanics of part-flooded beds”. Figure 2.12 presents a part-flooded column as it is interpreted by PICARO and WHITE (1993). This column presents two distinct regions, distinguished by the saturation of the medium. The upper zone is called by the authors as the “percolating-flow” region, in which the column is only partially saturated with liquid. The lower zone is the “saturated flow” region, composed by the flooded fraction of the column. The support is a perforate plate placed at the bottom of the column to sustain the sugarcane fibers. The terms H and h in Figure 2.12 are the heights of the column and the saturated flow region, respectively.

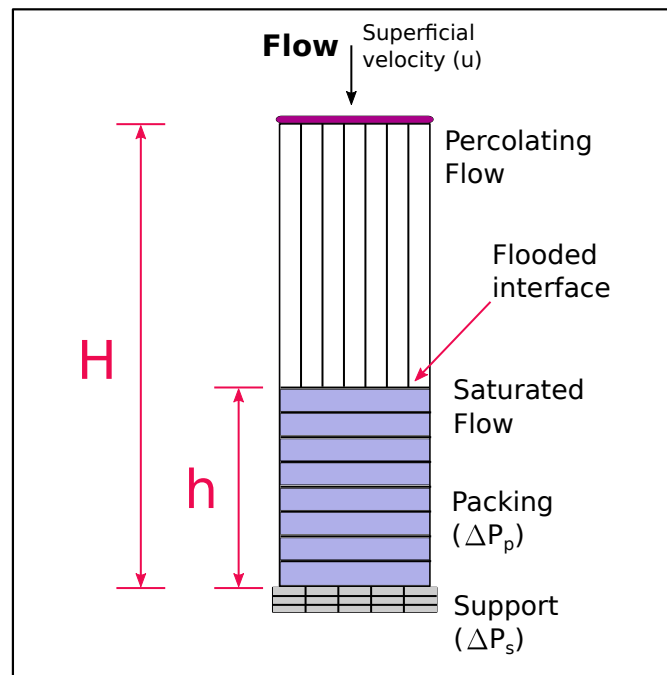


Figure 2.12: Schematic representation of a part-flooded bed. Adapted from PICARO and WHITE, 1993

The height of liquid inside the column was modeled by addressing to the fact that “the total pressure drop (in the column) must equal the hydrostatic-head of liquid” in the flooded zone (PICARO and WHITE, 1993). Putting the previous sentence into mathematical

terms leads to Eq 2.7. In this equation, ρ is the density of the liquid within the column. The right-hand terms of Eq 2.7 are the pressure drops promoted, respectively, by the packing of fibers and the support.

$$\rho gh = \Delta P_p + \Delta P_s \quad (2.7)$$

The authors computed the pressure drops by using the Forchheimer equation (Eqs 2.8 and 2.9). At the right-hand side of these equations, the first terms are the viscous contribution to pressure drop. Such viscous contribution has a conceptual congruence with Darcy's law. In its turn, the second terms account for the inertial influence on the pressure drop. The viscosity of the liquid is represented in these equations by μ . The elements a_1 and a_2 are constants characterizing the properties of a given medium. Addressing the congruence between the viscous element of Eq 2.8 and Darcy's law, the constant a_1 is the inverse of the permeability of the medium. The constants b_1 and b_2 summarize in their values the characteristics of the support plate (*e.g.*, geometry, void fraction).

$$\frac{\Delta P_p}{h} = a_1 \cdot \mu \cdot u + a_2 \cdot \rho \cdot u^2 \quad (2.8)$$

$$\frac{\Delta P_s}{h} = b_1 \cdot \mu \cdot u + b_2 \cdot \rho \cdot u^2 \quad (2.9)$$

PICARO and WHITE (1993) assessed the ability of Eqs 2.7 to 2.9 to describe data collected in an experimental column filled with sugarcane fibers. This assessment shows that the “the support plays a major role in the onset of the part-flooded bed and may greatly restrict the flow capacity of the bed”. The proposed model satisfactorily describes the experimental data only under operational conditions that minimize the amount of trapped air. Indeed, concerning operations with substantial amount of trapped air, this model presents a poor correlation with the collected data. In order to solve this correlation issue, the authors proposed empirical expressions “to account for the increased packing flow resistance as a result of entrapped air”. By coupling this empirical expressions with the previous equations, the model improves its ability to described the experimental data.

In another paper (PICARO *et al.*, 1994), the authors applied this model to a full-scale diffuser. As a result, the model along with the proposed empirical expressions are “consistent” with the data acquired in a real equipment.

2.4.6 Concluding remarks about Mathematical modeling

The previous works were fundamental to set the bases in which the present understanding of the extraction phenomenology via diffusers lays on. Unfortunately, there is a lack of recent works on phenomenological description of the extraction process using diffusers. Nowadays, many of the performed mathematical analyses have got concerned only with the overall mass balance along the whole equipment, thus treating the extraction process within a diffuser as “black-box” operation. In this scenario, it is gainful to restart the studies in the mathematical modeling of diffusers, since the evolution on computer processing allows for more detailed assessments of the extraction properties. Moreover, the new efforts on this modeling area should provide a formal mathematical base to the description of sucrose extraction from sugarcane beds. Bearing all of these in mind, the next chapter presents the mathematical formulation of the extraction process via diffuser developed in the present thesis.

Chapter 3

Mathematical formulation

In the this chapter, it is going to be presented the train of thoughts that led this study up to the current version of the model describing the sugar extraction in a diffuser. The literature sources that set the theoretical bases for the model concern traditional text books of transport phenomena in porous medium (e.g., [BEAR and BUCHLIN, 1987](#); [BEAR and BACHMAT, 1991](#)) and computational fluid-dynamics (e.g., [PATANKAR, 1980](#); [MALISKA, 2012](#)).

3.1 Phenomenological abstraction

In order to develop the mathematical representation of the extraction process, the sugarcane bed was interpreted as a fractured porous media. At a first glance, this abstraction may sound obvious. However, this interpretation is original and gives to the moving-bed diffuser model formal bases from the theories of transport phenomena in porous media. Moreover, it opens the studies of diffuser modeling to an area in constant development and with expressive volume of published work. Therefore, the theory of transport phenomena in porous medium guides the development of the proposed moving-bed diffuser model.

A fractured porous medium is a structure in which the void space can be divided into two regions, with different porosities ([BEAR and BACHMAT, 1991](#)). One of these regions is a higher-porosity network of fractures in which a fluid can move through the fibers of cane. The other one is composed by void spaces surrounded by the solid, which forms lower porosity zones disconnected among each other. A fluid penetrating those lower porosity regions is blocked by the fibers, remaining stagnated inside the porous media. In [Figure 3.1](#)

is presented a scheme of a sugarcane bed represented as a fractured media. The white regions are the void spaces, where a fluid can occupy them, and the yellow parts are the fibers in a section of a sugarcane bed. Also in this figure, it is possible to distinguish the two mentioned void regions and their differences in the porosity.

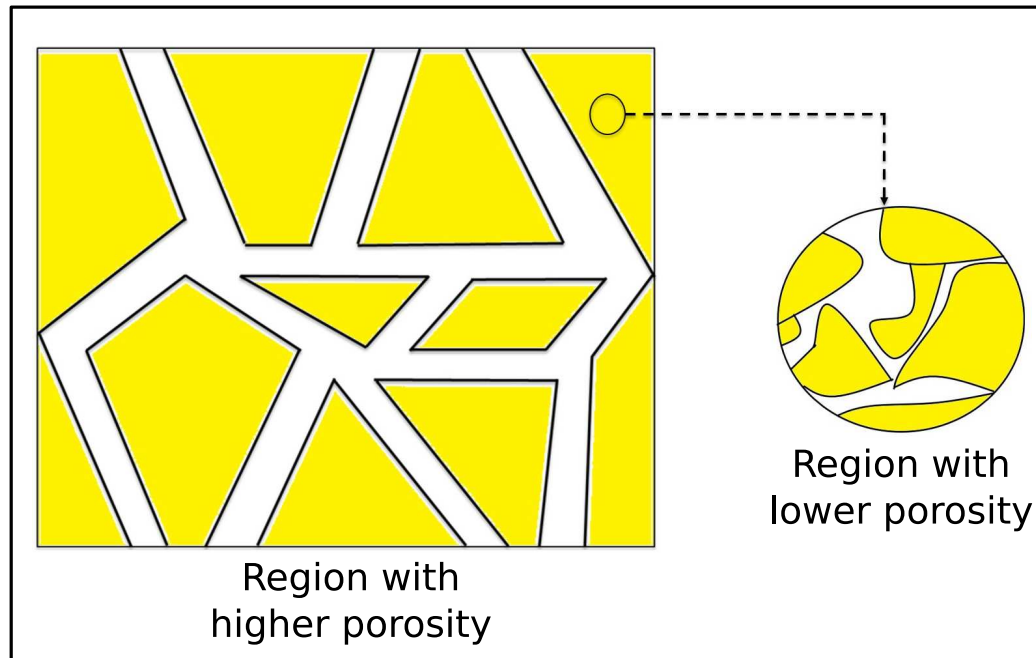


Figure 3.1: A section of a sugarcane bed represented as a fractured porous media. White and yellow regions represent, respectively, the void space and the sugarcane fibers.

Differences in mobility between the two void regions allow for the relation of extraction mechanisms with the liquid hydrodynamics inside a diffuser. It is assumed that lixiviation extraction takes place only in high-porosity zones (*i.e.*, fractures), promoted by a non-zero velocity of the percolating liquid in relation to fibers. It is worth to highlight the difference between a convective transport and lixiviation extraction. A convective transport takes place only in one phase while lixiviation extraction is a consequence of the interaction between the liquid and solid phases. In its turn, it is considered that diffusive extraction is performed exclusively in lower porosity regions, in which the trapped stagnant liquid remains in contact with the fibers for a long period. Liquid inside the two void regions is not isolated and exchanges sugar between such places by diffusion.

The sugarcane fibers were divided into two fractions. This interpretation separates the sugar content in the fibers into two parts, one extracted by lixiviation and other by diffusion. Figure 3.2 summarizes the proposed extraction phenomenon.

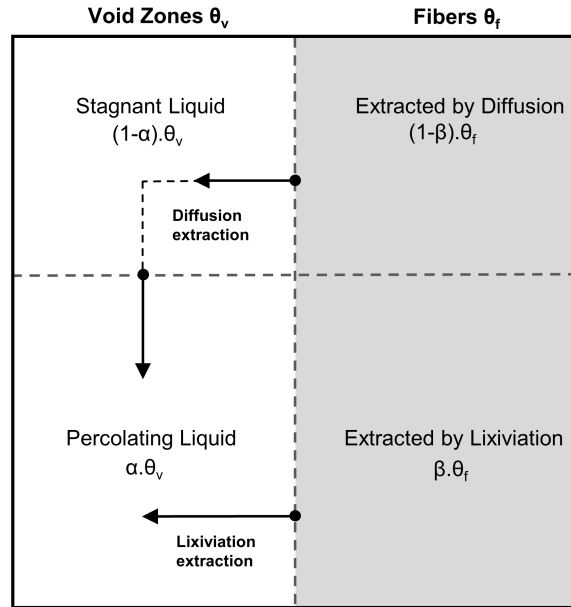


Figure 3.2: Schematic representation of the proposed extraction process. The volumetric fraction of the void spaces and fibers are represented by θ_v and θ_f , respectively. The fraction of the void space comprising the percolating liquid is accounted for the α term. The β term is the fraction of the fibers extracted by lixiviation.

3.2 Concerning the moving nature of sugarcane bed

The diffuser modeled in this study is of a moving bed type. Therefore, the number of velocity components presented in the model depends on the assumed referential. The proposed model was formulated following an Eulerian approach and a static referential (see section 4.1 for a more detailed discussion about this topic). Therefore, along with the descending vertical velocity, the percolating liquid has an horizontal movement promoted by the bed motion. The other three bed sections (*i.e.*, stagnant liquid and the two fiber fractions) are carried along the diffuser just by the bed movement. Thus, these three components have a horizontal velocity following the same direction of the bed motion. The velocity components for each bed section are represented in the Figure 3.3.

3.3 General assumptions

The following assumptions were taken into account to develop the model of the moving-bed diffuser.

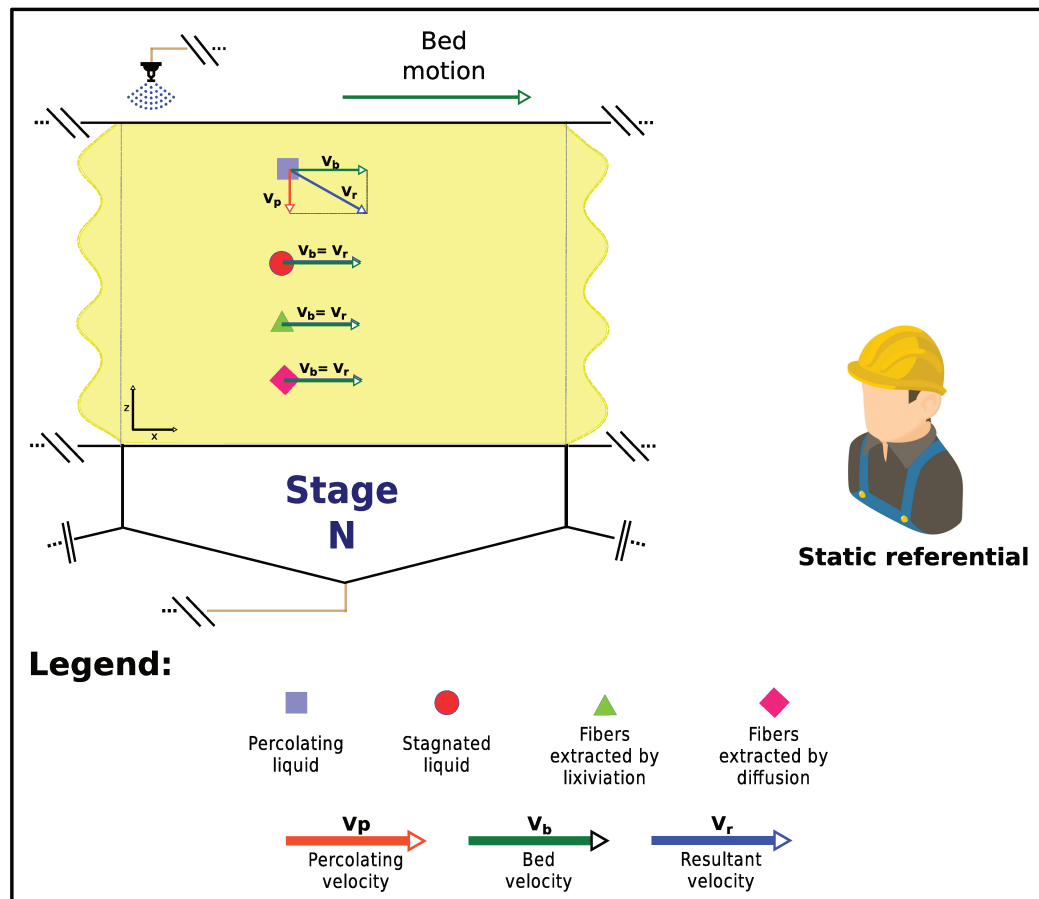


Figure 3.3: Velocity components for each bed section following an Eulerian approach and a static referential.

1. Model developed in two dimensions: length, in the x -axis, and width, in the z -axis;
2. Isothermal condition;
3. Static referential-Eulerian interpretation of the flux;
4. Momentum equation computed by the Darcy's equation;
5. Permeability of the media, viscosity and density of the percolating liquid are kept constant.

3.4 Model equations in infinitesimal scale

Following the phenomenological abstraction, the sugarcane bed is made up of four sections (*i.e.*, two void zones and the fiber content split in two fractions). Sugar content

in these four sections is transferred through the contact surface among them. The center of a phenomenological model is a balance equation of an extensive quantity (BEAR and BUCHLIN, 1987). Therefore, the proposed model is a set of four equations, each of them responsible to account for the sucrose mass balance in one of the four bed sections. As an initial approach, sucrose balance was performed by applying the conservation laws in infinitesimal volumes inside each bed section. Such volumes are assumed homogeneous, which allows the straightforward application of the conservation rules.

Sucrose balance is going to be developed in a generic infinitesimal volume, named as U (Figure 3.4). Such volume may be placed within any of the four bed sections. The cube shape is a simplification, once the geometry of the infinitesimal volumes may achieve any degree of complexity. The fluxes of sucrose in and out of the element are made through the surface S of the volume U and are depicted by the arrows. The generic form of the mass balance equation is also introduced in Figure 3.4, which can be stated as follow: for a generic volume U , surrounded by a surface S , the net accumulation of sugar is equal to the net influx of sucrose plus the net rate of production or degradation of sucrose. Each term of this balance equation is going to be detailed in the following sub-sections.

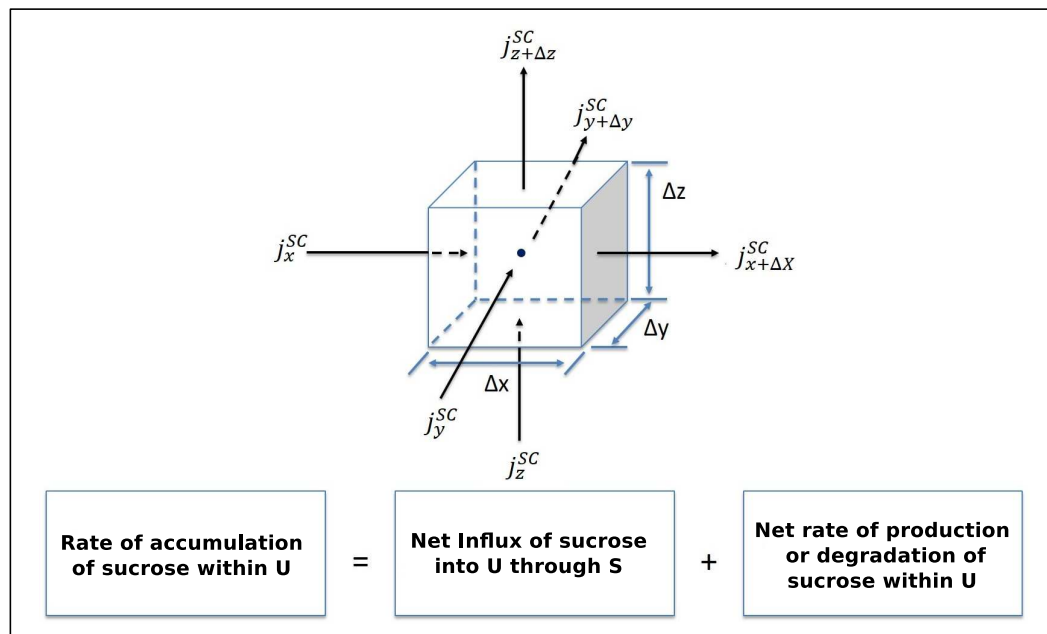


Figure 3.4: A generic infinitesimal volume U along with its sucrose fluxes. General form of the sucrose balance equation.

3.4.1 Accumulation of sucrose within U

Sucrose content, SC , within the volume U for one bed section is calculated through the Eq 3.1. The exponent γ is a generic bed section in which the volume U is placed ($\gamma = p$, percolating liquid, or e , stagnant liquid, or f_l , fiber fraction extracted by lixiviation, or f_d , fiber fraction extracted by diffusion). Moreover, C^γ is the sugar concentration in the volume U , valid for the γ bed section.

$$SC^\gamma = \int_U C^\gamma dU \quad (3.1)$$

As a consequence of the previous definition, accumulation of sucrose content in the volume U is obtained by the Eq 3.2. The last term of Eq 3.2 is legitimated by considering the volume U constant.

$$\frac{\partial SC^\gamma}{\partial t} = \frac{\partial}{\partial t} \int_U C^\gamma dU = \left(\int_U \frac{\partial C^\gamma}{\partial t} dU \right) \quad (3.2)$$

3.4.2 Net influx of sucrose into U

The net influx of sugar in the volume U is determined through the sum of all mass transfer occurring over the surface S . This quantity is computed by the following surface integral (Eq 3.3):

$$- \int_S \mathbf{j}^{\text{SC}} \cdot \boldsymbol{\nu} dS = - \int_U \nabla \cdot \mathbf{j}^{\text{SC}} dU \quad (3.3)$$

The term \mathbf{j}^{SC} is the flux of sugar in a infinitesimal area dS and $\boldsymbol{\nu}$ is unitary vector normal to the surface, pointing outward the volume U . The operation $\mathbf{j}^{\text{SC}} \cdot \boldsymbol{\nu}$ is an inner product between the vectors \mathbf{j}^{SC} and $\boldsymbol{\nu}$. This inner product produces a scalar that is the projection of \mathbf{j}^{SC} over the vector $\boldsymbol{\nu}$. The right-hand side of equation 3.3 comes from the application of the *Gauss Theorem*, which converts a surface integral into a volume integral. This theorem correlates a flux over a surface with the behavior of a vectorial field within the volume surrounded by it (VERSTEEG and MALALASEKRA, 1995). Therefore, the net influx is the sum of all sources minus the sum of all sinks inside U . The operator ∇ stands for the gradient of the net influx term.

The flux of sugar \mathbf{j}^{SC} can be divided into a convective and a diffusive contributions.

The convective flux is the sugar transfer promoted by the velocity V^γ of a γ section. The diffusive component accounts for the mass transfer stimulated by a gradient of sugar concentration. As a consequence, equation 3.4 presents the net influx in its disassembled form. The term $C^\gamma V^\gamma$ is the convective flux and j^γ is the diffusive flux of sugar in the γ section of the sugarcane bed.

$$-\int_U \mathbf{j}^{\text{SC}} dU = -\int_U \nabla \cdot (C^\gamma V^\gamma + j^\gamma) dU \quad (3.4)$$

3.4.3 Production or degradation of sucrose within U

The proposed phenomenological abstraction does not take into account the generation or degradation of sucrose during the extraction process performed inside a diffuser. Therefore, net sugar generation or degradation is not included in the sucrose balance over a infinitesimal volume U .

Substituting equations 3.2 and 3.4 in their respective positions of the mass balance equation, it is obtained the sugar balance in infinitesimal scale (Eq. 3.5):

$$\int_U \left[\frac{\partial C^\gamma}{\partial t} + \nabla \cdot (C^\gamma V^\gamma + j^\gamma) \right] dU = 0 \quad (3.5)$$

For a infinitesimal volume, the generic volume U tends to zero ($U \rightarrow 0$). Thus, equation 3.5 assumes its final form (Eq. 3.6):

$$\frac{\partial C^\gamma}{\partial t} + \nabla \cdot (C^\gamma V^\gamma + j^\gamma) = 0 \quad (3.6)$$

In order to apply Eq 3.6 directly to a sugarcane bed, an infinitesimal description of the properties which characterize the modeled system, such as sugar concentrations, porosity, and tortuosity is required. At this scale, each bed fraction occupies a distinct spacial domain and each point of the space belongs to a bed fraction (SZYMKIEWICZ, 2013). Due to the complex conformation of the fibers in bed, such degree of details is not available. Moreover, collecting data in infinitesimal scale is expensive and laborious. In order to overcome these limitations, the scale of the model equation is going to be changed, aiming a macroscopic representation of the sucrose extraction in a diffuser. Bearing this goal in mind, in the next section, it is going to be introduced the concepts behind the continuum hypothesis,

the representative elementary volume and the averaging rules. These three key concepts are the theoretical basis to convert the model equations into a macroscopic representation of the extraction process.

3.5 On the path to a macroscopic scale model

3.5.1 Continuum hypothesis

As an initial step to overcome the infinitesimal description of Eq. 3.6, this study made use of the continuum hypothesis valid for macroscopic subdivisions of the bed. Such macroscopic subdivisions will be named here as continuous volumes. For the sake of illustration, Figure 3.5-(a) presents a region of a sugarcane bed in which a generic system property Φ^γ (e.g., sucrose concentration, porosity) varies as function of the spatial position. The red-dashed square in Figure 3.5-(a) depicts a macroscopic continuous volume in which the continuum hypothesis is assumed valid. A more detailed treatment of continuum theory may be found at MÜLLER, (2014).

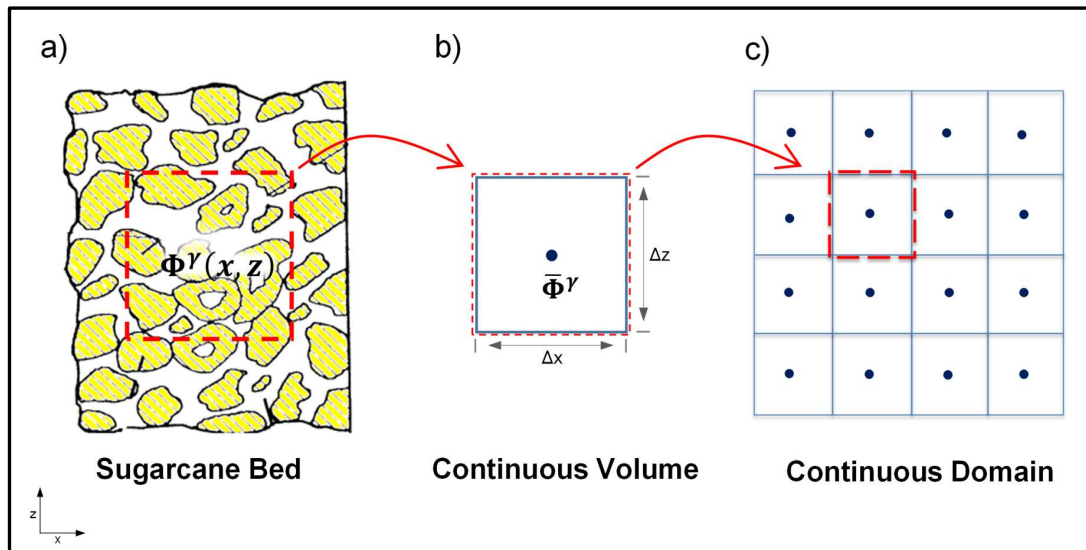


Figure 3.5: Continuum hypothesis applied to an illustrative scenario. (a) Region of a sugarcane bed described by a generic system property Φ^γ . Red dashed square represents the macroscopic subdivisions where the continuum hypothesis is assumed valid. (b) Continuous volume described by the average of a generic system property $\bar{\Phi}^\gamma$. (c) Sugarcane bed as union of continuous volumes.

Through the continuum hypothesis, the bed sections in a continuous volume no

longer occupy disjoint positions. Instead, the four sections fill the volumes as a continuum (Figure 3.5-(b)). In these volumes, properties of the modeled system do not vary as functions of the spatial position. In fact, each property is represented by its average over the continuous volume. In relation to the scenario illustrated in Figure 3.5, the generic property Φ^γ is described by its average value $\bar{\Phi}^\gamma$ in the continuous volume. Extending the continuum hypothesis to the whole modeled system, the sugarcane bed may be interpreted as an union of continuous volumes (Figure 3.5-(c)). It may be argued that such continuum approach is an oversimplification, which introduces uncertainties in the model. However, in face of the high complexity of the cane fibers conformation in the bed and the difficulty to collect data point-to-point in a full-scale diffuser, this simplification is justified and necessary to the feasibility of the proposed model.

3.5.2 Representative elementary volumes

The size of a continuum volume cannot be arbitrary. Different sizes may produce contrasting values of the average of the modeled system properties. In order to avoid these divergences and to obtain an universal methodology to define the size of the continuum volume, it is used the concept of *Representative Elementary Volumes (REV)*. For a generic continuous volume B , there is a range of volume sizes, called representatives, in which a measured property has a constant value. Therefore, the continuum volumes inside this range of sizes are characterized as REV. It is worth to stress the difference between the generic volumes U and B . The volume U is an infinitesimal generic volume, while B is a continuous macroscopic volume in which the four bed sections are distributed inside it as a continuum.

In an effort to clarify the core idea behind the *REV* concept, figure 3.6 shows, for instance, the average of the sugar concentration in a sugarcane bed as a function of the volume element size. From the center of the depicted volume element, it is gradually inserted volumes with increasing size (i.e., $B_1 < B_2 < B_3 < B_4$). It is possible to notice three different regions of the average sugar concentration value. The microscopic heterogeneity region concerns to the volumes in which the average sugar concentration values change due to the microscopic structure of the sugarcane bed. In the homogeneity region, the average concentration becomes constant. Volumes inside this zone are considered as REV. In the example presented in figure 3.6, the volume B_3 is a representative elementary volume. Increasing further the volume size, the value of the average concentration starts to change again as a result of the macroscopic heterogeneities of the medium (e.g., living the bed frontiers).

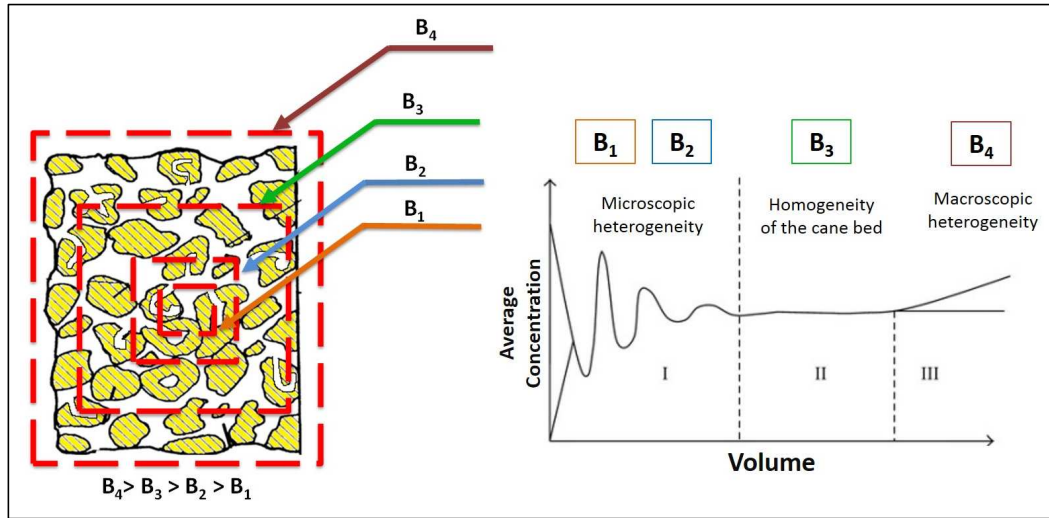


Figure 3.6: Average concentration of sugar in the cane bed as a function of the volume element size

3.5.3 Averaging rules

The mathematical technique responsible to convert the model equations into a macroscopic representation over a chosen *REV* is the averaging rules. These averaging rules seek the relation between the average of a quantity and the average value of the same property within a given *REV*. The average of a quantity would be obtained pondering this property point-to-point in the sugarcane bed. Through the average rules, this point-to-point knowledge is no longer necessary. The model equations becomes macroscopic balances of average values, valid over the whole considered *REV*. For the sake of the text fluidity, a detailed presentation of the averaging rules is delegated to Appendix A.

3.6 Model equations in macroscopic scale

The following step to avoid an infinitesimal sugar balance is to calculate the average of Eq 3.6 over a *REV*, named here as B_o . This procedure yields the average of the infinitesimal properties over B_o .

$$\frac{1}{B_o} \int_{B_o} \frac{\partial C^\gamma}{\partial t} dB_o = -\frac{1}{B_o} \int_{B_o} \nabla \cdot (C^\gamma V^\gamma + j^\gamma) dB_o \quad (3.7)$$

This equation assumes a more concise notation for the average procedure in the Eq 3.8.

$$\frac{\overline{\partial C^\gamma}}{\partial t} = -\overline{\nabla \cdot (C^\gamma V^\gamma)} - \overline{\nabla \cdot j^\gamma} \quad (3.8)$$

Eq 3.8 is valid over the whole B_o , thus considering simultaneously the four bed divisions. However, the proposed phenomenological abstraction differentiates each bed section. To preserve this differentiation, it is used the volume fraction of the bed sections (θ_γ), which relates B_o with its four continuum sub-domains (Eq 3.9). In this way, Eq. 3.9 represents the average of the infinitesimal properties in relation to only one γ section.

$$\theta_\gamma \frac{\overline{\partial C^\gamma}}{\partial t} = -\theta_\gamma \overline{\nabla \cdot (C^\gamma V^\gamma)} - \theta_\gamma \overline{\nabla \cdot j^\gamma} \quad (3.9)$$

However Eq. 3.9 still presents an infinitesimal nature, once its elements are averages of infinitesimal properties. Applying the averaging rules to Eq 3.9 yields a balance of average properties over a continuous volume B_o (Eq. 3.10). In this sense, the punctual knowledge concerning the system properties is about to be avoided.

$$\theta_\gamma \frac{\overline{\partial C^\gamma}}{\partial t} = -\theta_\gamma \overline{\nabla \cdot (C^\gamma V^\gamma + j^\gamma + \dot{C} V^\gamma)} + \sum_{\xi \in Q | \xi \neq \gamma} \langle C^\gamma (V^\gamma - V^\xi) \cdot \nu \rangle^{\gamma, \xi} \cdot \Lambda_{\gamma, \xi} + \sum_{\xi \in Q | \xi \neq \gamma} \langle j^\gamma \cdot \nu \rangle^{\gamma, \xi} \cdot \Lambda_{\gamma, \xi} \quad (3.10)$$

In Eq. 3.10, ξ is also a generic index; however, it represents a different section of the bed ($\xi \neq \gamma$). The set Q contains each bed division (*i.e.*, $Q = \{p, e, fi, fd\}$). The operator $\langle \cdot \rangle^{\gamma, \xi} \cdot \Lambda_{\gamma, \xi}$ represents the surface integrals that compute sugar transfer across the surface separating distinct bed sections. The specific area of the surface separating γ and ξ is represented by the term $\Lambda_{\gamma, \xi}$. The factor ν is a normal vector pointing outwards the same separating surface. For a generic γ , summation terms accounts for the interaction with the three other bed sections. Each term in the Eq 3.10 is going to be detailed in the following paragraphs.

The average convective contribution to the sugar transport is accounted for the term $\overline{C^\gamma V^\gamma}$, where $\overline{V^\gamma}$ stands for the average velocity of the γ section. The average diffusive flux of sugar, $\overline{j^\gamma}$, was described here by Fick's Law (Eq. 3.11). The diffusive coefficient D represents the mobility of sucrose in an aqueous solution.

$$\bar{j}^\gamma = -\nabla D \bar{C}^\gamma \quad (3.11)$$

$\overline{\dot{C}V}^\gamma$ is the average dispersion effect within the porous sugarcane bed. Dispersion rises in the bed due to the heterogeneity of the media. In a non-dispersed flow, the fluid-dynamics of the percolating liquid may be represented by a plug-flow model. However, dispersion introduces non-idealities in the flux, which makes different elements of the liquid staying different periods inside the bed (i.e., residence time distribution). According to [BEAR and BACHMAT \(1991\)](#), dispersion is proportional to the gradient of the balanced property (Eq. 3.12). The dispersive coefficient Ω introduces the tortuosity of the sugarcane bed to the model.

$$\overline{\dot{C}V}^\gamma = -\nabla \Omega \bar{C}^\gamma \quad (3.12)$$

The surface integrals (*e.g.*, terms with the operator $\langle \cdot \rangle^{\gamma,\xi} .\Lambda_{\gamma,\xi}$) account for the infinitesimal interaction between distinct sections of the bed. These terms translate to macroscopic scale the transfers of sugar among the bed portions. For the sake of illustration, [Figure 3.7](#) introduces a scheme of the frontier separating the γ and ξ portions of the cane bed, along with the vectors belonging to the terms present in the surface integrals. The integrals compute the influence of these vectors in the transference of sugar over the whole frontier. The insertion of these terms in the model allows for the mathematical representation of the sugar extraction.

The first surface integral represents the sugar transfer promoted by the motion of the γ section in relation to ξ , accounted for the relative velocity $(V^\gamma - V^\xi)$. There is a conceptual congruence between this element and the lixiviation extraction. The second surface integral element is the sugar transfer between γ and ξ through the diffusion mechanism. Calculating such surface integrals is not a trivial task, since it requires a complete description of the frontiers geometry separating the bed sections. Hence, we introduced a simplification of these elements based on the approach proposed by the classical work of [REIN \(1972\)](#) (Eqs. 3.13 and 3.14). The mass transfer rates are accounted for k_1 , lixiviation, and k_2 , diffusion, which are fitting parameters of the model.

$$\sum_{\xi \in Q | \xi \neq \gamma} \langle C^\gamma (V^\gamma - V^\xi) .\nu \rangle^{\gamma,\xi} .\Lambda_{\gamma,\xi} = \sum_{\xi \in Q | \xi \neq \gamma} k_1 (\bar{C}^\gamma - \bar{C}^\xi) \quad (3.13)$$

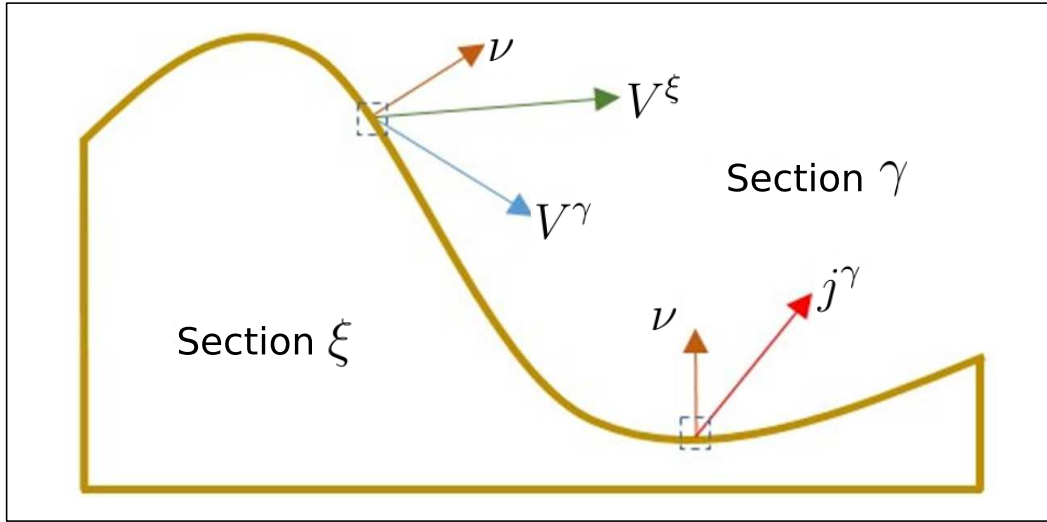


Figure 3.7: Schematic representation of a frontier between two portions of the sugarcane bed

$$\sum_{\xi \in Q | \xi \neq \gamma} \langle j \cdot \nu \rangle^{\gamma, \xi} \cdot \Lambda_{\gamma, \xi} = \sum_{\xi \in Q | \xi \neq \gamma} k_2 (\bar{C}^{\gamma} - \bar{C}^{\xi}) \quad (3.14)$$

Concerning volumetric fractions, the continuous domain was divided into θ_v , for the total void region (*i.e.*, percolating and stagnant zones) and $\theta_f (= 1 - \theta_v)$, for the volume fraction of the fibers. Each volumetric fraction is subsequently divided into two parts, in order to distinguish the volumetric fractions of the four bed sections. The parameter α divides θ_v into the percolating liquid content, $\alpha \cdot \theta_v$, and the stagnated content, $(1 - \alpha) \cdot \theta_v$. In terms of fibers, β splits θ_f into fractions for lixiviation extraction, $\beta \cdot \theta_f$, and for diffusion extraction, $(1 - \beta) \cdot \theta_f$ (see Figure 3.2). Both α and β are other two fitting parameters of the model.

Substituting Eqs 3.11, 3.12, 3.13 and 3.14 in Eq. 3.10 leads to the proposed model in its general form (Eq 3.15). Eq 3.15 needs to be particularized to each bed section in order to agree with the proposed phenomenological abstraction.

$$\theta_{\gamma} \frac{\partial \bar{C}^{\gamma}}{\partial t} = -\theta_{\gamma} \nabla \cdot (\bar{C}^{\gamma} \bar{V}^{\gamma} - \nabla \cdot D \bar{C}^{\gamma} - \nabla \cdot \Omega \bar{C}^{\gamma}) + \sum_{\xi \in Q | \xi \neq \gamma} k_1 (\bar{C}^{\gamma} - \bar{C}^{\xi}) + \sum_{\xi \in Q | \xi \neq \gamma} k_2 (\bar{C}^{\gamma} - \bar{C}^{\xi}) \quad (3.15)$$

3.6.1 Sugar content in the percolating liquid

The convective sugar transportation is performed by the bed velocity v_b (horizontal direction) and the percolating velocity v_p (vertical direction). Navier-Stokes equations may be used to compute the descending percolating velocity. However, such momentum balance requires a detailed representation of the conditions at the fluid-solid and fluid-fluid interfaces (SZYMKIEWICZ, 2013). Therefore, Navier-Stokes equations do not avoid an infinitesimal description of the extraction process. Applying the averaging rules also in the Navier-Stokes equations is an effective alternative to evade an infinitesimal characterization of the liquid flow. A mathematically rigorous averaging of the Navier-Stokes equations yields the Darcy's law equation (SZYMKIEWICZ, 2013), which is valid over macroscopic continuous volumes (*i.e.*, B_o). A detailed description of this averaging procedure may be found at AURIAULT *et al.* (2009) and BEAR (1972).

As a consequence of the above discussion, the percolating velocity is computed in this study by means of the Darcy's law equation, assuming a full saturated medium (Eq. 3.16). In this equation, K_p is the permeability of the media, which is directly related to the geometric characteristics of the void spaces. Viscosity and density of the percolating liquid correspond to μ and ρ , respectively, and g is the gravitational acceleration. Pressure gradient in the vertical axis accounts for the losses in the screen, which gives support and movement to the sugarcane bed.

$$v_p = -\frac{K_p}{\mu} \cdot \left[\frac{\Delta P_{sup}}{\Delta z} - \rho g \right] \quad (3.16)$$

The supporting screen may greatly restrict the flow capacity of the bed (PICARO *et al.*, 1994). Following the approach proposed by PICARO and WHITE (1993), pressure losses in the screen are computed in Eq. 3.17. The constant K_s represents the laminar flow resistance of the support, which is the function of the geometric characteristics of the screen.

$$\Delta P_{sup} = K_s \mu v_p \quad (3.17)$$

Substituting Eq. 3.17 in Eq. 3.16 leads to the percolating velocity equation (Eq. 3.18), where H stands for the bed height.

$$v_p = \frac{K_p \rho g}{\mu \left(1 + \frac{K_p K_s}{H}\right)} \quad (3.18)$$

The fifth general assumption (section 3.3) leads to a single value representing the percolating velocity throughout the sugarcane bed. However, it is a simplification of the modeled system. Permeability of the medium varies in a diffuser due to the deformable nature of the sugarcane fibers. In a real equipment, viscosity and density of the percolating liquid change due to fluctuations of system temperature and to variations of the sugar concentration. The variation of such parameters would generate a positive impact on representativeness and on generalization capacities of the model. On the other hand, it is infeasible to directly measure the distribution of these parameters in the bed for a full-scale diffuser under operation.

The validity of the aforementioned assumption is justified by some operational characteristics of a full-scale diffuser. Presence of two sets of lifting screws in moving-bed diffusers decreases variations of medium permeability. Homogenization action of the lifting screws corroborates to the constant permeability hypothesis. Temperature inside a diffuser is controlled to avoid high variations (REIN, 2013). Moreover, values of sugar concentration achieved during the operation of a diffuser do not lead to significant variations of density and viscosity of the percolating liquid. Given these two previous facts, it seems reasonable to assume constant values of viscosity and density related to the moving liquid.

The diffusive flux is neglected, once its effect is not representative in face of the dispersion promoted by the heterogeneity of the media. This simplification can be justified by comparing the magnitude order of the sucrose/water diffusion coefficient ($\sim 10^{-5} m^2/min$) with the dispersion coefficient in the sugarcane bed ($\sim 10^{-2} m^2/min$) (LOVE and REIN, 1980). According to the proposed phenomenological abstraction, the percolating liquid extracts sugar from the fibers through lixiviation (*i.e.*, from the f_l section), and through diffusion from the stagnant liquid. Therefore, both extraction terms are considered in the final form of the sugar balance (Eq. 3.19).

$$\alpha \theta_v \frac{\partial \bar{C}^p}{\partial t} = -\alpha \theta_v \left(\frac{\partial v_b \bar{C}^p}{\partial x} + \frac{\partial v_p \bar{C}^p}{\partial z} \right) + \alpha \theta_v \left(\frac{\partial^2 \Omega_x \bar{C}^p}{\partial x^2} + \frac{\partial^2 \Omega_z \bar{C}^p}{\partial z^2} \right) + k_1 (\bar{C}^{f_l} - \bar{C}^p) + k_2 (\bar{C}^e - \bar{C}^p) \quad (3.19)$$

3.6.2 Sugar content in the stagnant liquid

Inside a continuum volume, stagnant liquid is trapped by the fibers. Motionless in relation to the fibers implies non-existence of dispersive flux. Furthermore, it is assumed that each stagnant zone is isolated from each other and is homogeneous in relation to the sugar content. The homogeneous assumption leads to a null diffusive flux in the liquid inside each stagnated region. The stagnated liquid extracts sugar from the fibers by diffusion and transfers it to the percolating liquid using the same mechanism. Eq. 3.20 represents the sugar mass balance in the stagnant liquid.

$$(1 - \alpha) \theta_v \frac{\partial \bar{C}^e}{\partial t} = - (1 - \alpha) \theta_v \frac{\partial v_b \bar{C}^e}{\partial x} + k_2 \left(\bar{C}^{f_d} - 2\bar{C}^e + \bar{C}^p \right) \quad (3.20)$$

3.6.3 Sugar content in the fibers

We interpreted the sugar content of the two fiber fractions as isolated and homogeneous regions. As previously shown, this hypothesis leads to the absence of dispersive and diffusive fluxes. Sugar balance in the fiber fraction extracted by lixiviation is presented in Eq. 3.21.

$$\beta \theta_f \frac{\partial \bar{C}^{f_t}}{\partial t} = -\beta \theta_f \frac{\partial v_b \bar{C}^{f_t}}{\partial x} - k_1 \left(\bar{C}^{f_t} - \bar{C}^p \right) \quad (3.21)$$

Sugar content in fiber fraction extracted by diffusion is calculated in Eq. 3.22.

$$(1 - \beta) \theta_f \frac{\partial \bar{C}^{f_d}}{\partial t} = - (1 - \beta) \theta_f \frac{\partial v_b \bar{C}^{f_d}}{\partial x} - k_2 \left(\bar{C}^{f_d} - \bar{C}^e \right) \quad (3.22)$$

3.7 Boundary conditions

The Boundary conditions are presented in Figure 3.8. For the percolating liquid, the North side has two types of contour conditions: aspersion and non-aspersion regions (see Figure 4.1). In the aspersion regions, sugar concentration on the frontier is equal to the sugar concentration of the aspersion located over this point (C_{asp}), which can be stated as a Dirichlet boundary condition. For this study, the concentration of the aspersion over a stage n (C_{asp}^n) is the average sugar concentration of the percolating liquid leaving the next stage

($n + 1$). This boundary condition simulates the counter-current arrangement of the aspersion points.

We assumed non-aspersion regions and the West border as isolated frontiers. In these borders, absence of mass transfer is represented by a null Neumann boundary condition. For the East and the South borders, we considered a developed profile of the transported sugar, which can be also stated by a null Neumann boundary condition. Regarding the stagnant liquid and following the previous assumptions, the West border is isolated and the East border presents a developed profile of sugar concentration.

The pair of fiber equations have equal boundary conditions. For the West border, sugar concentration is set equal to the sugar concentration in the raw material entering the equipment (C_{rm}^{in}). As an assumption, East border have a developed profile of sugar concentration.

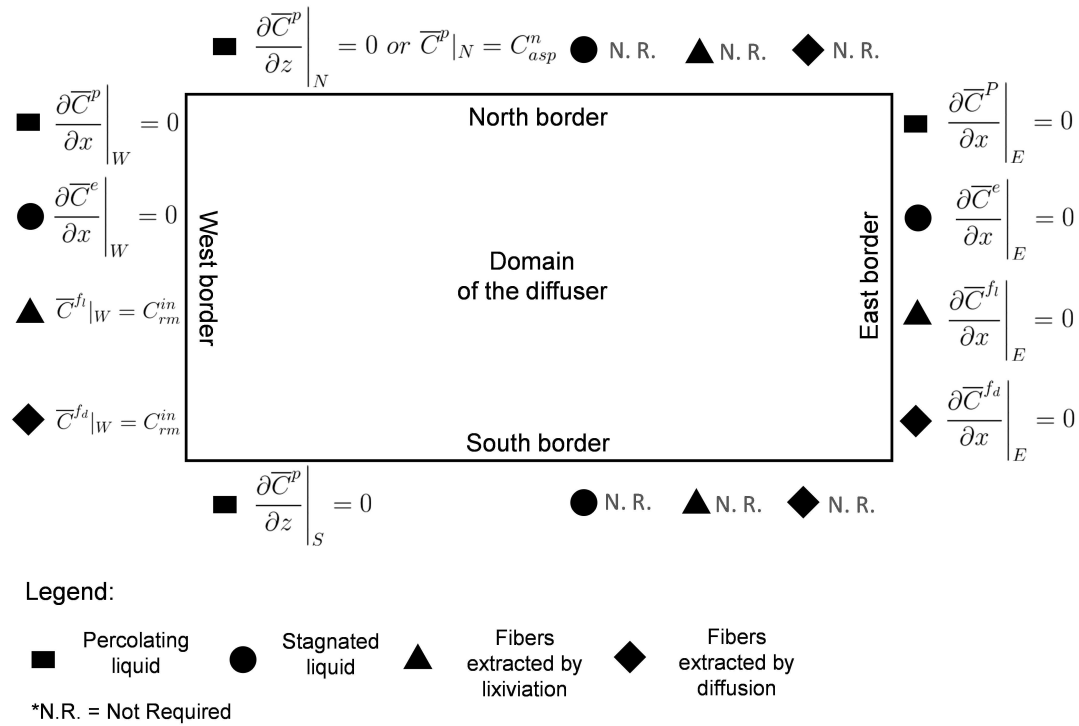


Figure 3.8: Boundary conditions for the four bed sections in each border of the diffuser.

3.8 Auxiliary equations

3.8.1 Bed height

Bed height is calculated in Eq. 3.23 (REIN, 2013). $Prod$ is the amount of sugarcane processed per second, Fc stands for the fiber content in the raw material, DPF is the fibers packing density in the bed, and $larg$ represents the bed width.

$$H = \frac{Prod.Fc}{DPF.v_b.larg} \quad (3.23)$$

3.8.2 Volume fractions in the bed portions

The total liquid “hold-up” (HU_t) is the amount of liquid (percolating and stagnant) retained by the sugarcane bed during operation. For a full saturated media, HU_t is an indicative of the extension of the void space. In this way, θ_v can be estimated by knowing the HU_t value, which is calculated in Eq. 3.24 (REIN and WOODBURN, 1974).

$$HU_t = 25.2 - 0.18DPF \quad (3.24)$$

With the value of HU_t , θ_v and θ_f are calculated by Eqs. 3.25 and 3.26, respectively.

$$\theta_v = \frac{DPF.HU_t}{\rho} \quad (3.25)$$

$$\theta_f = 1 - \theta_v \quad (3.26)$$

3.8.3 Converting concentration into °Brix

Concentration \overline{C}^γ is converted into °Brix value, $\overline{C}_{\circ Brix}^\gamma$, by Eq 3.27 (HUGOT, 1986). \overline{Puri} stands for the average purity of the sucrose solution over the whole equipment.

$$\overline{C}_{\circ Brix}^\gamma = \frac{100.\overline{C}^\gamma}{\rho.\overline{Puri}} \quad (3.27)$$

3.8.4 Extraction degree

Extraction degree is calculated using Eq 3.28 (REIN, 2013). In this equation, $SQ_{f_l}^{out}$ and $SQ_{f_d}^{out}$ are the sugar quantities leaving the diffuser in the f_l and f_d bed sections, respectively. SQ_{rm}^{in} is the sugar quantity in the raw material.

$$Ext = \left[1 - \frac{SQ_{f_l}^{out} + SQ_{f_d}^{out}}{SQ_{rm}^{in}} \right] .100 \quad (3.28)$$

3.9 Concluding remarks

It was presented in this chapter the proposed mathematical model of the extraction process in a moving-bed diffuser. The main concern of the previous discussion was to demonstrate the theoretical path that led this study up to the current version of the model. Concerning the former studies of mathematical modeling of diffusers, interpreting the sugarcane bed as a fractured medium represents an important novelty. Such interpretation provides a more formal theoretical base for the mathematical description of the extraction process within a fibrous sugarcane bed. It is expected that the efforts devoted to develop this new approach represents a bedrock for further developments of the model. In this sense, the future versions may include more complex phenomena, such as the extraction process in an unsaturated media. The next chapter is devoted to numerical issues behind the solution of the model equations. At the end, the simulation framework in its current version is going to be introduced.

Chapter 4

Numerical Solution

In this chapter, it is going to be introduced the computational implementation of the proposed mathematical model. First, the discretization procedure of the model's equations is going to be detailed. In a second part, it is going to be introduced the approaches used to account for the transient variations of the bed height and the percolating velocity. In the sequence, it is going to be presented the main features of the developed moving-bed diffuser simulator. It is also presented at the end of this chapter the strategies applied to fit the model's parameters, as well as to perform the optimization analysis.

4.1 Discretization procedure

The finite volume method (*FVM*) was used to discretize model equations. *FVM* is a numerical technique that converts differential equations representing conservation laws into discrete algebraic equations over finite volumes ([MOUKALLED *et al.*, 2016](#)). An important feature of the FVM is its strictly conservative nature at the discrete level, which is not an inherent characteristic of other discretization methods (*e.g.*, finite difference method, finite element method) ([MALISKA, 2012](#)). Moreover, *FVM* allows for a directly association between the physical interpretation and the mathematical representation of the modeled phenomenon ([VERSTEEG and MALALASEKRA, 1995](#)).

The resolution grid is the discrete representation of the sugarcane bed in which the *FVM* is applied (Figure 4.1-(a)). Such grid was designed in accordance with the Eulerian approach of the modeled process. In this approach, the value of the properties (*e.g.*, sucrose concentration) are described as fields, changing as function of space and time. The Eulerian

description does not consider the properties of any particular particle. Instead, the fields are obtained through the evaluation of the properties values along fixed points of the domain under study. Therefore, the resolution grid is the division of the real domain in fixed volumes. As presented in the chapter 3, this study assumes that such fixed volumes are continuous volumes in which the *REV* requirements are fulfilled. Despite the use of the term “volumes” to address the grid elements, the discrete representation of the bed is bi-dimensional. However, such bi-dimensionality is not prohibitive to apply the *FVM*, once it is assumed that the evaluated properties are distributed homogeneously in the width of the bed.

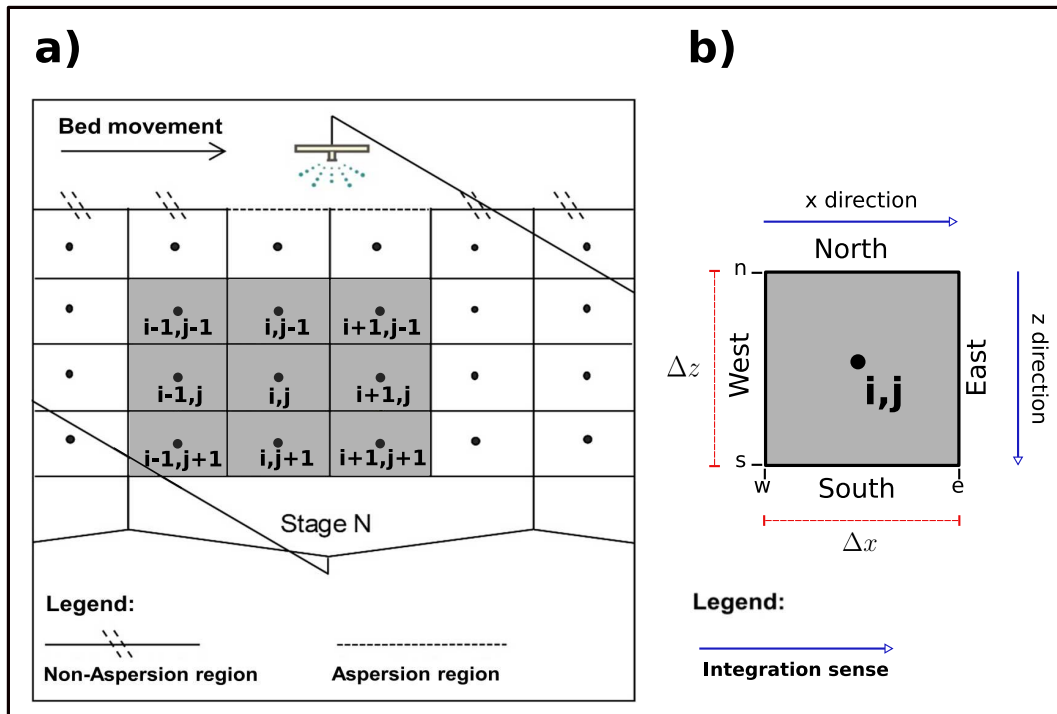


Figure 4.1: (a) Grid representation for a stage of a moving-bed diffuser. The highlighted volumes show the applied index rule for a generic volume centered in “ i,j ” and its nearest neighbors. North boundary divided into aspiration and non-aspiration regions. Number of volumes per stage presented and size of the aspiration zone are illustrative. (b) Generic volume of the grid along with its faces nomenclature as common used in the finite volumes method literature. Integration sense for both x and z directions.

In Figure 4.1-(a), the highlighted volumes show the applied index rule for a generic continuum volume centered in “ i,j ” and its nearest neighbors. Moreover, Figure 4.1-(b) presents a volume of the grid along with its faces nomenclature as common used in the *FVM* literature. The value of each intensive or extensive quantity is allocated at the center of the volume and is valid for the whole volume. Therefore, the continuum hypothesis is preserved for every discrete volume of the grid. The main procedure of *FVM* is the integration of the

model equations over each volume of the grid. Integration in each direction is performed from one face to the opposite one (arrows in Figure 4.1-(b)). In the following sub-sections, each term of the proposed extraction model is going to be integrated and hence discretized in a volume of the grid centered in “i,j”. For the sake of generality, the *FVM* is applied to a generic bed section γ .

4.1.1 Discretization of the convective terms

Eq 4.1 presents the integration of a convective term in the x direction. In this equation \bar{V}_x^γ is a generic velocity in the x direction (*e.g.*, bed velocity v_b). Integration is performed both in x and z directions. Since the derivative is done in relation to the x direction, \bar{C}^γ and \bar{V}_x^γ are assumed constant in the axis z . After the integration in z (second term in Eq 4.1), \bar{C}^γ and \bar{V}_x^γ become $\bar{C}_{:,j}^\gamma$ and $\bar{V}_{x|:,j}^\gamma$ to indicate that these values refer to the same vertical position of the volume in which the integration is being performed. Integrating in x direction requires the knowledge of $\bar{C}_{:,j}^\gamma$ and $\bar{V}_{x|:,j}^\gamma$ values on the frontiers West and East (third term in Eq 4.1). In a discretization procedure, the value of the quantities are allocated at center of the volume, giving to the grid a discrete nature. Therefore, it is required to use interpolation schemes that link the continuity of the real system to the discrete nature of the grid. In the other words, a quantity on a face have to be an interpolation of its values at the center of the surrounding volumes.

$$\begin{aligned} \int_w^e \int_n^s \theta_\gamma \frac{\partial \bar{C}^\gamma \bar{V}_x^\gamma}{\partial x} dz dx &= \theta_\gamma \Delta z \int_w^e \frac{\partial \bar{C}_{:,j}^\gamma \bar{V}_{x|:,j}^\gamma}{\partial x} dx = \\ &= \theta_\gamma \Delta z (\bar{C}_{e,j}^\gamma \bar{V}_{x|e,j}^\gamma - \bar{C}_{w,j}^\gamma \bar{V}_{x|w,j}^\gamma) \end{aligned} \quad (4.1)$$

The up-wind scheme was used in this study to interpolate the convective fluxes on the faces of the volumes. Such scheme is frequently used in computational fluid-dynamic studies due to its simplicity and physical coherence (MOUKALLED *et al.*, 2016). In this interpolation, the value of a quantity in the frontier is approximated to the value at the closest up-stream center. Representativeness of the up-wind scheme is justified by the parabolic nature of the convective term. A parabolic term is an one-way coordinate in which the conditions at a given location are influenced by changes in conditions of only one side of that location (MALISKA, 2012). Moreover, concerning the values for the grid Peclet number found in the modeled moving-bed diffuser system ($Pe \approx 10$), up-wind shows identical behavior

when compared to interpolation schemes with higher accuracy (*e.g.*, exponential scheme) (PATANKAR, 1980). Applying the up-wind approximation, the last term of equation 4.1 assumes its final discretized form (Eq 4.2).

$$\theta_\gamma \Delta z (\overline{C}_{e,j}^\gamma \overline{V}_{x|e,j}^\gamma - \overline{C}_{w,j}^\gamma \overline{V}_{x|w,j}^\gamma) = \theta_\gamma \Delta z (\overline{C}_{i,j}^\gamma \overline{V}_{x|i,j}^\gamma - \overline{C}_{i-1,j}^\gamma \overline{V}_{x|i-1,j}^\gamma) \quad (4.2)$$

The same procedure is applied to the convective term in which the derivative is done in relation to z direction (Eq 4.3). \overline{V}_z^γ is a generic velocity in the z direction (*e.g.*, percolating velocity v_p).

$$\int_n^s \int_w^e \theta_\gamma \frac{\partial \overline{C}^\gamma \overline{V}_z^\gamma}{\partial x} dz dx = \theta_\gamma \Delta x (\overline{C}_{i,j}^\gamma \overline{V}_{z|i,j}^\gamma - \overline{C}_{i,j-1}^\gamma \overline{V}_{z|i,j-1}^\gamma) \quad (4.3)$$

4.1.2 Discretization of the dispersion terms

A dispersion term in the x direction is integrated over a volume in the Eq 4.4. The dispersive coefficient Ω_x is assumed constant in the x direction. The first integration generates $\overline{C}_{:,j}^\gamma$ (second term in Eq 4.4), which means a constant behavior in the z -axis. After the integration in the horizontal direction, it is necessary to compute the derivative of $\overline{C}_{:,j}^\gamma$ in relation to x at the frontiers West and East (third term in Eq 4.4). Again it is necessary to represent the required values at the faces of the volume as interpolations. The used interpolation scheme has also to be a function exclusively of the \overline{C}^γ values at the center of the surrounding volumes.

$$\int_w^e \int_n^s \theta_\gamma \Omega_x \frac{\partial^2 \overline{C}^\gamma}{\partial x^2} dz dx = \theta_\gamma \Omega_x \Delta z \int_w^e \frac{\partial^2 \overline{C}_{:,j}^\gamma}{\partial x^2} dx = \theta_\gamma \Omega_x \Delta z \left(\left. \frac{\partial \overline{C}_{:,j}^\gamma}{\partial x} \right|_e - \left. \frac{\partial \overline{C}_{:,j}^\gamma}{\partial x} \right|_w \right) \quad (4.4)$$

The derivatives in the frontier are interpolated in this study by a central differences scheme. Such interpolation considers that a property at the frontier are dependent on the \overline{C}^γ value in the volumes both up and down stream. Moreover, this scheme leads to a linear variation of the properties at the faces of the volumes (VERSTEEG and MALALASEKRA, 1995) and captures the symmetry of a phenomenon with an elliptic type term (MOUKALLED *et al.*, 2016). Both characteristics are in accordance with the physical nature of the dispersion process. The central differences scheme is presented for the West and East faces in Eqs 4.5

and 4.6, respectively.

$$\left. \frac{\partial \bar{C}_{:,j}^\gamma}{\partial x} \right|_w = \frac{\bar{C}_{i,j}^\gamma - \bar{C}_{i-1,j}^\gamma}{\Delta x} \quad (4.5)$$

$$\left. \frac{\partial \bar{C}_{:,j}^\gamma}{\partial x} \right|_e = \frac{\bar{C}_{i+1,j}^\gamma - \bar{C}_{i,j}^\gamma}{\Delta x} \quad (4.6)$$

Substituting the central differences approximations in the Eq 4.4 yields the discretized form of the dispersion term in the x direction (Eq 4.7)

$$\begin{aligned} \theta_\gamma \Omega_x \Delta z \left(\left. \frac{\partial \bar{C}_{:,j}^\gamma}{\partial x} \right|_e - \left. \frac{\partial \bar{C}_{:,j}^\gamma}{\partial x} \right|_w \right) &= \theta_\gamma \Omega_x \Delta z \left(\frac{\bar{C}_{i+1,j}^\gamma - \bar{C}_{i,j}^\gamma}{\Delta x} - \frac{\bar{C}_{i,j}^\gamma - \bar{C}_{i-1,j}^\gamma}{\Delta x} \right) = \\ &= \frac{\theta_\gamma \Omega_x \Delta z}{\Delta x} (\bar{C}_{i+1,j}^\gamma - 2\bar{C}_{i,j}^\gamma + \bar{C}_{i-1,j}^\gamma) \end{aligned} \quad (4.7)$$

In relation to the dispersive term in the z direction, the discretization is performed also considering a central difference approximation, as presented in Eq 4.8.

$$\begin{aligned} \int_n^s \int_e^w \theta_\gamma \Omega_z \frac{\partial^2 \bar{C}^\gamma}{\partial z^2} dx dz &= \Omega_z \cdot \Delta x \left(\left. \frac{\partial \bar{C}_{i,:}^\gamma}{\partial z} \right|_s - \left. \frac{\partial \bar{C}_{i,:}^\gamma}{\partial z} \right|_n \right) = \\ &= \frac{\theta_\gamma \Omega_z \Delta x}{\Delta z} (\bar{C}_{i,j+1}^\gamma - 2\bar{C}_{i,j}^\gamma + \bar{C}_{i,j-1}^\gamma) \end{aligned} \quad (4.8)$$

4.1.3 Discretization of the extraction terms

The extraction terms do not appear in the model equations as derivatives. Therefore, these terms are assumed homogeneous within the volumes and their values are allocated at the center of the volumes. The integration of a lixiviation extraction term is presented in Eq 4.9.

$$\int_w^e \int_n^s k_1 (\bar{C}^\gamma - \bar{C}^\xi) dz dx = k_1 \Delta x \Delta z (\bar{C}_{i,j}^\gamma - \bar{C}_{i,j}^\xi) \quad (4.9)$$

In its turn, the diffusion extraction term is integrated and hence discretized in Eq 4.10

$$\int_w^e \int_n^s k_2 (\overline{C}^\gamma - \overline{C}^\xi) dz dx = k_2 \Delta x \Delta z (\overline{C}_{i,j}^\gamma - \overline{C}_{i,j}^\xi) \quad (4.10)$$

4.1.4 Time derivatives

The time derivatives are not going to be discretized in this study, once the method of lines is applied as solution approach in the transient state. The method of lines is a numerical procedure to solve partial differential equations (*PDE*). The basic idea of this method is to discretized all terms of the model, but leaving the time derivatives unchanged (SCHIESSER, 1991). Therefore, the PDEs become ordinary differential equations (*ODE*) (CHAPRA and CANALE, 2008), which may be solved straightforward by generally well established numerical methods (HAMDI *et al.*, 2007).

4.1.5 Mathematical model in the discretized form

The described discretization procedures were applied to the equations of the model (Eqs 3.19 to 3.22). As a result, Eqs 4.11 to 4.14 present the discretized sucrose balance for the four bed sections. As a general characteristic, the four equations show signal coherence, which is required for physical consistency of the discretized equations (PATANKAR, 1980). The boundary conditions are directly substituted in the discretized equations. At steady-state (*i.e.*, time derivative equal to zero), these four equations form a sparse system of linear algebraic equations. Due to the inter-stage connections promoted by the aspersion boundary conditions, the sparse linear algebraic system is unsymmetric. At the transient state, these equations form a systems of ODE.

$$\begin{aligned} \alpha \theta_v \frac{\partial \overline{C}_{i,j}^p}{\partial t} = & -\frac{\alpha \theta_v v_l}{\Delta x} (\overline{C}_{i,j}^p - \overline{C}_{i-1,j}^p) - \frac{\alpha \theta_v}{\Delta z} (v_{p|i,j} \overline{C}_{i,j}^p - v_{p|i,j-1} \overline{C}_{i,j-1}^p) \\ & + \frac{\alpha \theta_v \Omega_x}{\Delta x^2} (\overline{C}_{i-1,j}^p - 2\overline{C}_{i,j}^p + \overline{C}_{i+1,j}^p) + \frac{\alpha \theta_v \Omega_z}{\Delta z^2} (\overline{C}_{i,j-1}^p - 2\overline{C}_{i,j}^p + \overline{C}_{i,j+1}^p) \\ & + k_1 (\overline{C}_{i,j}^f - \overline{C}_{i,j}^p) + k_2 (\overline{C}_{i,j}^e - \overline{C}_{i,j}^p) \end{aligned} \quad (4.11)$$

$$(1 - \alpha) \theta_v \frac{\partial \overline{C}_{i,j}^e}{\partial t} = -\frac{(1 - \alpha) \theta_v v_l}{\Delta x} (\overline{C}_{i,j}^e - \overline{C}_{i-1,j}^e) + k_2 (\overline{C}_{i,j}^f - 2\overline{C}_{i,j}^e + \overline{C}_{i,j}^p) \quad (4.12)$$

$$\beta\theta_f \frac{\partial \overline{C_{i,j}^{f_i}}}{\partial t} = -\frac{\beta\theta_f v_l}{\Delta x} \left(\overline{C_{i,j}^{f_i}} - \overline{C_{i-1,j}^{f_i}} \right) - k_1 \left(\overline{C_{i,j}^{f_i}} - \overline{C_{i,j}^p} \right) \quad (4.13)$$

$$(1 - \beta)\theta_f \frac{\partial \overline{C_{i,j}^{f_d}}}{\partial t} = -\frac{(1 - \beta)\theta_f v_l}{\Delta x} \left(\overline{C_{i,j}^{f_d}} - \overline{C_{i-1,j}^{f_d}} \right) - k_2 \left(\overline{C_{i,j}^{f_d}} - \overline{C_{i,j}^e} \right) \quad (4.14)$$

In the discretized equations, bed velocity is out of the derivative, once this term is constant throughout the equipment. Although the fifth general assumption (section 3.3) leads to a constant percolating velocity in the sugarcane bed (as discussed in subsection 3.6.1), v_p is kept inside the derivative in the Eq 4.11. Such approach makes possible to vary this velocity across the bed height. In this sense, a percolating velocity profile may be considered during the solution procedure of the model equations. At the current version of the model, it is worth to stress that such profile is an external element of the model. This current external characteristic means that the profile is not generated by any internal equation of the model. However, the previous phrase may not be hold for future versions of the model. In this future scenario, the current configuration of the model (*i.e.*, v_p inside the derivative) will make easier the integration with the procedure in charge of generating the percolating velocity profile.

The transient state of the operational variables propagates in the bed with different velocities. Some of these variables propagates with velocities presenting the same magnitude of the bed velocity. Therefore, distinct parts of the bed sense the transient state of such variables in different periods of time. In this scenario, the large dimensions of a moving-bed diffuser works towards making such phenomenon even more pronounced. As a requirement, the solution procedure of the model must take into account the propagation of the operational variables that present such transient behavior. In this sense, the following two sections will discuss the transient behavior of two variables that presents a propagation velocity with the same magnitude of the bed velocity: bed height and percolating velocity. The final intention of these sections is to demonstrate the strategies applied in this study to consider the transient behavior of these variables in the solution procedure.

4.2 Bed height at transient state

In relation to the bed height, the transient state propagates in the system with a velocity equal to the bed velocity. For sake of illustration, Figure 4.2-(a) presents a sugarcane bed operating with a bed velocity V_1 and a bed height H_1 . If the velocity of the conveyor system that moves the bed is increased for a new value, V_2 , the whole bed sense this change equally and immediately. Even in the presence of some inertial effects, one is allowed to say that a velocity variation propagates in the bed with infinite velocity. Variations in the bed height, however, are not sense equally and immediately by the whole sugarcane bed (Figure 4.2-(b)). Provided that the amount of sugarcane fed into the diffuser is kept constant, an increase in the bed velocity promotes a decrease in the bed height that starts at the entrance of the diffuser. It is formed then a transient region that separates the bed into two zones: one with a new height and other with the old height (H_2 and H_1 , respectively). Such transient region propagates along the equipment with the same velocity of the bed until the whole system is at the new height (Figure 4.2-(c)). The same transient behavior happens to an increase of the bed height (Figure 4.3).

Assuming a constant sugarcane feed, the formation of the transient region is a consequence of the acceleration procedure that changes the velocity of the bed. In this sense, the zone presenting the new bed height (“New height” zones in Figures 4.2-(b) and 4.3) may be recognized as a region with fibers that entered the diffuser after the acceleration procedure. Moreover, the width of the transient region holds a directly proportional relation with the extent of the acceleration procedure. Therefore, faster acceleration processes make the width of the transient region decrease, thus leading to abrupt variations of the bed height. Despite the use of the word *propagation*, the transient region should not be understood as a type of “wave” that moves throughout the bed and performs the variation of the height. The term propagation is valid only for a static referential, in which an observer sees the variation of the height in fixed points of the bed as function of time. In fact, regarding a referential with the same velocity of the bed, the transient region is formed at the entrance of the diffuser and carried along the equipment by the bed motion.

So far, the formation of the transient regions was related with changes in the bed velocity. Other operational conditions, however, influence the formation of such transition regions. During operation, changes in the rate in which sugarcane is fed into the diffuser lead to variations in the bed height. Such variations take place also at the entrance of the diffuser, thus forming a transient region that propagates with the bed velocity to the remain

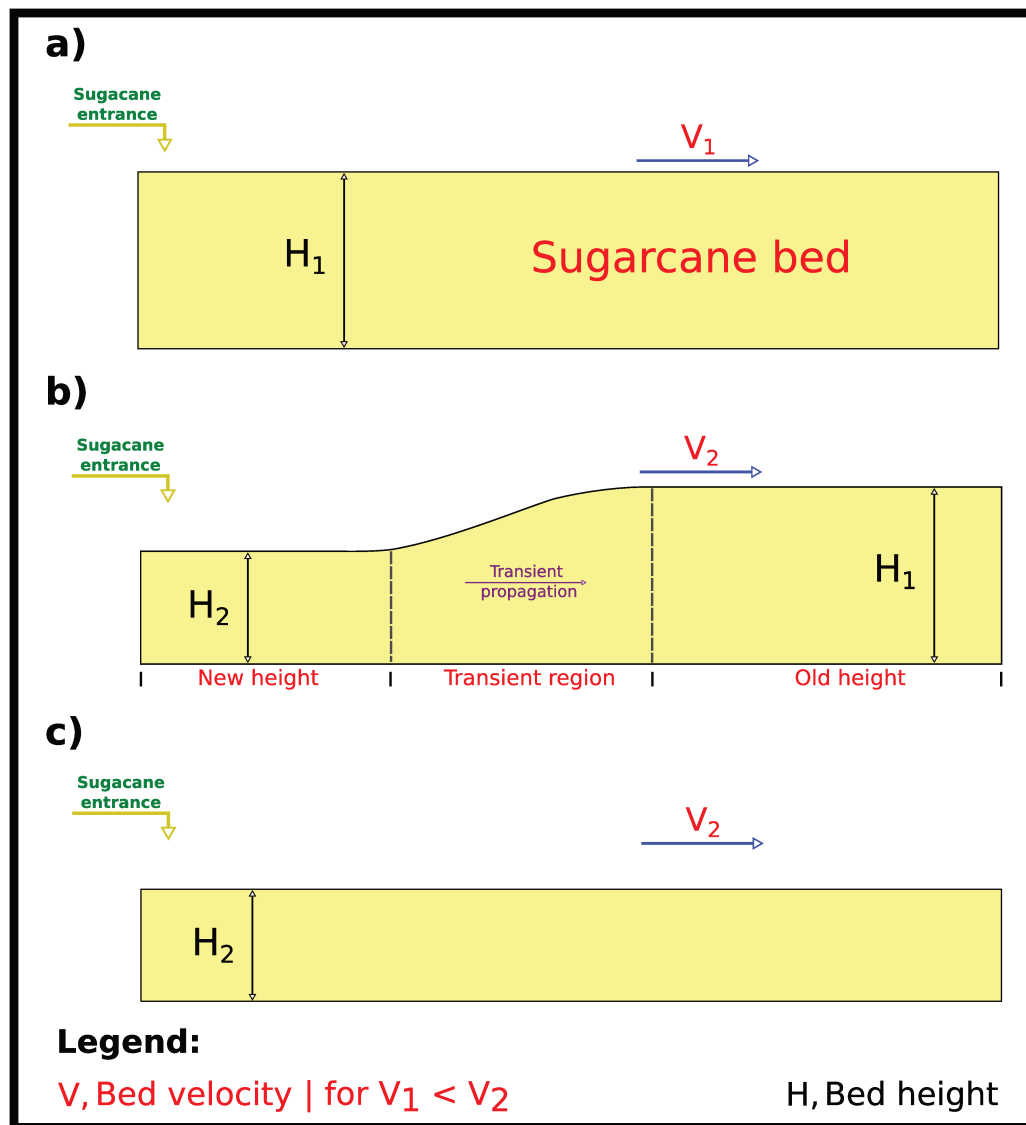


Figure 4.2: Schematic representation of the variation in the bed height promoted by an increase in the bed velocity. (a) A diffuser initially operating with a bed velocity V_1 and a bed height H_1 . (b) Bed velocity is increased to V_2 , but keeping the same amount of sugarcane fed into the equipment. It is formed three distinct regions in the bed: new and old height zones surrounding a transient region that propagates in the same sense of the bed velocity. (c) A new steady-state operational condition with bed height H_2 and bed velocity V_2 .

of the equipment. The width of the transient region has a directly proportional relation with the time required to change the rate in which sugarcane is fed into the equipment. Compaction effects may also promote variations in the bed height during the operation. In this case, the width of the transient regions is determined by the intensity and extension of the compaction effects. Lastly, the action of the lifting screws is another source of height variations. The lifting effect generates abrupt and fast changes in the bed height, which leads

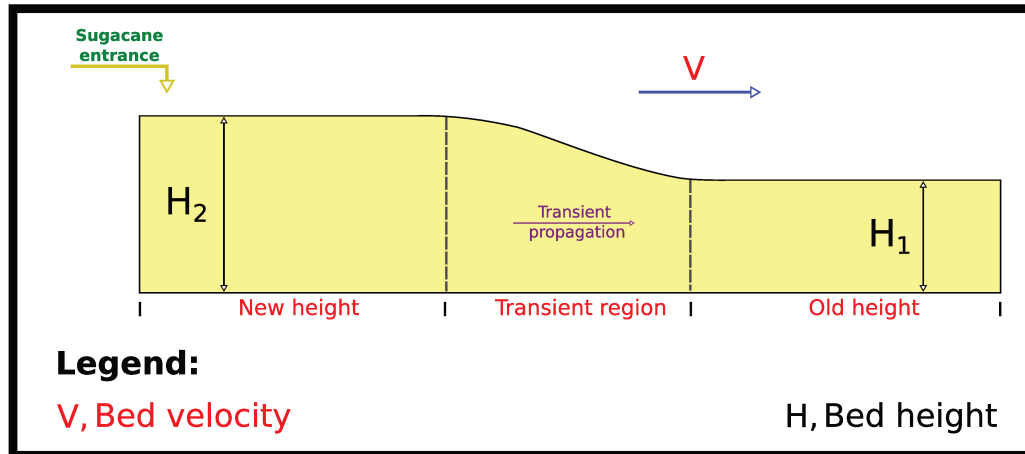


Figure 4.3: Transient behavior of the increase of the bed height.

to sharp transient regions.

4.2.1 Modifying the coordinate system

Whatever the source of the variations in the bed height, the grid has to represent an uneven bed. In the transient regions, the grid loses its orthogonality and the volumes no longer have equal size and shape (Figure 4.4-(a)). Furthermore, the grid varies as function of the time in order to capture the transient propagation of the bed height. In this variable scenario, the solution procedure has to be able to map the shape and size of the volumes in each new configuration of the grid. These mapping processes are cumbersome, thus leading to solution procedures with increased computational complexity and lower generality. The strategy used in this thesis to handle non-regular volumes bears on the fact that irregularities of the grid are characteristics of the Cartesian coordinates. Indeed, such irregularities may not be present in other coordinate systems. In principle, therefore, it is possible to describe the equations of the model in a different coordinate system in which the volumes of the grid are regular (Figure 4.4-(b)). This new coordinate system must preserve the regularity of the grid, no matter the configuration of the modeled process in Cartesian coordinates.

In order to convert the Cartesian system into the new coordinates representation, it is required the use of transformation functions (Eqs 4.15 to 4.17). Such functions translate each point in the Cartesian system, (x, z) , into a point in the new coordinates, (ψ, η) , and vice-versa. A grid representing a bed with variations in the height does not require transformations in the x -axis, once the shape and width of the volumes are constant in this direction. The

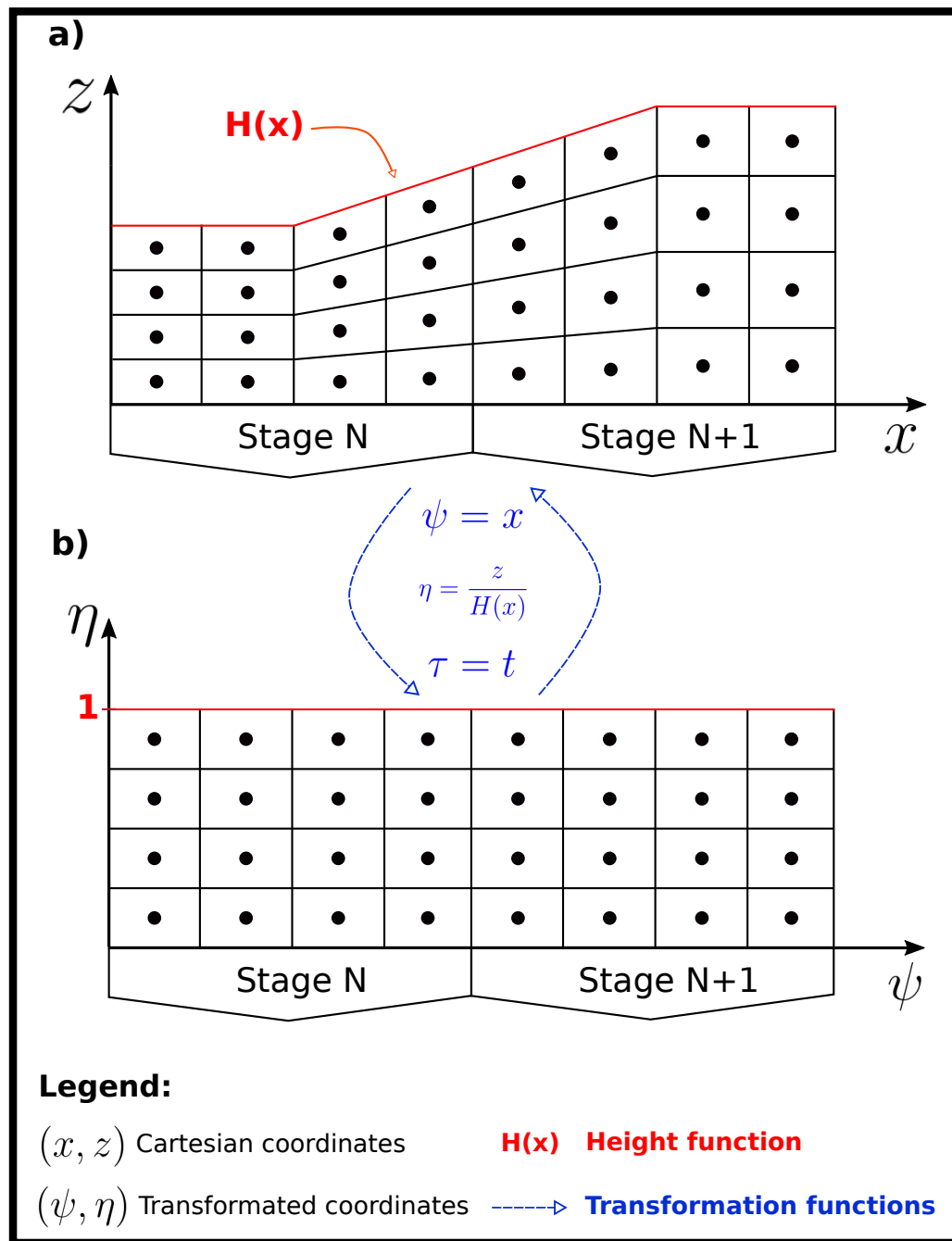


Figure 4.4: Schematic representation of the grid for two generic stages. (a) Solution grid in Cartesian coordinates presenting a non-regular grid in the transient regions. (b) Solution grid in the new coordinate system, in which the regularity of the volumes is always preserved. The blue equations are the transformation functions used to convert the Cartesian system into the new coordinates, and vice-versa.

equality in Eq 4.15 represents such absence of transformation requirements. In fact, such equality states that any change in the x direction, Δx , represents a equivalent variation

in the new coordinate system, $\Delta\psi$. In relation to the z -axis, however, a transformation is required to preserve the regularity of the volumes in the new coordinate system. The function proposed in Eq 4.16 normalize the bed height using the height distribution function $H(x)$, which relates each x position with a correspondent bed height. Therefore, the height of the bed is homogenized in the new coordinate system (*i.e.*, $H(\psi) = 1$), thus leading to a grid with regular volumes (TANNEHILL *et al.*, 1997). Eq 4.17 states an equal time relation between the two coordinate systems.

$$\psi = x \tag{4.15}$$

$$\eta = \frac{z}{H(x)} \tag{4.16}$$

$$\tau = t \tag{4.17}$$

The equations of the model were developed in Cartesian coordinates. It is required then to convert the model in order to allow it to simulate the extraction process in the new coordinate system. Such conversion must guarantee that the simulation results are equal to those that would be achieved using the Cartesian system. In other words, the model equations must lead to results that are *invariant* in relation to the chosen coordinate system. The conversion strategy applied to generate an invariant model uses methods from the tensorial calculus. It is important to stress in advance that this thesis does not intend to be a complete material concerning tensorial analysis. In fact, the following discussion will focus only on aspects of the theory that are considered relevant for the comprehension of the conversion procedure of the model. A more interested reader may find a complete material about tensorial calculus in SANCHEZ FILHO (2016), GRINFELD (2013), and, in a less extent, MALISKA, (2012)

4.2.2 An invariant model

The tensorial calculus is a set of mathematical techniques that acknowledges the importance of a coordinate system and, simultaneously, avoids selecting a particular coordinate for as long as possible (GRINFELD, 2013). These techniques leads to analytical expressions that are valid in all coordinate systems at the same time. In oder to achieve such invari-

ant behavior, the tensorial methodology uses metrics that converts a given expression into a generic coordinate system. By doing so, the generic scheme has all the advantages of a coordinate system (*i.e.*, clear correspondence between geometry and algebra), without facing the drawbacks of a particular coordinate system (*e.g.* irregular volumes). The conversion metrics are responsible to transmit the geometric and time characteristics of a specific coordinate to the generic scheme of coordinates. This geometric consistency guarantees that the results simulated by the model in the Cartesian coordinates are equal to those achieved in the generic scheme.

It is valid to stress that the generic coordinates may represent any coordinate system, even the one proposed in Figure 4.4-(b) and described by the Eqs 4.15 to 4.17. In this case, the conversion metrics will describe the geometric and time relations between the Cartesian system, (x,z) , and the new coordinates, (ψ,η) . In two dimension, there are six metrics to convert an expression into the new coordinates (Eqs 4.18 to 4.23). These metrics relate changes in the Cartesian system with variations in the (ψ, η) coordinates. Moreover, the time metrics (*i.e.*, ψ_t and η_t) are responsible to translate the motion of the grid in the Cartesian coordinates to the new coordinates system.

$$\psi_x = \frac{\partial \psi}{\partial x} \quad (4.18)$$

$$\psi_z = \frac{\partial \psi}{\partial z} \quad (4.19)$$

$$\eta_x = \frac{\partial \eta}{\partial x} \quad (4.20)$$

$$\eta_z = \frac{\partial \eta}{\partial z} \quad (4.21)$$

$$\psi_t = \frac{\partial \psi}{\partial t} \quad (4.22)$$

$$\eta_t = \frac{\partial \eta}{\partial t} \quad (4.23)$$

Another important element of the coordinate conversion is the Jacobian of the transformation, J , presented in Eq 4.24. The operator “**det**” stands for the determinant of the given matrix.

$$J = \det \begin{bmatrix} \psi_x & \psi_z \\ \eta_x & \eta_z \end{bmatrix} \quad (4.24)$$

The conversion of the model (Eqs 3.19 to 3.22) using the metrics presented above is going to be illustrate for the sucrose balance in the percolating liquid (Eq 3.19). The three other equations are converted following a similar procedure, thus only the final form of these expressions are going to be presented at the end of this subsection. Eq 3.19 is rearranged in order to assemble the terms with equal derivative (Eq 4.25).

$$\begin{aligned} \alpha\theta_v \frac{\partial \bar{C}^p}{\partial t} + \alpha\theta_v \frac{\partial}{\partial x} \left(v_b \bar{C}^p - \frac{\partial \Omega_x \bar{C}^p}{\partial x} \right) + \alpha\theta_v \frac{\partial}{\partial z} \left(v_p \bar{C}^p - \frac{\partial \Omega_z \bar{C}^p}{\partial z} \right) \\ = k_1 (\bar{C}^{f_i} - \bar{C}^p) + k_2 (\bar{C}^e - \bar{C}^p) \end{aligned} \quad (4.25)$$

It is proposed four expression (Eqs 4.26 to 4.29) in order to simplify Eq 4.25. Such simplification has the intention to reduce the size of this expression to allow a better visualization of the conversion procedure.

$$Q = \bar{C}^p \quad (4.26)$$

$$L = v_b \bar{C}^p - \frac{\partial \Omega_x \bar{C}^p}{\partial x} \quad (4.27)$$

$$M = v_p \bar{C}^p - \frac{\partial \Omega_z \bar{C}^p}{\partial z} \quad (4.28)$$

$$S = k_1 (\bar{C}^{f_i} - \bar{C}^p) + k_2 (\bar{C}^e - \bar{C}^p) \quad (4.29)$$

Substituting these simplifications in Eq 4.25 leads to a more concise equation (Eq 4.30).

$$\alpha\theta_v \frac{\partial Q}{\partial t} + \alpha\theta_v \frac{\partial L}{\partial x} + \alpha\theta_v \frac{\partial M}{\partial z} = S \quad (4.30)$$

The *chain rule* is applied to translate the partial derivatives into the new coordinate system, as demonstrate in Eqs 4.31 and 4.33. It is worthwhile to highlight the presence of the four conversion metrics in these two expressions.

$$\frac{\partial Q}{\partial t} = \frac{\partial Q}{\partial \psi} \cdot \frac{\partial \psi}{\partial t} + \frac{\partial Q}{\partial \eta} \cdot \frac{\partial \eta}{\partial t} + \frac{\partial Q}{\partial \tau} \cdot \frac{\partial \tau}{\partial t} = \frac{\partial Q}{\partial \psi} \cdot \psi_t + \frac{\partial Q}{\partial \eta} \cdot \eta_t + \frac{\partial Q}{\partial \tau} \cdot 1 \quad (4.31)$$

$$\frac{\partial L}{\partial x} = \frac{\partial L}{\partial \psi} \cdot \frac{\partial \psi}{\partial x} + \frac{\partial L}{\partial \eta} \cdot \frac{\partial \eta}{\partial x} + \frac{\partial L}{\partial \tau} \cdot \frac{\partial \tau}{\partial x} = \frac{\partial L}{\partial \psi} \cdot \psi_x + \frac{\partial L}{\partial \eta} \cdot \eta_x \quad (4.32)$$

$$\frac{\partial M}{\partial z} = \frac{\partial M}{\partial \psi} \cdot \frac{\partial \psi}{\partial z} + \frac{\partial M}{\partial \eta} \cdot \frac{\partial \eta}{\partial z} + \frac{\partial M}{\partial \tau} \cdot \frac{\partial \tau}{\partial z} = \frac{\partial M}{\partial \psi} \cdot \psi_z + \frac{\partial M}{\partial \eta} \cdot \eta_z \quad (4.33)$$

The term $\frac{\partial \tau}{\partial t}$ in equation 4.31 is equal to “1” according to Eq 4.17. Moreover, the red terms in Eqs 4.32 and 4.33 are equal to zero, since time is not dependent on the space coordinates. Introducing the chain rule expressions into Eq 4.30 and dividing all terms by the Jacobian of the transformation lead to Eq 4.34.

$$\begin{aligned} \frac{\alpha \theta_v}{J} \frac{\partial Q}{\partial \tau} + \alpha \theta_v \left(\frac{\partial Q}{\partial \psi} \cdot \frac{\psi_t}{J} + \frac{\partial Q}{\partial \eta} \cdot \frac{\eta_t}{J} \right) + \alpha \theta_v \left(\frac{\partial L}{\partial \psi} \cdot \frac{\psi_x}{J} + \frac{\partial L}{\partial \eta} \cdot \frac{\eta_x}{J} \right) \\ + \alpha \theta_v \left(\frac{\partial M}{\partial \psi} \cdot \frac{\psi_z}{J} + \frac{\partial M}{\partial \eta} \cdot \frac{\eta_z}{J} \right) = \frac{S}{J} \end{aligned} \quad (4.34)$$

The conversion metrics and the Jacobian are out of the derivative terms. In order to achieve a conservative equation, it is required that the metrics and Jacobian become part of the derivative procedure. The strategy applied to accomplish this requirement is based on the approach proposed by MALISKA (2012). This approach inserts those elements into the derivatives by means of restoring the derivative of a product. In this sense, it is added and subtracted in Eq 4.34 the terms presented in Eq 4.35.

$$Q \frac{\partial \psi_t J^{-1}}{\partial \psi}, \quad Q \frac{\partial \eta_t J^{-1}}{\partial \eta}, \quad L \frac{\partial \psi_x J^{-1}}{\partial \psi}, \quad L \frac{\partial \eta_x J^{-1}}{\partial \eta}, \quad M \frac{\partial \psi_z J^{-1}}{\partial \psi}, \quad M \frac{\partial \eta_z J^{-1}}{\partial \eta} \quad (4.35)$$

The resulting expression is presented in Eq 4.36.

$$\begin{aligned}
& \frac{\alpha\theta_v}{J} \frac{\partial Q}{\partial \tau} + \alpha\theta_v \frac{\partial Q}{\partial \psi} \frac{\psi_t J^{-1}}{\partial \psi} + \alpha\theta_v \frac{\partial Q}{\partial \eta} \frac{\eta_t J^{-1}}{\partial \eta} + \alpha\theta_v \frac{\partial L}{\partial \psi} \frac{\psi_x J^{-1}}{\partial \psi} + \alpha\theta_v \frac{\partial L}{\partial \eta} \frac{\eta_x J^{-1}}{\partial \eta} \\
& + \alpha\theta_v \frac{\partial M}{\partial \psi} \frac{\psi_z J^{-1}}{\partial \psi} + \alpha\theta_v \frac{\partial M}{\partial \eta} \frac{\eta_z J^{-1}}{\partial \eta} - \alpha\theta_v L \left(\frac{\partial \psi_x J^{-1}}{\partial \psi} + \frac{\partial \eta_x J^{-1}}{\partial \eta} \right) \\
& - \alpha\theta_v M \left(\frac{\partial \psi_z J^{-1}}{\partial \psi} + \frac{\partial \eta_z J^{-1}}{\partial \eta} \right) - \alpha\theta_v Q \left(\frac{\partial \psi_t J^{-1}}{\partial \psi} + \frac{\partial \eta_t J^{-1}}{\partial \eta} \right) = \frac{S}{J}
\end{aligned} \tag{4.36}$$

The red terms in Eq 4.36 are equal to zero. The proof for the previous assertion may be found at Figure 4.5. The green term is also equal to zero, which may be proved by using the relations deduced at Figure 4.5 and the following equations:

$$\psi_t = -\psi_x x_\tau - \psi_z z_\tau \tag{4.37}$$

$$\eta_t = -\eta_x x_\tau - \eta_z z_\tau \tag{4.38}$$

The elements Q , L , M , and S are no longer necessary in their lumped form, thus Eqs 4.26 to 4.29 are substituted in Eq 4.36. After some rearrangements, it is obtained the Eq 4.39.

$$\begin{aligned}
& \frac{\alpha\theta_v}{J} \frac{\partial \bar{C}^p}{\partial \tau} + \alpha\theta_v \frac{\partial}{\partial \psi} (\bar{C}^p J^{-1} [\psi_t + v_b \psi_x + v_p \psi_z]) + \alpha\theta_v \frac{\partial}{\partial \eta} (\bar{C}^p J^{-1} [\eta_t + v_b \eta_x + v_p \eta_z]) \\
& - \alpha\theta_v \frac{\partial}{\partial \psi} \left(\psi_x J^{-1} \frac{\partial \Omega_x \bar{C}^p}{\partial x} + \psi_z J^{-1} \frac{\partial \Omega_z \bar{C}^p}{\partial z} \right) \\
& - \alpha\theta_v \frac{\partial}{\partial \eta} \left(\eta_x J^{-1} \frac{\partial \Omega_x \bar{C}^p}{\partial x} + \eta_z J^{-1} \frac{\partial \Omega_z \bar{C}^p}{\partial z} \right) \\
& = k_1 J^{-1} (\bar{C}^{f1} - \bar{C}^p) + k_2 J^{-1} (\bar{C}^e - \bar{C}^p)
\end{aligned} \tag{4.39}$$

Eq 4.39 still present partial derivatives in the (x, z) system. Such derivatives are converted to the new coordinates by also applying the chain rule (Eqs 4.40 and 4.41).

$$\frac{\partial \Omega_x \bar{C}^p}{\partial x} = \frac{\partial \Omega_x \bar{C}^p}{\partial \psi} \cdot \psi_x + \frac{\partial \Omega_x \bar{C}^p}{\partial \eta} \cdot \eta_x \tag{4.40}$$

The transformation functions between the coordinate systems may be defined in a generic way by the following equations:

New coordinates	Cartesian coordinates
$\psi = \psi(x, z)$	$x = x(\psi, \eta)$
$\eta = \eta(x, z)$	$z = z(\psi, \eta)$

Derivating these equations yields
(in matrix form) the expressions below:

$\begin{bmatrix} d\psi \\ d\eta \end{bmatrix} = \underbrace{\begin{bmatrix} \psi_x & \psi_z \\ \eta_x & \eta_z \end{bmatrix}}_A \begin{bmatrix} dx \\ dz \end{bmatrix}$	$\begin{bmatrix} dx \\ dz \end{bmatrix} = \underbrace{\begin{bmatrix} x_\psi & x_\eta \\ z_\psi & z_\eta \end{bmatrix}}_B \begin{bmatrix} d\psi \\ d\eta \end{bmatrix}$
---	---

The symmetry of these expressions leads to two important relations
between the conversion metrics:

$A = \underbrace{B^{-1}}$	and	$\det[A] = J = \frac{1}{\det[B]}$
\downarrow	Where	$B^{-1} = J \begin{bmatrix} z_\eta & -x_\eta \\ -z_\psi & x_\psi \end{bmatrix}$

Comparing A with B^{-1} , it is straightforward to find the following relations:

$\psi_x = J \cdot z_\eta$	$\eta_x = -J \cdot z_\psi$
$\psi_z = -J \cdot x_\eta$	$\eta_z = J \cdot x_\psi$

Substituting the above relations in the red terms of Eq 4.36 makes
those terms equal to zero. The J in the relations is canceled with
those in the denominator of the red terms.

Figure 4.5: Proof for the zero value of the red terms in the Eq 4.36.

$$\frac{\partial \Omega_z \bar{C}^p}{\partial z} = \frac{\partial \Omega_z \bar{C}^p}{\partial \psi} \cdot \psi_z + \frac{\partial \Omega_z \bar{C}^p}{\partial \eta} \cdot \eta_z \quad (4.41)$$

Substituting Eqs 4.40 and 4.41 in Eq 4.39 and performing some rearrangements lead to the final form of the sucrose balance of the percolating liquid in the new coordinates (Eq 4.42).

$$\begin{aligned}
& \frac{\alpha\theta_v}{J} \frac{\partial \bar{C}^p}{\partial \tau} + \alpha\theta_v \frac{\partial}{\partial \psi} \left(\bar{C}^p J^{-1} [\psi_t + v_b \psi_x + v_p \psi_z] \right) + \alpha\theta_v \frac{\partial}{\partial \eta} \left(\bar{C}^p J^{-1} [\eta_t + v_b \eta_x + v_p \eta_z] \right) \\
& - \alpha\theta_v \frac{\partial}{\partial \psi} \left(\psi_x^2 J^{-1} \frac{\partial \Omega_x \bar{C}^p}{\partial \psi} + \psi_z^2 J^{-1} \frac{\partial \Omega_z \bar{C}^p}{\partial \psi} \right) \\
& - \alpha\theta_v \frac{\partial}{\partial \eta} \left(\eta_x^2 J^{-1} \frac{\partial \Omega_x \bar{C}^p}{\partial \eta} + \eta_z^2 J^{-1} \frac{\partial \Omega_z \bar{C}^p}{\partial \eta} \right) \quad (4.42) \\
& - \alpha\theta_v \frac{\partial}{\partial \psi} \left(2\psi_x \eta_x J^{-1} \frac{\partial \Omega_x \bar{C}^p}{\partial \eta} + 2\psi_z \eta_z J^{-1} \frac{\partial \Omega_z \bar{C}^p}{\partial \eta} \right) \\
& = k_1 J^{-1} \left(\bar{C}^{fi} - \bar{C}^p \right) + k_2 J^{-1} \left(\bar{C}^e - \bar{C}^p \right)
\end{aligned}$$

Applying the same procedure to the three other equations of the model (Eqs 3.20 to 3.22) yields the Eqs 4.43 to 4.45, all of them in the new coordinates.

$$\begin{aligned}
& \frac{(1-\alpha)\theta_v}{J} \frac{\partial \bar{C}^e}{\partial \tau} + (1-\alpha)\theta_v \frac{\partial}{\partial \psi} \left(\bar{C}^e J^{-1} [\psi_t + v_b \psi_x] \right) \\
& + (1-\alpha)\theta_v \frac{\partial}{\partial \eta} \left(\bar{C}^e J^{-1} [\eta_t + v_b \eta_x] \right) = k_2 J^{-1} \left(\bar{C}^{fa} - 2\bar{C}^e + \bar{C}^p \right) \quad (4.43)
\end{aligned}$$

$$\begin{aligned}
& \frac{\beta\theta_f}{J} \frac{\partial \bar{C}^{fi}}{\partial t} + \beta\theta_f \frac{\partial}{\partial \psi} \left(\bar{C}^{fi} J^{-1} [\psi_t + v_b \psi_x] \right) \\
& + \beta\theta_f \frac{\partial}{\partial \eta} \left(\bar{C}^{fi} J^{-1} [\eta_t + v_b \eta_x] \right) = -k_1 J^{-1} \left(\bar{C}^{fi} - \bar{C}^p \right) \quad (4.44)
\end{aligned}$$

$$\begin{aligned}
& \frac{(1-\beta)\theta_f}{J} \frac{\partial \bar{C}^{fa}}{\partial t} + (1-\beta)\theta_f \frac{\partial}{\partial \psi} \left(\bar{C}^{fa} J^{-1} [\psi_t + v_b \psi_x] \right) \\
& + (1-\beta)\theta_f \frac{\partial}{\partial \eta} \left(\bar{C}^{fa} J^{-1} [\eta_t + v_b \eta_x] \right) = -k_2 J^{-1} \left(\bar{C}^{fa} - \bar{C}^p \right) \quad (4.45)
\end{aligned}$$

The geometrical conversion metrics may be computed analytically by applying Eqs 4.18 to 4.21 in the transformation functions (Eqs 4.15 and 4.16). In relation to the proposed transformation, therefore, the geometrical metrics are presented in Eqs 4.46 to 4.49.

$$\psi_x = \frac{\partial \psi}{\partial x} = \frac{\partial x}{\partial x} = 1 \quad (4.46)$$

$$\psi_z = \frac{\partial \psi}{\partial z} = \frac{\partial x}{\partial z} = 0 \quad (4.47)$$

$$\eta_x = \frac{\partial \eta}{\partial x} = \frac{\partial Z.H(x)^{-1}}{\partial x} = -\frac{Z}{H(x)^2} \cdot \frac{\partial H(x)}{\partial x} \quad (4.48)$$

$$\eta_z = \frac{\partial \eta}{\partial z} = \frac{\partial Z.H(x)^{-1}}{\partial z} = \frac{1}{H(x)} \quad (4.49)$$

The time conversion metrics are computed using Eqs 4.37 and 4.38. A change in the bed height promotes only vertical variations in the grid. This fact and Eq 4.47 lead to Eq 4.50. It is important to highlight that this study follows an Eulerian approach and a static referential to develop the model equations (see section 3.2). Therefore, the grid is assumed fixed in the horizontal direction and the bed motion is interpreted as a horizontal convective flux of the percolating liquid. Regarding the η direction, the time metric is presented by Eq 4.51. The approach used to compute z_τ is detailed at Figure 4.6.

$$\psi_t = 0 \quad (4.50)$$

$$\eta_t = -\eta_z z_\tau = -\frac{1}{H(x)} \cdot \frac{\partial Z}{\partial \tau} = -\frac{1}{H(x)} \cdot \frac{\partial Z}{\partial t} \quad (4.51)$$

At least, the Jacobian of such transformation is calculated in Eq 4.52.

$$J = \det \begin{bmatrix} \psi_x & \psi_z \\ \eta_x & \eta_z \end{bmatrix} = \det \begin{bmatrix} 1 & 0 \\ -\frac{Z}{H(x)^2} \cdot \frac{\partial H(x)}{\partial x} & \frac{1}{H(x)} \end{bmatrix} = \frac{1}{H(x)} \quad (4.52)$$

4.2.3 Invariant mathematical model in the discretized form

The invariant mathematical model was discretized also by the *Finite volumes method*, following the procedures described in section 4.1. Convective and dispersion terms are likewise approximated by the up-wind and central differences schemes, respectively. Integration of the cross derivative terms (*i.e.*, $\frac{\partial}{\partial \psi} \frac{\partial}{\partial \eta}$) leads to the requirement of computing “ $\frac{\partial}{\partial \eta}$ ” on both

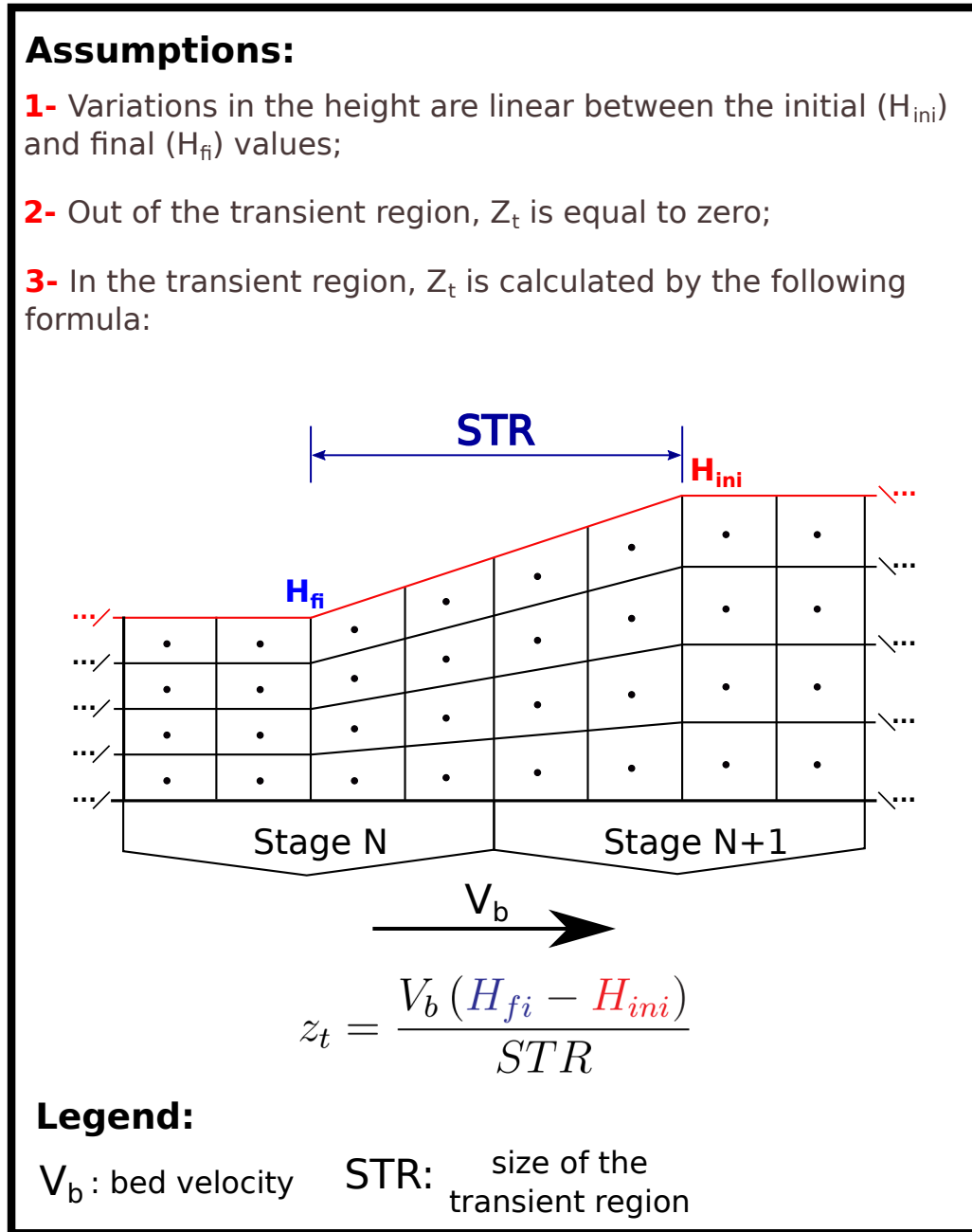


Figure 4.6: Approach used in this thesis to compute z_τ in the model equations.

West and East faces of the volumes. In this sense, the central difference scheme of these cross terms are computed in accordance with the following two equations:

$$\left. \frac{\partial \bar{C}^p}{\partial \eta} \right|_w = \frac{\bar{C}_{i,j-1}^p + \bar{C}_{i-1,j-1}^p - \bar{C}_{i,j+1}^p - \bar{C}_{i-1,j+1}^p}{4\Delta\eta} \quad (4.53)$$

$$\left. \frac{\partial \bar{C}^p}{\partial \eta} \right|_e = \frac{\bar{C}_{i,j-1}^p + \bar{C}_{i+1,j-1}^p - \bar{C}_{i,j+1}^p - \bar{C}_{i+1,j+1}^p}{4\Delta\eta} \quad (4.54)$$

Therefore, Eqs 4.55 to 4.58 present the invariant model equations in the discretized form. The metrics ψ_x and ψ_z are already substituted in these equations. It is interesting to notice that the terms of these equations reduces to those in the Cartesian coordinates (*i.e.*, original model) for a system without height variation.

$$\begin{aligned} \alpha\theta_v J_{i,j}^{-1} \frac{\partial \bar{C}_{i,j}^p}{\partial t} &= -\frac{\alpha\theta_v v_b}{\Delta\psi} (\bar{C}_{i,j}^p J_{i,j}^{-1} - \bar{C}_{i-1,j}^p J_{i-1,j}^{-1}) \\ &\quad -\frac{\alpha\theta_v}{\Delta\eta} (\bar{C}_{i,j}^p J_{i,j}^{-1} \eta_t - \bar{C}_{i,j-1}^p J_{i,j-1}^{-1} \eta_t) \\ &\quad -\frac{\alpha\theta_v v_b}{\Delta\eta} (\bar{C}_{i,j}^p J_{i,j}^{-1} \eta_{x|i,j} - \bar{C}_{i,j-1}^p J_{i,j-1}^{-1} \eta_{x|i,j-1}) \\ &\quad -\frac{\alpha\theta_v}{\Delta\eta} (v_{p|i,j} \bar{C}_{i,j}^p J_{i,j}^{-1} \eta_{z|i,j} - v_{p|i,j-1} \bar{C}_{i,j-1}^p J_{i,j-1}^{-1} \eta_{z|i,j-1}) \\ &\quad +\frac{\alpha\theta_v \Omega_x}{\Delta\psi^2} (\bar{C}_{i+1,j}^p J_e^{-1} - \bar{C}_{i,j}^p [J_e^{-1} + J_w^{-1}] + \bar{C}_{i-1,j}^p J_w^{-1}) \\ &\quad +\frac{\alpha\theta_v \Omega_x}{\Delta\eta^2} (\bar{C}_{i,j+1}^p J_s^{-1} \eta_{x|s}^2 - \bar{C}_{i,j}^p [J_s^{-1} \eta_{x|s}^2 + J_n^{-1} \eta_{x|n}^2] + \bar{C}_{i,j-1}^p J_n^{-1} \eta_{x|n}^2) \\ &\quad +\frac{\alpha\theta_v \Omega_z}{\Delta\eta^2} (\bar{C}_{i,j+1}^p J_s^{-1} \eta_{z|s}^2 - \bar{C}_{i,j}^p [J_s^{-1} \eta_{z|s}^2 + J_n^{-1} \eta_{z|n}^2] + \bar{C}_{i,j-1}^p J_n^{-1} \eta_{z|n}^2) \\ &\quad +\frac{\alpha\theta_v \Omega_x}{2\Delta\psi\Delta\eta} (\bar{C}_{i,j-1}^p [\eta_{x|e} J_e^{-1} - \eta_{x|w} J_w^{-1}] + \bar{C}_{i+1,j-1}^p \eta_{x|e} J_e^{-1} \\ &\quad -\bar{C}_{i,j+1}^p [\eta_{x|e} J_e^{-1} - \eta_{x|w} J_w^{-1}] - \bar{C}_{i+1,j+1}^p \eta_{x|e} J_e^{-1} - \bar{C}_{i-1,j-1}^p \eta_{x|w} J_w^{-1} \\ &\quad +\bar{C}_{i-1,j+1}^p \eta_{x|w} J_w^{-1}) + k_1 J_{i,j}^{-1} (\bar{C}_{i,j}^{f1} - \bar{C}_{i,j}^p) + k_2 J_{i,j}^{-1} (\bar{C}_{i,j}^e - \bar{C}_{i,j}^p) \end{aligned} \quad (4.55)$$

$$\begin{aligned} (1-\alpha)\theta_v J_{i,j}^{-1} \frac{\partial \bar{C}_{i,j}^e}{\partial t} &= -\frac{(1-\alpha)\theta_v v_b}{\Delta\psi} (\bar{C}_{i,j}^e J_{i,j}^{-1} - \bar{C}_{i-1,j}^e J_{i-1,j}^{-1}) \\ &\quad -\frac{(1-\alpha)\theta_v}{\Delta\eta} (\bar{C}_{i,j}^e J_{i,j}^{-1} \eta_{t|i,j} - \bar{C}_{i,j-1}^e J_{i,j-1}^{-1} \eta_{t|i,j-1}) \\ &\quad -\frac{(1-\alpha)\theta_v v_b}{\Delta\eta} (\bar{C}_{i,j}^e J_{i,j}^{-1} \eta_{x|i,j} - \bar{C}_{i,j-1}^e J_{i,j-1}^{-1} \eta_{x|i,j-1}) \\ &\quad +k_2 J_{i,j}^{-1} (\bar{C}_{i,j}^{fd} - 2\bar{C}_{i,j}^e + \bar{C}_{i,j}^p) \end{aligned} \quad (4.56)$$

$$\begin{aligned}
\beta\theta_f J_{i,j}^{-1} \frac{\partial \bar{C}_{i,j}^{fi}}{\partial t} &= -\frac{\beta\theta_f v_b}{\Delta\psi} \left(\bar{C}_{i,j}^{fi} J_{i,j}^{-1} - \bar{C}_{i-1,j}^{fi} J_{i-1,j}^{-1} \right) \\
&\quad - \frac{\beta\theta_f}{\Delta\eta} \left(\bar{C}_{i,j}^{fi} J_{i,j}^{-1} \eta_{t|i,j} - \bar{C}_{i,j-1}^{fi} J_{i,j-1}^{-1} \eta_{t|i,j-1} \right) \\
&\quad - \frac{\beta\theta_f v_b}{\Delta\eta} \left(\bar{C}_{i,j}^{fi} J_{i,j}^{-1} \eta_{x|i,j} - \bar{C}_{i,j-1}^{fi} J_{i,j-1}^{-1} \eta_{x|i,j-1} \right) \\
&\quad \quad \quad - k_1 J_{i,j}^{-1} \left(\bar{C}_{i,j}^{fi} - \bar{C}_{i,j}^p \right)
\end{aligned} \tag{4.57}$$

$$\begin{aligned}
(1-\beta)\theta_f J_{i,j}^{-1} \frac{\partial \bar{C}_{i,j}^{fa}}{\partial t} &= -\frac{(1-\beta)\theta_f v_b}{\Delta\psi} \left(\bar{C}_{i,j}^{fa} J_{i,j}^{-1} - \bar{C}_{i-1,j}^{fa} J_{i-1,j}^{-1} \right) \\
&\quad - \frac{(1-\beta)\theta_f}{\Delta\eta} \left(\bar{C}_{i,j}^{fa} J_{i,j}^{-1} \eta_{t|i,j} - \bar{C}_{i,j-1}^{fa} J_{i,j-1}^{-1} \eta_{t|i,j-1} \right) \\
&\quad - \frac{(1-\beta)\theta_f v_b}{\Delta\eta} \left(\bar{C}_{i,j}^{fa} J_{i,j}^{-1} \eta_{x|i,j} - \bar{C}_{i,j-1}^{fa} J_{i,j-1}^{-1} \eta_{x|i,j-1} \right) \\
&\quad \quad \quad - k_2 J_{i,j}^{-1} \left(\bar{C}_{i,j}^{fa} - \bar{C}_{i,j}^e \right)
\end{aligned} \tag{4.58}$$

Integration of the dispersive terms introduces the requirement to compute the “ η ” metrics and the Jacobian on the volumes faces. These conversion factors are computed by the average between the values of such terms in the centers of the two nearest volumes, as presented in Eqs 4.59 to 4.68. Such approach to computed those terms are justified based on the numerical determination of the conversion factors on the frontiers of the volumes. A numerical determination uses the local shape of the grid to obtain the conversion factors on the volumes faces, not using the analytical expression presented in Eqs 4.46 to 4.52. A thorough presentation of such numerical procedure may be found at MALISKA (2012)

$$\eta_{x|w} = \frac{\eta_{x|i-1,j} + \eta_{x|i,j}}{2} \quad (4.59)$$

$$\eta_{x|e} = \frac{\eta_{x|i+1,j} + \eta_{x|i,j}}{2} \quad (4.60)$$

$$\eta_{x|n} = \frac{\eta_{x|i,j-1} + \eta_{x|i,j}}{2} \quad (4.61)$$

$$\eta_{x|s} = \frac{\eta_{x|i,j+1} + \eta_{x|i,j}}{2} \quad (4.62)$$

$$\eta_{z|n} = \frac{\eta_{z|i,j-1} + \eta_{z|i,j}}{2} \quad (4.63)$$

$$\eta_{z|s} = \frac{\eta_{z|i,j+1} + \eta_{z|i,j}}{2} \quad (4.64)$$

$$J_w = \frac{J_{i-1,j} + J_{i,j}}{2} \quad (4.65)$$

$$J_e = \frac{J_{i+1,j} + J_{i,j}}{2} \quad (4.66)$$

$$J_n = \frac{J_{i,j-1} + J_{i,j}}{2} \quad (4.67)$$

$$J_s = \frac{J_{i,j+1} + J_{i,j}}{2} \quad (4.68)$$

The new coordinate system demands the definition of additional boundary conditions. These new boundary conditions are a consequence of the extra terms that emerges in the model due to the coordinates transformation. Figure 4.7 summarizes the new configuration of boundary conditions. Regarding the percolating liquid, the cross derivative term requires the value of the derivative $\frac{\partial \bar{C}^p}{\partial \eta}$ on both west and east borders. It is assumed then a null Noumann boundary condition in these boundaries, in order to account for a isolated west frontier and a east border with a developed profile of the transported sugar. Acknowledging a correspondence between x and ψ and also between z and η , the other boundary conditions are satisfied by those already presented to the percolating liquid in the Cartesian system (Figure 3.8).

The sugar balances of the stagnant liquid and the fiber fractions in the new coordinate system requires the definition of two extra boundary conditions. On the the north face, it is assumed an isolated condition for these three bed fractions. In relation to the south border, the sugar profile is defined as developed for each of the three sugar balances. Therefore, such extra boundary conditions are represented by a null Neumann condition. Concerning the west and east borders, these three sugar balances have the same boundary conditions as

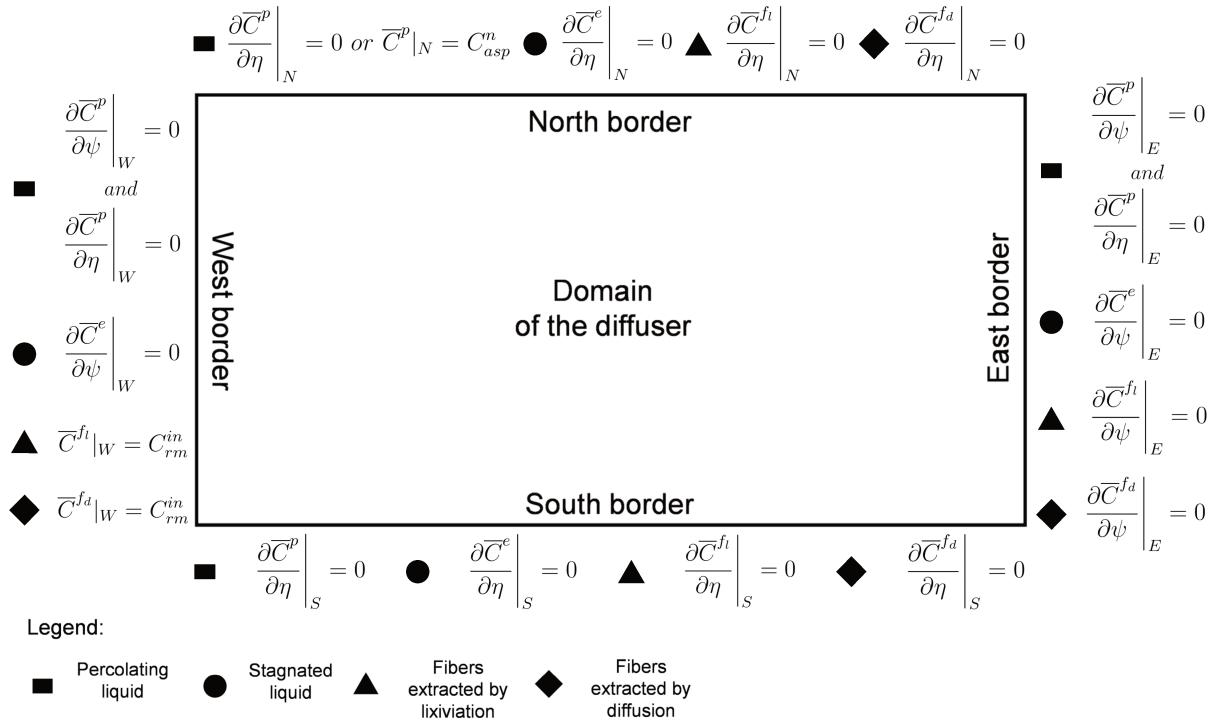


Figure 4.7: Boundary conditions for the four bed sections in the new coordinates system.

designated for the Cartesian coordinates. As done in the Cartesian scenario, all the boundary conditions are directly substituted in the discretized equations.

4.3 Percolating velocity at the transient state

The discretized form of the percolating liquid balance (either Eqs 4.11 or 4.55) allows for the variation of v_p across the bed height. Changes in the percolating velocity directly or indirectly explain the effects of several variables (e.g., imbibition rate, bed density, fiber content of sugar cane) on the extraction performance. Up to this point, however, this velocity profile was assumed static, thus being immutable along the time. Alike in the bed height scenario, a variation in the percolating velocity is not sensed by every point of the grid at the same time. Actually, a change in the percolating velocity in a given point of the grid propagates to other parts of the grid with a finite velocity. It is the intention of this section, therefore, to present how this thesis abstracts such transient phenomenon in a procedural way and how it was included in the dynamic solution of the model.

For sake of illustration, Figure 4.8 presents a schematic representation of the v_p propagation phenomenon as it is interpreted by this study. Figure 4.8-(a) shows a section of a

grid in which all volumes have initially a equal percolating velocity. At time t_1 , a modification on the percolating velocity is promoted above the volume with index “ $i, j - 2$ ”. The liquid with a new percolating velocity (red arrows) descends the grid, thus forming a propagation front (PF) (dashed red line). Such front has a velocity equal to the new percolating velocity. As PF moves downward through the volumes, the initial percolating velocity is replaced by the new value (Figure 4.8-(b)). It is assumed that a volume has its percolating velocity changed only when PF crosses the center of this very volume. In Figure 4.8-(b), for instance, PF has entered the volume with the index “ i, j ”, but not crossed the center. Therefore, the volume “ i, j ” still preserves its initial percolating velocity. After crossing the given grid section (Figure 4.8-(c)), PF leaves behind all grid volumes at the new percolating velocity configuration.

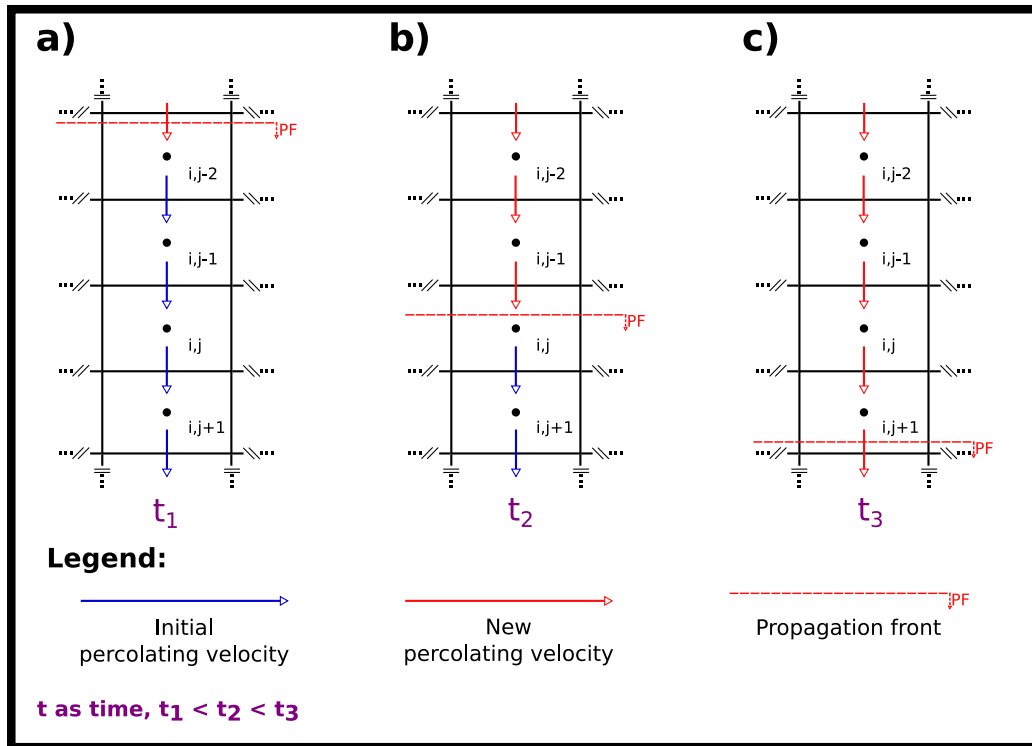


Figure 4.8: Section of a grid at three distinct times (*i.e.*, $t_1 < t_2 < t_3$). (a) Initial period when a propagation front (PF) enters in the section. (b) As PF penetrates the grid, the initial percolating velocity in the volumes is replaced by the new value. (c) Each volume in the given section presenting the new percolating velocity. It is important to highlight that this abstraction is assumed valid whatever coordinate system is considered.

It is not required modifications in the grid structure in order to describe the transient behavior of the percolating velocity. Indeed, the phenomenon presented in the previous paragraph is valid whatever coordinate system is considered. Right before the transient so-

lution, it must be defined the source of the percolating velocity variation. Such source is defined as the position in the grid where the percolating velocity is modified. As a consequence, location and extension of this source define the initial position of the percolation front. At each interaction of the transient solution, the position of PF is updated taking into account its velocity (*i.e.*, the new percolating velocity) and the integration step. Therefore, as the interactions move onward, the percolating velocity is also update in the volumes of the grid. Despite the use of the word “source” in the singular along this paragraph, the solution procedure at transient state may handle multiple sources of percolating velocity variation.

4.4 Simulation framework

The moving-bed diffuser model was computationally implemented in *Python* programming language (Figure 4.9). The discretized equations at steady state are solved using a supernodal LU factorization routine suited to handle large, sparse, nonsymmetric systems of linear algebraic equations (DEMMELE *et al.*, 1999). This routine is available in the *Scipy* library (JONES *et al.*, 2001). Dynamic simulations are performed using the classical Runge–Kutta method of 4th order of accuracy (HAIRER *et al.*, 1993) as the integration routine for the system of ODEs. In parallel with the 4th order method, the integration procedure is also performed by a first order Runge-Kutta method (*i.e.*, the Euler’s method). By comparing the 4th order solutions with the 1st order outcomes, it is possible to estimate the local errors of the integration procedure (CHAPRA and CANALE, 2008; HAIRER *et al.*, 1993).

Simulation inputs are provided by the end-user of the framework, with the intention to define the characteristics of the equipment, the operational conditions, and the processed raw material. The size of the resolution grid can also be changed. The outcomes displayed by the simulation are °Brix curve, °Brix distribution in the sugarcane bed, and extraction degree. In order to perform a simulation, an end-user does not need to interact with the solution, parameters fitting and results display routines. The practical use of the framework does not require advanced abilities related to computer programming or any knowledge on numerical methods. In fact, the simulation framework was developed to be an user-friendly tool.

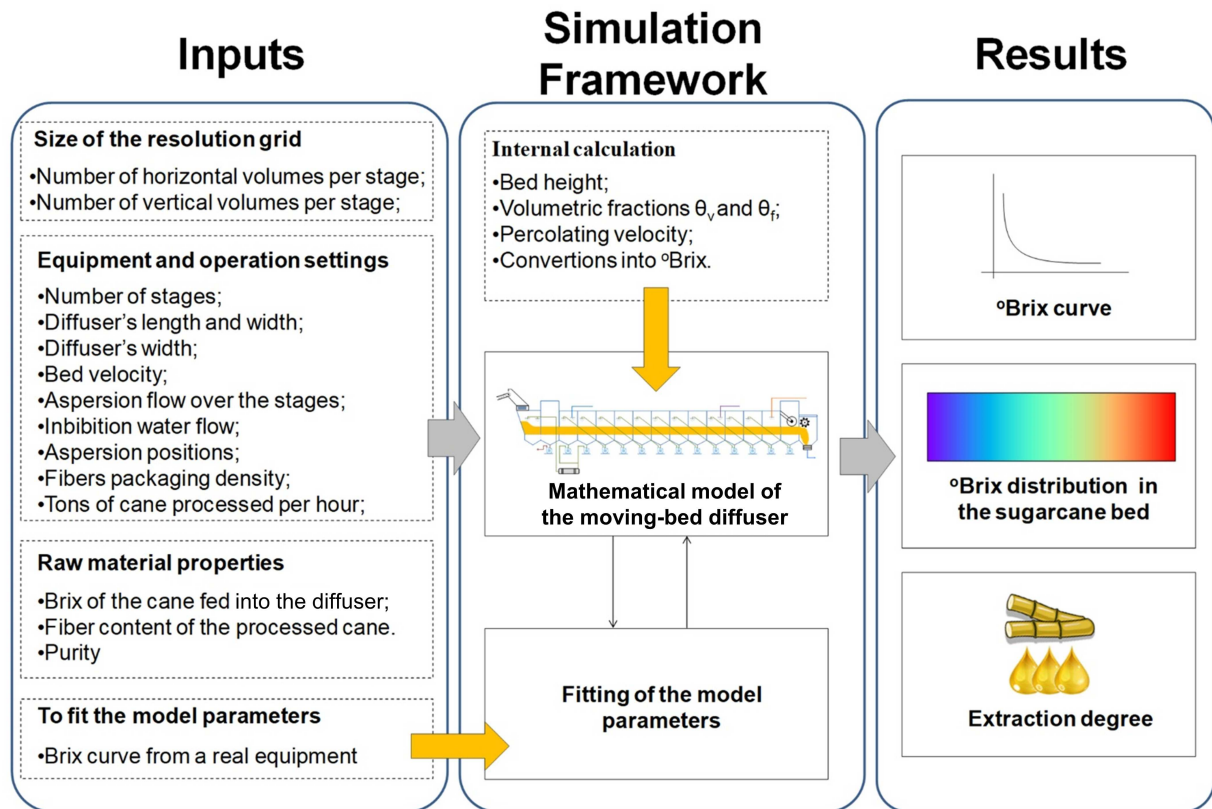


Figure 4.9: Main features of the moving-bed diffuser simulation framework.

4.4.1 Fitting model parameters

Model parameters (k_1 , k_2 , α and β) are fitted using a genetic algorithm (GA). There are a vast number of works in literature about parameters estimation using GA (*e.g.*, LI *et al.*, 2012; OTEIZA and BRIGNOLE, 2016; MARTINEZ VILLEGAS *et al.*, 2017). This procedure is a random search and optimization method based on the principle of natural selection and genetics (SASTRY *et al.*, 2014). In the simulation framework, the implementation of GA in Python programming language was performed using the *DEAP* (Distributed Evolutionary Algorithms in Python) package (FORTIN *et al.*, 2012).

In the GA algorithm implemented in this work, the initial population is generated using Latin Hypercube sampling in order to spread the candidate solutions more evenly across the searching domain. The performance criteria (*e.g.*, *fitness*) considered here measures how close the °Brix curve calculated by the model and a real °Brix curve collected in a full-scale equipment are (Eq. 4.69). In Eq. 4.69, summation is performed over each stage of the diffuser, from 1 to N_{st} . Selection of the candidate solutions is performed by a tournament method. Two-point crossover and Gaussian mutation are inserted in the GA algorithm to improve the

searching procedure.

$$fitness = \sum_{n=1}^{N_{st}} (C_{\circ Brix,n}^{real} - C_{\circ Brix,n}^{model})^2 \quad (4.69)$$

The bootstrap method was applied to quantify the uncertainty associated with each fitted parameter. The bootstrap is a widely applicable statistical tool (JAMES *et al.*, 2013) and is an efficient approach to assess accuracy of model parameters using a limited data set (ZHANG, 2004; HASTIE *et al.*, 2009). This method construct new data sets by repeatedly sampling randomly observations from the original one with replacement. The fitting procedure is performed to each new bootstrap observation, generating a group of different fitted parameters. After it, average and standard deviation of the parameters are calculated by Eqs. 4.70 and 4.71, respectively. In these equations Υ can be k_1 , k_2 , α or β . G is the number of new data sets constructed by the bootstrap method. Figure 4.10 summarizes the main steps of the implemented fitting procedure.

$$\bar{\Upsilon} = \frac{1}{G} \sum_{i=1}^G \Upsilon_i \quad (4.70)$$

$$s_{\Upsilon} = \sqrt{\frac{1}{G-1} \sum_{i=1}^G (\bar{\Upsilon} - \Upsilon_i)^2} \quad (4.71)$$

4.4.2 Optimization procedure

The simulation framework has an embedded optimization routine. In relation to a given scenario, such routine uses the developed model to find the best operational configuration that leads to the maximum achievable extraction degree and the steeper decrease of the \circ Brix curve. Therefore, the simulation framework as presented in this thesis has two objective functions: the extraction degree and the slope of the \circ Brix curve at the initial stages. The optimization of the decreasing slope of the \circ Brix curve focus on the initial stages of the equipment because such approach leads to a faster extraction process. In the optimization procedures performed in this thesis, the decreasing slope of the \circ Brix curve is increased by seeking the maximum difference of the \circ Brix values between the first and the second stages. The objective function of the optimization procedure is presented in Eq 4.72. Note that each

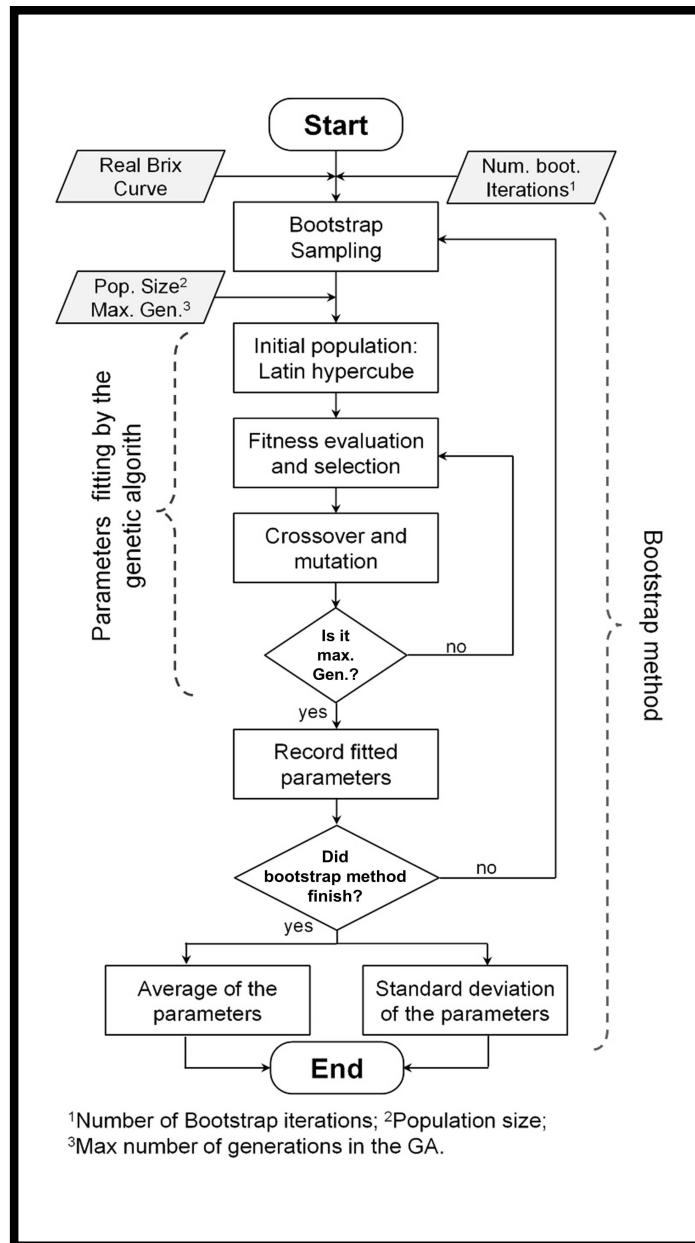


Figure 4.10: Schematic representation of the fitting procedure. Gray colored boxes are inputs provided by the end users.

term of the objective function is normalize to fit between 0.0 and 1.0.

$$obj. function = \frac{(Ext. degree \%)}{100\%} + \frac{(C_{\circ Brix,1}^{model} - C_{\circ Brix,2}^{model})}{C_{\circ Brix,rm}^{in}} \quad (4.72)$$

As in the procedure to fitting the parameters of the model, the optimization routine is done by a Genetic Algorithm. Except for the bootstrap method and the objective function,

the GA routine to optimize the extraction degree is the same as described in the previous subsection (Figure 4.11). Specific to the optimization purpose, the initial population is a set of operational configurations (*i.e.*, optimization variables). The computational implementation of the optimization routine is also done by using the *DEAP* package.

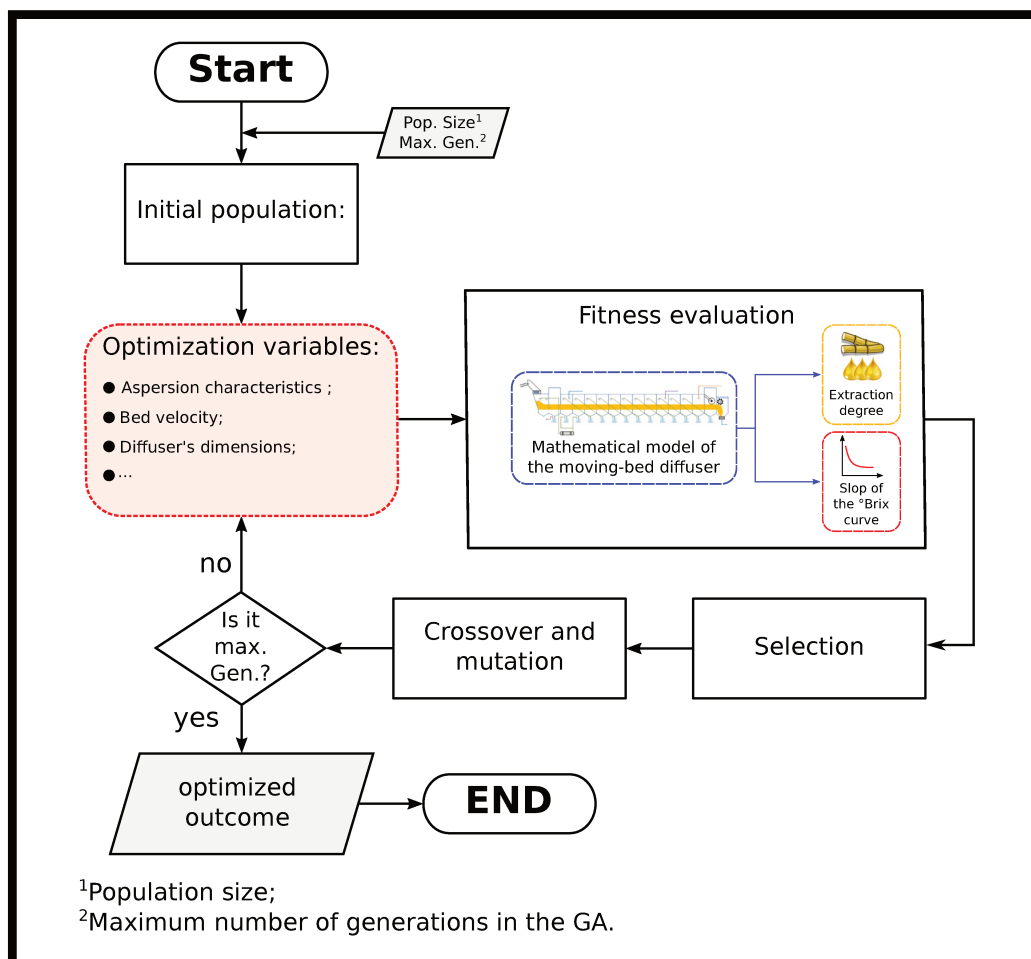


Figure 4.11: Schematic representation of the optimization procedure. Gray colored boxes are either an input (top of the scheme) or an output (bottom of the scheme) of the optimization procedure.

4.5 Concluding remarks

The present chapter was essential to translate into computational terms the mathematical description of the extraction process proposed in the Chapter 3. Therefore, the model equations are now embedded in a Simulation Framework, which introduces a “usability-layer” to the computational procedures in charged of solving the model equations. This fact opens

room for the possibility of using the developed Simulation Framework at the daily routine of sugarcane mills as well as at research institutions. The next chapter explores the potential of the developed Simulation Framework to account for the operation of a full-scale moving-bed diffuser.

Chapter 5

Performance of the Simulation Framework

This chapter will explore the capacity of the simulation framework to represent the expected behavior of a full-scale moving-bed diffuser under operation. This task is accomplished by using data collected in a real diffuser as a case study. Along with such exploration, it is going to be presented and discussed the main features of the developed simulator. It is worth to highlight that this chapter does not have the intention to exhaust all the possibilities of the simulator. Nevertheless, the following sections will provide a “big picture” of the potential of such framework to assist design and operation of diffusers.

5.1 Case Study

The case study refers to a full-scale moving bed diffuser located in a mill in Central-Western Brazil. This equipment is a chainless moving-bed diffuser built by *Bosch Rexroth*. Table 5.1 presents the characteristics and operational conditions of the equipment. The operational conditions come from the personal contact with the diffuser operators. Raw material properties were collected from the industrial daily reports. Both operational conditions and raw material properties represents typical values achieved in the daily routine of the mill. One is allowed to interpret “typical values” as averages along the harvest season. These average values consider only regular days, which are days without atypical operation conditions (*e.g.*, broken equipments, start-up or shutdown conditions).

The Dispersion coefficients for vertical and horizontal directions are assumed equal. The value considered in this study for the dispersion coefficients was reported by [LOVE and REIN \(1980\)](#). The value used for the permeability of the media is the one presented by [LOUBSER and JENSEN \(2015\)](#) concerning a sugarcane bed at common operation conditions. The laminar flow resistance K_s is computed considering that the supporting screen promotes a pressure loss equivalent to 1 m of the sugarcane bed being conveyed ([PICARO et al., 1994](#)).

Table 5.1: Characteristics and operational conditions of the equipment from a full-scale moving-bed diffuser located in a mill in Central-Western Brazil.

Input	Value	Unity
Equipment and operation settings		
Number of stages	14	–
Diffuser’s length	60.0	m
Diffuser’s width	12.0	m
Bed velocity	0.85	m/min
Imbibition%fiber	2.8	kg_{water}/kg_{fiber}
Fibers packing density	87.0	kg_{fibers}/m_{bed}^3
Tons of cane processed	699.3	ton/h
$\Omega_{x,z}$	10^{-2}	m^2/min
K_p	10^{-8}	m^2
Raw material properties		
Brix of the cane fed	18.1	$^{\circ}Brix$
Fiber content of the processed cane	0.1199	kg_{fiber}/kg_{cane}
Average Purity	0.87	$kg_{sucrose}/kg_{soluble\ solids}$
Parameters calculated by the simulator		
Bed height	1.59	m
Percolating velocity	0.4	m/min
θ_v	0.78	–

The following sections use this case study as the baseline scenario to perform the assessments. The aforementioned “exploration of the simulation framework” is going to be divided into three sections. In the first one, it is presented the framework calculations at steady state. The following section focus on the dynamic simulations. This very section discusses the effectiveness of the approaches applied in this study to consider bed height variations and percolating velocity propagations. At least, the third section is devoted to some optimization analyses.

Before the assessments, however, it is important to present the configurations of the computer used to perform all the simulations. Table 5.2 summarizes the main configurations of the personal laptop used in the following studies.

Table 5.2: Configurations of the computer used to perform all the simulations

Brand and type:	Dell Inspiron 5457
Operational system:	Ubuntu 18.04.01 LTS
Processor:	Intel Core i-7 CPU 2.50 GHz x 4
RAM:	16 GB
Cache:	8 GB

5.2 Steady state simulations

5.2.1 Solution procedure

A mesh sensitivity analysis was performed in order to find a trade-off between the accuracy of the results and computational effort to solve the model equations. The °Brix curve is used as an indication of the solution behavior (Figure 5.1). For this case, accuracy relates to the capacity of the results to follow the expected downward tendency displayed by the ideal °Brix curve. This ideal curve is calculated using the operational conditions presented in Table 5.1.

The labels of the curves in Figure 5.1 are the size of the grid per stage of the diffuser (*e.g.*, 6X6 means 6 vertical volumes and 6 horizontal volumes per stage). For smaller number of volumes, the °Brix curves change their shape considerably as the grid sizes vary. When the number of volumes increases, changes in the °Brix curve shape start to decrease, assuming progressively an asymptotic value wherever the accuracy condition is satisfied. An asymptotic group was defined as a collection of grid sizes in which the results do not change whenever there is an increase in the number of volumes in the grid. For this case study, it was assumed that an asymptotic group exists for grids with sizes equal or higher than 20X20.

Time required to perform a simulation as a function of the number of volumes in the grid is presented in Figure 5.2 for the stage sizes inside the asymptotic group. Smaller grid volumes need longer solution procedures, which is prohibitive for tasks requiring successive simulations, as in the fitting procedure proposed in this study. Since increasing the number of volumes does not lead to noticeable differences in the outputs, the following discussions are based on simulations performed in a 20X20 grid per stage. This grid size presents a fast solution and belongs to the asymptotic group.

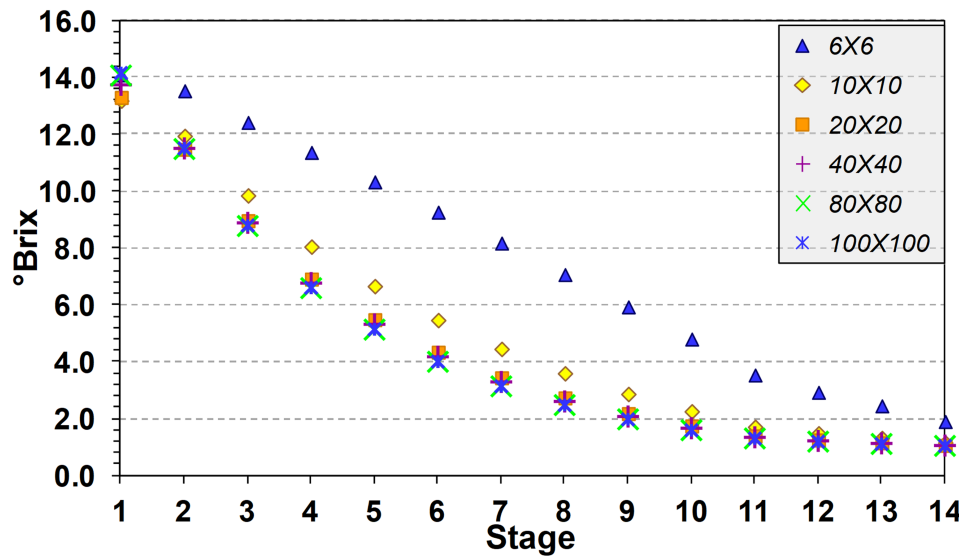


Figure 5.1: °Brix curves from the moving-bed diffuser simulation framework as a function of the resolution grid size. Labels represent the size of the grid per stage (*e.g.*, 6X6 means 6 vertical volumes and 6 horizontal volumes per stage).

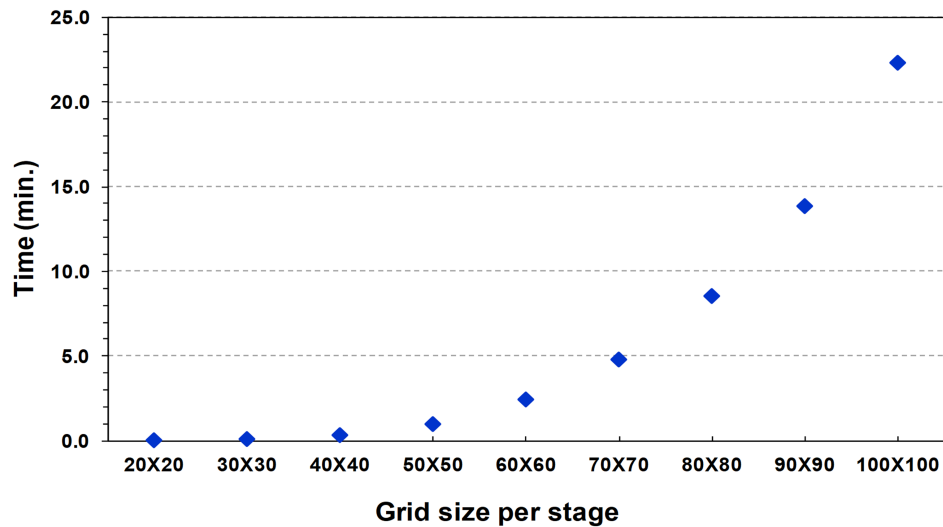


Figure 5.2: Time in minutes to perform a simulation as function grid size per stage.

5.2.2 Fitted parameters

The fitting procedure was performed using an ideal °Brix curve. Deviations from the ideal regime have many sources (*e.g.*, flooding, inorganic impurities, mechanical failures), which are often hard to define, measure, and describe in a mathematical model. The ideal curve was used to avoid such deviations, thus fitting the parameters of the model in a well defined scenario.

Figure 5.3 shows the ideal °Brix curve and fitted results of one hundred bootstrap iterations (dashed lines). Lines instead of dots were used to emphasize the shapes of the fitted curves and how they are distributed around the ideal contour. Bootstrap iterations present narrower dispersion above the fourth stage. Precision of outcomes is due to the ability of the model to represent the arrangement of points in this region. Dashed lines present an opposite behavior below the fourth stage. The model looks unable to describe the S-shape of the ideal curve, specially between first and second stages. Bootstrap curves have three trends in this region according to their attempt to fit one of the first two points or an intermediate position. These trends causes the broader dispersion.

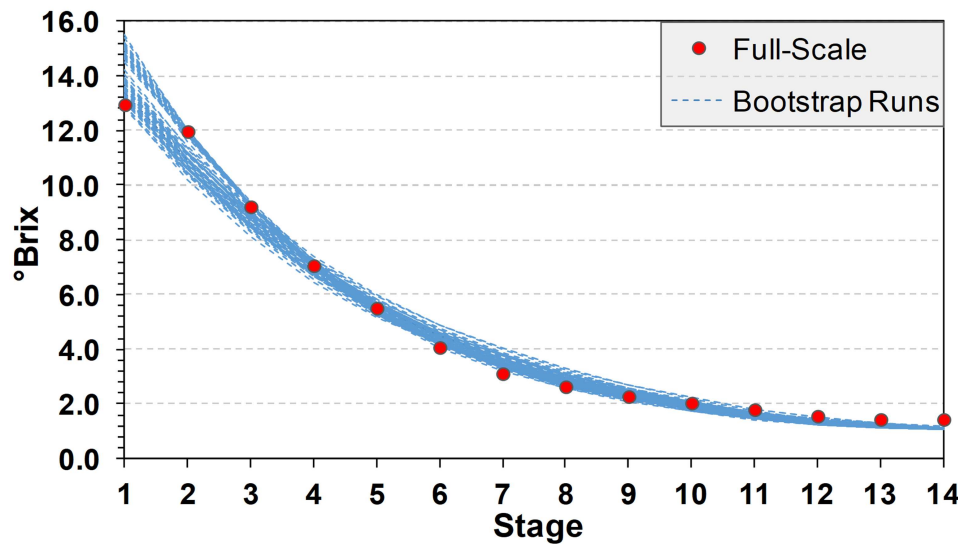


Figure 5.3: Ideal °Brix curve used and fitted results of one hundred bootstrap iterations.

The linear interpretation of the extraction mechanisms used in this study (Eqs. 3.13 and 3.14) is the possible cause for the inflexibility observed in the model. Linear mechanisms may not represent accurately the phenomenology of extraction in the first stage. In the front of the diffuser, sugarcane enters in contact with the extracting liquid for the first time. This initial contact is hard to represent mathematically due to a complex interaction among liquid and fibers. A non-linear model describing extraction in the first stage may solve this problem. On the other hand, solution procedure becomes more complex, thus leading to an increase in computational time.

The °Brix curve simulated using the average of the parameters fitted in bootstrap iterations (Table 5.3) accurately describes the downward tendency of ideal points (Figure 5.4), even for the initial stages. Thus, it was considered unnecessary to increase complexity of the solution procedure for a small gain in representativeness. For this reason, the linear

interpretation of the extraction mechanisms was maintained.

Table 5.3: Averages and standard deviations of the fitted parameters in bootstrap iterations.

Parameter	Average	Std. deviation	Unity
k_1	0.4	0.2	s^{-1}
k_2	0.009	0.005	s^{-1}
α	0.42	0.03	%
β	0.24	0.08	%

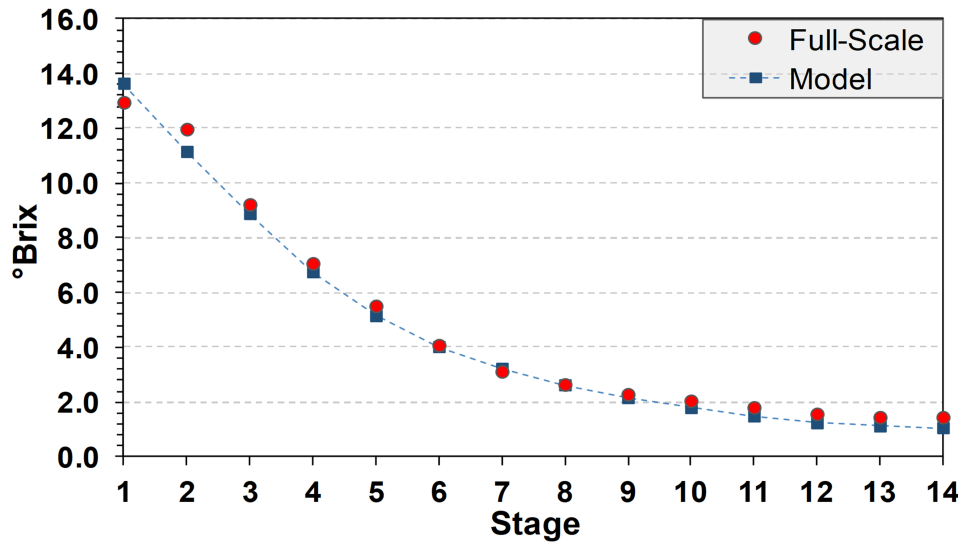


Figure 5.4: °Brix curve simulated using the average of parameters fitted through the bootstrap iteration.

The average value of k_1 (Table 5.3) is about 45 times larger than k_2 . This outcome matches the one found by REIN (2013), who reports that sucrose transfer by lixiviation is around 50 times higher than diffusion extraction in a moving-bed diffuser operation. The fitted extraction rates have standard deviations with the same order of magnitude in relation to their averages. These high deviations have two sources. The first relates to the fitting procedure in which variations of k_1 and k_2 also reflect the attempt of the model to represent the S-shape of the ideal curve. Besides, outcomes are more sensitive to changes in α and β , given that they define the volumetric extent of the four bed sections. As a consequence, fluctuations in k_1 and k_2 altered less the quality of the fitting procedure, thus leading to a wide range of suitable values for the extraction rates.

The second source concerns the complex phenomena these two parameters represent through their values. Magnitudes of the extraction rates result from an intricate interaction

among many variables, which are not homogeneously distributed over the bed. As a consequence, extraction rates in a real equipment have different values at distinct positions. If it was possible to measure such rates directly, the standard deviation related to them would be high. From this perspective, a wide range of k_1 and k_2 values also reflects the intrinsic variability of the modeled system.

Unfortunately, it was not possible to compare the fitted extraction rates with those presented by REIN and WOODBURN (1974), once the model formulation and the processes from which data were collected are different. The model proposed in this thesis considers stagnant liquid as an individual fraction, whereas the other study treated static liquid as an integral part of the fibrous structure. REIN and WOODBURN (1974) collected data from a pilot column diffuser processing bagasse instead of a full-scale moving bed equipment handling cane. Although REIN (1974) applied their model to a moving-bed diffuser, the values of the extraction rates are assumed equally to those already fitted in the pilot column.

Average values of α and β reveal a prevalence of stagnant zones. This tendency is consistent with the fibrous nature of the modeled system. The presence of stagnant zones in fibrous bed has no parallel in a granular systems (KYAN *et al.*, 1970). In relation to diffusers, the hydrophilic quality of sugarcane fibers fosters the existence of such regions (REIN and WOODBURN, 1974). Furthermore, heterogeneous shapes and sizes of fibers promote a tortuous network of void spaces (REIN, 1972), which increases the presence of dead-end regions. In relation to the extraction rates, standard deviations of α and β show more certainty in the fitted values. It indicates lower variability of the phenomena represented by these two parameters.

The following subsections explore the capacity of the simulator to represent the expected behavior of a real diffuser towards changes in some operational conditions. These assessments do not exhaust all the possibilities of the simulator; they demonstrate, however, the potential of such tool to assess performance of moving-bed diffusers.

Fitted parameters were assumed to be valid for the new values related to the new operational conditions. This assumption allows for exploring the qualitative behavior of the diffuser in relation to changes in these operational conditions. Quantitative accuracy of this assumption requires validation through direct experimentation in the moving-bed diffuser under operation. However, it is not feasible to perform unrestricted experimentation in a full-scale diffuser, once it may significantly reduce sugarcane juice extraction during the daily routine of a sugarcane mill. Moreover, concerning an industrial diffuser, it is difficult

to isolate the effects on extraction due to changes in a single operation condition. Therefore, future works may focus on the development of an experimental rig to provide a controlled environment, in which the quantitative accuracy of this assumption may be assessed.

5.2.3 Dimensions of the diffuser

Number of stages and width are the dimensions of the diffuser considered in the present analyses. Length of each stage is kept constant, thus the extent of the diffuser is defined only by the number of stages. Assuming the scenario presented in Table 5.1, it was performed simulations varying the number of stages, between 10 to 18. Such limits represent common sizes of diffusers under operation at the mills. Table 5.4 presents the extraction degree achieved for each simulated value of number of stages. Extraction degree rises along with the number of stages, which is an expected tendency. Moreover, the gain in the extraction level becomes only incremental above 14 stages. As reported by REIN (2013), such asymptotic relation between sugar extraction and number of stages is an observed behavior in full-scale diffusers. In a more generalist view, this asymptotic relation is an inherent phenomenon of stage-based solid-liquid extractors (TREYBAL, 1981), which represents the limit of the extraction process.

Table 5.4: Extraction degree according to the number of stages in a moving-bed diffuser.

Number of stages	Extraction
-	%
10	88.8
12	93.9
14	94.2
16	94.4
18	94.6

°Brix curves also exhibit an asymptotic relation with the size of the diffuser (Figure 5.5). This behavior is also an expected tendency, which may be endorsed by the same arguments as presented for the extraction degree. During the design of a diffuser, such °Brix curve analyses provides valuable information about the required size of a diffuser to achieve a desired extraction level. Concerning the conditions reported in the Table 5.1, for instance, a diffuser with 18 stages means an unnecessary long equipment to achieve only an incremental gain of extraction. Performing the extraction using the current diffuser with 14 stages leads to comparable results with those achieved in equipments with 16 or 18 stages. Economically,

this type of insight would be very interesting, as no money would be spent on building a longer diffuser.

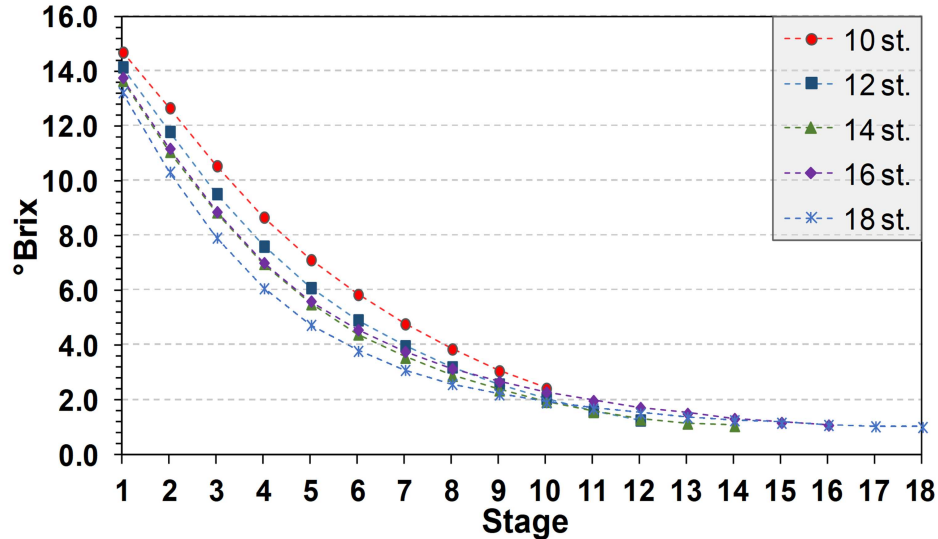


Figure 5.5: °Brix curves simulated for different number of stages.

Figure 5.6 presents the simulated °Brix gradation within the sugarcane bed for three different numbers of stages (10, 14, and 18). The dashed lines are *isolines*, which depicts regions with equal value of °Brix. Position of the isolines is an indicative of the sugar gradient along the equipment. Increasing the number of stages, the distance between two consecutive isolines grows at the second half of the diffuser. This higher distance means a lower sugar gradient, which represents consequently a reduction in the extraction rate at this region. This drop of the extraction agrees with the already observed asymptotic tendency.

The configuration of the isolines at the beginning of the diffuser gets narrower as the number of stages grows. As a consequence of this higher sugar gradient, the simulated °Brix gradations show an increasing in the extraction rate for the initial stages of a longer diffuser. It may be explained by the fact that the extraction process gets closer to a pure counter-current operation as the number of stages rises. Getting closer to a counter-current arrangement enhances the sugar concentration difference between liquid and solid (PAYNE, 1969), thus leading to higher extraction rates at the front of the equipment for longer diffusers.

The influence of the width in the performance of the diffuser was assessed by comparing the current configuration, 12 m, with a higher value, 15 m. This higher value is the widest diffuser manufactured by *Bosch Rexroth* (designer of the equipment under study). In this assessment, it is kept constant the throughput of sugarcane. As presented in Table 5.5,

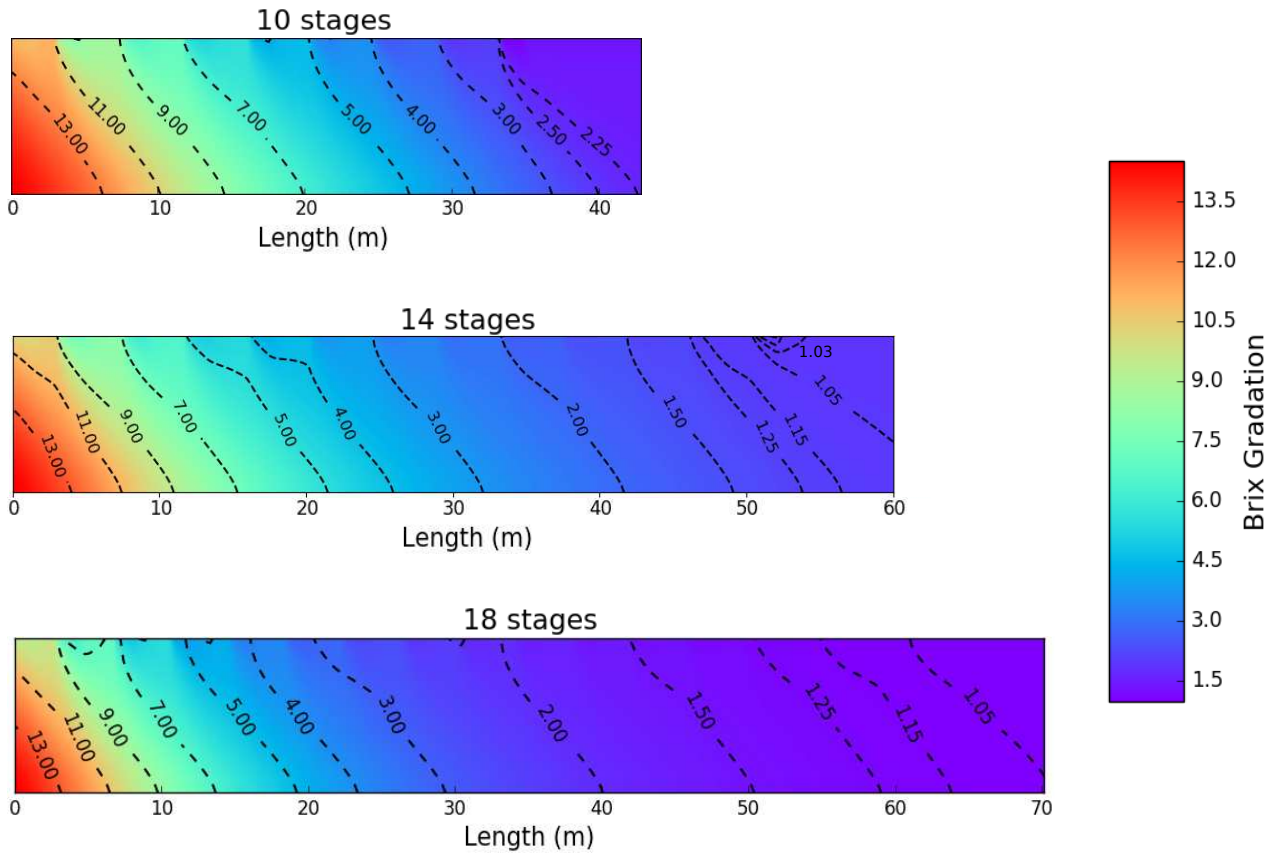


Figure 5.6: Simulated °Brix distribution for moving-bed diffusers with 10, 14, and 18 stages, respectively. Regions of same °Brix value are represented by dashed lines (isolines).

extraction degree rises along with the width. This increment on extraction is an anticipated tendency, once the area available for extraction rises (REIN, 2013). However, such growth is not substantial and may not be profitable in face of the cost of acquiring a new equipment or modifying an existing one. An incremental increase of the extraction may be a consequence of the reduction on the bed height and the unchanged configuration of the aspersion positions. These two facts may act on detriment of the gains that would be achieved by increasing the area available for extraction.

Table 5.5: Extraction degree as function of the width of the diffuser

Width	Extraction
m	%
12.0	94.2
15.0	94.6

Despite the evolution of the extraction degree shows only a slightly benefit, the analysis of the °Brix curves (Figure 5.7) provides some insights that argues in favor of the

increase of the width. The increase of the extraction area using a wider diffuser promotes a rise of the sugar gradient, with positive impacts on the extraction rate along the diffuser. A higher sugar gradient may be also observed in the simulated °Brix gradations (Figure 5.8). Isolines are shifted leftward and the distance among them are reduced at the front of the diffuser for the 15 m width scenario, thus indicating a faster variation of the sugar concentration. This tendency leads to two possible alternatives that may be advantageous. The first one is the possibility to reduce the number of stages for a wider diffuser, but keeping the sugarcane throughput constant. The second alternative maintain the number of stages unchanged and increases the width of the equipment. As a consequence, this second alternative opens room for a more flexible operation in which a higher sugarcane throughput is allowed without detriments of the extraction degree.

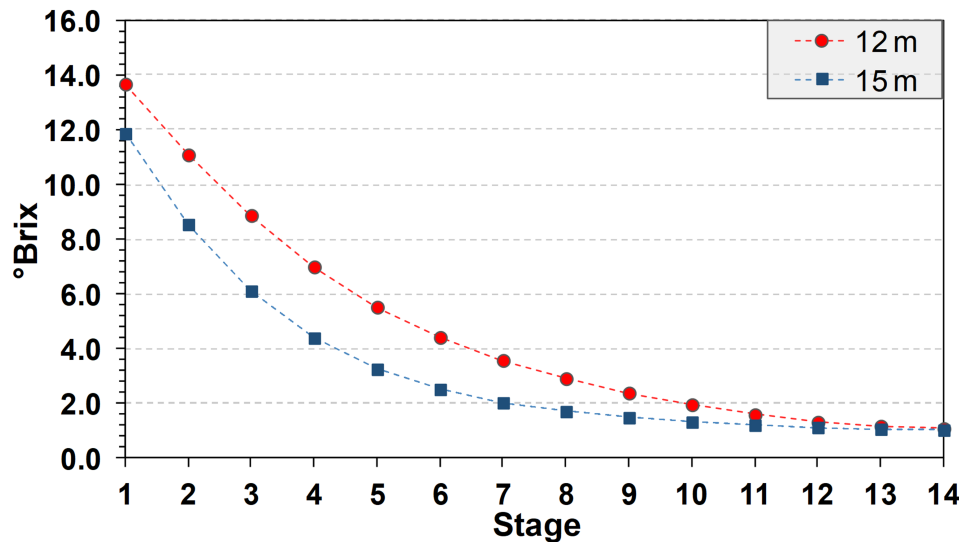


Figure 5.7: °Brix curve as function of the width of the diffuser.

5.2.4 °Brix in the raw material

In the current subsection, it is performed an analysis to evaluate the effect on the simulated results of a variation in the °Brix value of the raw material. Two scenarios of °Brix are used in the following assessment: 18.0 (as presented in Table 5.1) and 14.0 °Brix. In comparison with the scenario reported in the case study, the °Brix curve regarding the raw material with lower °Brix (Figure 5.9) shows a visible reduction in the °Brix values for almost all the stages (*i.e.*, from the first to 10th stage). Such reduction is coherent with an environment with lower sucrose concentration imposed by a feedstock with lower °Brix level.

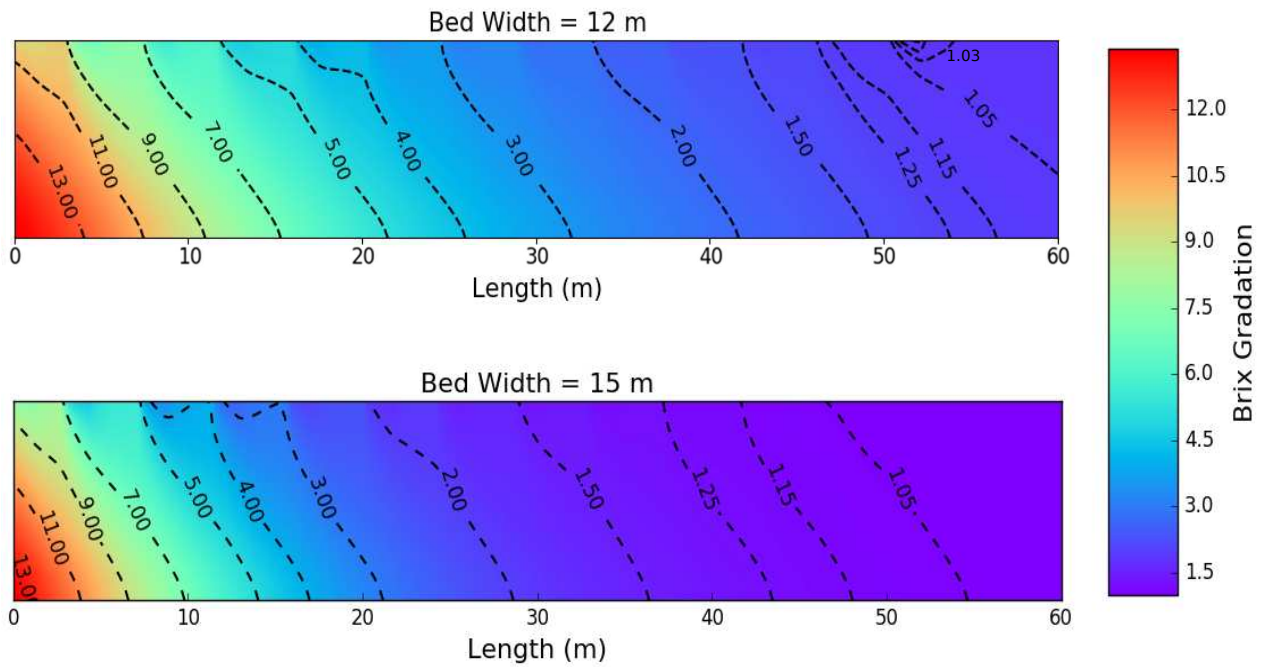


Figure 5.8: Simulated °Brix distribution as function of the width of the diffuser. Regions of the same °Brix value are represented by dash lines (isolines).

Especially at the initial stages of the diffuser, the simulated °Brix curve for the row material possessing a higher °Brix exhibits a faster reduction of the °Brix values between two successive stages. Such tendency may also be noticed in the °Brix distributions (Figure 5.10), in which the isolines for the feedstock with lower °Brix are slightly more spaced at first half of the equipment. A higher °Brix gradient for the scenario with higher °Brix values is a consequence of a greater difference of sucrose concentration between the fibers of the raw material and the extracting liquid. A more pronounced °Brix gradient fosters the extraction rate, which may lead to higher extraction degrees. As presented in Table 5.6, the simulated extraction degrees agrees with this expected tendency.

Table 5.6: Extraction degree as function of the °Brix value in the raw material

°Brix in the raw material	Extraction %
18.0	94.2
14.0	92.9

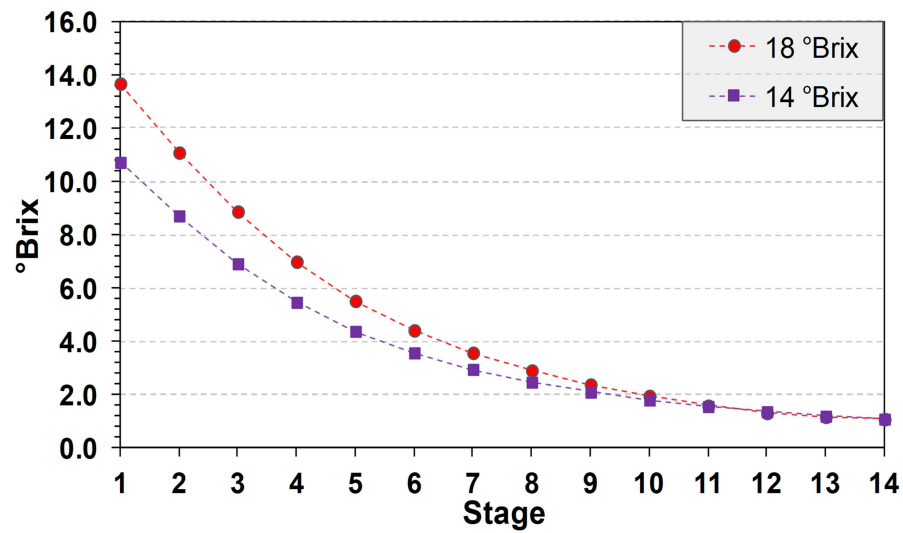


Figure 5.9: Simulated °Brix curves regarding two °Brix values in the raw material: 18.0 and 14.0 °Brix.

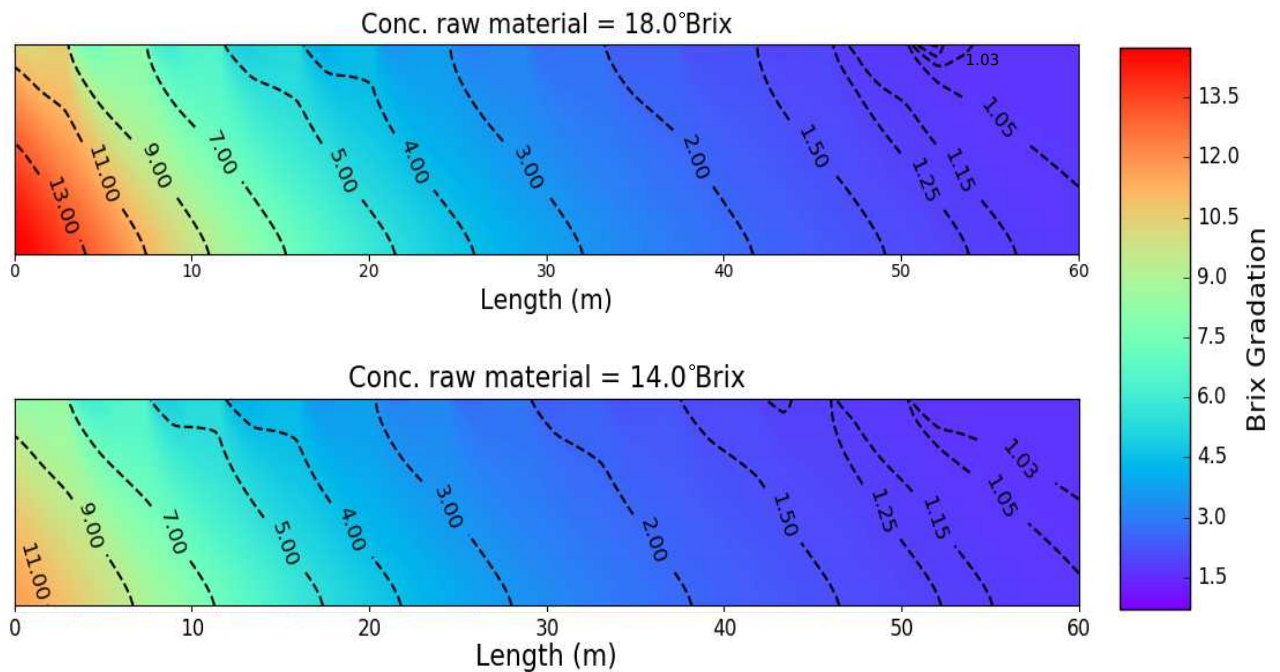


Figure 5.10: Simulated °Brix distribution for two °Brix values in the raw material: 18.0 and 14.0 °Brix. Regions of the same °Brix value are represented by dash lines (isolines).

5.2.5 Bed velocity

Two velocities are used in this assessment: 0.85 m/min (value reported in Table 5.1) and 0.95 m/min . Table 5.7 shows the simulated extraction degree for these two levels. A

lower extraction is achieved by increasing bed velocity. This behavior is a consequence of different residence times inside the diffuser in these two scenarios. A lower v_b value represents a longer period that the fibers remains inside the equipment. Moreover, decreasing v_b implies in an increase of the bed height, which leads to a longer retention time of the percolating liquid inside the bed during an aspersion-percolation cycle. According to these two previous facts, the slower velocity scenario represents a longer residence time of both fibers and percolating liquid. Since a longer residence time means a better solid-liquid contact (REIN, 2013), a slower velocity leads to a positive impact on extraction (MUNSAMY and BACHAN, 2006)

Table 5.7: Simulated sugar extraction degree as a function of the bed velocity.

Bed Velocity	Extraction
<i>m/min</i>	%
0.85	94.2
0.95	93.8

Increasing the bed velocity represents a higher convective flux in the horizontal direction. Since aspersion positions are kept constant in the two scenarios, higher horizontal flux improves recirculation of the percolating liquid (REIN and INGHAM, 1992). It promotes deviation from the stage-wise operation (LOVE and REIN, 1980), thus smoothing the °Brix gradient. Figure 5.11 shows the simulated °Brix distribution in the bed for both velocity values. As a consequence of the higher convective horizontal flux, the position of the lines shifts towards the end of the diffuser for faster bed velocities. Moreover, the distance between two consecutive isolines increases in the faster scenario, which is an evidence for the aforementioned reduction in the °Brix gradient. °Brix curves exhibit the same tendency regarding the °Brix gradient (Figure 5.12).

Reduction in the °Brix gradient for a faster bed velocity represents a decrease in the extraction rate along the diffuser. The models of the extraction mechanisms (Eqs 3.13 and 3.14) are able to represent such behavior. Figure 5.13 is used to support the previous assertion. In this figure, v_b is a generic bed velocity. Increasing v_b (*i.e.*, $v_b + \text{increment}$) leads to an intensification of the horizontal convective flux. As a consequence of this higher flux, the percolating liquid is carried to regions with lower °Brix (movement promoted by the resultant velocity v_{r2} in Figure 5.13). Once the extraction mechanisms are described as proportional to the difference of sugar concentration between two distinct bed sections, the contact with lower °Brix regions decrease the extraction rate. The agreement between the real phenomenon and the mathematical representation testify in favor of the chosen model for the extraction mechanisms.

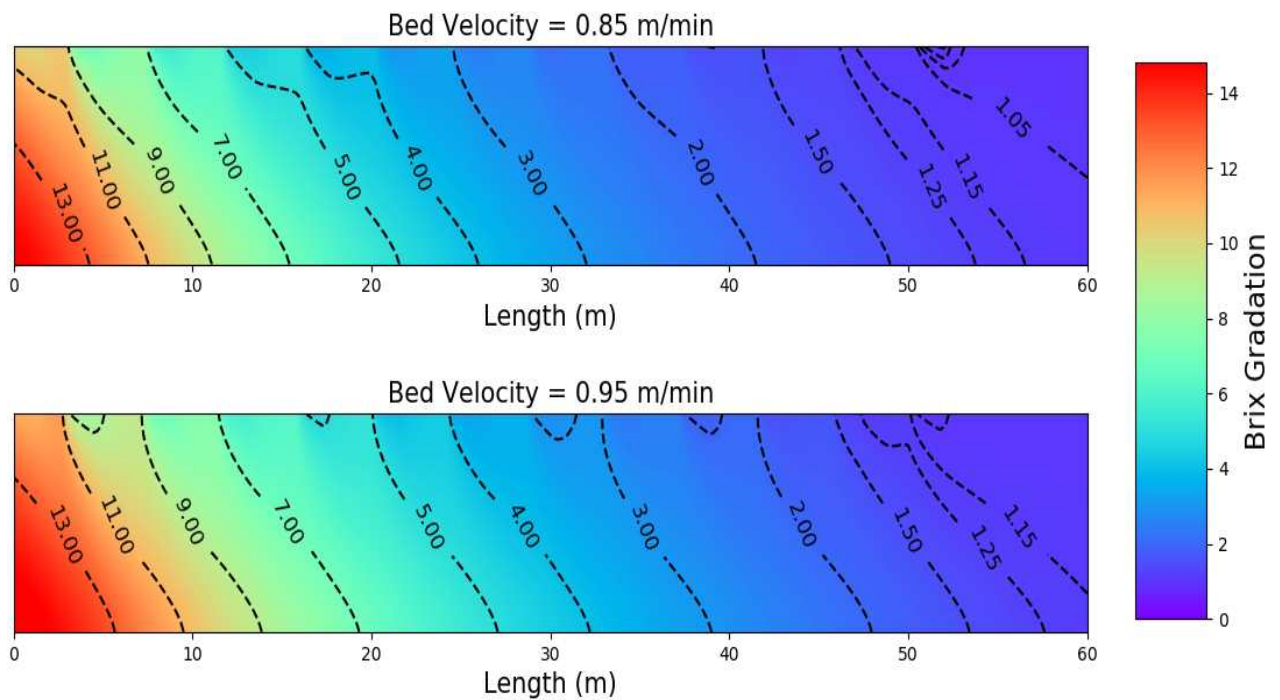


Figure 5.11: Simulated °Brix distribution for bed velocities of 0.85 and 0.95 m/min . Regions of the same °Brix value are represented by dash lines (isolines).

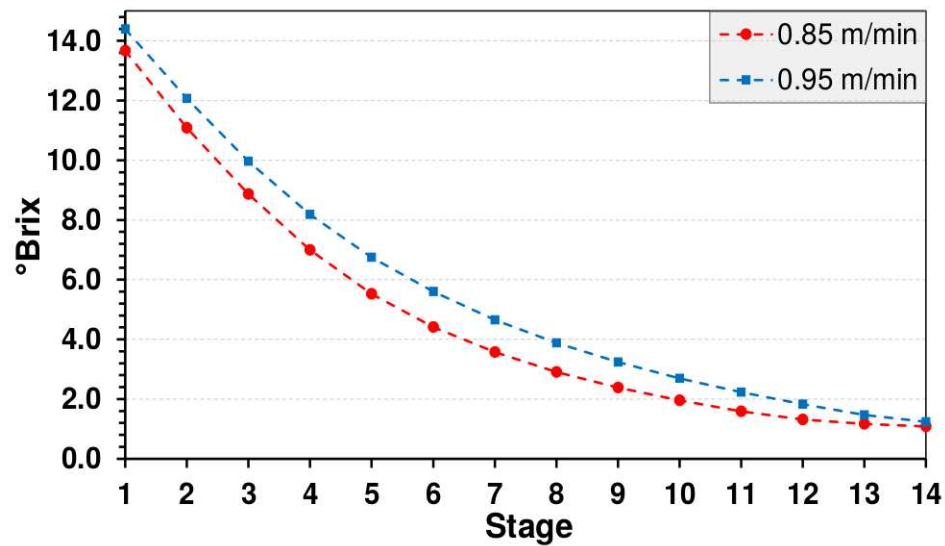


Figure 5.12: °Brix curve for bed velocities of 0.85 and 0.95 m/min .

5.2.6 Imbibition characteristics

In a sugarcane mill, the amount of imbibition water added into a diffuser is frequently measured in relation to the quantity of fibers being processed (*i.e.*, kg_{water}/kg_{fiber}). Keeping constant the amount of fibers, the present analysis assesses the influence of an increase in the

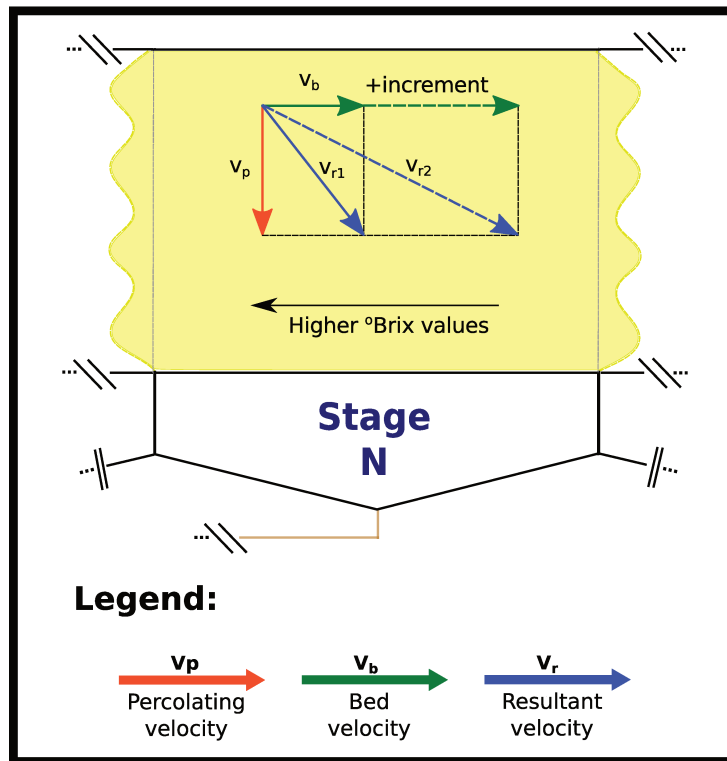


Figure 5.13: Resultant trajectory of the percolating liquid inside the bed for two bed velocities: v_b and $v_b + \text{increment}$.

imbibition from 2.8 (as reported in Table 5.1) to $3.5 \text{ kg}_{\text{water}}/\text{kg}_{\text{fiber}}$. The new imbibition value represents a common operation condition as frequently found in the literature. Many authors report that increasing the amount of imbibition water in a diffuser has a positive impact on sugar extraction (e.g., REIN, 2013; MUNSAMY and BACHAN, 2006; REIN and INGHAM, 1992). This positive relation is captured by the simulated extraction degree (Table 5.8).

Table 5.8: Extraction degree as function of the amount of imbibition water

Imbibition $\text{kg}_{\text{water}}/\text{kg}_{\text{fiber}}$	Extraction %
2.8	94.2
3.5	95.1

Higher imbibition values fosters the extraction rate, thus leading to an increase in the sugar gradient along the equipment (MUNSAMY and BACHAN, 2006; REIN and INGHAM, 1992). The $^{\circ}\text{Brix}$ curves (Figure 5.14) show the expected increase in the sugar gradient. Operating the diffuser with an imbibition of $3.5 \text{ kg}_{\text{water}}/\text{kg}_{\text{fiber}}$ promotes a steeper decrease of the $^{\circ}\text{Brix}$ value, thus indicating a higher sugar extraction along the equipment. The simulated $^{\circ}\text{Brix}$ gradation (Figure 5.15) corroborates with the tendency presented by the $^{\circ}\text{Brix}$ curve.

Concerning the higher imbibition scenario, the isolines are shifted towards the entrance of the diffuser and achieve lower values of °Brix at the rear of the equipment. Moreover, these very isolines display a closer configuration at the initial stages of the diffuser. These facts point towards a greater sugar gradient, which entails a more intense sugar extraction along the diffuser.

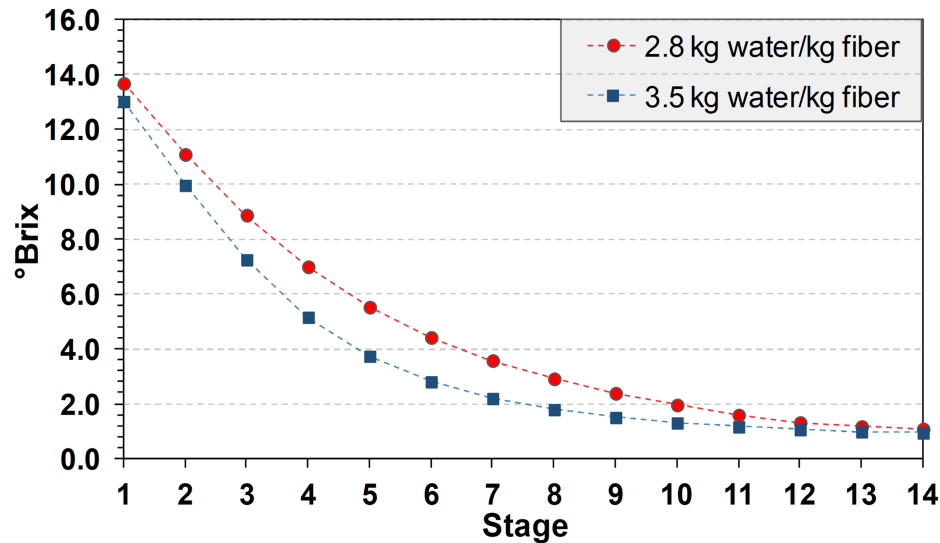


Figure 5.14: °Brix curves simulated considering two different amounts of imbibition water: 2.8 and 3.5 kg_{water}/kg_{fiber} .

Regarding the diffuser under assessment in this case study, it is not feasible to change the position of the imbibition water application. Indeed, most of the equipments operating under commercial purposes present an imbibition configuration that may be varied only within a limited range. Although such variation has a restricted practical applicability, it has a huge importance for the design of new equipments. In this sense, the following analysis focus on the understanding of the impacts that changing the imbibition position have on the operation of a moving-bed diffuser. It is worth to highlight that the results presented bellow concerns the operational conditions display at Table 5.1; extrapolations for different operational characteristics may not be valid.

The imbibition is located at 51 m in the equipment used as case study. Four different positions were applied to assess the influence of this location on the operational performance: 15, 30, 45, and 60 m . These four new positions represent each quarter of a diffuser with 60 m long. Table 5.9 displays the simulated extraction degree achieved for each considered imbibition position. Extraction degree has its higher simulated value (94.2 %) at the position in which the real diffuser is currently operating (51 m). Positioning the imbibition in a

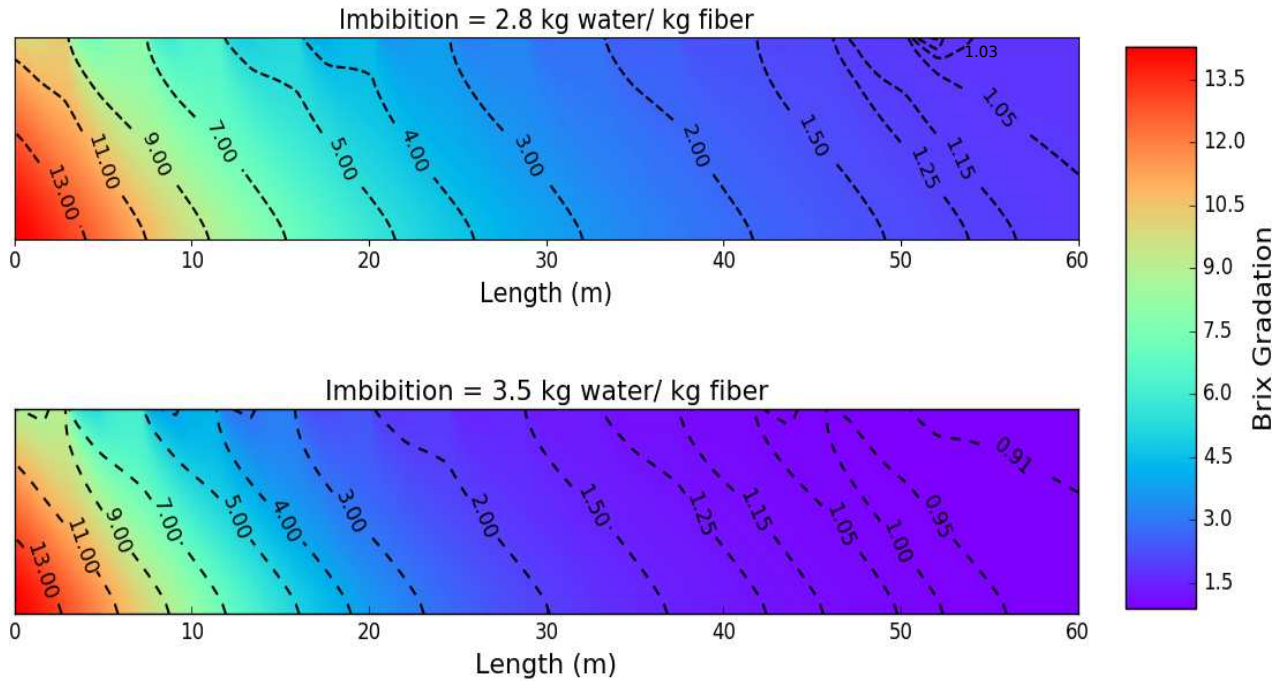


Figure 5.15: °Brix gradation for two amounts of imbibition water: 2.8 and 3.5 kg_{water}/kg_{fiber} . Regions of the same °Brix value are represented by dash lines (isolines).

different position leads to a reduction on the extraction degree. Such reduction may be explained by an abrupt interference in the sucrose gradient.

Table 5.9: Extraction degree concerning distinct imbibition positions

Imbibition position	Extraction
m	%
15	88.8
30	92.0
45	93.7
51	94.2
60	92.6

The stage-base operation and a well set counter-current arrangement of the aspersion positions promote a gradual decreasing of the sugar concentration (PAYNE, 1969). In an ideal condition, such gradual tendency leads, in the limit, to the lower sugar concentration at the last stage, which represents the maximum achievable extraction degree. Any external insertions into the equipment must be performed without disturbing this gradual decreasing of the °Brix value (REIN, 2013). Concerning the present analysis, disturbing the ideal gradual slope of the °Brix (*i.e.*, gradual sugar gradient) means the insertion of imbibition in a region of the bed with sugar concentration different of the sugar content in the imbibition water.

In this scenario, the gradual slope is modified, thus leading to a negative impact on the extraction degree. Regarding the interaction between sugar concentration in the imbibition water and within the sugarcane bed, three distinct conditions emerges inside the equipment.

The first condition is the insertion of imbibition in a position with sugar concentration higher than the one of the imbibition water. In this case, the insertion of imbibition abruptly increase the sugar gradient, particularly in the vicinity of the point that the imbibition water enters into the equipment. Examples of this condition may be seen at Figures 5.16 and 5.17 concerning the imbibition positions at 15, 30, and 45 *m*. Nonetheless, such intensification of the sugar gradient leads to an equilibrium condition with a higher °Brix value, which may be witnessed in the more elevated asymptotic value of the °Brix curves and the higher values achieved by the isolines at the rear of the equipment. As the imbibition position moves towards the end of the diffuser, the second condition emerges: similar sugar concentration in the imbibition water and within the bed. Concerning this condition, sugar gradient varies more smoothly along the equipment, as the isolines configuration shows for the scenario with imbibition position at 51 *m* (Figure 5.17). Therefore the Brix variation tends to the ideal gradual decreasing of the sugar content. The third condition is imbibition water possessing higher °Brix value than the sugarcane bed environment. It promotes an increase of the sugar content within the bed, thus leading to a higher Brix value at the asymptotic region (see Figures 5.16 and 5.17 for imbibition at 60 *m*).

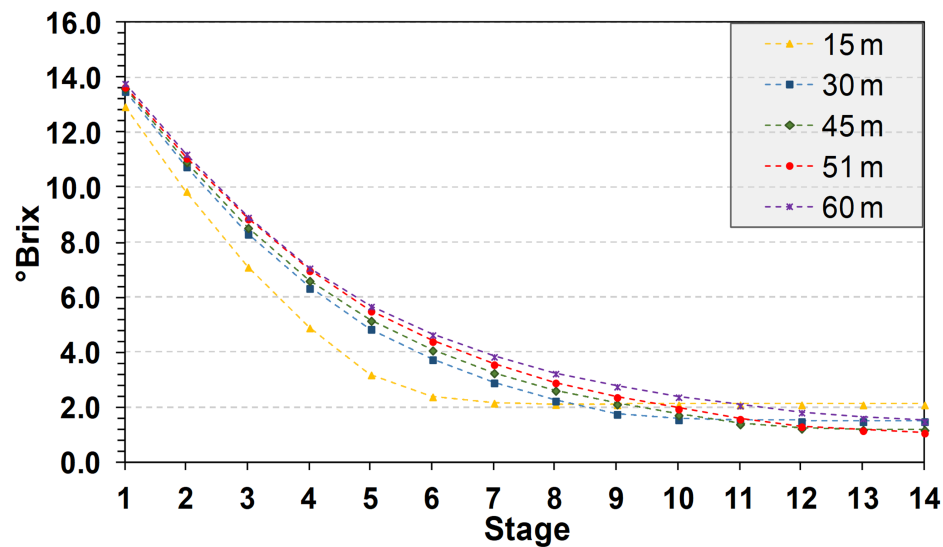


Figure 5.16: °Brix curve simulated considering distinct positions of the imbibition. The position 51 *m* is the current configuration of the diffuser. The four remaining positions (*i.e.*, 15, 30, 45, and 60 *m*) relate to each quarter of a diffuser with 60 *m* long.

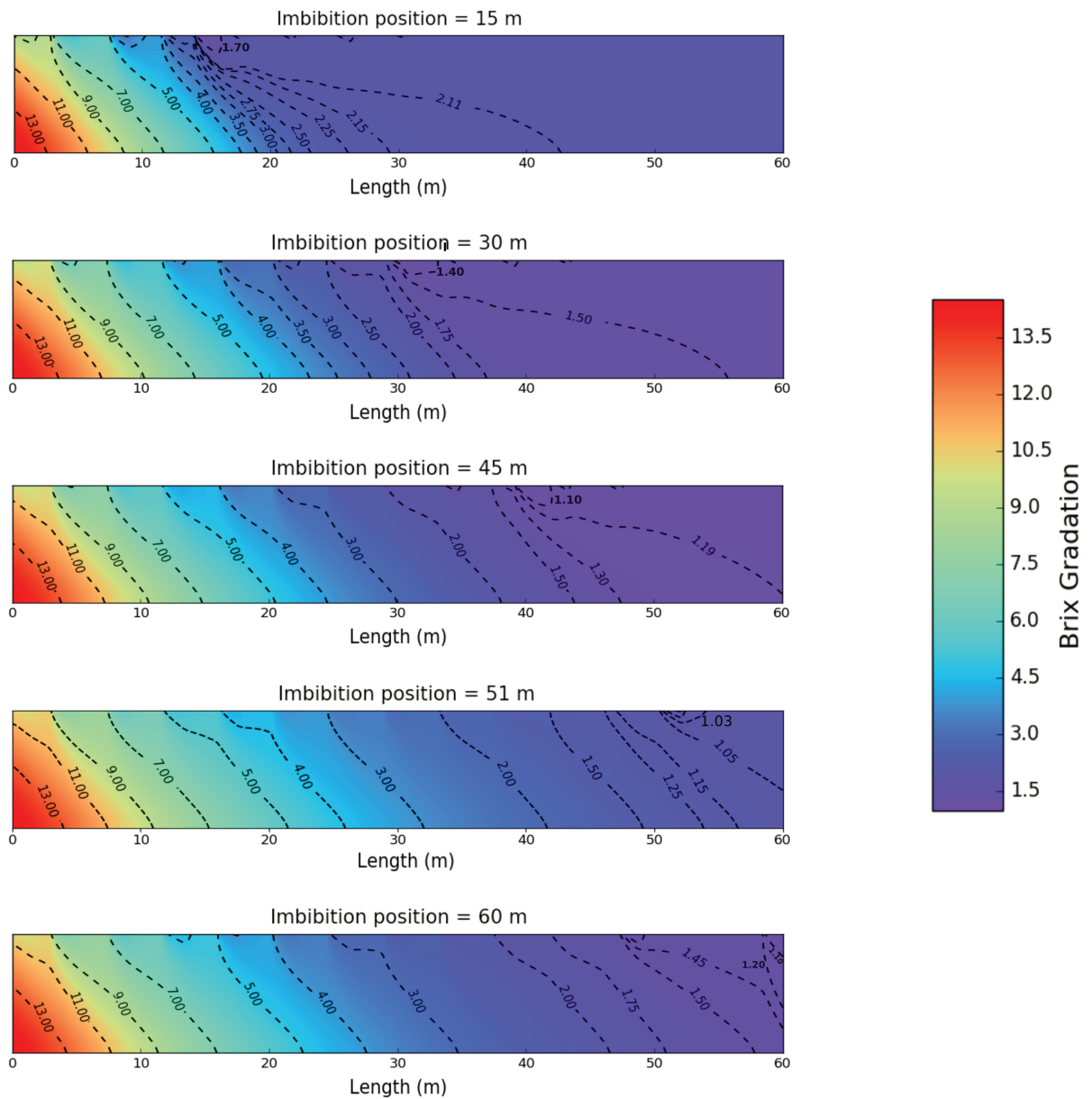


Figure 5.17: Simulated °Brix gradation concerning distinct positions of the imbibition. The position 51 m is the current configuration of the diffuser. The four remaining positions (*i.e.*, 15, 30, 45, and 60 m) relate to each quarter of a diffuser with 60 m long. Regions of the same °Brix value are represented by dash lines (isolines).

Bearing the previous discussion in mind, inserting the imbibition water at 51 m leads to the lower disturbance of the ideal decreasing of the sugar concentration. This fact is the reason for this scenario had achieved the higher extraction degree. However, it does not necessarily mean that the equipment is operating exactly at the ideal point and no further extraction improvements are possible by adjusting the imbibition position. Moreover, imbibition position at 51 m leading to the best scenario is a particularity of the

current operational characteristics. In different operational conditions, the outcomes may be diametrically distinct. In this sense, the developed simulation framework arises as an useful tool to seek the ideal imbibition position for a given operational configuration. The previous analysis is also applicable for the positioning of each aspersion point and the weak-juice return to the diffuser.

A particular characteristic of the operation used as case study is the imbibition water with a concentration of around 1.0 °Brix. According to the engineers responsible for the operation of this diffuser, such concentration is due to the reuse of water from the downstream processes. The following assessment is going to explore the impact on the extraction performance promoted by a decrease of 30% in the imbibition water concentration. Such reduction is a target operation condition aimed by the mill where the data were collected. Provided that the imbibition position is kept constant (at the original position, *i.e.*, 51 m), decreasing the imbibition water concentration leads to an increase in the extraction degree (Table 5.10). A lower concentration promotes a higher sucrose difference between the imbibition water and the sugarcane bed environment. As a consequence, a greater sucrose difference fosters the extraction rate, not only in the vicinity of the imbibition but also across the whole equipment. A higher extraction rate along the equipment may be seen in the evolution of the °Brix curves between the two assessed scenarios (Figure 5.18).

Table 5.10: Extraction degree values for three sugar concentrations in the imbibition water

Sugar conc. imbib.	Extraction
°Brix	%
1.0	94.2
0.7	96.0

The simulated °Brix distribution (Figure 5.19) provides a more detailed view of the variation in the sugar gradient within the bed. The lower concentration of the imbibition water intensify the sugar variation near the point of imbibition entrance. Therefore, the isolines get closer and reach a lower °Brix value than the higher concentration scenario. Concerning the other parts of the diffuser, the increase of the sugar gradient for the lower concentration condition may be recognized in the shifting of the isolines towards the front of the diffuser. The predicted improvements of the extraction performance may be an evidence that justify the intention of the mill to reduce the sugar concentration in the imbibition water. Moreover, a further improvement on extraction may be achieved by changing the imbibition position to adequate the operation to the new concentration value.

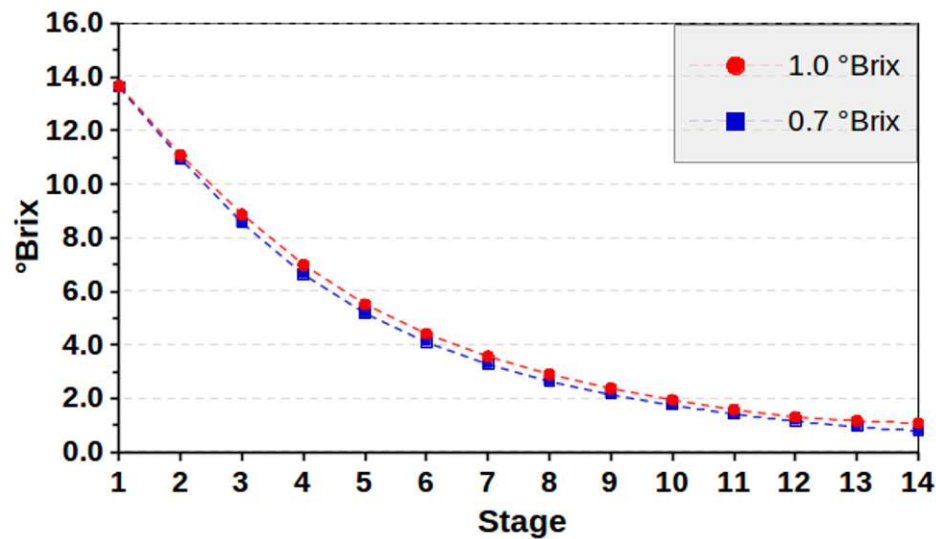


Figure 5.18: Simulated °Brix curves concerning two distinct sugar concentrations of the imbibition water.

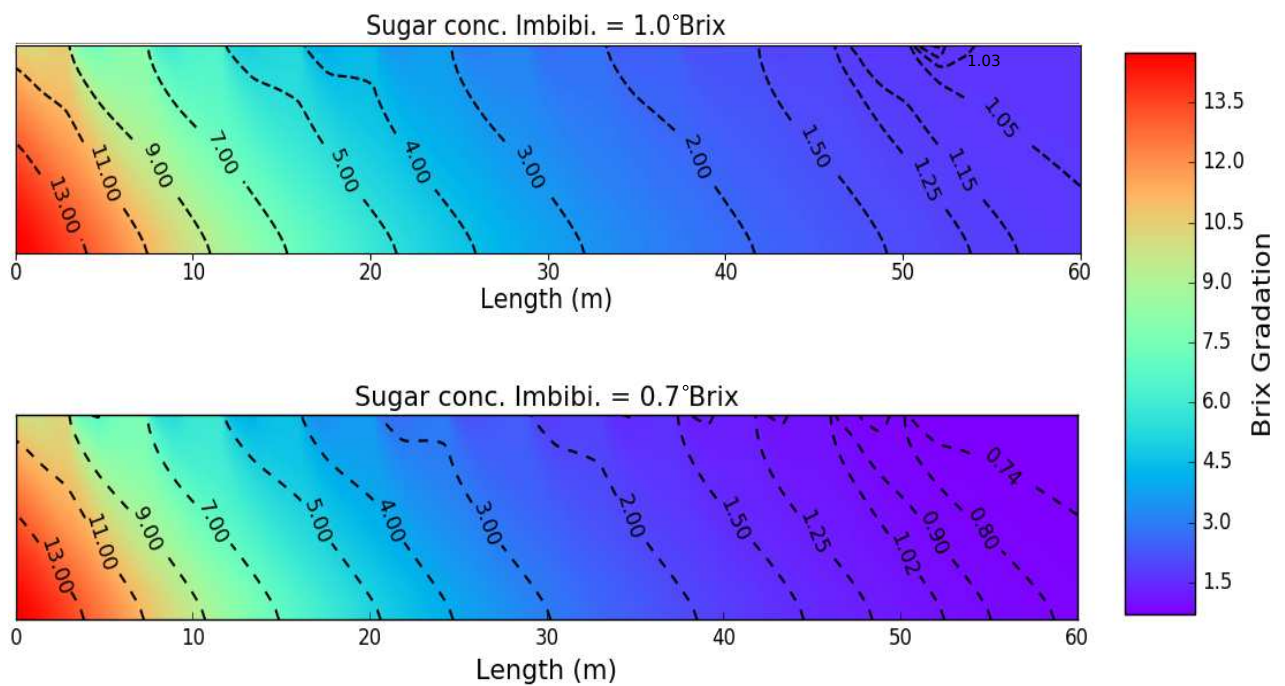


Figure 5.19: Simulated °Brix gradation concerning two distinct sugar concentrations of the imbibition water. Regions of the same °Brix value are represented by dash lines (isolines).

5.2.7 Percolating velocity

So far, the previous analyses were conducted assuming a constant percolating velocity in the sugarcane bed. Therefore, a single value (0.4 m/min as reported by the Table 5.1) was

used to represent the downward motion of the liquid in the whole modeled system. Changes in the percolating velocity directly or indirectly explain the effects of several variables on the extraction performance (as discussed in subsection 2.3.2). Instead of assessing individually each of these variables, the following analyses skip the intermediate steps and focus directly on the percolating velocity. Therefore, this subsection has the underlying intention to explore the capacity of the model to represent the expected behavior of the extraction process towards changes in v_p along the equipment. These analyses is going to be divided into two groups: one considering the v_p constant in the sugarcane bed and the other assuming a percolating velocity profile.

5.2.7.1 Percolating velocity constant in the bed

The first group of analyses evaluate the effects on the simulation outcomes promoted by an increase in the percolating velocity from 4.0 to 5.0 m/min in the whole sugarcane bed. Increasing the v_p value throughout the sugarcane bed leads to an increase in the extraction degree (Table 5.11). Such tendency is expected according to literature, since a higher percolating velocity improves the solid-liquid contact (REIN, 1971) and reduce the amount of sucrose recovered by the slower diffusion mechanism (REIN and INGHAM, 1992). Moreover, higher percolating velocities decrease the extent of the stagnant zones (REIN and WOODBURN, 1974), thus contributing for a faster extraction by the lixiviation mechanism. As a consequence of this scenario, transfer rates increase within the sugarcane bed, which contributes to higher extraction levels. It is worth to stress, however, that an unlimited increase of liquid flow is not possible, once it causes flooding in the bed (LOVE and REIN, 1980)

Table 5.11: Simulated extraction degree values for two percolating velocities. Each velocity is assumed valid in the whole equipment.

Percolating velocity <i>m/min</i>	Extraction %
0.4	94.2
0.5	95.0

Figure 5.20 captures the expected increment in the transfer rate due to an increase in the percolating velocity. For a percolating velocity of 0.5 m/min , a lower distance between successive isolines reflects a higher gradient of sugar. Besides, dashed lines have their position shifted leftwards, which indicates a faster extraction process. Simulated °Brix curves also

display an increase in the °Brix gradient for a superior percolating velocity (Figure 5.21). In relation to the faster percolating scenario, therefore, Figures 5.20 and 5.21 show °Brix values achieving a stationary region for a smaller length of the equipment. Such observation is important during the design and operation of a diffuser, since it provides insights about the required dimensions of this equipment and the flexibility of the operational process to achieve a desirable extraction level. In the former phrase, flexibility means the capacity to address variations in the operational process (*e.g.*, change of the cane throughput, variation in the aspersion characteristics) without jeopardizing the extraction degree.

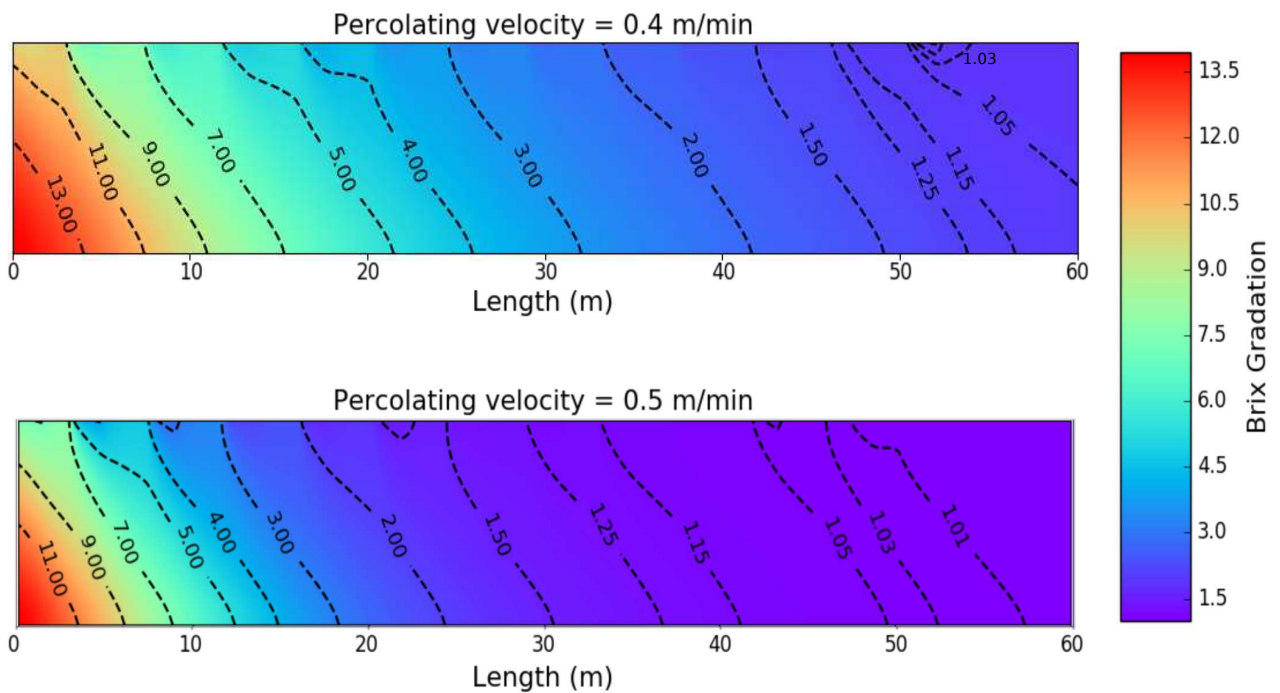


Figure 5.20: Simulated °Brix distribution inside the sugar cane for percolating velocities of 0.4 and 0.5 m/min. Regions of the same °Brix value are represented by dash lines (isolines)

Variations in the gradient of sugar promoted by an increase in v_p are coherent with the proposed extraction models (Eqs 3.13 and 3.14). Provided that v_b and the aspersion positions are kept constant, an increment in the percolating velocity (from v_p to $v_p + increment$ in Figure 5.22) leads to an intensification of the vertical flux of the percolating liquid. A higher downward flux reduces the length of the horizontal movement of the liquid inside the sugarcane bed. The percolating liquid thus enters in contact with regions of the bed possessing higher °Brix values (movement promoted by the resultant velocity v_{r2} in Figure 5.22). The contact with higher °Brix regions enhance the sugar difference among the percolating liquid and the other three bed sections. As a consequence, the extraction rates increase, once

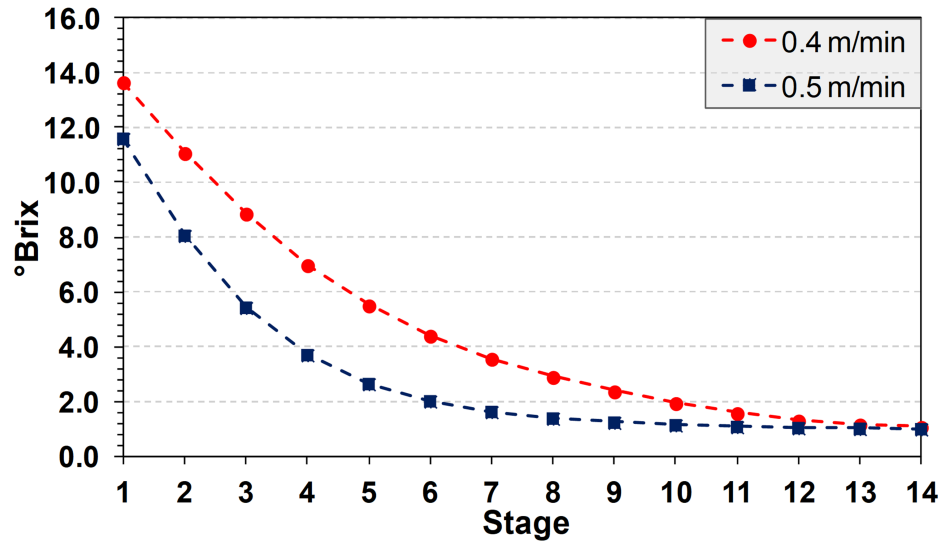


Figure 5.21: °Brix curve for percolating velocities of 0.4 and 0.5 m/min .

the proposed extraction models describe extraction as proportional to the sugar difference among the bed sections. Alike in the bed velocity analyses, the agreement between the real phenomenon and the mathematical description testify in favor of the chosen model for the extraction mechanisms.

5.2.7.2 Percolating velocity variation in the bed

The second group of analysis assesses the effects on the simulated outcomes promoted by variations on the percolating velocity along the equipment. As a consequence, it is going to be evaluated the capacity of the simulation framework to deal with changes in the v_p value. Such evaluation is important to throw light on the capacity of the model to handle more complex scenarios, such as the extraction process in unsaturated sugarcane beds. Figure 5.23 shows the four cases of v_p profiles applied in following assessments. The v_p profiles considered in the current study have as lower and upper limits the percolating velocities values used in the former analyses (*i.e.*, 0.4 and 0.5 m/min). It is important to highlight that these cases have an exploratory intention and do not strictly represent a real operation condition measured in the equipment.

The four cases are proposed to understand the impact on extraction performance promoted by different v_p magnitudes in distinct regions of the bed. Cases 1 and 3 represent abrupt variations in the percolating velocity. Concerning these two cases, changes in the v_p magnitude are promoted at the middle of the diffuser, thus dividing the equipment into two

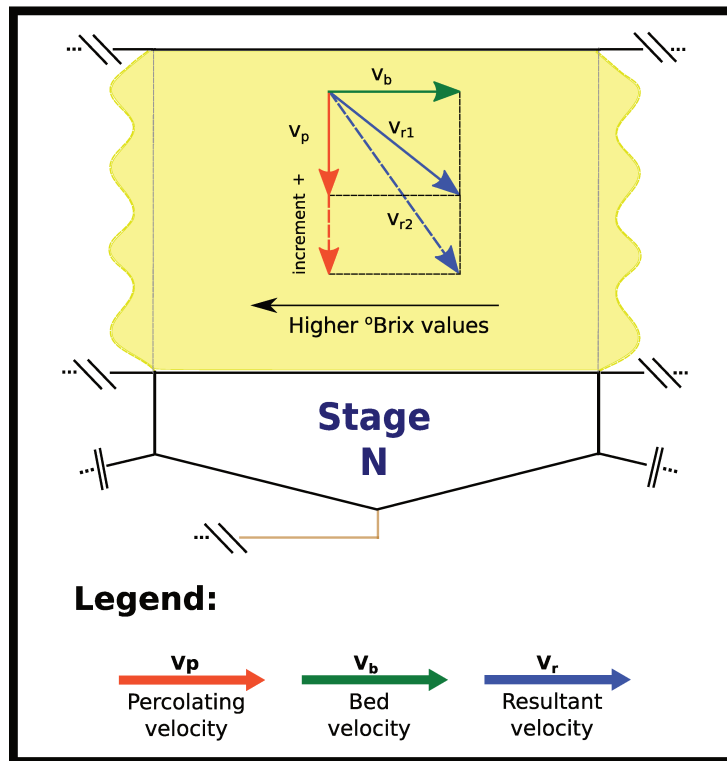


Figure 5.22: Resultant trajectory of the percolating liquid inside the bed for two percolating velocities: v_p and $v_p + \text{increment}$.

regions. By doing this division, it is possible to distinguish the impact of the v_p magnitudes on the extraction characteristics at each region of the equipment. Cases 2 and 4 represent a gradual variation of the v_p along the equipment. For the sake of simplicity, these variations are described in the assessments following a linear relation with the length of the equipment. The even cases are proposed, therefore, to assess the extraction performance in the absence of abrupt variations of the percolating velocity.

Table 5.12 presents the simulated extraction degree for each case. As a general observation, each scenario has an extraction value laying between those achieved by operating the diffuser with a single v_p value. It is an expected tendency, since these cases may be seen as intermediate conditions between the extraction process being performed with percolating velocities at 0.4 or 0.5 m/min . Limiting the assessment only to the extraction degrees, it was not found differences between abrupt and gradual variations in the percolating velocity. The explanation of these tendency may be seen by extending the analysis to the $^{\circ}Brix$ curves (Figure 5.24). Despite the different shape of the curves, either abrupt or gradual v_p variations leads to very close $^{\circ}Brix$ values at the front and end of the diffuser. Since extraction degree is computed by comparing the status of the bed at the two extremes of the equipment (Eq 3.28),

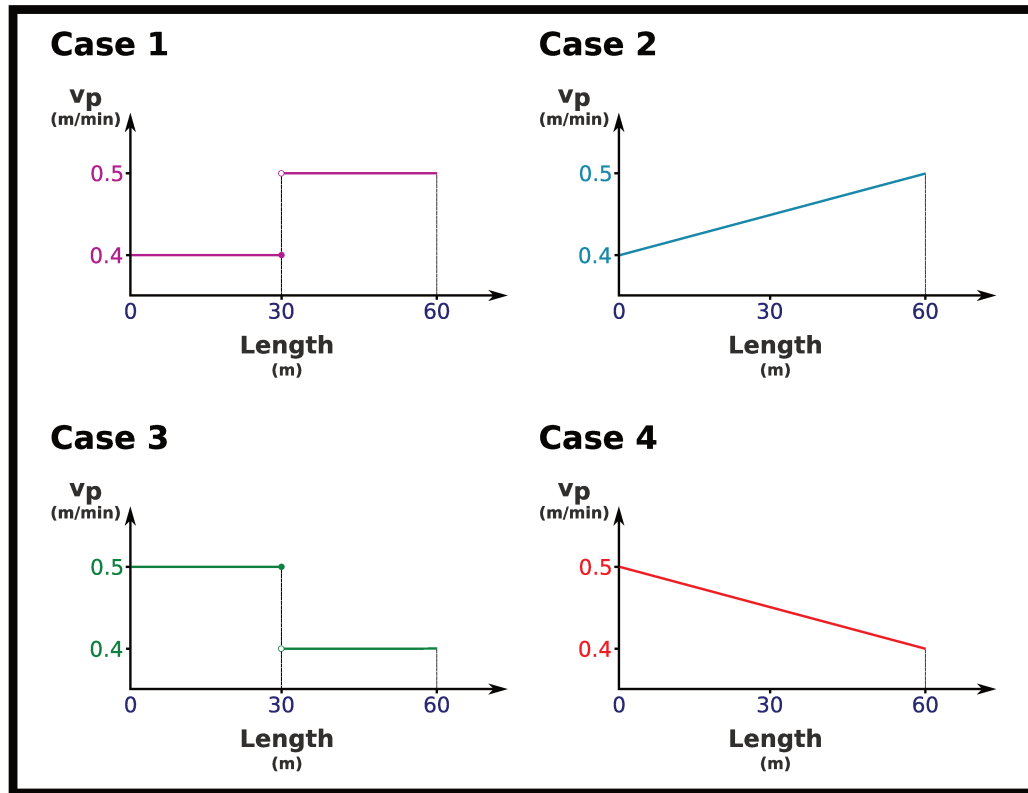


Figure 5.23: Percolating velocity profiles regarding the cases 1 to 4.

it is reasonable to expect equal extraction degrees between cases 1 and 2 as well as between cases 3 and 4.

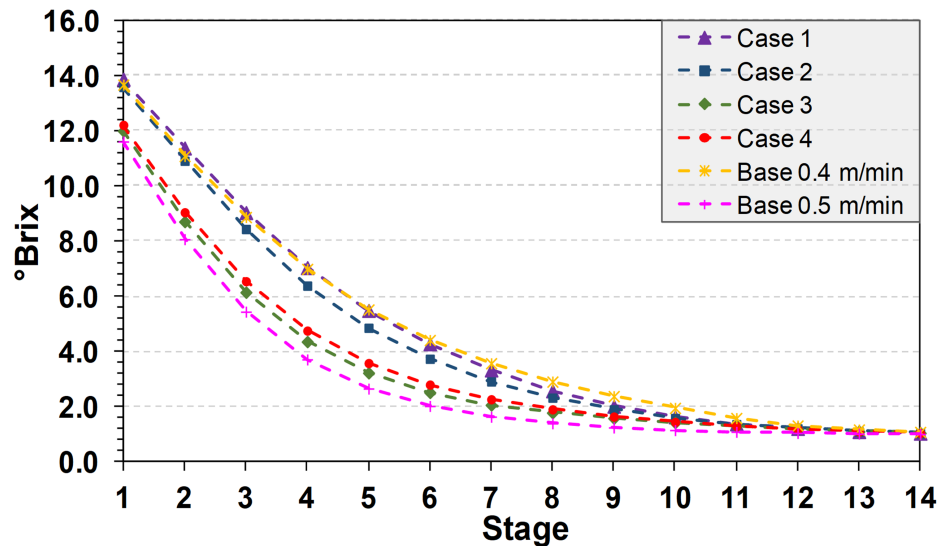
The higher extraction levels are those achieved by cases 1 and 2. These two cases have as a common characteristic the fact of the higher v_p values taking place at the second half of the diffuser. At this region, the extraction rate decreases due to a reduction of the sucrose difference among each bed section. However, higher v_p in this region fosters the extraction rate by increasing the vertical convective flux. In the real operation, such higher convective flux corresponds to a greater renewal of liquid in the bed. Moreover, a higher v_p value enhances the influence of the imbibition water on the extraction process. Therefore, it is expected to achieve higher extraction values by operating the diffuser with higher v_p values at the rear of the equipment.

Operating the diffuser with a higher v_p value at the first half of the equipment has a positive impact on the sugar gradient. Such positive impact is noticed by the steeper decrease of the °Brix values displayed by the °Brix curves of cases 3 and 4 (Figure 5.24). Moreover, the isolines of the °Brix distributions (Figure 5.25) are shifted leftward for cases 3 and 4, thus indicating a greater extraction rate. In this sense, °Brix distribution endorses the increase in

Table 5.12: Simulated extraction degrees regarding the cases 1 to 4.

Cases	Extraction
–	%
1	94.7
2	94.7
3	94.5
4	94.5

the sugar gradient displayed by the °Brix curves. As previously discussed (see 5.2.7.1), such increase in the sugar gradient at the initial stages of the diffuser are a direct consequence of a higher downward percolating velocity. Despite the advantage of cases 1 and 2 regarding the extraction degree, cases 3 and 4 requires a shorter diffuser to achieve their maximum extraction value. As pointed out before, it also opens room for more flexible extraction processes.

**Figure 5.24:** Simulated °Brix curves for the cases 1 to 4. The °Brix curves of the two constant v_p scenarios are also displayed in this figure (base 0.4 and 0.5 m/min).

It is also worthwhile to compare the effects on the sugar gradient of abrupt and gradual variations of v_p . In relation to cases 1 and 2, a gradual variation of the percolating velocity leads to a steeper decrease of the °Brix value, especially at the initial stages of the diffuser. Cases 3 and 4, however, displays an opposite tendency in which the abrupt variation scenario contributes to a higher °Brix gradient at the front of the equipment. The two previous tendencies may be seen in the Brix curves of Figure 5.24 and in the position of the isolines of Figure 5.25. Case 2 (3) presents, in general, higher v_p values in the initial

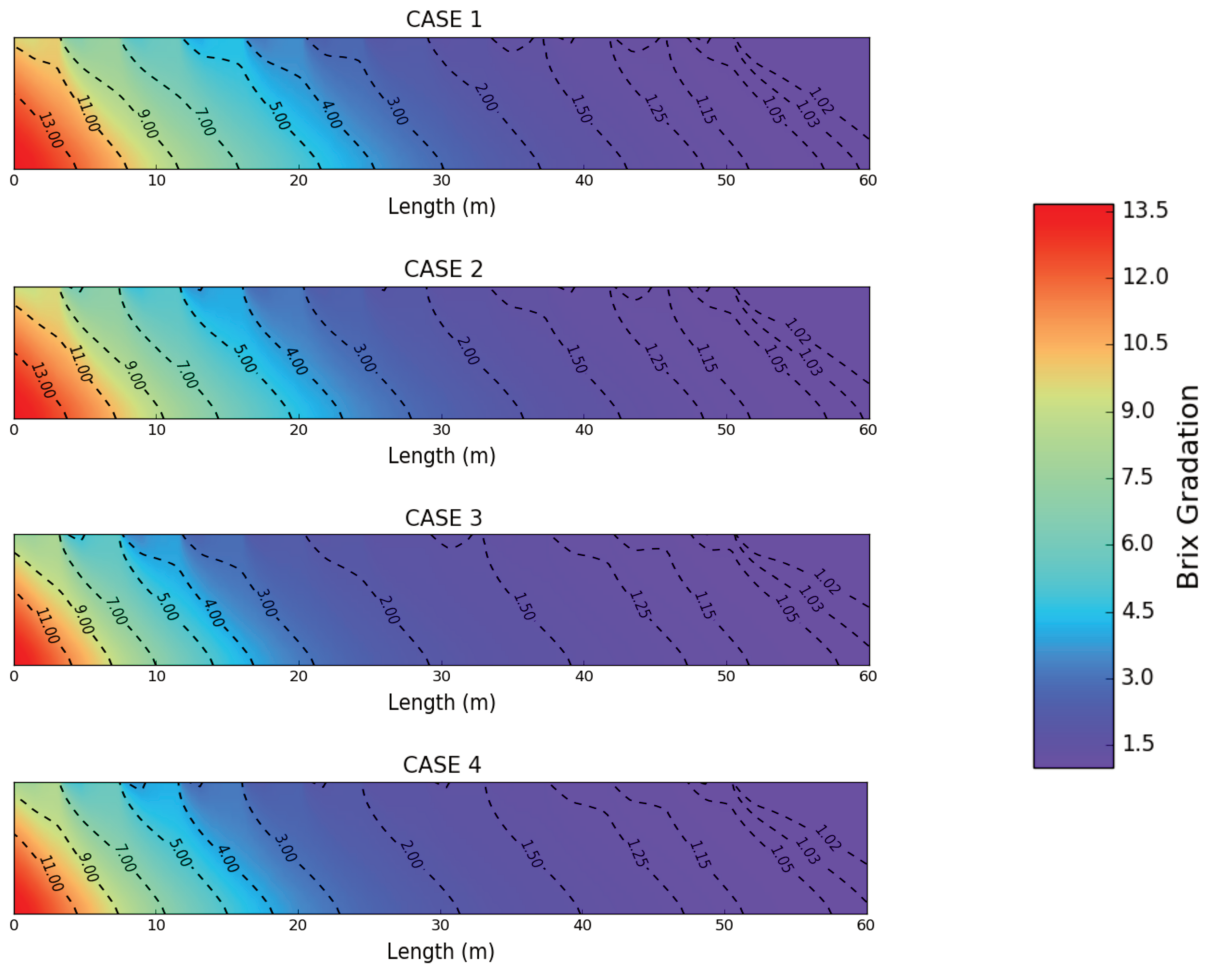


Figure 5.25: Simulated °Brix distribution regarding the cases 1 to 4. Regions of the same °Brix value are represented by dash lines (isolines).

stages of the equipment than case 1 (4). Using the same arguments posed in the former paragraph (*i.e.*, increasing v_p leads to a greater extraction rate), such higher v_p is the cause of the steeper decrease of the °Brix values observed in the cases 2 and 3.

A fifth case is proposed in order to assess the influence of the lifting screws in the extraction performance (Figure 5.26). This case is a more realistic scenario and may be interpreted as a combination of cases 1 and 4. The upper limit of v_p (*i.e.*, 0.5 m/min) is assigned to the entrance of the equipment. A gradual reduction of the percolating liquid takes place inside the equipment following the same rate of decrease as presented in the case 4. In a real equipment, such gradual decrease in v_p occurs due to the rearrangement of the fibers into a more packed conformation and the compaction effects promoted by the aspersion of liquid over the bed. In the modeled equipment, there are two sets of lifting screws: one at 17 m and the other at 48 m . These screws revolves the bed and reduces the compaction

effects, thus leading to an abrupt increase in the percolating velocity. It is assumed that the v_p value is restored to the upper limit after crossing a set of lifting screws. The linear reduction of the v_p value continues after each set of screws.

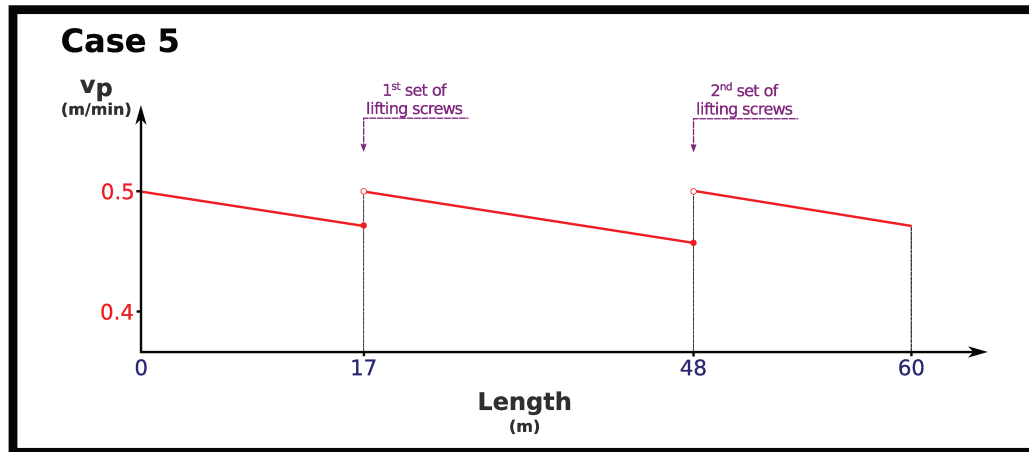


Figure 5.26: Percolating velocity profile regarding the case 5.

The presence of the lifting screws leads to an operation condition in which v_p value is kept near the upper limit throughout the sugarcane bed. The extraction degree achieved in the case 5 is 94.7 %, which is higher than the value presented for case 4. Such fact may be explained by the conservation of a higher percolating velocity at the second half of the diffuser, thus leading to the same phenomenon reported before in relation to cases 1 and 2. Another feature of case 5 is a higher °Brix gradient at the first half of the diffuser (see °Brix curve at Figure 5.27) in comparison with cases 1 and 2. The position of the isolines in the °Brix distribution of case 5 (Figure 5.28) agrees with the steeper °Brix reduction displayed by the °Brix curve. Such reduction tendency are explained by the same reasons as presented before in relation to cases 3 and 4: higher v_p values at the initial stages of the equipment leads to a greater °Brix gradient.

The five cases demonstrates the importance of maintain the percolating velocity (*i.e.*, liquid flow within the sugarcane fibers) as high as possible throughout the bed. Such fact is in accordance with the expected behavior of a full-scale diffuser and was extensively reported in the literature (see subsection 2.3.2). The analysis performed in the five cases also demonstrates the importance of the lifting screws to the extraction performance. Moreover, case 5 has extraction characteristics (*i.e.*, shape of the °Brix curve, position of the isolines in the °Brix distribution) closer to the scenario in which the diffuser operates with a constant v_p at the upper limit (0.5 *m/min* for the cases proposed in this thesis). This result advocates in favor of the hypothesis that the presence of the lifting screws may endorse the fifth general

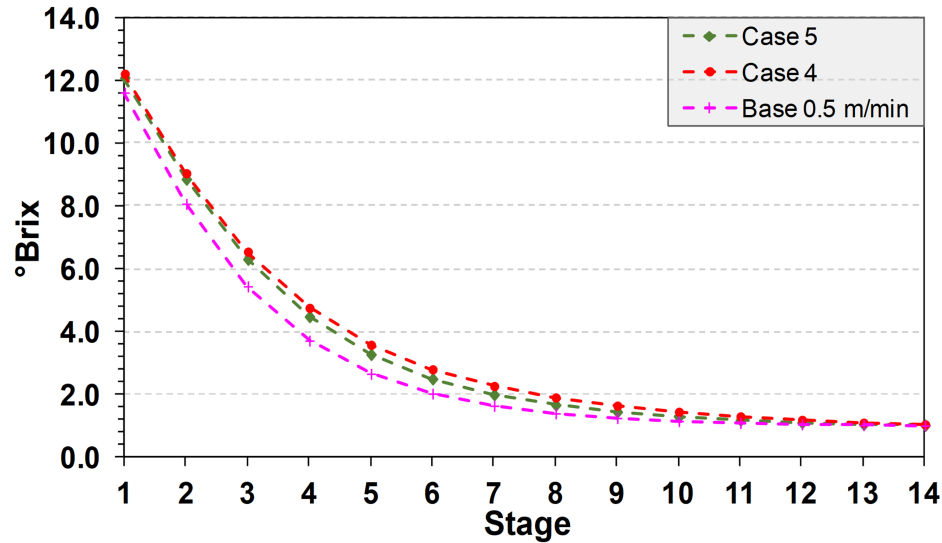


Figure 5.27: Simulated °Brix curves for case 5 in comparison with case 4 and base case of constant v_p at 0.5 m/min .

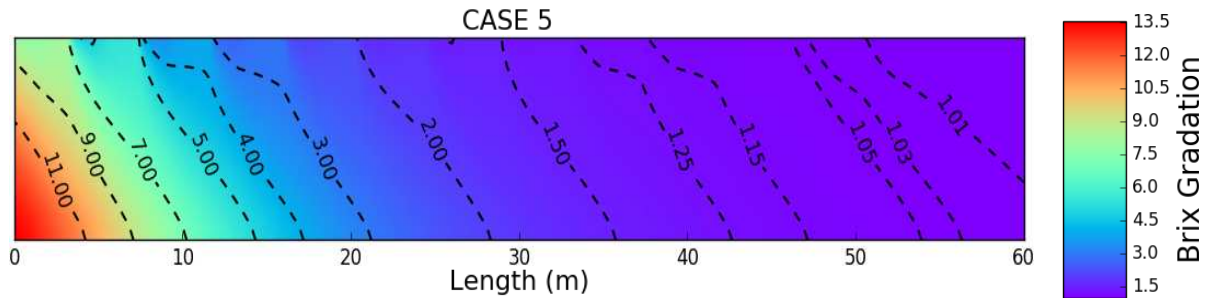


Figure 5.28: Simulated °Brix distribution for case 5. Regions of the same °Brix value are represented by dash lines (isolines).

assumption (section 3.3) and, as consequence, support the simplification of using a single v_p value to represent the liquid flux in the whole bed (see subsection 3.6.1).

5.2.8 Concluding remarks about the steady-state simulations

The system of linear algebraic equations representing the proposed model in its discretized form is well-posed. Such conclusion is based on the three factors proposed by *Hadamard* to define the “well-posedness” of a mathematical problem (*TANNEHILL et al.*, 1997). First and second factors concern, respectively, the existence of a solution and its uniqueness. The discretized model at steady-state fulfill these two requirements, since it has solution and the results are unique for each simulated scenario. The third factor demands

that the solution must depend continuously on the data. In other words, the solutions can not have abrupt or drastic changes promoted by slightly variations in the value of the model's parameters. The discretized model satisfies the third condition, since, whenever a change is promoted in the base scenario, the solution is able to achieve a new, feasible, and consistent result.

Under a constructivist perspective, validity (or truth) of a model is determined by its coherence/consistence with a set of beliefs that are accepted as true (TOLK, 2013). Regarding the scope of the thesis, this set of beliefs embraces the phenomenology of the extraction process and the expected, observed behavior of a diffuser under operation in an industrial facility. The simulations performed in the current section lead to results coherent and consistent with the extraction phenomenology as well as with the expected and observed features of a full-scale diffuser during operation. By following this constructivist perspective, therefore, the previous simulations and analyses testify in favor of the validity of the developed model concerning its ability to represent the real system.

The constructivist yardstick may sound a weak approach to testify the validity/truth of the proposed model, especially for someone who compares it with the positivist perspective. In the positivist view, validity/truth is assigned to a model based on its strict correspondence with a fact of reality (TOLK, 2013). This strict correspondence is evaluated by measuring the difference among data collected in a real system (*i.e.*, °Brix distribution, °Brix curve) and the results of the simulations. As a consequence, the positivist approach is not directly applied for models of systems in which data is hard or even impossible to be collected (SCHMID, 2005). A moving-bed diffuser in an industrial facility is exactly this type of system, in which unrestricted experimentation is not allowed or not feasible. Moreover, once the set of beliefs is understood and determined in the constructivist perspective, validity/truth of a model is as rigidly defined as it would be in the positivist approach (TOLK, 2013). In this sense, the constructivist interpretation of the simulations is maintained in the past assessments as well as in the following analyses.

5.3 Dynamic simulations

This section is going to revisit some of the steady-state analysis performed in the previous section in order to assess their transient behavior. The evolution of the °Brix curves as well as the °Brix distributions, as function of time, is going to be the base of the following

assessments. The transient simulations are going to be presented both as figures in the current text (*i.e.*, “the traditional way”) and also as *YouTube* videos. At *YouTube*, it is possible to see each transient behavior as an animation, thus allowing a better visualization of the phenomena under analysis. The digital version of this thesis (*i.e.*, the pdf file) has direct links to all of the videos. In order to access a video related to a specific figure, a reader may click on the link “[YouTube](#)” at the label of the respective figure. Regarding a reader with a printed version of the thesis, it is also provided at the label of each figure the *URL* of the video.

It is important to give a disclaimer in relation to the animations of the °Brix distributions. The isolines presented in these videos do not have labels as those displayed by the figures embedded in the text. This fact is due to the impossibility of satisfactorily animate such labels. However, it is still possible to fully understand these videos by using the figures of the thesis as visual guides.

5.3.1 °Brix in the raw material

This subsection explores the transient behavior of the extraction process as a consequence of a change in the °Brix of the raw material. As a matter of fact, the present analysis extends the assessment presented in the subsection 5.2.4. Therefore, the initial condition is a diffuser operating with a raw material possessing 18 °Brix. The simulated transient state captures the variation in the extraction process promoted by a feedstock with 14 °Brix. The integration process of the system of ODEs was performed using five different time steps: 1.0, 0.5, 0.1, 0.05, and 0.01 seconds. Such sensitivity analysis has the intention to assess the effect of the integration steps on the numerical stability of the simulations. Moreover, this analysis is also a way to assess the variations in the simulated results promoted by different time steps. Regarding the numerical stability, the integration process becomes unstable by using the integration step of 1.0 second. Moreover, such instability leads to results that diverges completely from the new steady state of the system. Concerning the other four integration steps (*i.e.*, 0.5, 0.1, 0.05, *and* 0.01 s), all of them are numerically stable and converges to the new steady state of the system.

In relation to each time step below 1.0 s, the integration process using a 4th or a 1st order Runge-Kutta method leads to almost equal results along each transient procedure. Figure 5.29 presents the evolution of the average of the estimated local error over the first hour of the transient processes. This figure was generated using the time step of 0.5 s, but

similar results are achieved for the other three stable integration steps. The magnitude of the differences between the solutions simulated by the two Runge-Kutta methods is 10^{-8} °Brix for the four stable time steps over most part of the first hour of the simulated transient procedure. Moreover, these errors present a progressive decrease that leads to a constant magnitude of 10^{-9} °Brix for the rest of the dynamic procedure. Such facts indicate that the estimated local errors are small and evolves towards a stable condition, which means that the modeled system progresses as function of time in a smooth way. A smooth transient behavior means the absence of abrupt or sharp variations in the °Brix value at each volume of the solution grid.

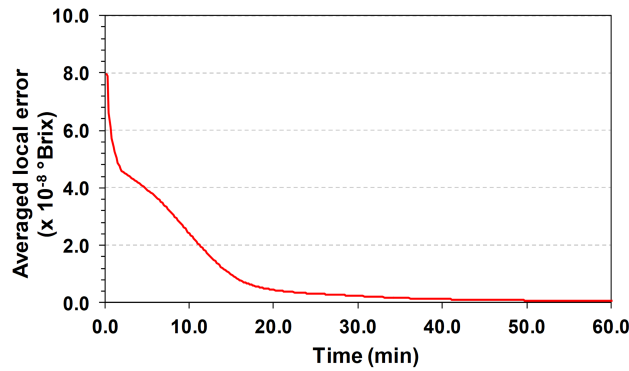


Figure 5.29: Evolution of the average of the estimated local error over the first hour of the transient process. Figure generated using a time step of 0.5 s. Such errors concerns the transient state promoted by a variation in the °Brix of the raw material from 18 to 14 °Brix.

Provided that the time steps do not lead to numerical instabilities, another consequence of a smooth transient process is a lower sensibility of the simulated results towards changes in the integration step. This tendency is observed in the simulated results, since the outcomes achieved by the stable time steps (*i.e.*, 0.5, 0.1, 0.05, and 0.01 s) are quite close during the whole integration procedure. For instance, the simulated results using the time steps of 0.5 and 0.01 s present differences in which the magnitude order is of 10^{-5} °Brix in all iterations of the transient solutions. At this point, it is important to discuss the time required to perform a transient procedure. Table 5.13 shows the time required to simulate 10 min of the present transient process as function of the integration step. According to this results, it is not worth to perform a longer simulation using a lower time step (*e.g.*, 0.01 s), since the differences of the results simulated using distinct time steps are small. Therefore, the transient behavior of the °Brix curve and the °Brix distribution presented in the following discussion are simulated using a integration step of 0.5 s.

The evolution of the Brix curve as function of time is presented in the Figure 5.30.

Table 5.13: Simulation time, as function of the integration step, required to simulate 10 *min* of a transient process promoted by a variation in the °Brix of the raw material from 18 to 14 °Brix.

Time step	Simulation time
<i>s</i>	<i>min</i>
0.5	0.75
0.1	3.6
0.05	7.3
0.01	34.8

Every time lapse displayed in this Figure present two motionless curves regarding the initial condition (*i.e.*, raw material with 18 °Brix) and the new steady state (*i.e.*, diffuser processing a feedstock with 14 °Brix). The transient curve, in their turn, moves from the initial position towards the new steady state. As time goes by, such movement starts at the front of the equipment and propagates to the remain of the diffuser. It is as expected behavior since the modification in the simulated system is promoted at the entrance of the equipment by changing the boundary conditions of the two fiber sections (*i.e.*, the C_{rm}^{in} value). This rightward propagation of the transient behavior may also be noticed in the evolution of the isolines of the °Brix distribution (Figure 5.31). At each time lapse of the Figure 5.31, the isolines are progressively shifted towards the entrance of the diffuser. Over the course of time, such variation in the isolines positions starts at the front of the equipment and spreads to the remain of the sugarcane bed.

The simulated transient phenomenon present a variation in its intensity along the diffuser and over the simulated time span. At this point of the discussion, it is highly recommended to stop the reading procedure in order to pay some extra attention on the YouTube videos. The °Brix curves and the °Brix distribution presents a faster variation in the first hour of the transient process, especially at the front of the equipment. After this initial period, the °Brix curve and the position of the isolines change with a progressive slower pace. This fact is a result of the reduction in the difference of the °Brix distribution between the transient system and the new steady state. Such reduction happens along the diffuser, as well as over the simulated time span concerning the equipment as a whole. The gradual reduction of this Brix differences decreases the driven force of the transient phenomenon over the course of the simulation procedure. In fact, such behavior agrees with the mathematical nature of the proposed extraction models (Eqs 3.13 and 3.14), which describes the mass transfer in the system as proportional to the difference of the sucrose concentration among the bed sections. The modeled system achieves the new steady-states in about 7.0 hours.

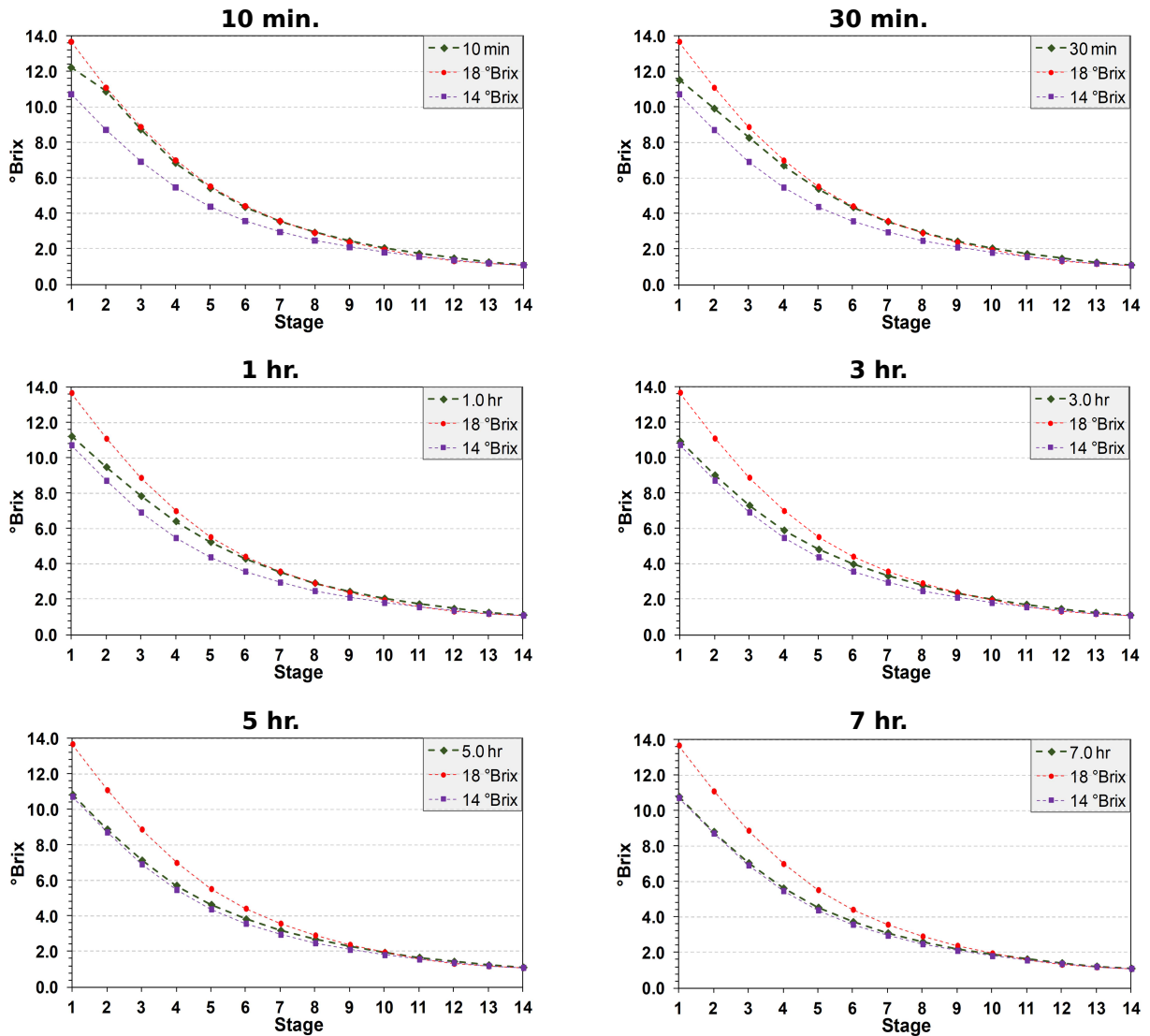


Figure 5.30: Evolution of the °Brix curve as function of time promoted by a variation in the °Brix of the raw material from 18 to 14 °Brix ([YouTube](https://youtu.be/bvxyZX9h3hc)). URL: <https://youtu.be/bvxyZX9h3hc> .

5.3.2 Imbibition position

Among the analyses concerning the imbibition properties (subsection 5.2.6), the variation in the aspersion position of the imbibition water from from 51 (*i.e.*, base case) to 15 *m* was the one that promotes the most drastic changes of the extraction characteristics. In order to assess the stability of the simulations to handle intense transient processes, the following discussion is going to assess the dynamic behavior of this shifting in the aspersion position of the imbibition water. As done in the previous subsection, it is performed the

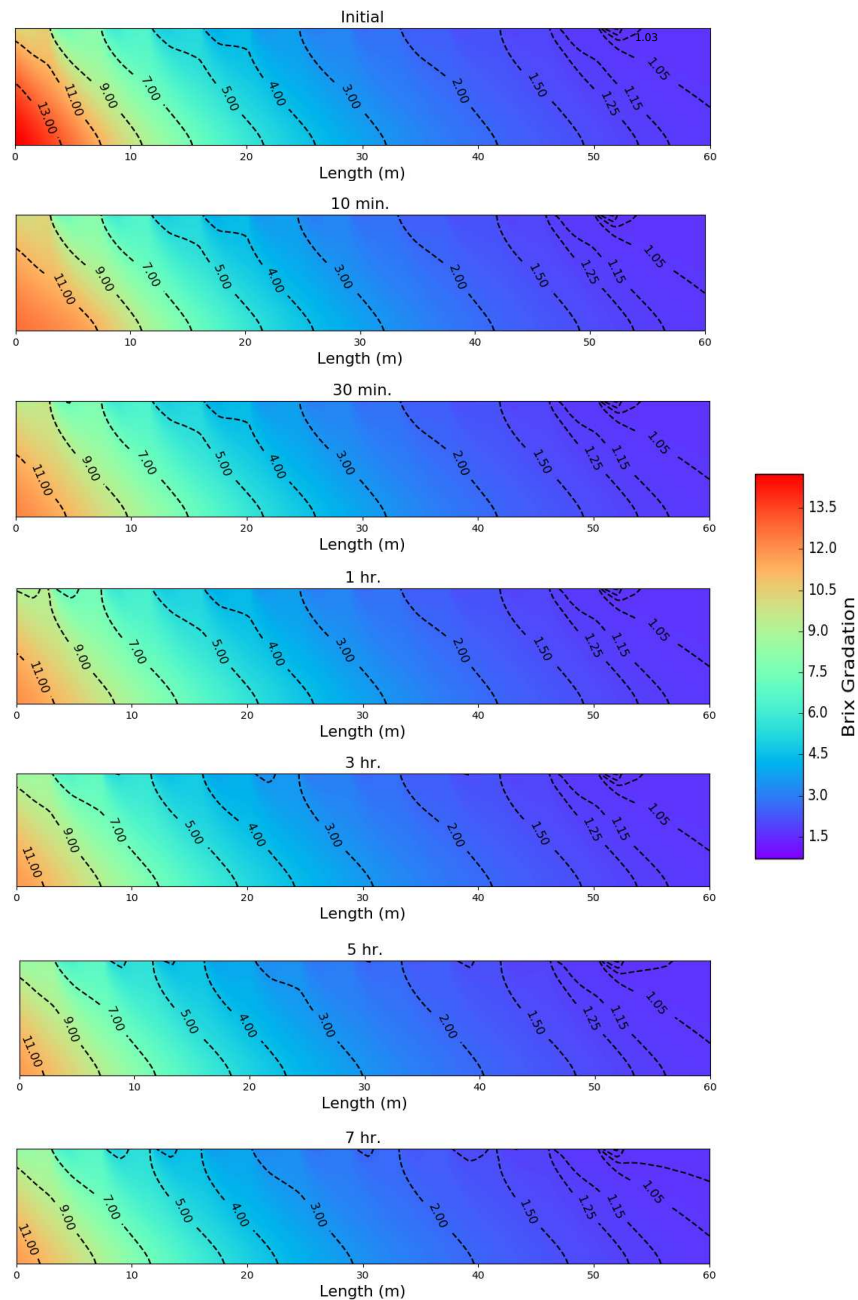


Figure 5.31: Evolution of the °Brix distribution as function of time promoted by a variation in the °Brix of the raw material from 18 to 14 °Brix ([YouTube](https://youtu.be/IpbjiYEZEwo)). URL: <https://youtu.be/IpbjiYEZEwo> .

sensitivity analysis of the integration step using the same values of time: 1.0, 0.5, 0.1, 0.05, and 0.01 seconds. Once again, the time step of 1.0 s leads to numerical instabilities that make the solution to diverge from the new steady state. The other four time steps, in their turn, are stable and converge to the new steady condition.

The local errors of the transient process are estimated for each of the stable time steps (*i.e.*, 0.5, 0.1, 0.05, and 0.01 *s*). The analysis displayed in Figure 5.32 is the one performed using a time step of 0.5 *s*. However, this analysis is also valid for the other integration steps, since each of them leads to similar results. Over the initial 10.0 *s* of the transient processes (Figure 5.32-(a)), the difference of the solutions computed using a 4th or a 1st order Runge-Kutta method have a magnitude order of 10^{-6} °Brix. This magnitude is higher than the one computed for the variation in the °Brix of the raw material. Such higher magnitude is a consequence of a more intense transient process at the beginning of the simulated period. A pronounced dynamic behavior leads to less smooth variations of the °Brix values in each volume of the grid. Therefore, it is expected higher differences among the results computed by integration methods with different order of accuracy, since a higher order method is capable to better represent the less smooth variations in the transient state.

After the initial shock promoted by the abrupt variation in the imbibition position, the average of the estimated local errors presents a fast decrease. Indeed, over the course of the first hour of the simulated process (Figure 5.32-(b)), the local errors achieve a constant magnitude of 10^{-8} °Brix. Such decrease of the errors is a consequence of the reduction in the intensity of the transient process. In relation to the outcomes of the simulations, it is observed a lower sensitivity of the results towards changes in the integration steps. The difference between the results simulated using the time steps of 0.5 and 0.01 *s* has the magnitude order of 10^{-4} °Brix. The simulation times are similar to those present in the Table 5.13, since the computational procedures are equal to those performed in the previous transient assessment (*i.e.*, variation in the °Brix of the raw material). In this scenario, therefore, it is also not worth to perform longer simulations because the differences among the results achieved using distinct time steps are small.

Figure 5.33 presents the evolution of the °Brix curve over the course of time for the present transient phenomena. This Figure as well as the °Brix distribution as function of time (Figure 5.34) are simulated using a time step of 0.5 *s*. The two static °Brix curves displayed in the Figure 5.33 represent the initial condition (*i.e.*, imbibition position at 51 *m*) and the new steady state (*i.e.*, imbibition position at 15 *m*). The evolution of the Brix curve shows that the transient process starts near the 4th stage, which is at the region of the new aspersion position of the imbibition water. From this initial point, the transient behavior propagates to the front and rear of the diffuser. The time frames of the Brix distribution (Figure 5.34) also show the same tendency. The disturbance of the isolines starts at the top of the sugarcane bed, close to the 15 *m* of the equipment. As time goes by, the transient process

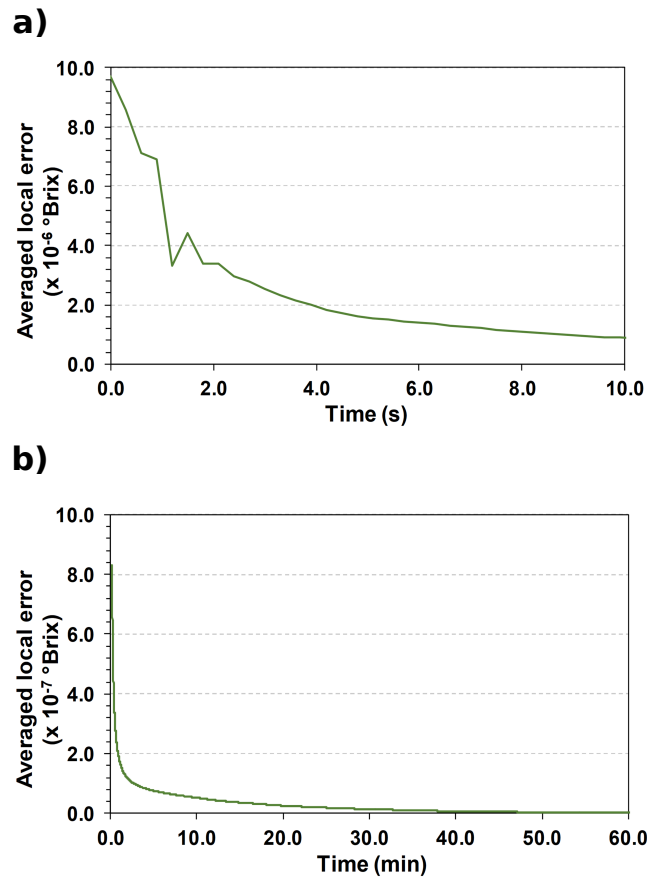


Figure 5.32: Evolution of the average of the estimated local error over (a) the initial 10 s of the transient process and (b) from 10.0 s to 1.0 hour of the same dynamic procedure. Figure generated using a time step of 0.5 s. These errors concerns the transient state promoted by a change in the aspersion position of the imbibition water from 51 to 15 m.

propagates to the bottom of the bed as well as to both front and rear of the equipment.

The intensity of the transient phenomenon is not uniform along the diffuser. Such fact is better observed in the evolution of the isolines positions as function of time (Figure 5.34). The isolines at the rightward of the new imbibition position have a more intense variation than those located leftwards. This fact emerges mainly by the influence of the rightward convective flux assumed during the modeled procedure as well as the effect of the counter-current arrangement of the aspersions. Such influences are responsible to propagate the variations in the °Brix values towards the end of the diffuser. In their turn, the regions of the bed before the embibition position (*i.e.*, leftward) sense the transient phenomena by means of the dispersion effect and also by the counter-current aspersions. Comparing the rightward convective flux with the dispersion flux, the former is more intense than the latter.

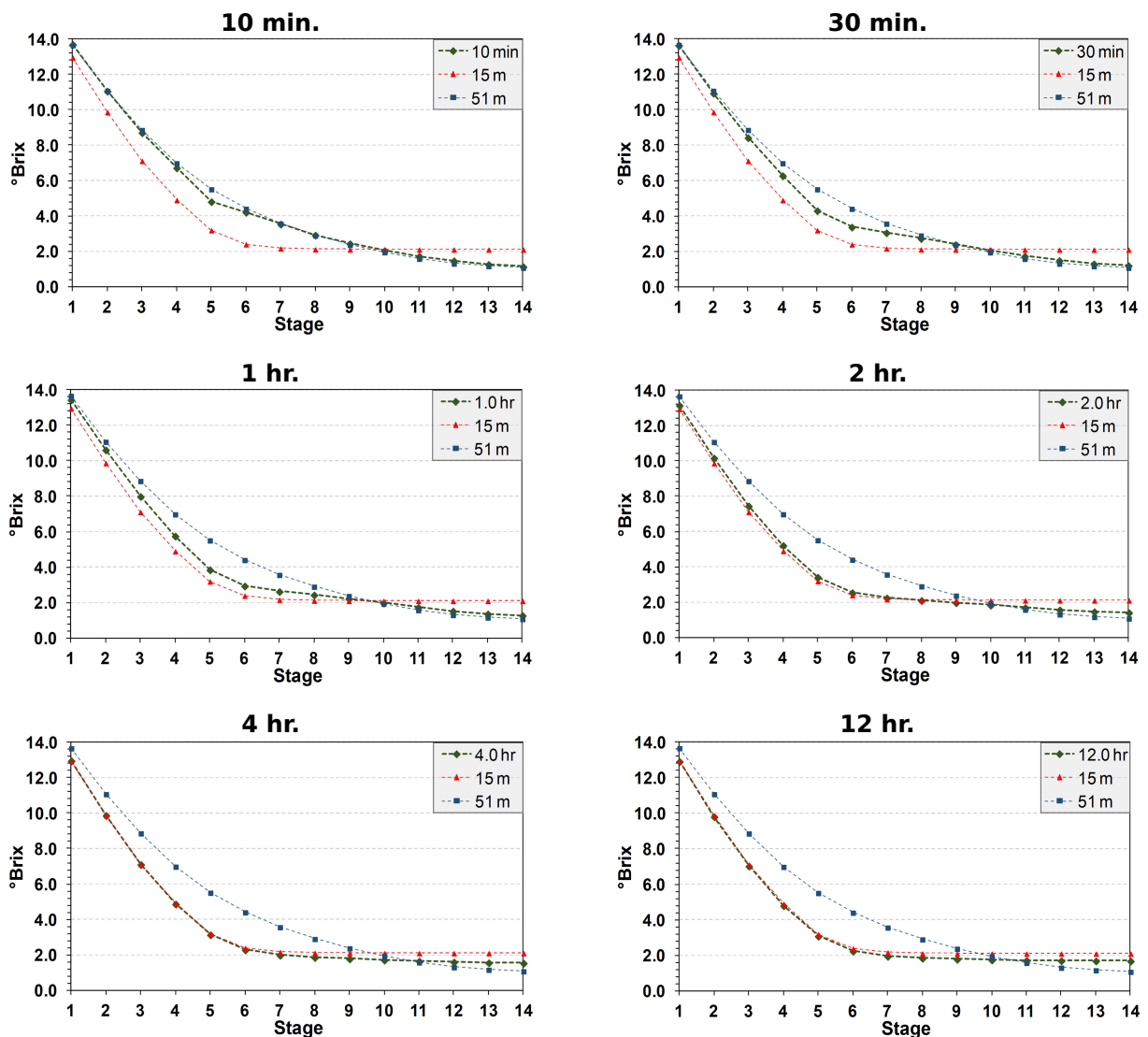


Figure 5.33: Variation in the °Brix curve as function of time promoted by a change in the aspersion position of the imbibition water from 51 to 15 *m* ([YouTube](https://youtu.be/93sYuNQry3A)). URL: <https://youtu.be/93sYuNQry3A> .

In relation to the aspersion positions, the leftward region possesses less counter-current aspersion points than the rightward region. These two facts, therefore, lead to a more intense variation in the °Brix values at the rightward of the new imbibition position.

The intensity of the transient phenomena varies also over the course of time. At the beginning of the transient process, both the °Brix curve and the °Brix distribution present faster variations in their initial conditions. However, as the extraction environment comes closer to the new stationary condition, the °Brix curve and the isolines positions present a reduction of their transient pace. Such reduction is explained by the same reason as

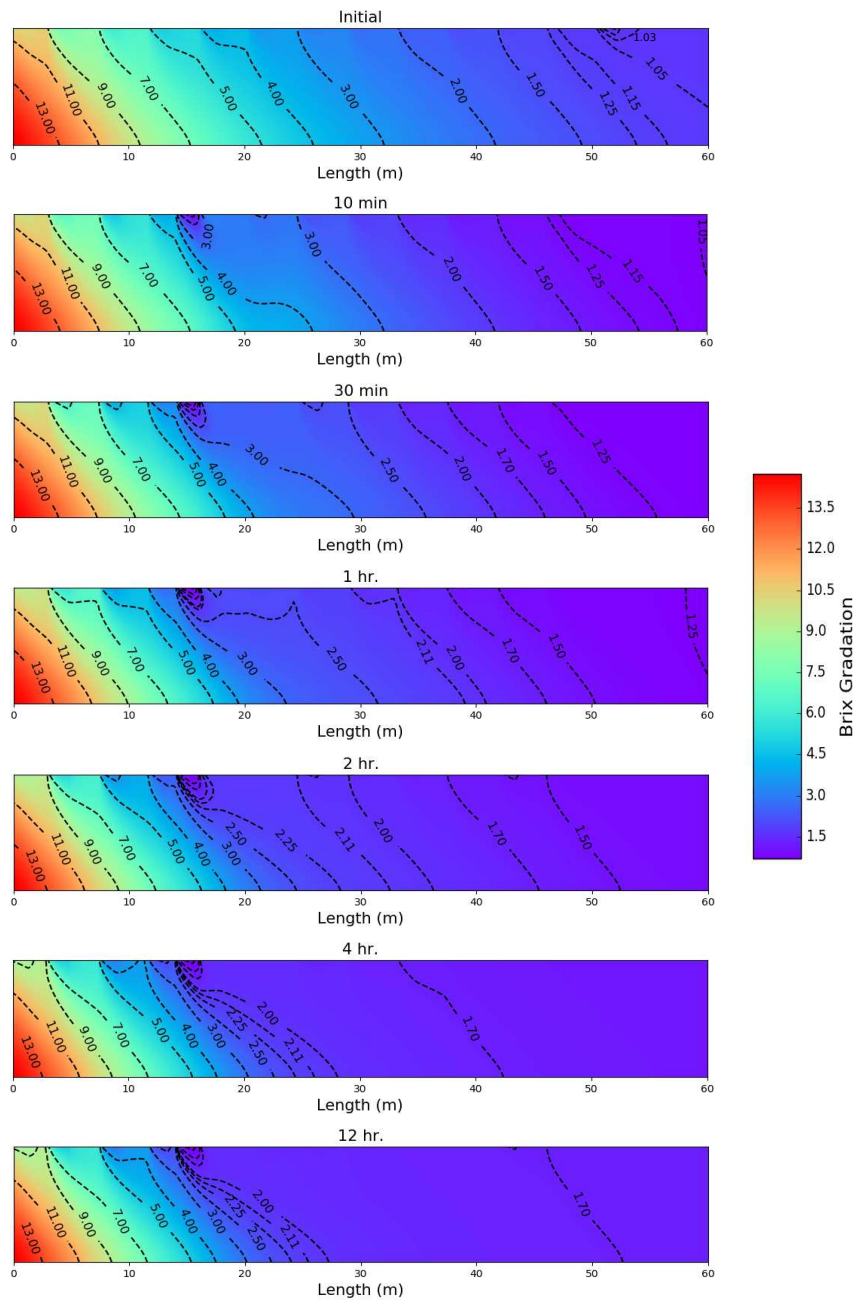


Figure 5.34: Variation in the °Brix distribution as function of time promoted by a change in the aspersion position of the imbibition water from 51 to 15 m ([YouTube](https://youtu.be/yqIMbLWtVSc)). URL: <https://youtu.be/yqIMbLWtVSc> .

discussed in the previous subsection: the driving force of the transient phenomenon, which is the differences of the °Brix values between the transient system and the new steady state, reduces over the passage of time. Such reduction in the transient pace over the course of the time makes the extraction environment after the 7th stage to take a long period to achieve the steady condition (see the YouTube video of the Figure 5.33).

5.3.3 Percolating velocity

The present assessment explores the transient behavior of a variation in the percolating velocity from 0.4 to 0.5 m/min . This assessment is performed considering the change in the v_p value over two approaches. The first one is an instantaneous shift in the percolating velocity, in which all of the volumes of the grid sense the v_p variation at the same time at the very beginning of the transient procedure. The second approach assumes that the new v_p value propagates within the sugarcane bed, following the procedure described in the section 4.3. It is assumed that such propagation presents a single source that embraces the whole top of the diffuser's bed. Therefore, the propagation front, which extends along the whole extension of the diffuser, descends the bed from the top to the bottom of the equipment. These two propagation approaches are going to be addressed along this subsection as the scenarios without propagation and with propagation, respectively. The following discussion has as the underlying intention to compare these two approaches in order to understand the impact on the transient simulations promoted by these two distinct propagation regimes of the percolating velocity.

Both propagation approaches present equal results in relation to the sensitivity analysis of the integration steps. Indeed, such results are similar to those already discussed in the two previous subsections: numerical instabilities emerging for the time step of 1.0 s and stable and convergent results regarding the four other integration steps (*i.e.*, 0.5, 0.1, 0.05, and 0.01 s). Concerning the comparison between the outcomes computed using a 4th and 1st order Runge-Kutta methods, the four stable integration steps lead to similar results for each of the propagation regimes. Therefore, the following analysis of the estimated local errors are based in simulations using the integration step of 0.5 s .

Figure 5.35 presents the averages of the estimated local errors over the first hour of the transient phenomenon for a v_p variation without propagation (frames a and b) and with propagation (frames c and d). The scenario with v_p variation without propagation has a estimated local error with magnitude order of 10^{-7} °Brix over the first minute of the transient phenomena (Figure 5.35-(a)). After this initial period, the averages of the differences between the 4th and 1st order Runge-Kutta methods drop to the magnitude order of 10^{-8} °Brix and, at the end of the first simulated hour, achieve a stable condition with a magnitude order of 10^{-9} °Brix (Figure 5.35-(b)). A higher local error at the beginning of the transient process is a consequence of the instantaneous variation of the percolating velocity. Such variation promotes a more intense change of the extraction characteristics, which is better described

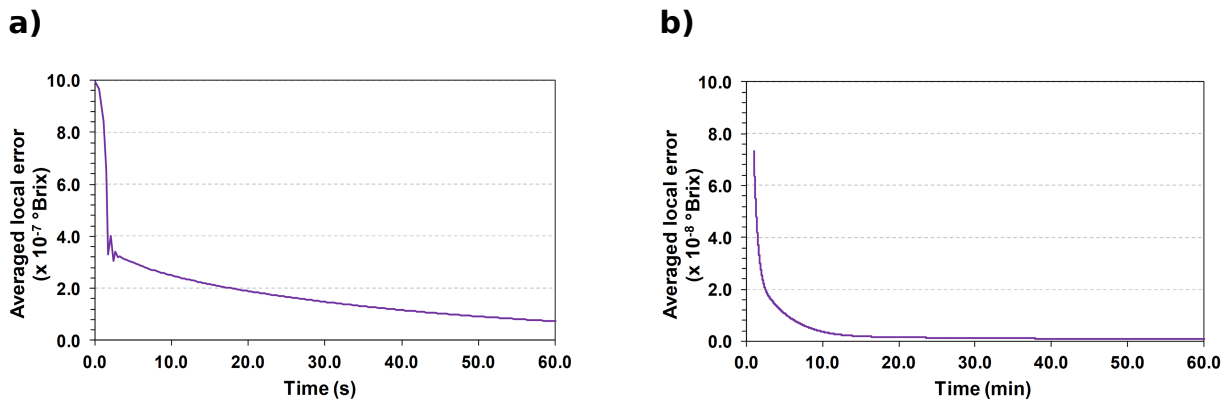
by a higher order integration method. Since all the volumes of the grid sense the transient effect at the same time, the observed fast drop of the local errors is consequence of a fast accommodation of the extraction environment to the transient phenomenon.

The averages of the estimated local errors captures the proposed propagation regime of the percolating velocity, especially for the first 5 minutes of the simulated transient procedure (Figure 5.35-(c)). In the Figure 5.35-(c)), it is possible to notice 20 peaks of the estimated local error. The number of peaks is equal to the amount of volumes in the vertical direction of the grid. Therefore, it is reasonable to relate those peaks with the progressive change of the v_p value in each of the 20 horizontal sections of the grid (remember that the present grid is a 20X20 per stage type). When the propagation front promotes a change in the v_p value of a horizontal section, the transient phenomena sense an increase in its intensity. Such increase is followed by a raise of the values of the local errors. The magnitude of the peaks increases as the propagation front gets closer to the bottom volumes of the grid. It is an expected tendency, since the bottom volumes impact the whole extraction system through their role in the counter-current aspersions.

After each peak observed in the regime with propagation, the local errors present a fast decrease. These fast decreases are evidences of the stability of the transient simulations over the course of the propagation procedure. Concluding the propagation process, the local errors no longer present the observed peaks and their magnitude order decreases up to 10^{-9} °Brix by the end of the first simulated hour, thus displaying the same behavior of the scenario without propagation.

Within the set of the stable time steps, the results simulated using distinct integration steps are quite close over the transient process. Such similarity among the results are observed in the two propagation regimes. Concerning the scenario without propagation, the differences among the °Brix values computed using the integration steps of 0.5 and 0.01 s present a magnitude order of 10^{-4} °Brix over the first simulated minute. After this initial period, the magnitude order of these differences drop progressively up to 10^{-5} °Brix. Regarding the scenario with propagation, the simulated results of the time steps 0.5 and 0.01 s have a difference with magnitude order of 10^{-3} °Brix over the first five simulated minutes. After this five minutes, this magnitude also display a progressive decreasing, thus achieving after the first simulated hour a constant magnitude order of 10^{-5} °Brix. The tendencies presented in this paragraph are consistent with the decreasing behavior of the estimated local errors regarding the scenarios with and without propagation.

Without V_p propagation:



With V_p propagation:

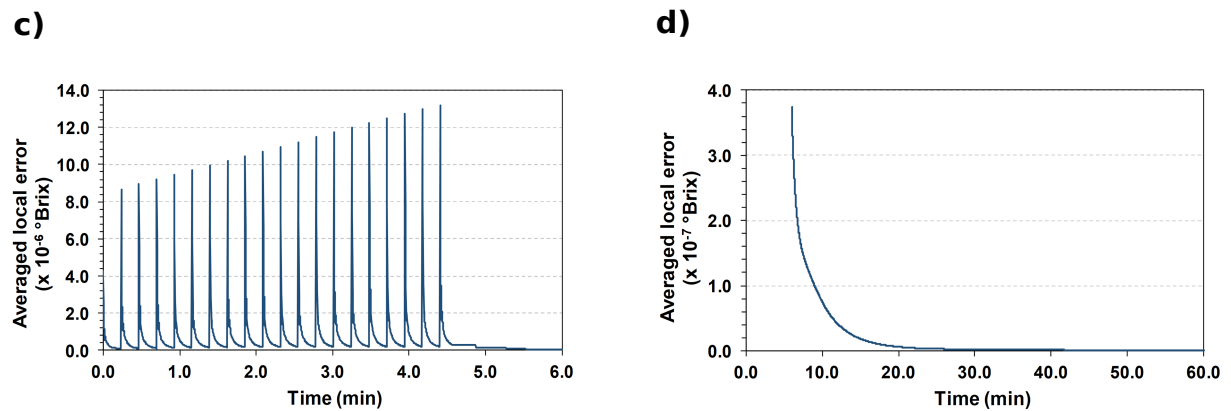


Figure 5.35: Evolution of the average of the estimated local error over the time promoted by a variation of the percolating velocity from 0.4 to 0.5 m/min , without propagation (frames a and b) and with propagation (frames c and d). Frame (a) regards the first simulated minute and frame (b) presents the average of the estimated local errors from 1 min to 1 hour. In their turn, frame (c) is the initial 6 minutes of simulation and frame (d) shows the the average of the estimated local errors from 6 min to 1 hour.

The times required to performed the simulations of the regime without propagation are comparable to those already presented in the Table 5.13. This fact is a consequence of the similarity between the computational procedures of the “without propagation case” and those implemented to simulate the transient state of a variation in the °Brix of the raw material. In each iteration of the transient solution, the simulations with v_p propagation need to update the system of $ODEs$ in order to account for the propagation phenomenon. Due to the update procedure, the extent of the simulations are higher (Table 5.14) than the time values achieved by the regime without propagation. Since the simulated outcomes yielded by

different time steps are quite close for both propagation regimes, the following assessments are going to be performed using the higher integration step (*i.e.*, 0.5 s) so as to reduce the duration of the simulations.

Table 5.14: Simulation time, as function of the integration step, required to simulate 10 *min* of a transient process promoted by a variation of the percolating velocity from 0.4 to 0.5 *m/min*, with propagation.

Time step	Simulation time
<i>s</i>	<i>min</i>
0.5	2.6
0.1	14.1
0.05	28.3
0.01	143.1

Concerning the scenario without v_p propagation, the time lapses of the transient motion of the °Brix curve are displayed in the Figure 5.36. The fixed curves in the Figure 5.36 represent the old and new steady-state conditions. The shifts faced by the Brix curve over the course of time are not local. It means that the current modeled system does not have a source of variations from where the transient phenomenon spreads to the other regions of the bed (as in the cases discussed in the previous two subsections). Indeed, since the very beginning of the transient process, the whole curve sense equally the variation in the v_p value. Such behavior is also capture by the evolution of the isolines positions displayed in the °Brix distribution (Figure 5.37). It is possible to notice in the Figure 5.37 that the isolines start their leftward motion at the same time and move together towards the new steady-state position. This non-local variation in the extraction system is an expected tendency, since the change in the operation condition is promoted simultaneously in every volume of the grid.

The °Brix curve of the scenario with v_p propagation (Figure 5.38) also shows a non-local variation. Over the course of the transient simulation, the points of the °Brix curve are synchronized in their movement, as an unit that obeys the same underlying tendency. This fact is an anticipated one, since the propagation front extends along the whole sugarcane bed, thus affecting at the same time the °Brix values along the extension of the diffuser. The isolines in the °Brix distribution (Figure 5.39) show, for the first five simulated minutes, a variation of the their position that starts at the top of the diffuser and spreads progressively to the bottom of the equipment (this behavior is better observed in the YouTube video). Such variation of the isolines position across the height of the equipment reflects the propagation of the change in the v_p value.

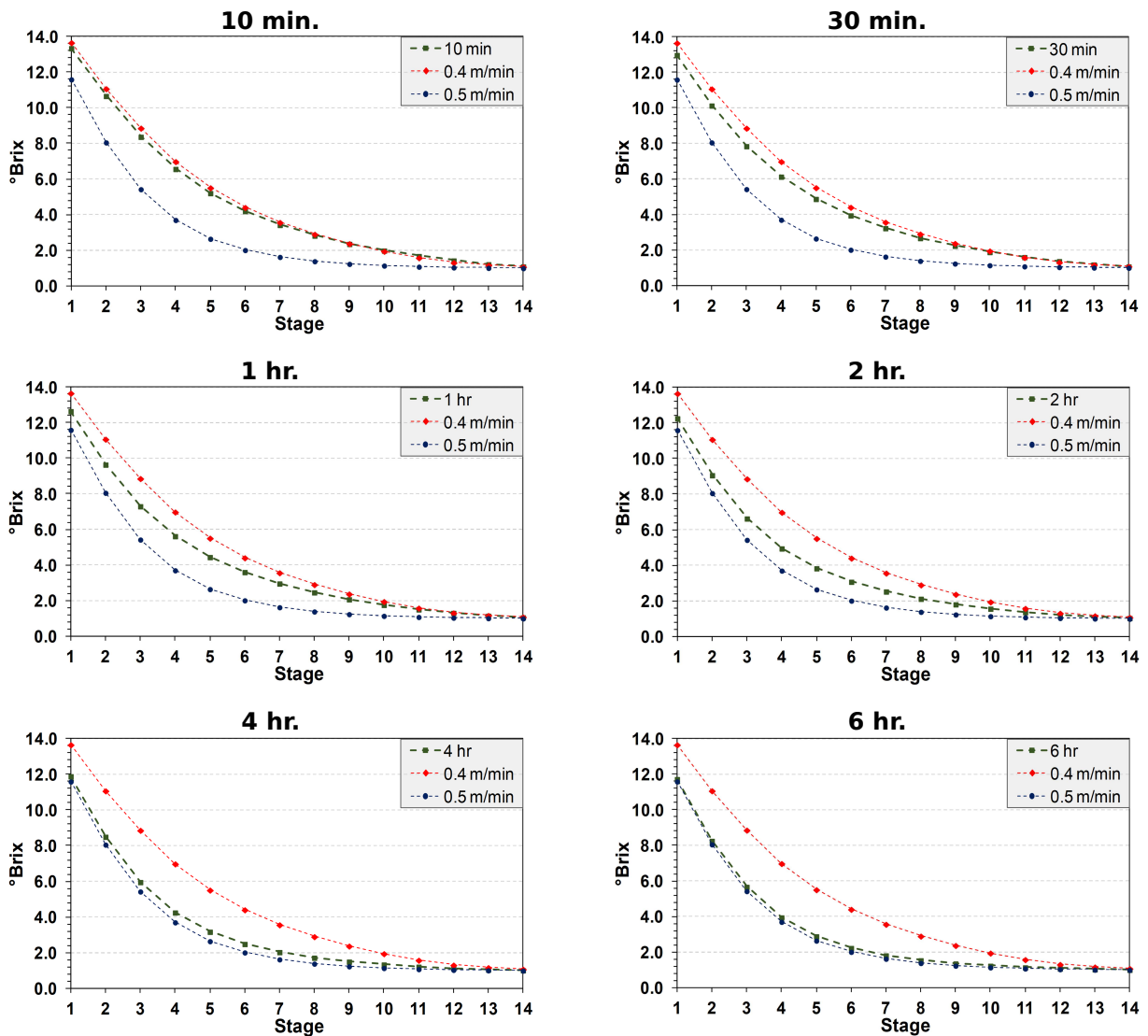


Figure 5.36: Evolution of the °Brix curve as function of time promoted by a variation of the percolating velocity, **without propagation**, from 0.4 to 0.5 m/min ([YouTube](https://youtu.be/1kWPWhI2OV8)). URL: <https://youtu.be/1kWPWhI2OV8> .

In relation to the initial condition (*i.e.*, $v_p = 0.4 m/min$), the Brix curve of the “with propagation scenario” presents an increase in the °Brix values during the propagation procedure. This fact may be explained by an imbalance of the vertical convective flux between the regions of the bed above and below the propagation front. A higher v_p value means a more intense convective flux coming from the volumes above the propagation front. However, the region of the bed below the propagation front has lower outlet convective flux, since it have not undergone to change in the v_p value yet. This lack of balance between the inlet and outlet convective flux leads to the observed increase of the °Brix values in the region

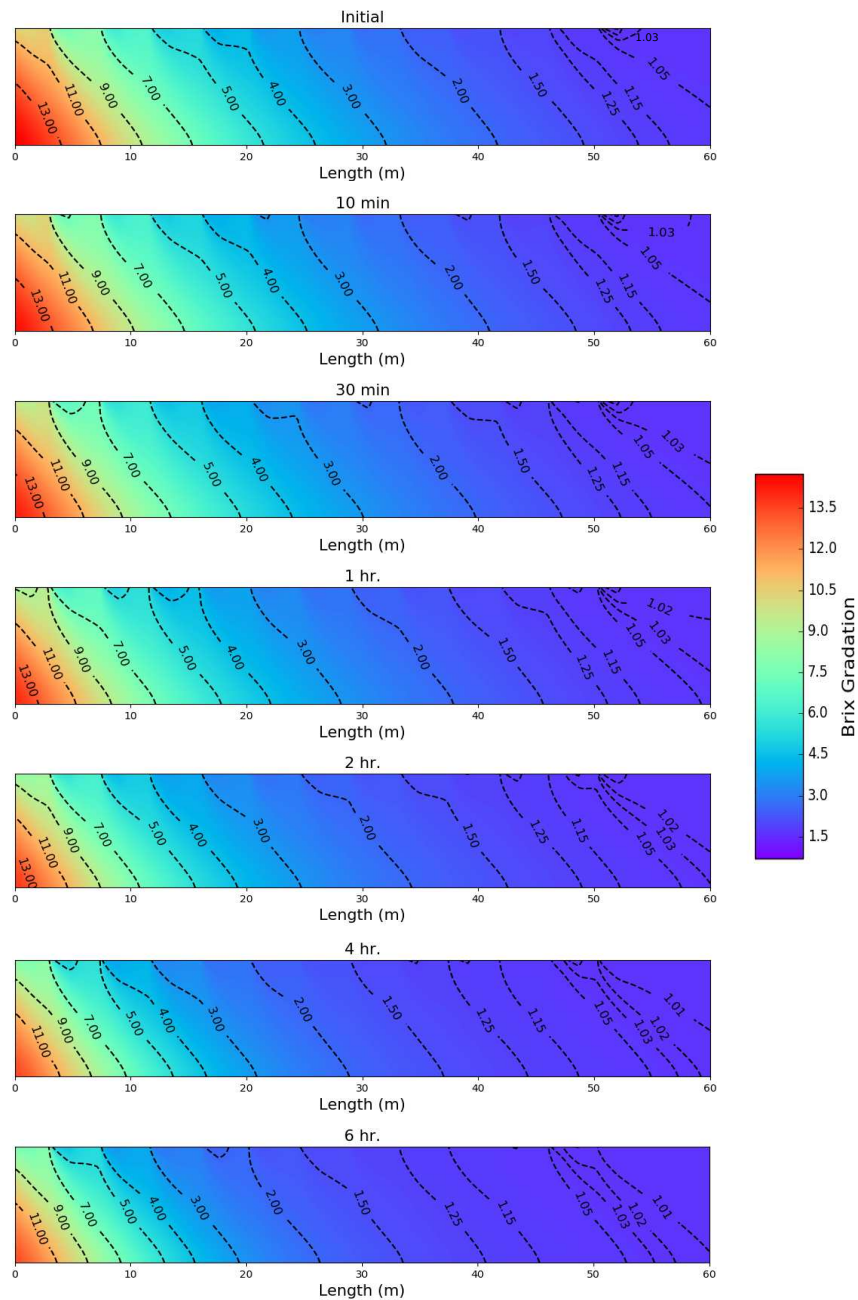


Figure 5.37: Evolution of the °Brix distribution as function of time promoted by a variation of the percolating velocity, **without propagation**, from 0.4 to 0.5 m/min ([YouTube](https://youtu.be/Z6YezFR4iOI)). URL: <https://youtu.be/Z6YezFR4iOI> .

of the bed below the propagation front. Ceasing the propagation procedure, the extraction environment behaves similar to the case without v_p propagation and moves progressively towards the new steady state.

The two propagation regimes achieves to the same new steady state, since the two

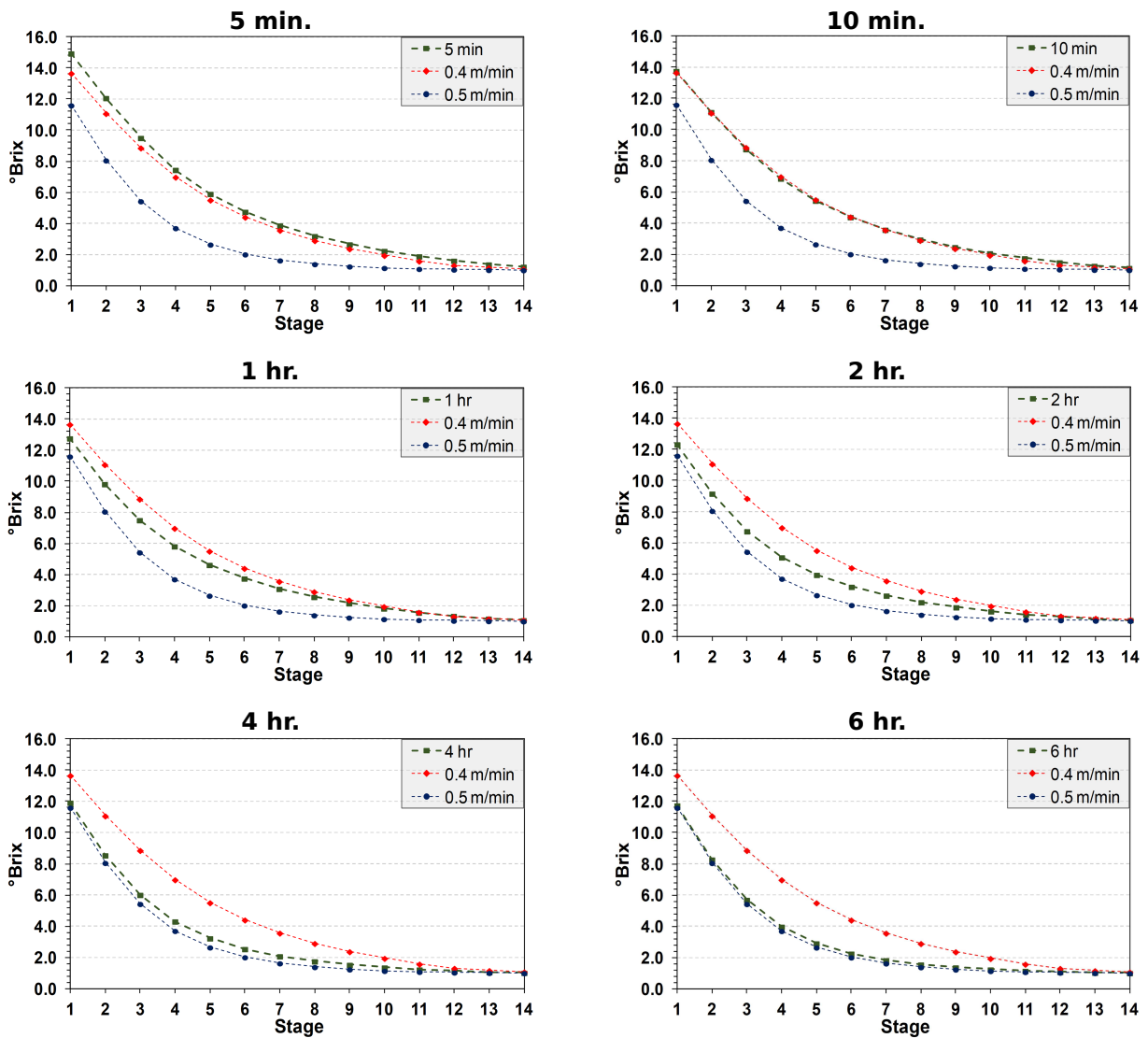


Figure 5.38: Evolution of the °Brix curve as function of time promoted by a variation of the percolating velocity, **with propagation**, from 0.4 to 0.5 m/min ([YouTube](https://youtu.be/57zytbI7_KY)). URL: https://youtu.be/57zytbI7_KY .

assessed scenarios present the same percolating velocity after the propagation procedure. The proposed abstraction of the propagation of v_p delays the extraction system in relation to the scenario without propagation. Such delay is around 10 *min*, which is not a remarkable difference in face of the time required to achieve the new steady state. The two propagation regimes reach the new steady-state in about 6.0 hours. As the transient systems get closer to the new steady state, the differences in the extraction environment between the simulated transient processes become small.

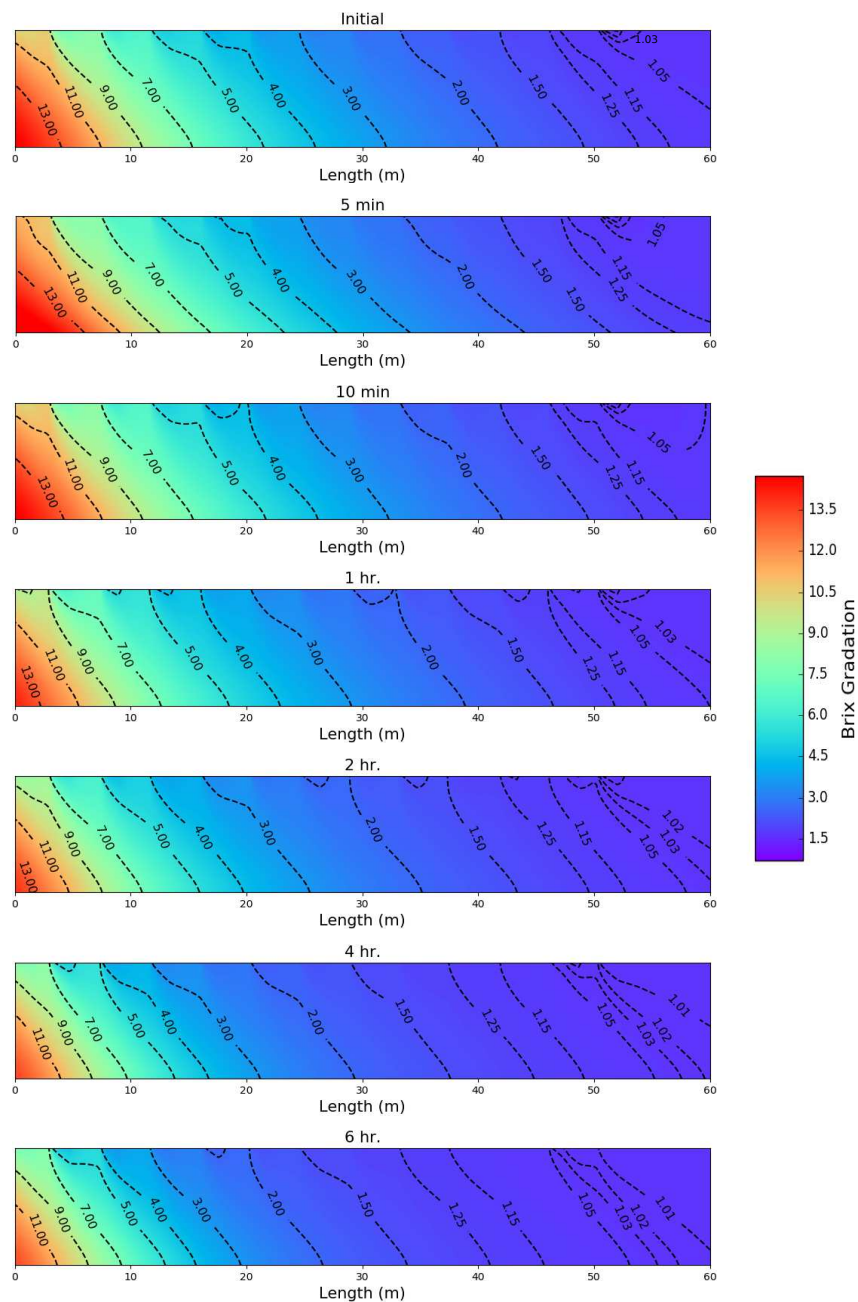


Figure 5.39: Evolution of the °Brix distribution as function of time promoted by a variation of the percolating velocity, **with propagation**, from 0.4 to 0.5 m/min ([YouTube](https://youtu.be/suBdLIroGrc)). URL: <https://youtu.be/suBdLIroGrc> .

5.3.4 Bed velocity

The present subsection deals with the assessment of the transient behavior of the extraction system towards a change in the bed velocity. The following analysis is an extension of the steady-state simulation performed in the subsection 5.2.5. Over the course of the

transient process, the effect of the v_b variation in the bed height is going to be assessed under two regimes. The first one is an instantaneous variation of the bed height at the very beginning of the transient phenomenon. In this regime, the whole sugarcane bed sense a sudden, abrupt change in the bed height. The second regime assumes a gradual variation of the bed height. In this second regime, it is going to be possible to evaluate the impact in the simulated results of the approach proposed in the section 4.2 (*i.e.*, the translation of the model equations into an invariant new coordinate system).

5.3.4.1 Instantaneous variation of the bed height

Regarding the regime with an instantaneous variation in the bed height, the numerical results have similar tendencies as presented and discussed in the three previous subsections. In this sense, transient simulations become unstable and divergent from the new steady state condition when the integration step is equal to 1.0 s. Indeed, after additional numerical inspections, such observation may be generalized by stating that the numerical instabilities is a constant for simulations using integration steps equal or higher than 1.0 s. Although it was implicit in the previous subsections, it is worth to state clearly that this generalization is also valid for all transient simulations presented in this thesis so far. Therefore, it is reasonable to conclude that this numerical instabilities is an underlying property of the transient simulations implemented in the present study. The most likely source of this instabilities lay on the interaction between the mathematical properties of the model equations and the ability of the integration procedure to capture the transient variations in these very mathematical properties for time steps equal or higher than 1.0 s.

The other four times steps (*i.e.*, 0.5, 0.1, 0.05, and, 0.01 s) lead to stable solutions that converge smoothly to the new steady condition. The average of the local errors, as function of time, displayed in the Figure 5.40 are acquired using a time step of 0.5 s. These results are quite similar to those achieved by performing the simulations using the other three stable integration steps. Regarding the initial two minutes of simulation (Figure 5.40-(a)), the average of the differences between the results simulated using a 4th and 1st order Runge-Kutta methods has a magnitude order of 10^{-7} °Brix. The local error has a decreasing tendency that achieves a magnitude of 10^{-8} °Brix, by the end of the initial two minutes, and a magnitude of 10^{-9} °Brix at the conclusion of the first simulated hour (Figure 5.40-(b)).

Comparing the evolution of this local errors with the one displayed by the case with v_p variation without propagation (Figure 5.35- (a) and (b)), the former scenario has a slower

decrease of the errors than the latter. It may be explained by the amount of variations in the extraction environment that the scenarios have to accommodate. The simulation with change in the v_p value has to handle only with the change in the percolating velocity. Along with the alteration of the bed velocity, the transient phenomenon simulated in the present subsection has to deal with a variation in the bed height. Moreover, a change in the bed height promotes a small alteration of the v_p value (see Eq 3.18). Therefore, an extraction environment facing a change in the bed velocity has to accommodate the variation in at least three operational variables, which leads to the observed slower decrease of the estimated local errors.

Despite the relative slower reduction of the estimated local errors, the decreasing tendency displayed in the Figure 5.40 argues in favor of the stability of the simulations with instantaneous change in the bed height. Moreover, the small magnitude of the estimated local errors indicates a non-intense and smooth transient phenomenon. This fact results in a small sensitivity of the simulated results to changes in the integration step. In fact, for the first two minutes of simulation, the differences among the results computed by using any two distinct time steps have a magnitude order of 10^{-4} °Brix. After this initial period, the differences drop to a magnitude of 10^{-5} °Brix. The simulation procedure under assessment does not require updates of the *ODEs* over the transient procedure, which leads to simulation periods similar to those already reported in Table 5.13. Bearing the simulation periods in mind and acknowledging the small differences in the results achieved by using distinct stable time steps, the following assessments are performed applying the integration step of 0.5 s.

Figure 5.41 presents the evolution of the °Brix curve over the course of time. The transient process starts in each region of the bed at the same time. This synchronize behavior may be observed in the °Brix curve motion: each point of this curve senses the transient phenomenon at the same time, since the very beginning of the simulations. The synchronicity of the transient process is also present in the evolution of the °Brix distribution (Figure 5.42). As the °Brix distribution evolves, the isolines shift their position in a coordinate way from the old to the new steady-state condition. Therefore, the transient process under assessment does not have local sources of variations, which matches with the expected tendency of an instantaneous variation in the whole extraction environment.

In relation to the regime with v_p variation without propagation, so far in the present subsection, the simulated extraction environment displays a slower variation in its concentration distribution. Such observation indicates a lower intensity of the transient process, which may be a result of a small driving force of the transient phenomenon. As already defined in

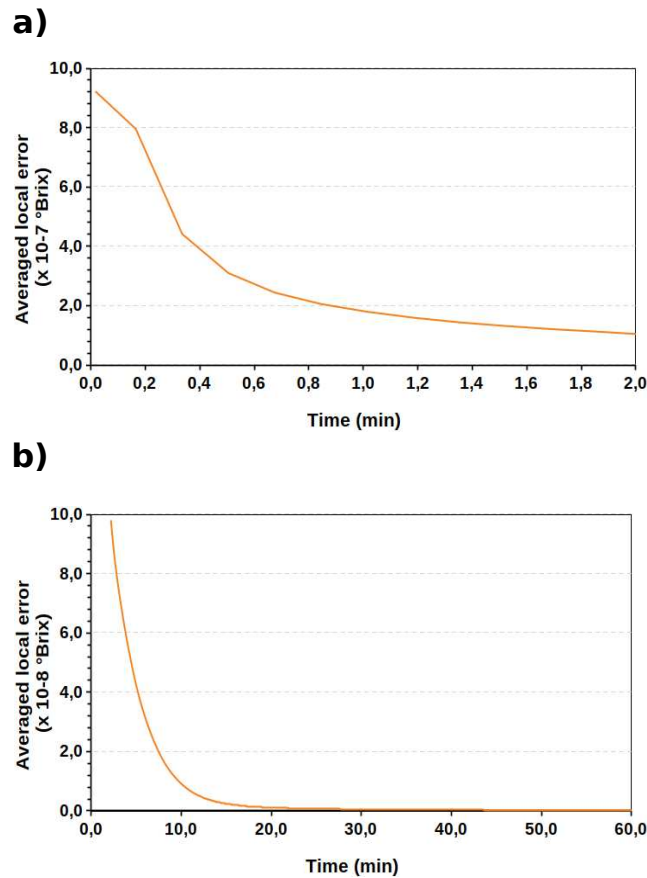


Figure 5.40: Average of the estimated local errors acquired during the transient simulation of a system facing a change in the bed velocity from 0.85 (base case) to 0.95 m/min , with instantaneous variation in the bed height. Frame (a) presents the first two minutes of the transient process and frame (b) displays the evolution of the average of the local errors up to the end of the first simulated hour. Errors acquired using a time step of 0.5 s.

the previous subsections, the driving force is the concentration difference between the old and the new steady-state conditions. The two motionless curves displayed in the Figure 5.41 are closer than those simulated for the regime with v_p variation without propagation. Moreover, the isolines change their positions only over a short range, which makes the concentration distributions quite similar in both old and new steady-state conditions. Therefore, the driving force regarding the regime with instantaneous bed height variation is not pronounced, leading to the observed slow variation of the transient system. The pace of the transient phenomena push the extraction environment to the new steady condition in about 6.0 hours.

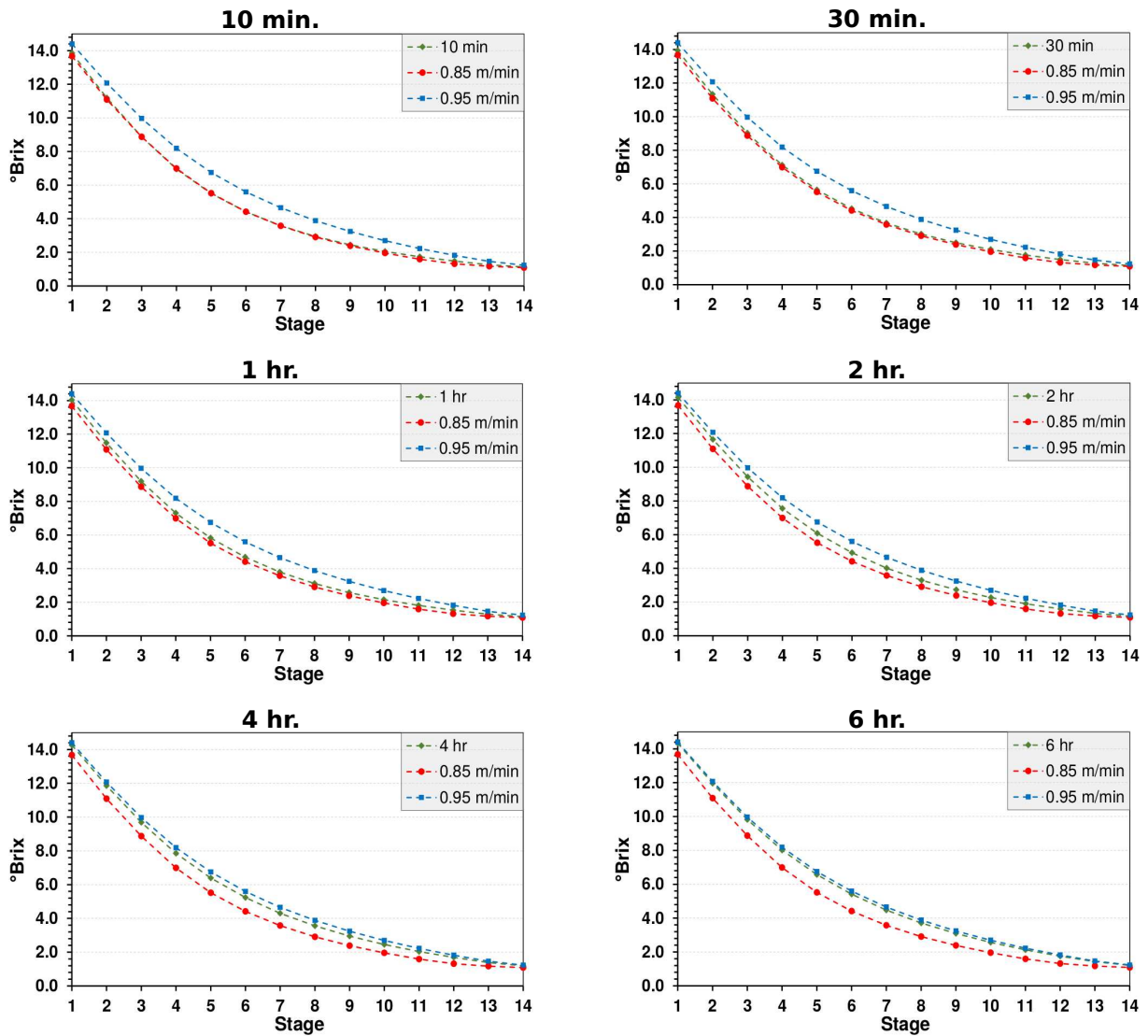


Figure 5.41: °Brix curve, as function of time, of a system facing a change in the extraction characteristics promoted by a variation in the bed velocity from 0.85 (base case) to 0.95 m/min , with instantaneous modification of the bed height. The two motionless curves displayed in the frames of this Figure are the old and the new steady-state conditions ([YouTube](https://youtu.be/nLAOyvi2tKE)). URL: <https://youtu.be/nLAOyvi2tKE> .

5.3.4.2 Gradual variation of the bed height

The simulations of the regime with gradual variation in the bed height were performed with the model equations in the new coordinates (ψ, η) . Concerning the two assessed v_b levels, Figure 5.43 shows the °Brix distributions at steady-state (*i.e.*, even bed height) simulated in the new coordinates system. These °Brix distributions are equal to those simulated with the model equations in the Cartesian system (Figure 5.11). Moreover, equal °Brix

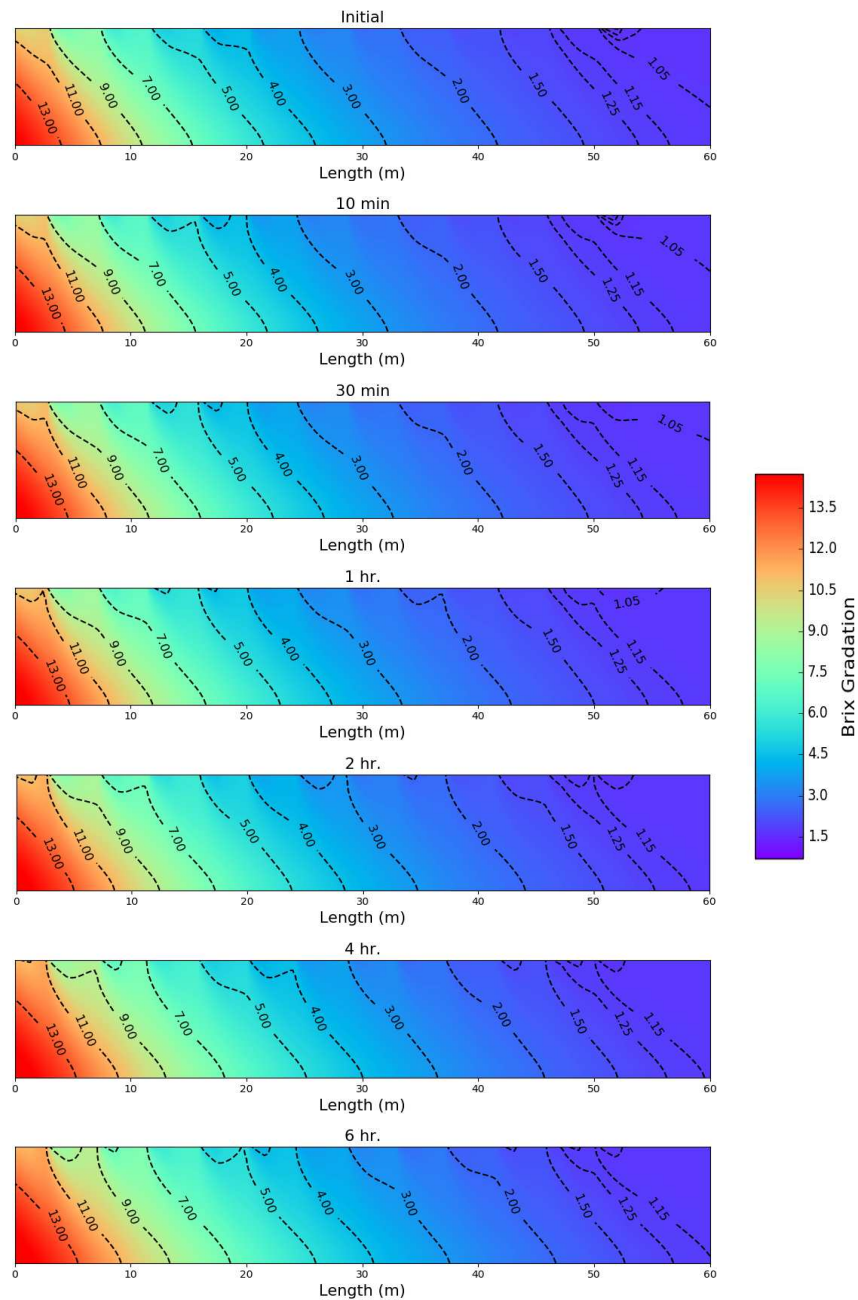


Figure 5.42: °Brix distribution, as function of time, of a system facing a change in the extraction characteristics promoted by a variation in the bed velocity from 0.85 (base case) to 0.95 m/min , with instantaneous modification of the bed height ([YouTube](https://youtu.be/O63LOvRgPEA)). URL: <https://youtu.be/O63LOvRgPEA> .

distributions lead to identical °Brix curves simulated in the two coordinates systems. Such equality among the simulated results is also observed by repeating, in the new coordinates, the other assessments performed in this chapter so far, both at steady and transient states. Therefore, the model equations in the new coordinates present the desired invariant nature

in relation to the outcomes computed by using the model in the Cartesian system.

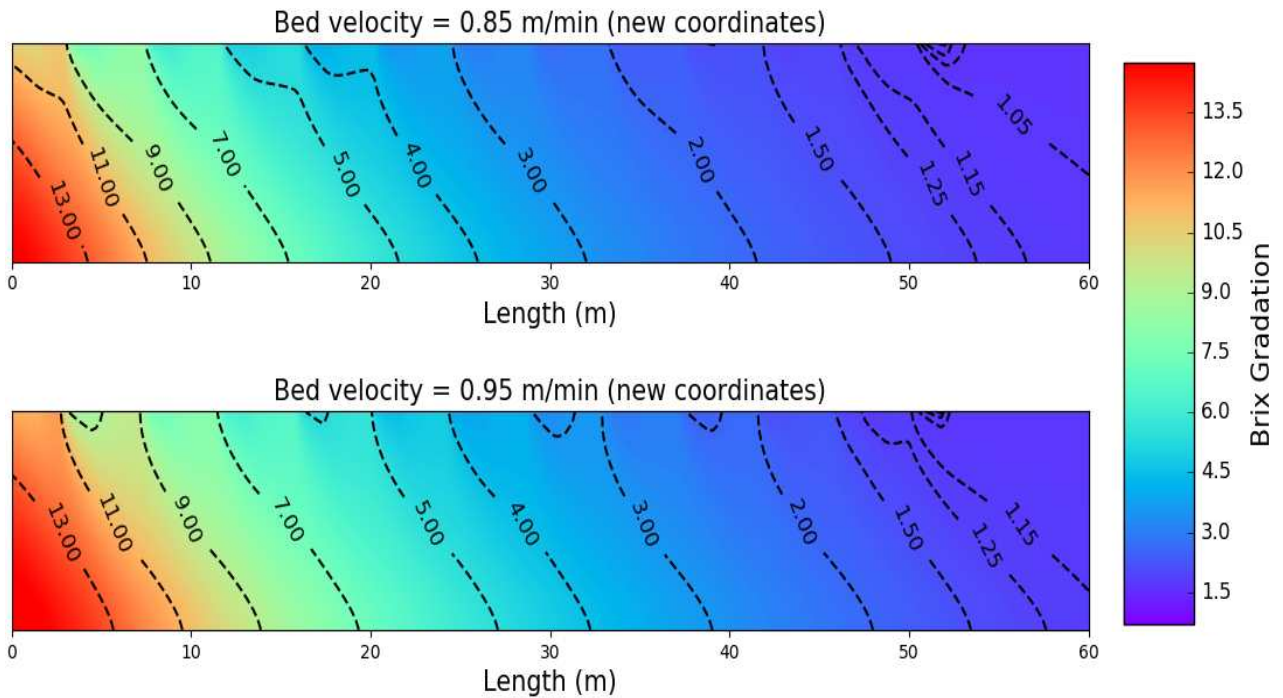


Figure 5.43: Simulated °Brix distribution for bed velocities of 0.85 and 0.95 m/min in the new coordinates system.

By performing the sensitivity analyze of the integration steps, it was found that the transient simulations are numerically unstable, even for the lower assessed time step (*i.e.*, 0.01 s). The most likely source of this numerical issues is the new terms that emerges in the model equations due to the presence of the dispersion effects. The evidence that support the role of the new dispersion terms in the observed numerical instabilities are twofold. First, regarding the simulations without gradual bed height variations, the presence of the dispersion terms in their traditional mathematical form do not affect the numerical stability of the simulations. The previous evidence is observed regardless of the coordinates system in which the model equations are written.

The second evidence is based on the fact that, by neglecting the dispersion effects, the transient simulations with gradual variations in the bed height become stable and convergent for time steps lower than 1.0 s . As far as the analyses can tell, the critical effect in the numerical stability promoted by the new dispersion terms may be a result of an erroneous definition of the boundary conditions. The discretized form of these new terms impose to the solution procedure the requirement to define additional boundary conditions, especially in relation to the cross-derivative terms. In the present study, such definition were

performed by comparing the mathematical features of the new boundary conditions with those of the contour conditions already defined to the Cartesian coordinates. Therefore, the new boundary conditions were deduced by following a resemblance criteria, which lacks some phenomenological support. The interaction of these new boundary conditions with the other discretized terms may lead to unstable conditions at the frontiers, which then spreads to the inner volumes of the grid.

Unfortunately, it was not found in the literature, as well as through the personal contact with professionals with more technical and methodological expertise, a solution for such numerical instabilities. Different boundary conditions were proposed for the new terms, but without successful results. Therefore, the definition of suitable boundary conditions for the new dispersion terms is an unsolved question, opened for suggestions. It is important to clarify that this thesis does not suggest that numerical stability and convergence argue in favor of the accuracy of a given boundary condition. The critical point here is that unstable simulations prevent the analyses of the simulated outcomes. Without convergent outcomes, it is not possible to understand the conceptual implications of the approach applied to simulated a gradual variation in the bed height. For the sake of such conceptual understanding, the following analyses were performed without the presence of the dispersion effects.

The simulations of the transient process with gradual variation in the bed height were performed assuming three values for the *STR* (*i.e.*, Size of Transient Region): 10, 15, and 20 *m*. This sensitivity analysis allows for assessing the impact on the extraction characteristics promoted by three distinct intensities of the bed height variation. The simulations performed using different *STR* values are unstable for time steps equal or higher than 1.0 *s*. The numerical stability displayed by the other integration steps (*i.e.*, 0.5, 0.1, 0.05, and 0.01 *s*) makes it possible to assess the evolution of the average of the estimated local errors over the course of the simulations (Figure 5.44).

The magnitude of the local errors increase with the reduction of the *STR* value. It is an expected tendency, since smaller transient regions leads to more intense transient process. As a consequence of this higher intensity, the differences between the results computed using a 4th or 1st order Runge-Kutta method are more pronounced. The three curves in the Figure 5.44 are constituted by small peaks. These peaks occur when the transient region achieves a new vertical section of the grid and disturbs the extraction environment, thus locally increasing the intensity of the transient processes. Another general feature of these errors is the drop of the their values after the occurrence of a peak. Such behavior indicates that the errors do not have the tendency to build up, which testifies in favor of the numerical

stability of the transient simulations.

The three curves present two major leaps in the values of the errors. The first leap happens when the transient system is initially disturbed by the entrance of the transient region in the extraction environment. The second and more pronounced leap occurs exactly when the transient region finish its entrance, thus being completely inside the equipment for the first time. After those leaps, the simulations are capable to accommodate the upsurge of the intensity of the transient processes, thus leading to the reduction of the local errors. Such accommodation tendency, therefore, is also an indicative of the stability of the simulations. Independently of the STR value, the magnitude of the local errors is small. Such small magnitude leads, as discussed before, to outcomes less sensitive to the value used as time step in the integration process. Moreover, the transient procedure needs a constant update of the $ODEs$ system, thus requiring a simulation time similar to those already reported in Table 5.14. In this sense, the following analysis are performed using the higher stable time step (*i.e.*, 0.5 s).

Figures 5.45 to 5.47 present the simulated $^{\circ}\text{Brix}$ distributions, as function of time, for the three STR values. By focusing only on the first and last time-frames of these Figures, it possible to notice the effect of the omission of the dispersion terms on the simulated extraction environment. Without dispersion, the isolines are no longer “S-shape” type of curves; but getting closer to a straight line. This change is a consequence of the absence in the model of terms with elliptic nature. Therefore, the mass transport within the diffuser becomes a pure parabolic phenomenon, governed only by one-way type of terms (*i.e.*, the convective terms). As a general observation concerning the concentration distribution in the scenarios without dispersion, the isolines display a rightward shift in their positions, especially at the bottom of the bed.

In the simulated $^{\circ}\text{Brix}$ distributions (Figures 5.45 to 5.47), the vertical dashed lines at the times 10 and 30 *min*, and 1 *hr* depict the frontiers of the transient regions. In the Figure 5.45 at 10 *min*, the isolines at the left-hand side of the transient frontier are “stretched” downward by the effect of the height variation. The same behavior may be observed in the other $^{\circ}\text{Brix}$ distributions (Figures 5.46 and 5.47), but with less intensity. Such phenomenon may be explained by the relation between the new convective terms present in the sucrose balance of the percolating liquid (blue and red terms in the Figure 5.48). Due to the approach proposed in this work to compute z_{τ} in the model equations (Figure 4.6), the convective fluxes with the metric η_t are higher than those with the metric η_x . Therefore, there is an increase in the convective downward flux in the regions of the bed under transient variation in its

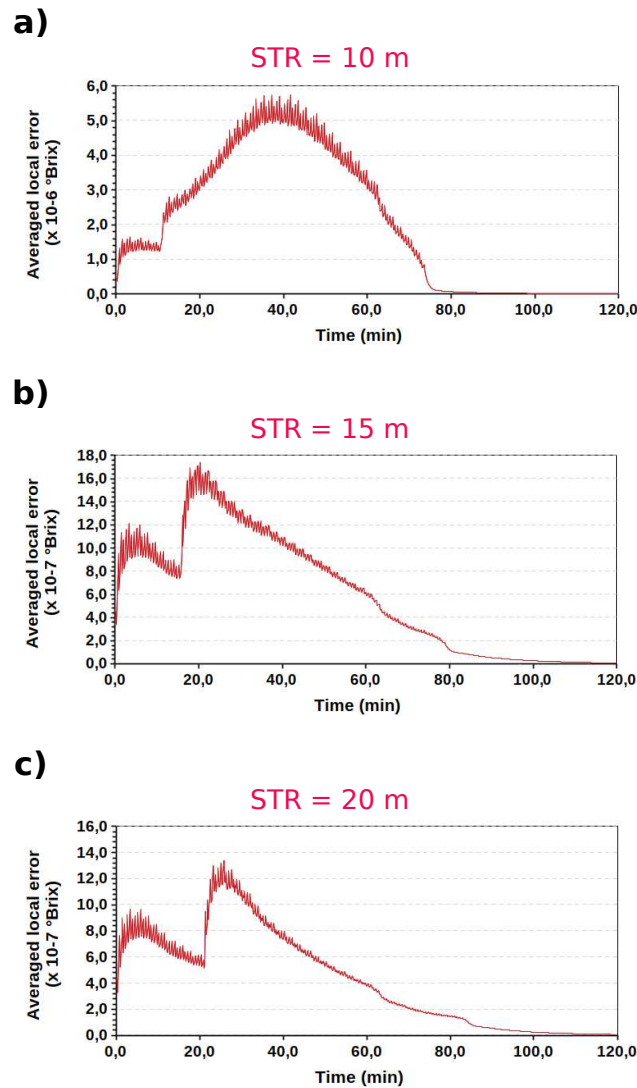


Figure 5.44: Average of the estimated local errors acquired during the transient simulation of a system facing a change in the bed velocity from 0.85 (base case) to 0.95 m/min , with gradual variation in the bed height. Errors acquired using a time step of 0.5 s.

height. This higher convective flux is the cause of the stretching behavior as well as the leftward shifting in the position of the isolines within the transient region.

As the transient region leaves behind a given zone of the bed, the extraction environment in this very zone stops to sense the effects of the height variation. With the consequent reduction of the downward convective flow, the isolines are no longer under a vertical stretching effect. Therefore, the isolines recovery a spatial disposition similar to that displayed by zones of the bed at the right-hand side of the transient region. This behavior of the isolines is better observed in the YouTube videos. As the transient region moves along the bed (*e.g.*,

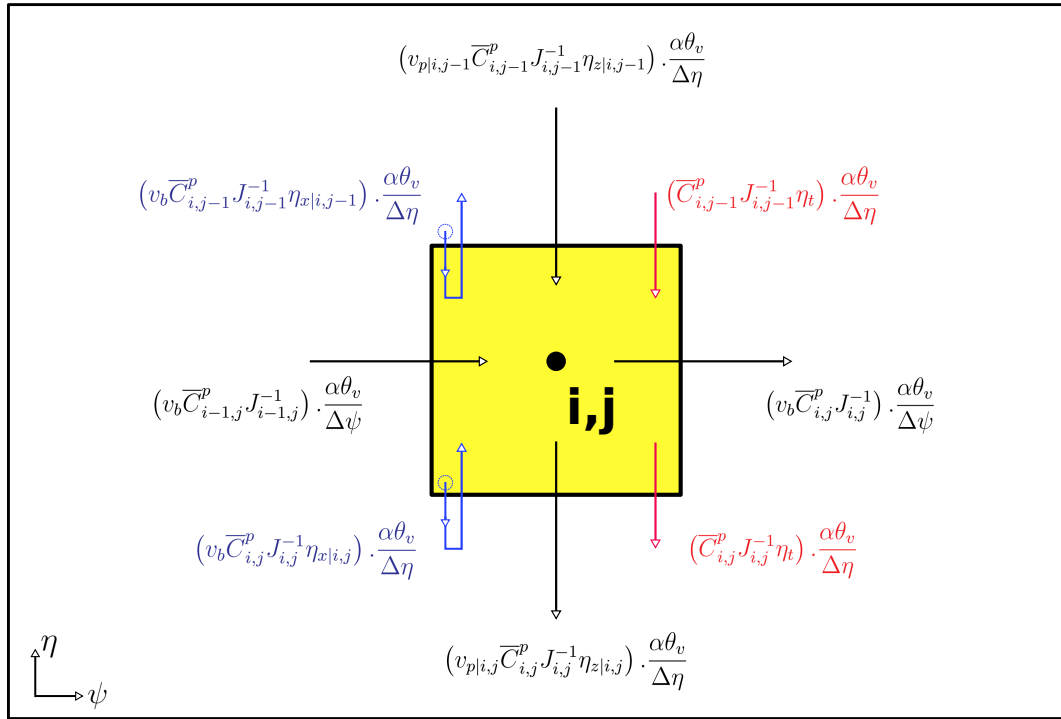


Figure 5.48: Convective fluxes of the sucrose balance of the percolating liquid regarding a generic volume of the grid (i,j) in the new coordinates system.

in *their* positions”, and so on). Figure 5.49 presents a thought experiment to help in the understanding of the those jagged patterns. Such experiment follows the transient behavior of two generic isolines, which are interpreted as real elements of a sugarcane bed.

At the beginning of the thought experiment, the sugarcane bed in question has its velocity changed. Outside of a transient region, the two isolines sense the transient variation of the bed velocity at the same time and in equal intensity all over their extension. Therefore, the isolines during their motion do not cross each other (Figure 5.49-(a)), since they move in the same direction with similar intensity and in a synchronized way. In a transient region, however, the sections of the isolines inside it sense a higher vertical downward flux (Figure 5.49-(b)). This higher flux deforms the sections of the isolines inside the transient region. As a result of such deformation, the isolines may cross each other, thus leading to the emergence of mixture points as well as the overlap of the lines (Figure 5.49-(c)). In this scenario, the presence of mixture points and overlap zones are the proposed causes of the simulated jagged patterns.

The simulated °Brix curves, as function of time, are presented in the Figures 5.50 to 5.52. The motionless curves in these Figures are the old and new steady-state conditions,

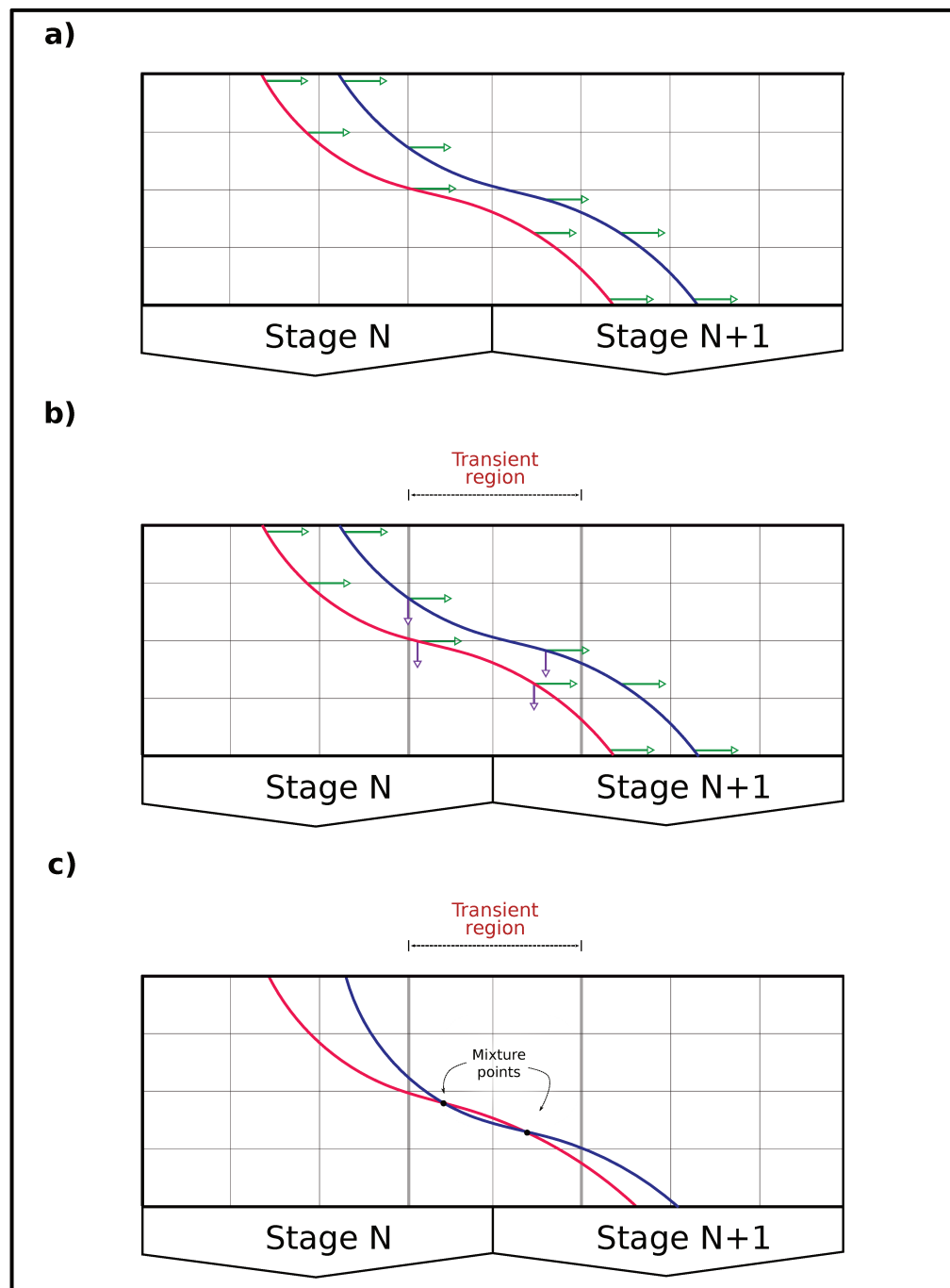


Figure 5.49: Schematic representation of a thought experiment in which two generic isolines are interpreted as real entities of a sugarcane bed. During the experiment, it is analyzed the transient behavior of the isolines promoted by a variation in the bed velocity with gradual change in the bed height.

but regarding the scenarios without dispersion. As general tendency, the fixed $^{\circ}$ Birx curves do not display many differences in relation to those acquired in the simulations with the dispersion effect (Figure 5.41). The differences are noticed only in the initial stages of the

diffuser, in which the °Brix values are slightly smaller. This effect may also be explained by the absence in the model of terms with elliptic nature.

The vertical dashed lines in the Figures 5.50 to 5.52 depict the frontiers of the transient regions. The aforementioned increase in the vertical downward flux inside the transient regions may be interpreted, in essence, as a higher percolating velocity. Therefore, it is expected that the °Brix curve in those regions behave similar to scenarios facing a rise in the v_p value (*e.g.*, see Figure 5.21). Such expectation is fulfilled, since the °Brix curves show the anticipated reduction in the °Brix values for the zones inside the transient regions. The intensity of this reduction holds an inverse relation with the STR value, which is, again, an expected tendency.

No matter the STR value under consideration, as the entire transient region quits the bed, the whole system starts to move towards the new steady-state condition. The characteristics of this transient path are quite similar to those discussed for the scenario with instantaneous variation in the bed height. However, it is possible to notice a particular feature of this path towards the new steady-state condition: a faster transient process, especially at the beginning of the transient path. Such feature is a consequence of a larger concentration difference (*i.e.*, driven force) between the system at the new-steady state and the extraction environment right after the transient region quits the bed. A lower STR value means that the transient region leaves the bed faster than in those scenarios with higher STR values. Therefore, the simulations with STR value equal to 10 m achieves first the new steady-state condition, followed by the scenarios with STR values equal to 15 and 20 m , respectively. As a general tendency, the transient processes achieve the new stationary condition in about 7 hr , which is 1 hr longer than the simulated transient process with instantaneous variation in the bed height.

The main question that pop up from the previous discussions may be placed as follow: Are the simulated results real? Unfortunately, there are not data in the literature concerning assessments of systems with gradual variation in the bed height. Moreover, such assessment is hard (or even impossible) to be performed in an industrial equipment. Without real bases to guide the analyses, the results of the simulations with gradual variation in the bed height have to be interpreted under a dual nature. On one hand, results coming from the numerical simulations may be directly connected to a consistent physical interpretation, which is draw from the observation of the modeled real system. On the other hand, the results may be just a numerical phenomenon, without any meaning out of the simulations realm. In this scenario, the question above may be tackled only by pondering these two natures in

STR = 10 m

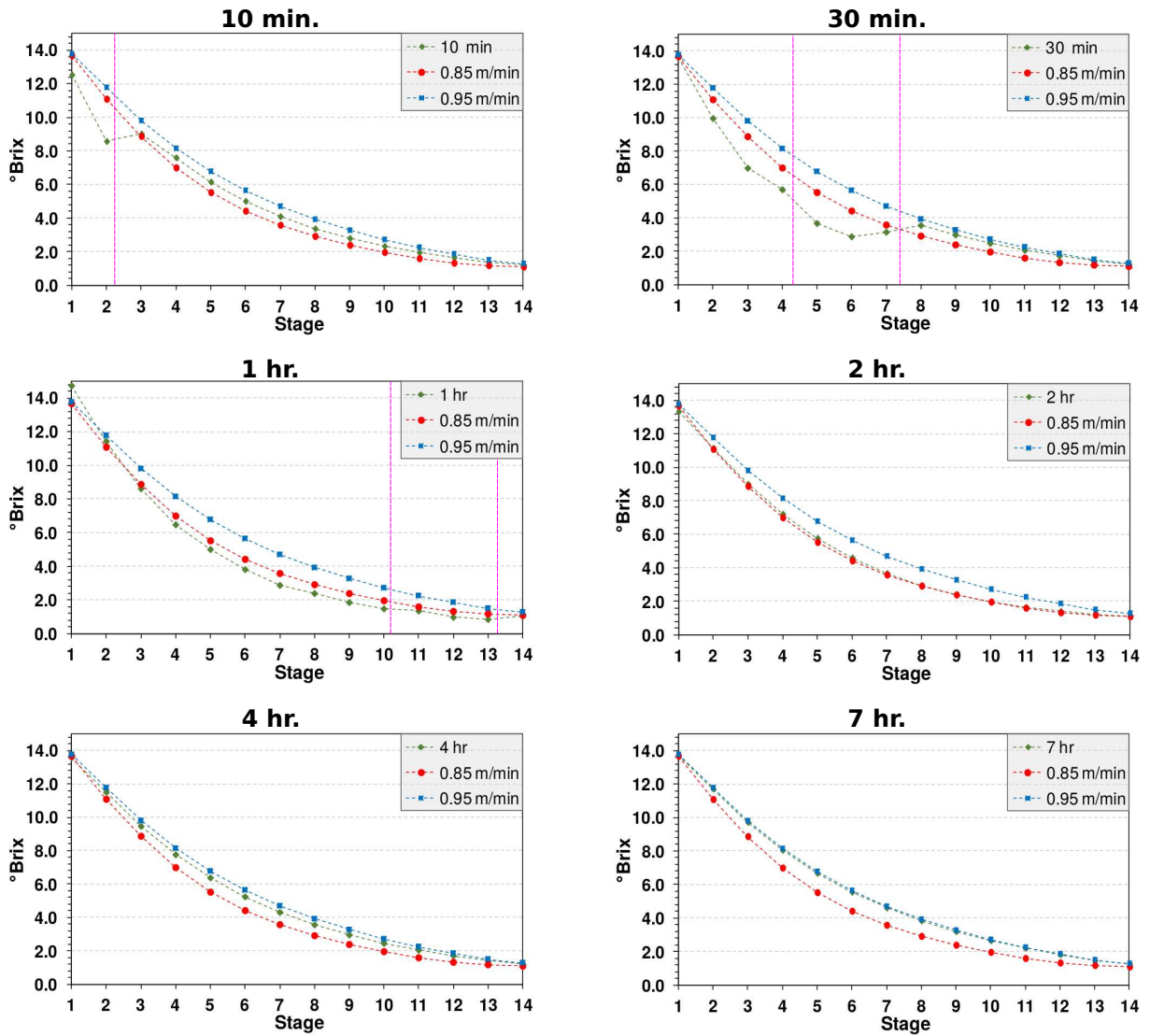


Figure 5.50: °Brix curve evolution as function of time for a variation in the bed velocity from 0.85 (base case) to 0.95 m/min , with gradual modification of the bed height. Size of the transient region (STR) is equal to 10 m . Vertical dashed lines depict the frontiers of the transient regions ([YouTube](https://youtu.be/k6m95zJwwyc)). URL: <https://youtu.be/k6m95zJwwyc> .

order to assess their likelihood of being the right answer. By following this strategy, the next paragraphs discuss the nature of the above simulated outcomes.

The particularities of the transient behavior under assessment may be directly connected to the presence of the new convective terms. Such additional elements rise in the model from the numerical representation of the geometric variations faced by the bed in

STR = 15 m

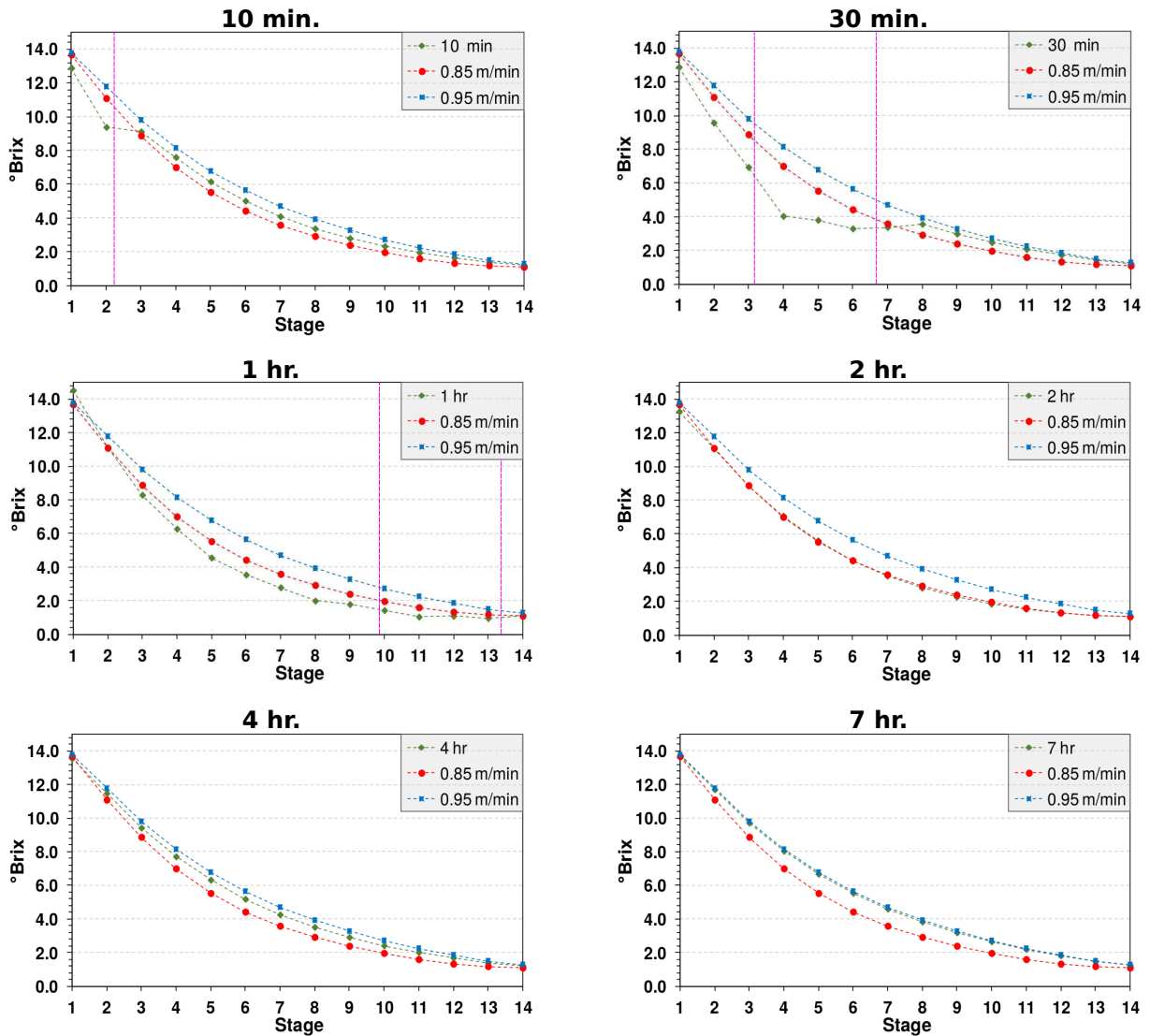


Figure 5.51: °Brix curve evolution as function of time for a variation in the bed velocity from 0.85 (base case) to 0.95 m/min , with gradual modification of the bed height. Size of the transient region (STR) is equal to 15 m . Vertical dashed lines depict the frontiers of the transient regions ([YouTube](https://youtu.be/aMh2eZ3JOEc)). URL: <https://youtu.be/aMh2eZ3JOEc> .

the Cartesian system. In an opposite sense, the mathematical characteristics of these very numerical representations are determined by the way in which this study interprets the gradual variation of the bed height. Such interpretation, therefore, is the base from which the phenomenological meaning of the new convective terms may arise. Provided that this interpretation is prone to happen in the reality of the modeled process, the phenomenological

STR = 20 m

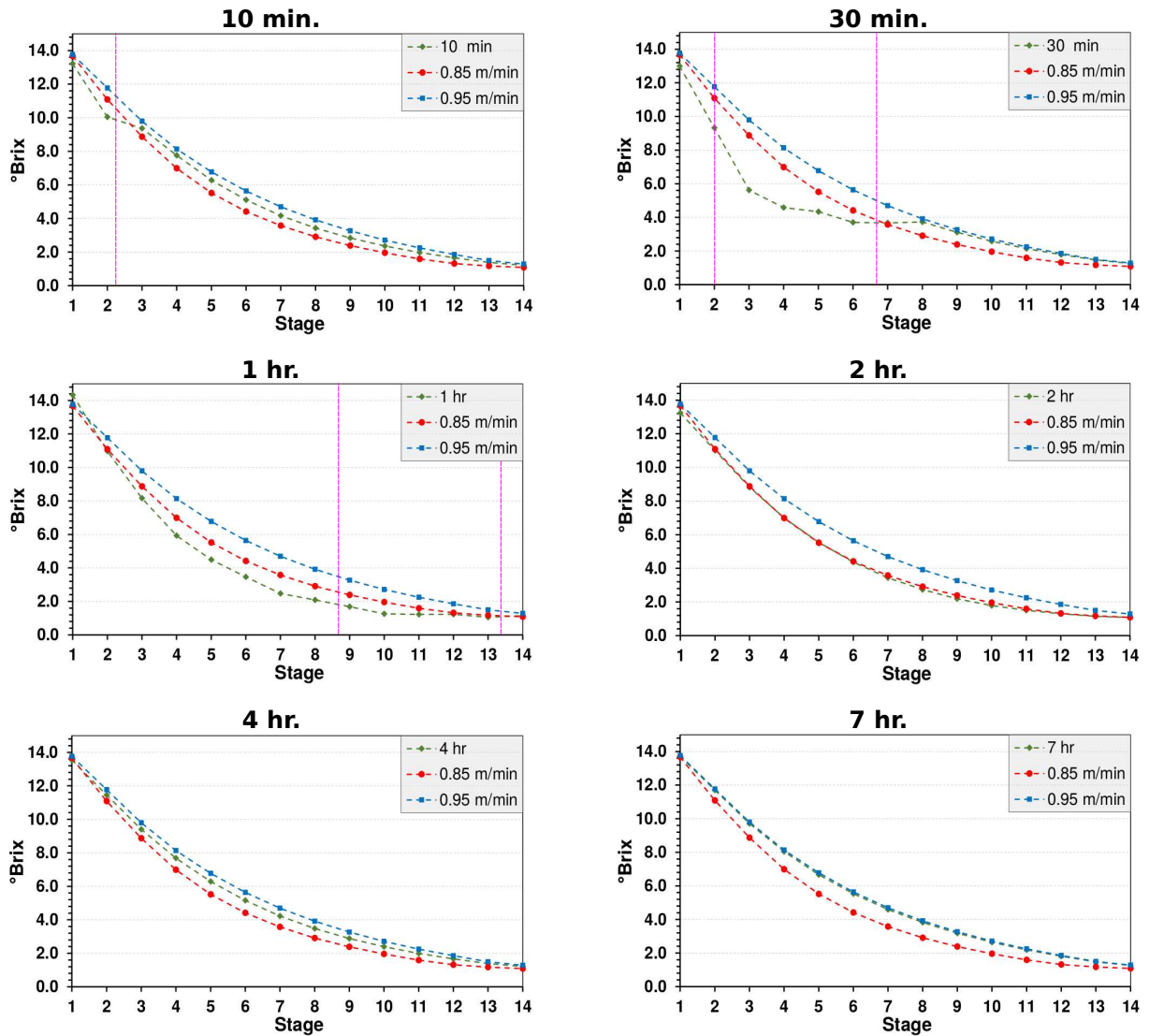


Figure 5.52: °Brix curve evolution as function of time for a variation in the bed velocity from 0.85 (base case) to 0.95 m/min , with gradual modification of the bed height. Size of the transient region (STR) is equal to 20 m . Vertical dashed lines depict the frontiers of the transient regions ([YouTube](https://youtu.be/-cgK8HDE0dY)). URL: <https://youtu.be/-cgK8HDE0dY> .

meaning coming from it is responsible to prevent a pure numerical explanation of the simulated results.

The mathematical features of the convective element with the η_t term is defined by the linear description of the variation of the bed height (see Figure 4.6). Such description is in accordance with the Eulerian interpretation of the modeled system. In relation to a

static referential, therefore, a transient region crossing a vertical section of the bed promotes a linear decreasing of the local height. Moreover, for a motionless observer focusing on a fixed point of the bed, such gradual decreasing resembles a compaction effect. This effect may be a candidate for a physical interpretation of the simulated results. By doing so, the compaction effect may explain the geometric variations of the bed during its gradual transition. Moreover, the higher downward flux observed in the simulations may be caused by the squeezing of the sugarcane fibers promoted by the same compaction effect.

Despite the appeal to explain the simulation results by the presence of the compaction effect, it is important to explore the reality of such effect in the context of a variation of the bed velocity. As aforementioned, the proposed description of the bed height variation agrees with the Eulerian interpretation of the modeled process; but it is not quite representative of the real phenomenon (see section 4.2). In fact, a Lagrangian interpretation gives a better picture of the modeled real phenomenon: the transient region as a segment of the bed that is carried along the equipment by the conveyor system of the diffuser. In this Lagrangian interpretation, the proposed linear decreasing of the bed height is no longer necessary. Moreover, acknowledging the transient region as a section of the bed that moves along the diffuser, such region is by no means under a compaction effect. Therefore, the compaction effect is present in the simulation results as a direct consequence of the Eulerian interpretation of the modeled system.

As far as the current knowledge about moving-bed diffuser operation can tell, it is not possible to dissociate that compaction effect from the Eulerian interpretation. Therefore, regarding the present scenario, the convective element with the η_t term has, unfortunately, a pure numerical nature. The other additional convective element (*i.e.*, the one with the η_x term) still holds its physical interpretation, since it emerges to account the geometric variations of the bed. The previous conclusions, however, do not argue against the proposed linear decreasing of the bed height as a whole; but only against its scope of applicability. For instance, imagine a sugarcane bed facing a compaction effect promoted by the aspersion of liquid onto its top. In this case, the linear decreasing of the height still holds, and the convective element with the η_t term gains a phenomenological nature.

Regarding a scenario facing a variation in the bed velocity, the most suitable way to describe the η_t term is still an unsolved issue. It is expected, therefore, that the previous paragraphs had motivated a future discussion about the best way to solve this open question.

5.3.5 Concluding remarks about the dynamic simulations

As a general tendency, the system of *ODEs* that represents the model equations in their discretized form is well-posed, thus leading to simulations possessing numerical stability for time steps lower than 1.0 s. However, The numerical instabilities that emerge in the simulations with gradual bed height variations due to the presence of the new dispersion terms are still a unsolved problem, open for suggestions. The stable transient simulations yield results coherent and consistent with the phenomenology of the sucrose extraction from sugarcane as well as with the observed behavior of the moving-bed diffuser under operation. Therefore, under a constructivist perspective, the assessments performed in this section also testify in favor of the validity of the proposed model.

It is important to highlight the period of times required to achieved the new steady states according to the simulations performed in this section. In all simulations, the new steady-states are achieve in no less than 6.0 *hrs*. It is important to stress that this period of times are valid, each one of them, for a controlled variation in a single variable. It means that the other operational conditions are kept constant during the entire simulation procedure. This fact opens room for a critical analysis of the operation of a moving-bed diffuser at an industrial facility. In a sugarcane mill, the operational characteristics change constantly. In other words, the variations faced by a real moving-bed diffuser do not take place in a controlled environment. Therefore, it is reasonable to expect that the period of time between two variations in the extraction properties are smaller than the simulated times required to achieve a new steady-state. In this sense, a full-scale diffuser may never achieve a steady-state condition in a real operation process.

5.4 Optimization analyses

The simulation framework may also be used as an optimization tool. Such feature is an important, useful one in the daily routine of an industrial facility, since it opens room for the possibility to seek operational conditions that improve the extraction performance. In this sense, this section is going to present the optimization capabilities of the simulation framework. It is not the intention of the following presentation to inspect all the possible combinations of the optimization variables included in the model. In fact, the coming analyses have as main objective to discuss the potential of the developed model as a base to perform optimization procedures.

5.4.1 Aspersion positions

According to a study reported by REIN and INGHAM (1992), an active change in the aspersion positions during the operation of a diffuser is an effective way to seek improvements in the extraction process. From a quotation of that study, “it has been show that varying the point of application of juice enables the diffuser performance to be optimized (...)”. In this sense, the aspersion positions should not be fixed, but changing in order to answer to variations in the characteristics of the extraction environment. It is important to stress the active nature of such approach, thus understanding it as an efficient and possible way to control the diffuser performance on a daily basis at a sugarcane mill.

However, the active shifting in the aspersion positions is seldom performed at industrial facilities, despite the benefits that it may bring to the extraction process. This fact may be explained by practical circumstances particular to each sugarcane mill. Among such circumstances, one of the most critical issues is the lack of a tool that relates a change in the extraction environment with the required variation in the aspersion positions. In the absence of such tool, the variation in the aspersion points becomes an uncertain and laborious procedure, thus relying a lot on the heuristic expertise of the diffuser operator. The simulation framework developed in this thesis has the potential to fill the gap of the absence of the this predictive tool.

In the assessments performed in the previous sections, the aspersion points are fixed at the positions correspondent to those measured in the real equipment used as case study. Using these “real” aspersion points as midpoints, the following optimization procedures seek the best aspersion position in an interval around those midpoints. For instance, Figure 5.53 illustrates an initial aspersion position (*i.e.*, midpoint = 0.0 *m*), which is allowed a clearance of $\pm R$ *m* to the variation of the aspersion point. Therefore, the optimization procedure is going to seek inside that clearance a new position that improves both the extraction degree and the decreasing slope of the °Brix curve. According to REIN and INGHAM (1992), the aspersion positions in a full-scale diffuser may be changed up to the length of one stage, both right and leftward. For that reason, the *R* value used in the following optimizations is 4.5 *m* (*i.e.*, the length of a stage).

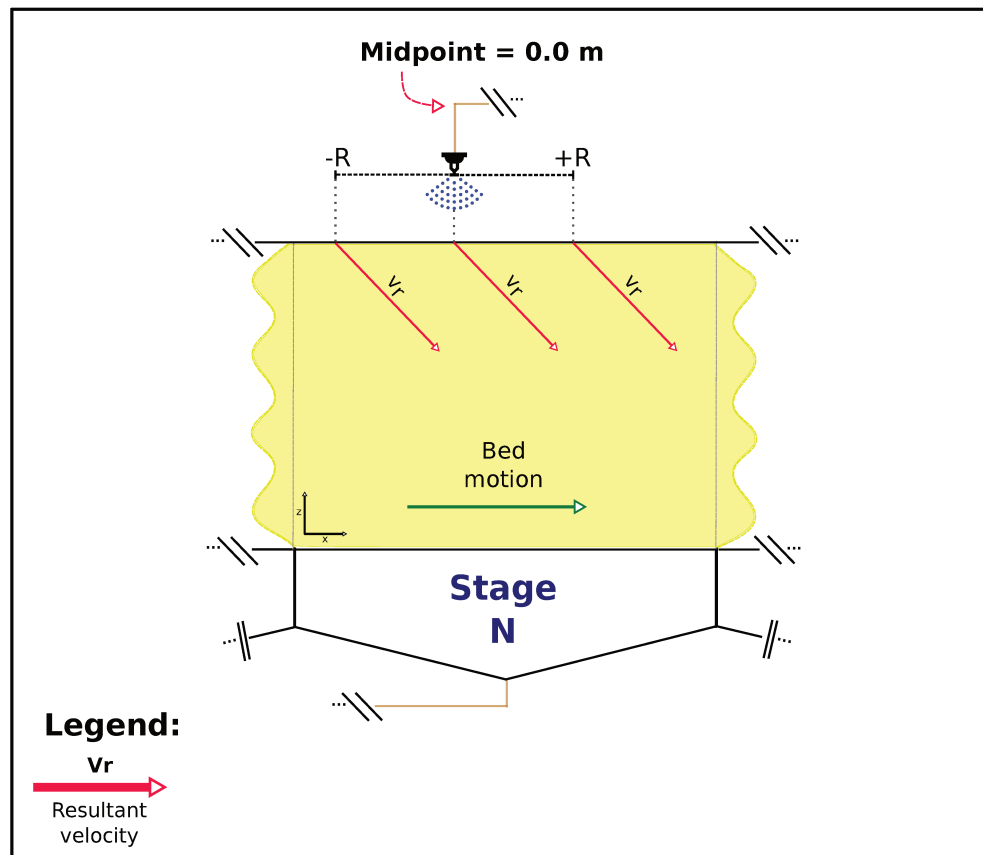


Figure 5.53: Schematic representation of the variation in the aspersion position.

5.4.1.1 Optimizing the base case

This subsection explores the potential to improve the extraction performance of the base case (*i.e.*, the one described in Table 5.1) by changing the aspersion positions. Aspersions have their positions changed in conjunct. It means the optimization procedure seeks a single shifting value valid for all the application points. It is worth to highlight that such single-shifting is just one of the possible approaches to perform an optimization procedure. In fact, the simulation framework enables the end-user to perform optimization analyses treating the aspersion points either individually or as groups of any desired configuration. The present optimization analysis was performed using a population of 10 candidate solutions. This value was defined by following a traditional rule of thumb that sets the amount of candidate solutions to ten times the number of optimization variables (SIVANANDAM and DEEPA, 2008). The number of iterations of the optimization procedure is 10,000.

Figure 5.54 presents the optimization results concerning the base case. Despite the use of a larger number of iterations (*i.e.*, 10,000 iterations), the evolution of the fitness value

(Figure 5.54-(a)) shows that an upper limit is reached in less than 50 iterations. Indeed, in relation to the generations above 50 iterations, the fitness value remains practically constant, displaying only tiny increments. The time required to perform 50 iterations is 4.8 *min*. Therefore, the optimized configuration may be achieved in a short period of time, which is important to enable the use of the simulation framework as an optimization tool in the daily routine of sugarcane mills.

The relative small number of iterations to achieve the optimized configuration may be explained by the features of the implemented genetic algorithm as well as by the morphology of the searching-domain. Regarding the *GA*, the generation of the initial population by the Latin hypercube sampling method spreads the initial candidate solutions evenly in the searching-domain. Such approach allows a better exploration of the morphology of the searching-domain, which makes it easier to find the global optimum and avoid the local solutions. Moreover, the presence of the genetic operators, such as the Gaussian mutation, leads to a faster exploitation of the best candidate solutions.

In relation to the morphology of the searching-domain, its characteristics are defined by the mathematical features of the model equations. In special, the linear nature of the extraction terms prevents the occurrence of complex morphologies (*e.g.*, intense or abrupt variations, extensive amount of peaks and valleys, and so on), which would emerge within the searching-domain due to the presence of non-linearities. The non-complexity of the morphology makes the searching for the optimum solution straightforward and faster. Therefore, a simple and smooth searching-domain coupled with the searching abilities of the implemented *GA* explain the observed small number of iterations required to achieve the optimum solution.

Figure 5.54-(b) shows the °Brix curve of the base case scenario in comparison with the °Brix curve of the optimized solution. In relation to the aspersion midpoints, the optimum solution is the one in which the aspersion positions are shifted in 68.1 *cm* towards the entrance of the equipment (*i.e.*, -68.1 *cm* in relation to the midpoints). As demonstrated in the Figure 5.54-(b), such shifting in the aspersion positions leads to a faster decrease of the °Brix curve, which is a positive contribution to the flexibility of the extraction process. Moreover, operating the diffuser in this optimum condition leads to a extraction degree of 94.8 %. This improvement in the extraction degree is only incremental, but may represents a substantial gain in profit in face of the great amount of sugarcane processed in a full-scale diffuser.

Figure 5.55 presents the °Brix distribution for the base case as well as the one for

Aspersion positions as optimization variable, Base case

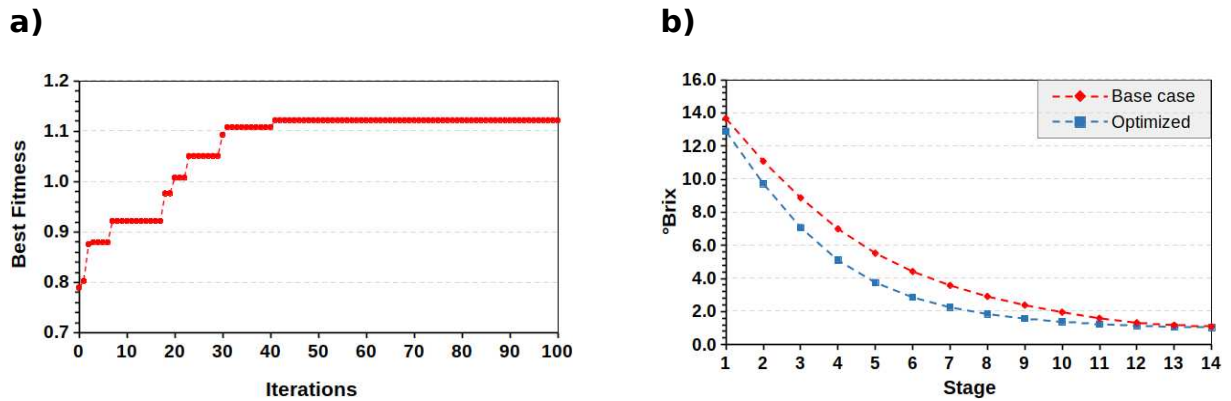


Figure 5.54: Results of the optimization procedure that aims to improve the extraction performance of the base case by changing the aspersion positions as a conjunct. (a) Fitness evolution (*i.e.*, objective function) over the course of the optimization procedure. (b) °Brix curve for the base case in comparison with the °Brix curve for the optimized scenario.

the optimized scenario. It is notice that anticipating the aspersion positions in 68.1 *cm* leads to a leftward shifting in the positions of the isolines. As a consequence, the isolines at the entrance of the equipment get closer to each other. Such closer configuration is an expected behavior concerning an extraction process with a faster decrease of the Brix values in the initial stages of the diffuser. At the rear of the diffuser, the leftward shifting in the isolines positions also leads, in relation to the base case, to lower values of °Brix. These lower values means an improvement of the sucrose extraction, which is in agreement with the higher extraction degree achieved in the optimum scenario.

5.4.1.2 Optimizing a scenario with bed velocity equal to 0.95 *m/min*

Increasing the bed velocity to a value of 0.95 *m/min*, but keeping the other operational conditions equal to the base case lead to a reduction in the extraction degree as well as in the °Brix gradient along the sugarcane bed (see subsections 5.2.5 and 5.3.4). Despite the reduction in the sugarcane processing time, the drop in the extraction may represent an important drawback for the economic sustainability of the mill. In this scenario, the active control of the aspersion positions is a cunning way to improve the extraction performance, without necessarily reducing the bed velocity. Therefore, this subsection applies the previous optimization approach to seek a new aspersion configuration in order to improve the extraction performance of the scenario with $v_b = 0.95$ *m/min*. As done before, this opti-

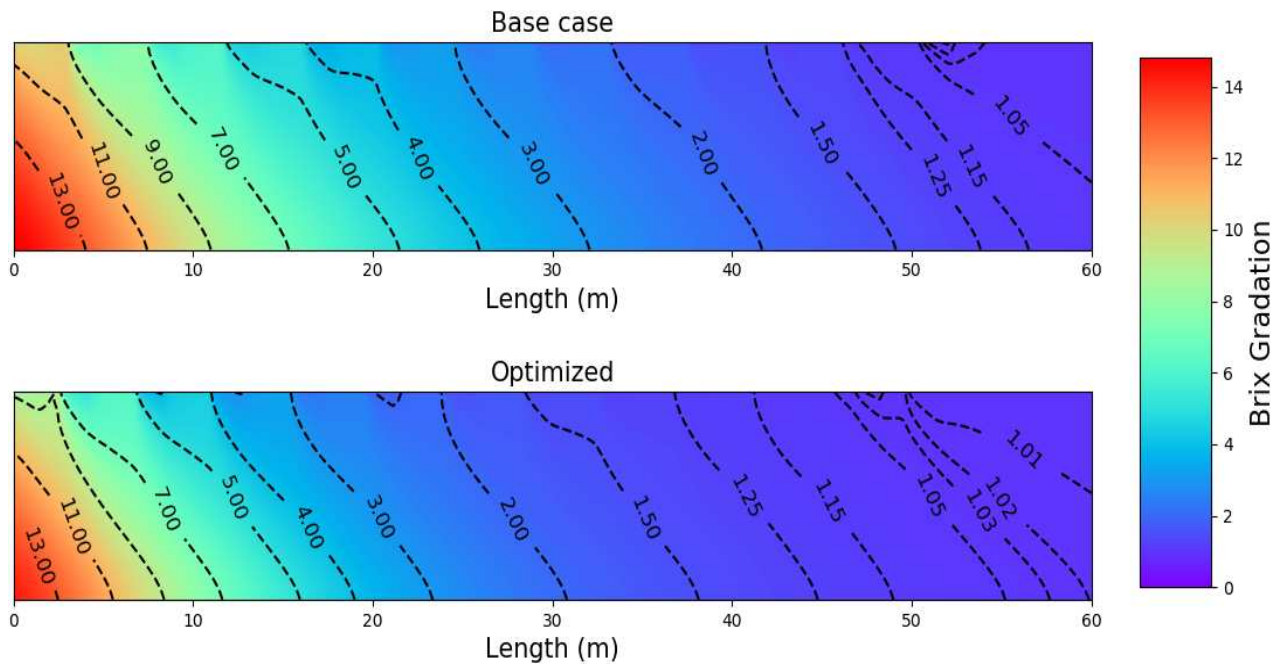


Figure 5.55: °Brix distribution for the base case and for the optimized scenario concerning an optimization procedure that aims to improve the extraction performance by changing the aspersion positions as a conjunct.

mization procedure was performed with a population of 10 individuals, evolving along 10,000 iterations of the genetic algorithm.

Figure 5.56-(a) presents the evolution of the fitness value (*i.e.*, the objective function) over the course of the first 100 iterations. Above these 100 iterations, the fitness remains practically constant, not presenting any remarkable variation in its optimum value. Therefore, one is allowed to conclude that the present optimization procedure achieves the optimum solution in less than 100 iterations. This relative fast optimization procedure is also a consequence of a smooth and non-complex searching domain, and the efficient searching features of the implemented *GA*. The genetic algorithm, as it is implemented in this thesis, takes around 10 *min* to perform 100 iterations. Therefore, the current optimization procedure is suitable to be performed in the daily routine of a sugarcane mill.

The optimum condition is as shifting of each aspersion point in 38.0 *cm* towards the entrance of the equipment (*i.e.*, -38.0 *cm* in relation to the midpoints). This optimum condition generates a °Brix curve with a spatial disposition similar to the °Brix curve of the base case (Figure 5.56-(b)). In relation to the non-optimized scenario, the aspersions in their optimal positions yield a higher °Brix gradient in the initial stages of the diffuser. Moreover,

the extraction degree concerning the optimized scenario is 94.1 %, which is higher than the value achieved by the non-optimized scenario (*i.e.*, 93.8 %) and similar to the extraction degree of the base case (*i.e.*, 94.2 %). These results testify in favor of the advantages of controlling the aspersion positions. As a matter of fact, the optimum result demonstrates that a small adjustment in the aspersion positions may restore the extraction performance to a condition equivalent to the scenario before the increasing of the bed velocity (*i.e.*, the base case).

Aspersion positions as optimization variable, $v_b = 0.95 \text{ m/min}$

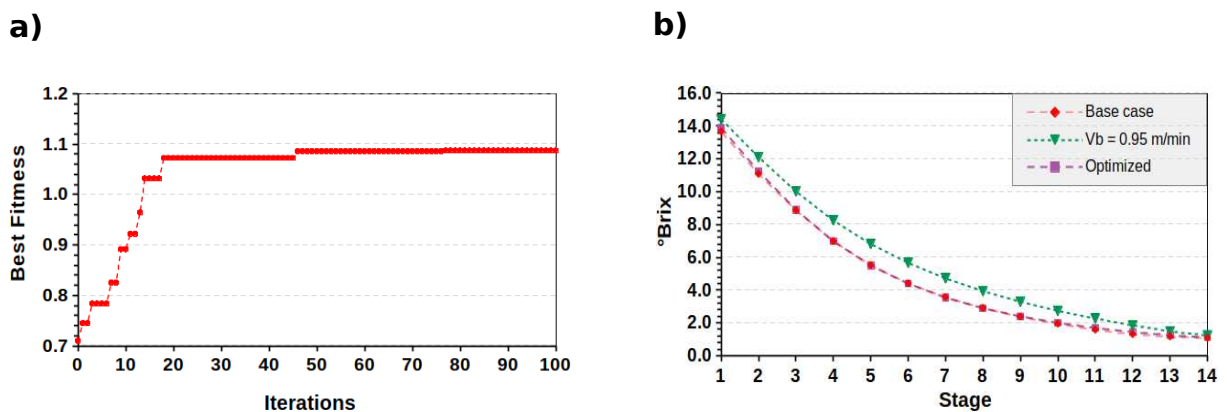


Figure 5.56: Results of the optimization procedure in which the main goal was to improve the extraction performance of a scenario in which the bed velocity is 0.95 m/min . (a) Fitness evolution (*i.e.*, objective function) over the course of the optimization procedure. (b) °Brix curves for the base case and the scenario with $v_b = 0.95 \text{ m/min}$ in comparison with the °Brix curve for the optimized scenario.

Provided that the aspersion positions are kept constant, increasing the bed velocity leads to a more pronounced recirculation effect. In this sense, the percolating liquid within a given region of the diffuser leaves the bed in a position beyond the spot that would preserve a pure counter-current flux. In order to guarantee that the percolating liquid leaves the bed in the right position, the aspersion have to be replaced to a position before their initial location. By doing so, the recirculation effect is reduced and the pure counter-current flux is restored. The optimum solution founded by the optimization procedure follows exactly such tendency of replacement of the aspersion positions. Therefore, the optimum result is consistent with the phenomenology of an extraction process in a moving-bed diffuser.

Figure 5.57 presents the °Brix distributions concerning the scenarios without and with optimization. It is possible to notice that adjusting the aspersion points in accordance with the optimum solution makes the isolines to shift their position leftward. Such leftward

shifting leads to a °Brix distribution similar to the one simulated for the base case. These analogous °Brix distributions agree with the aforementioned similarity between the simulated extraction degrees as well as with the closeness of the two °Brix curves.

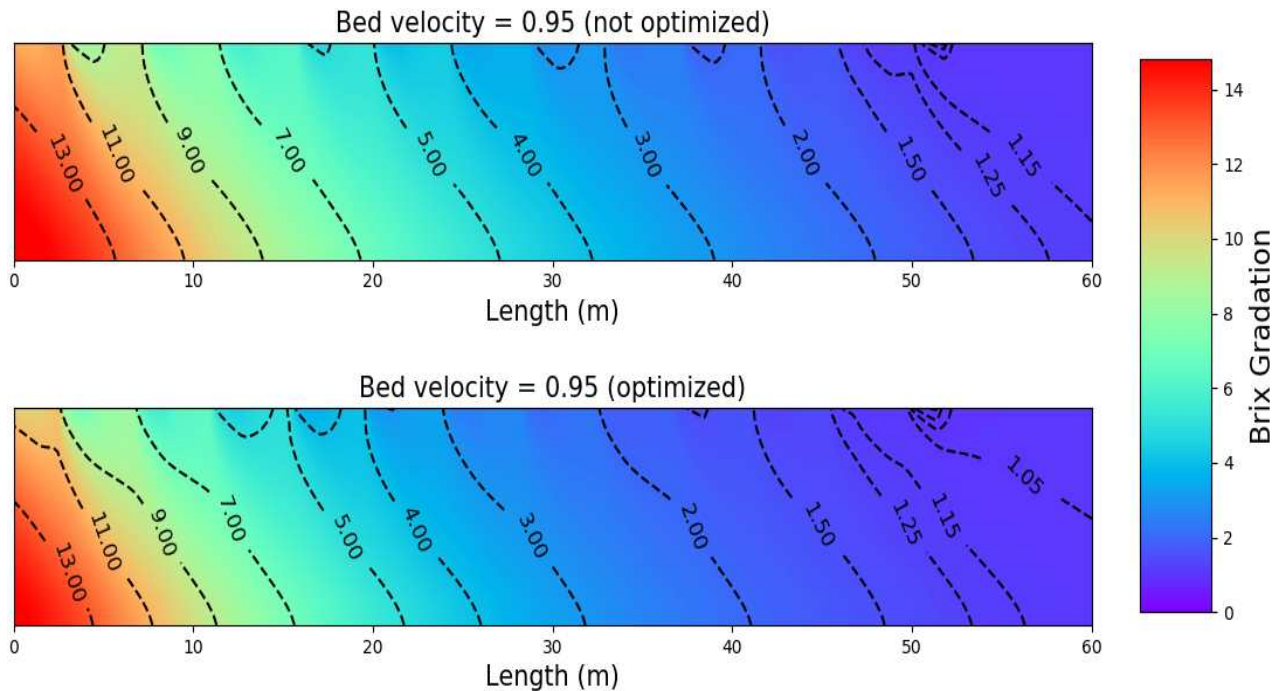


Figure 5.57: °Brix distributions regarding the scenarios with $v_b = 0.95 \text{ m/min}$ with and without optimization.

5.4.2 Imbibition rate

Another important operational variable used at a sugarcane mill to control the extraction performance is the imbibition rate. By changing the amount of imbibition water added to a diffuser, it is possible to control the liquid distribution in the whole equipment. During the extraction process, such water control is important to guarantee an efficient liquid-solid contact and prevent the occurrence of flooding. In fact, according to [MUNSAMY and BACHAN \(2006\)](#), the imbibition rate is a control variable that has a remarkable potential to impact the extraction performance. In this sense, the following analyses applies the optimization features of the developed Simulation Framework to seek improvements in the extraction performance by changing the imbibition rate.

The amount of imbibition water added into a diffuser is set in relation to the quantity of fibers being processed (*i.e.*, kg_{water}/kg_{fiber}). According to [REIN \(2013\)](#), in common

operation conditions, the imbibition rate in a moving-bed diffuser may vary from 2.0 up to 4.0 kg_{water}/kg_{fiber} . In the optimization procedure, therefore, lower and upper limits of the imbibition rate was defined in accordance with this reference. As done in the previous subsection, the base case is used as the baseline to perform the following optimization procedures. Since only one variable (*i.e.*, content of imbibition water) is used in the optimization process, the number of candidate solutions is set to 10 individuals. Moreover, the total amount of generations of the *GA* is 10,000.

The evolution of the fitness value over the course of the *GA* iterations (Figure 5.58-(a)) shows that the objective function reach a upper limit in less than 100 iterations. Indeed, a general conclusion is achieved after repeating the optimization procedure several times: it is not necessary to use a large number of iterations (*i.e.*, 10,000), since the same optimum condition is always reached in less than one hundred generations of the *GA*. The optimum value is the one in which the diffuser operates with the imbibition rate at its upper limit (*i.e.*, 4.0 kg_{water}/kg_{fiber}). Operating the extraction in the highest allowed imbibition value leads to an increase of the °Brix gradient in the initial stages of the diffuser. Such tendency may be observed by comparing the Brix curve of the base with the one of the optimized scenario (Figure 5.58-(b)).

Imbibition rate as optimization variable, base case

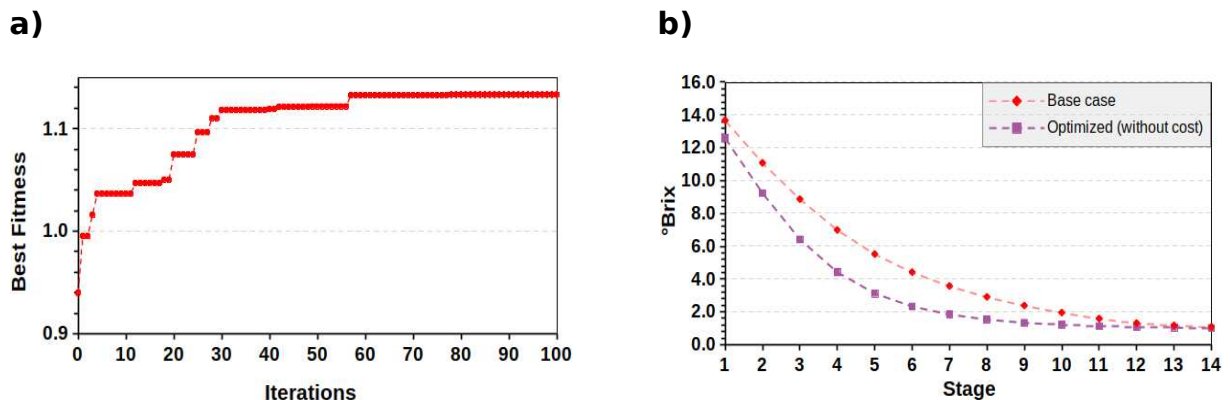


Figure 5.58: Optimization results regarding the procedure to seek improvements in the extraction performance by changing the imbibition rate. (a) Fitness evolution (*i.e.*, objective function) over the course of the optimization procedure. (b) °Brix curves for the base case with and without optimization.

The °Brix distribution simulated using the optimum imbibition value (Figure 5.59) also display the observed increase in the °Brix gradient, especially in the initial stages of the

diffuser. In comparison with the base case without optimization, the isolines displayed in the Figure 5.59 are dislocated towards the entrance of the diffuser. Moreover, particularly at the first 15 m of the equipment, the isolines are closer to each other, thus indicating a faster reduction of °Brix value. The extraction degree reached in this optimized scenario is 95.2 %, which is higher than the value simulated for the base case.

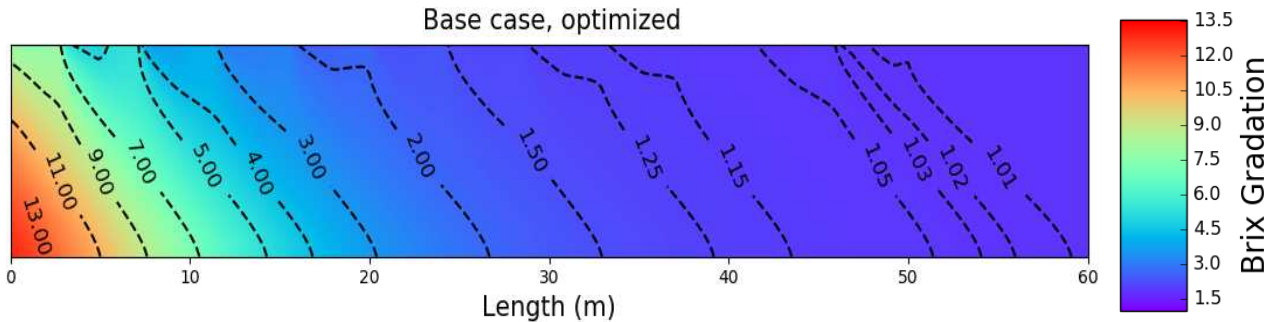


Figure 5.59: °Brix distribution simulated considering the optimum value of the Imbibition rate (*i.e.*, $4.0 \text{ kg}_{\text{water}}/\text{kg}_{\text{fiber}}$).

The previous optimization result is a trivial one. Neglecting a potential flooding condition, “higher imbibition rates will invariably result in higher extractions” (REIN, 2013). Moreover, operating a diffuser with high imbibition rate “will enable a smaller diffuser to be utilized to achieve a given extraction” (REIN, 2013). Therefore, without performing any optimization procedure, someone slightly acquainted with the operation of a moving-bed diffuser may easily conclude that the maximum imbibition rate leads to the best extraction performance. However, by increasing the water content within the bed, there is a rise of energy and steam consumption, majorly in the unit operation in charge of concentrate the extracted juice. In this scenario, the improvements reached in the extraction performance must be balanced against the additional costs imposed by a higher energy/steam consumption.

In order to include the cost evaluation in the optimization analyses, the objective function (Eq 4.72) needs to be modified. This modification means the inclusion of a cost element in the objective function in order to balance the other two terms. In the present analyses, this cost term is a simplification. It is assumed that the upper limit of the optimization variable (*i.e.*, $4.0 \text{ kg}_{\text{water}}/\text{kg}_{\text{fiber}}$) imputes the maximum operational cost ($Cost_{imb}^{max}$) to the process. The actual value of $Cost_{imb}^{max}$ is not important, since the costs are normalized between 0 and 1 by using this very maximum value. Therefore, $Cost_{imb}^{max}$ is equal to 1 in the objective function (*i.e.*, $Cost_{imb}^{max}/Cost_{imb}^{max} = 1$). The costs in relation to the other imbibition values are computed by the 0.6-rule (PETERS and TIMMERHAUS, 1991), as presented in the

Eq 5.1 for a generic imbibition value i .

$$Cost_{imb}^i = Cost_{imb}^{max} \cdot \left(\frac{Imbibition^i}{Max. Imbibition} \right)^{0.6} = 1.0 \cdot \left(\frac{Imbibition^i}{4.0} \right)^{0.6} \quad (5.1)$$

The modified objective function is described in the Eq 5.2. The cost element appears at the denominator because it has to be minimized by the optimization procedure.

$$obj. function = \frac{(Ext. degree \%)}{100\%} + \frac{(C_{\circ Brix,1}^{model} - C_{\circ Brix,2}^{model})}{C_{\circ Brix,rm}^{in}} + \frac{1}{1 + Cost_{imb}^i} \quad (5.2)$$

The above optimization procedure was repeated using the modified objective function. Figure 5.60-(a) shows the evolution of the fitness value over the course of the optimization process. In comparison with the former optimization procedures, the fitness value achieves the optimum solution in a higher number of iterations. Despite this apparently slower optimization process, the fitness behavior still follows the common tendency of the previous analyses: an constant objective function for iterations above 100. Therefore, the present optimum procedure may be considered fast and suitable for applications in the daily routine of a mill. In this present scenario, the optimum amount of imbibition water is $3.3 \text{ kg}_{water}/\text{kg}_{fiber}$, which is definitely not a trivial result.

This optimum value is higher than the one applied to the base case ($2.8 \text{ kg}_{water} / \text{kg}_{fiber}$). As a result, it leads to an increasing in the extraction degree (94.8%) in relation to base scenario. Moreover, the °Brix gradient increases in comparison with the initial condition, as it may be noticed in the simulated °Brix curve (Figure 5.60-(b)) as well as in the rightward shifting of the position of the isolines displayed in the °Brix distribution (Figure 5.61). The presence of the cost term prevents the optimization procedure to reach the upper limit of the optimization variable. As a consequence, both extraction degree and °Brix gradient are limited by the cost imposition, thus not achieving the better extraction performance displayed by the analysis without financial assumption. In this scenario, therefore, the gains in the extraction performance reached by applying the maximum allowed imbibition rate are not so advantageous in face of the increasing in the process cost.

It is worth to stress that this cost analysis is an simplification of a real assessment designed to infer the financial sustainability of a sugarcane mill. In a real scenario, process cost

Imbibition rate as optimization variable with cost assumption

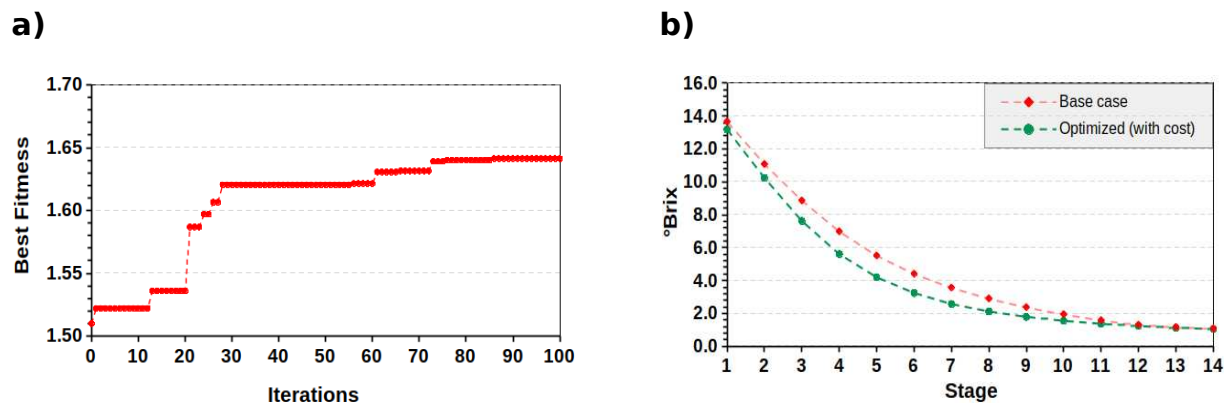


Figure 5.60: Optimization results regarding the procedure to seek improvements in the extraction performance by changing the imbibition rate, with cost assumption. (a) Fitness evolution (*i.e.*, objective function) over the course of the optimization procedure. (b) °Brix curves for the base case in comparison with the optimized scenario assuming a cost assumption.

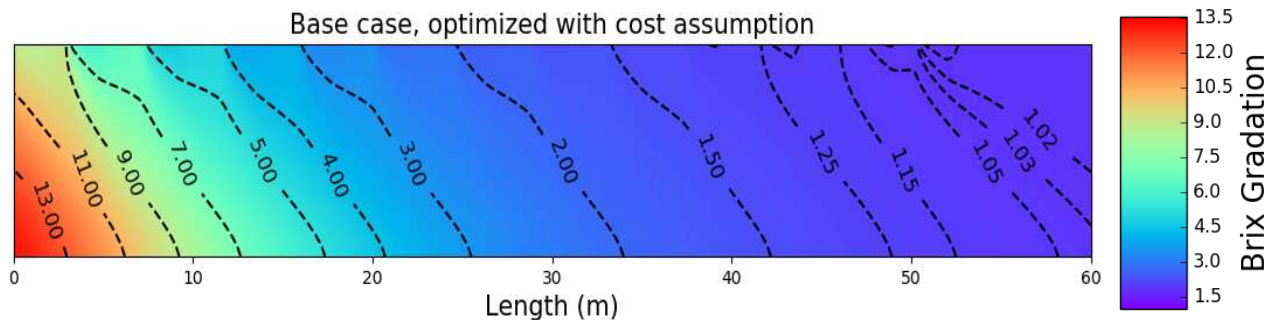


Figure 5.61: °Brix distribution regarding the procedure to seek improvements in the extraction performance by changing the imbibition rate, with cost assumption.

is influenced by many variables, which interact with each other in a non-trivial way. Modeling the financial relations among the operational variables by itself is a complex task, which is not included in the scope of the present thesis. However, despite the oversimplification in relation to a real assessment, the previous cost assumption fulfill its designate intention: to demonstrate the potential of the Simulation Framework to handle multi-objective functions with terms possessing divergent goals (*i.e.*, maximization or minimization).

5.4.3 Size of the moving-bed diffuser

This subsection is going to explore the potential of the Simulation Framework to handle design optimizations. This type of assessment is important to guide the conception of a diffuser's layout in order to reach some desired performance criteria. The design parameter optimized in the following optimization analyses is the number of stages (N_{st}). The other layout variables (*e.g.*, width of the equipment) are fixed. Along with the number of stages, the former optimization variables (*i.e.*, aspersion positions and imbibition rate) are also included in the coming optimization procedures. Therefore, the assessments performed in the present subsection are mixed-integer optimizations.

Figure 5.62 is a schematic representation of the implemented mixed-integer optimization routine. The set of N_{st} values used in the optimization process is $\{10, 12, 14, 16, 18\}$. Therefore, the complete optimization routine (Figure 5.62-(a)) seeks within the N_{st} set the value that leads to the best extraction performance. Due to the integer nature of the variable “number of stages”, the optimization task may be divided into 5 sub-scenarios (Figure 5.62-(b)), each one of them representing a value of the N_{st} set. An optimization procedure is performed for each sub-scenario (Figure 5.62-(c)) in order to improve the extraction performance by manipulating the aspersion positions and the imbibition rate. The results of the 5 optimization procedures are compared among each other (Figure 5.62-(d)) with the intention to rank the sub-scenarios by their optimum value. The sub-scenario with the best optimum value is the final solution of the complete optimization procedure (Figure 5.62-(e)).

The optimization procedures of the sub-scenarios were performed considering the cost assumption of the imbibition rate (Eq 5.2). In each sub-scenario, the number of candidate solutions is 20 and the total amount of iterations performed in the optimization procedure is 1,000. A lower number of iterations is used in this analysis because the former optimization procedures showed that it is not required 10,000 iterations to reach the optimum solution. Table 5.16 presents the results of the optimization of each sub-scenario. The cost assumption leads to optimization results in which the imbibition rates are near to the lower limit (*i.e.*, $2.0 \text{ kg}_{water}/\text{kg}_{fiber}$). The reduction in the imbibition rates are compensated by a leftward shifting in the aspersion positions (negative values in Table 5.16). The best optimized solution is the one in which the extraction process is performed using a diffuser with 18 stages.

Figure 5.63 details the optimization results of the sub-scenario presenting the best optimization performance (*i.e.*, $N_{st} = 18$). The higher fitness value is reached in less than 400

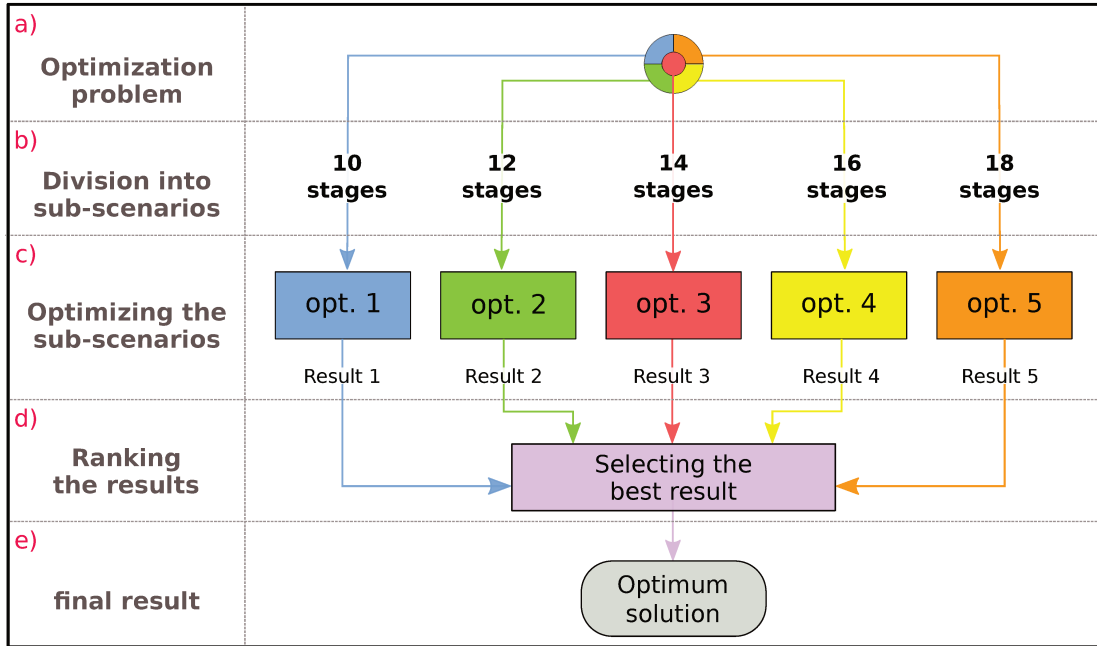


Figure 5.62: Schematic representation of the implemented mixed-integer optimization routine.

Table 5.15: Optimization results concerning each sub-scenario describe in Figure 5.62

N_{st}	Asp. posi. shift*	Imbibition rate	Best Fitness
—	m	kg_{water}/kg_{fiber}	—
10	-0.46	2.9	1.62
12	-1.16	2.2	1.69
14	-1.12	2.4	1.70
16	-1.62	2.3	1.72
18	-1.55	2.2	1.73

*Negative values represents leftward shifting in the asp. positions.

iterations (Figure 5.63-(a)). The larger number of iterations required to achieve the optimum solution is a direct consequence of the increase in the number of optimization variables (two, in the present analysis, instead of one, as it was done in previous assessments). Figure 5.63-(b) depicts the simulated °Brix curve for the best optimum scenario. The optimum curve presents a higher °Brix gradient than the base case. Regarding an extraction process performed in a diffuser with 18 stages, but without optimization, the optimum curve also display a stepper decrease of the °Brix value, specially in the initial stages of the diffuser. Moreover, still in relation to the non-optimized scenario with 18 stages, the optimum curve achieves lower °Brix values at the end of the equipment. Such lower °Brix at the rear of the diffuser is in agreement

with the higher extraction degree simulated using the optimum conditions ($\approx 94.8\%$).

Optimization results concerning the sub-scenario with 18 stages

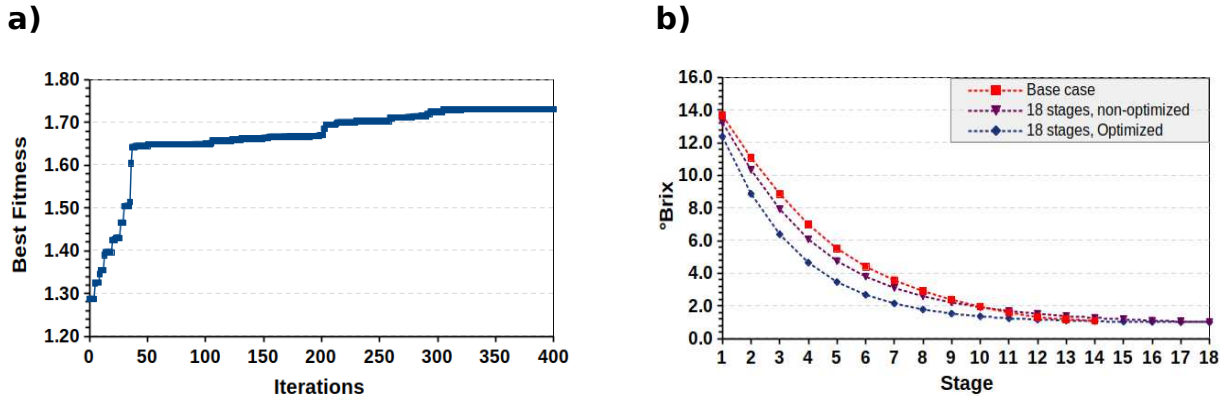


Figure 5.63: Details of the optimization procedure concerning the sub-scenario with the best optimum solution ($N_{st} = 18$). (a) Fitness evolution over the course of the optimization procedure. (b) °Brix curves regarding the extraction process performed in a diffuser with 18 stages, both optimized and non-optimized, in comparison with the °Brix curve of the base case.

However, the previous optimization result is also a trivial one, since one may intuitively achieve the same conclusion without performing any optimization procedure. Indeed, the steady-state simulations performed in the sub-section 5.2.3 have already alluded to the advantages of performing the extraction process in longer diffusers. A complete design assessment must consider the capital required to build the equipment. Such capital issues insert in the optimization process the requirement to ponder between extraction performance and the financial assets available to fulfill the goals intended during the design of the diffuser. With the intention to explore the role of the financial burden in the design of an equipment, it is proposed a new term to be included in the objective function in order to account for the capital required to build a diffuser.

This new capital term is defined in the same manner as done before to include the imbibition water cost in the objective function (Eq 5.1). Therefore, the longer diffuser ($N_{st} = 18$) assumes the maximum cost ($Cost_{N_{st}}^{max}$) and the other costs ($Cost_{N_{st}}^i$) are computed by the 0.6-rule. In this way, the objective function in its new modified version is presented in the Eq 5.3. The optimization results concerning each number of stage are displayed in Table 5.16. The best solution is no longer the one achieved by using the longer diffuser. In fact, the new cost assumption leads the optimization procedure to achieve the best solution for a diffuser with 12 stages. This result indicates that the gains in extraction performance

do not compensate in face of the raise in the costs required to build a longer diffuser.

$$\begin{aligned}
 \text{obj. function} = & \frac{(\text{Ext. degree } \%)}{100\%} + \frac{(C_{\circ\text{Brix},1}^{\text{model}} - C_{\circ\text{Brix},2}^{\text{model}})}{C_{\circ\text{Brix},rm}^{\text{in}}} \\
 & + \frac{1}{1 + \text{Cost}_{imb}^i} + \frac{1}{1 + \text{Cost}_{Nst}^i}
 \end{aligned} \tag{5.3}$$

Table 5.16: Values of the objective function considering cost assumption of the diffuser's size.

N_{st}	Best Fitness
10	2.20
12	2.25
14	2.24
16	2.24
18	2.23

The °Brix curves for a diffuser with 12 stages, with and without optimization, is presented in Figure 5.64. It is possible to notice that the optimized curve shows a faster decrease of °Brix curve and achieves, as well, a lower value of °Brix at the end of the equipment. In comparison with a 18 stage diffuser (also displayed in Figure 5.64), the new optimum scenario has a lower °Brix gradient, but achieves a similar level of °Brix values at the rear of the equipment. Such similarity leads to close values of the extraction degree: 94.8 % for the optimized 12 stage scenario. However, it is worth to point out that the lower °Brix gradient leads to less flexible extraction process. This fact may be an evidence for the reason why the full-scale diffuser used in the case study has 14 stages: to balance the performance and flexibility of extraction with the capital cost required to build the diffuser.

5.4.4 Concluding remarks about the optimization analyses

The analyses performed in this section demonstrate the potential of the Simulation Framework to be used as an optimization tool. Such potential may be converted into important contributions to the sugarcane sector. In this desired scenario, these contributions embrace the design of new equipments as well as the searching of improvements in the extraction performance on a daily basis at a sugarcane mill. As a general tendency, the optimum results are achieved in a not so large number of iterations, which testify in favor of the

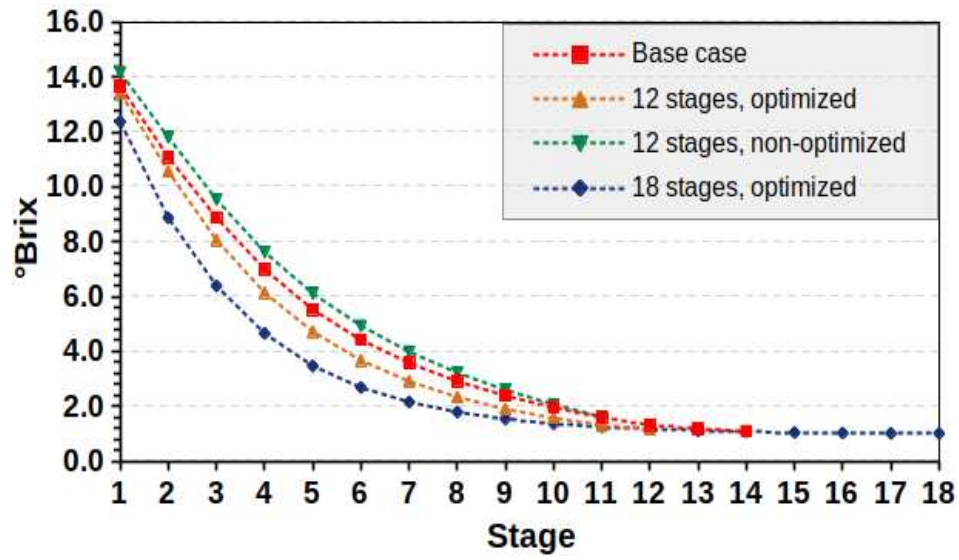


Figure 5.64: °Brix Curves for a 12 stage diffuser, with and without optimization, in comparison with the base case and the scenario regarding a optimized 18 stage diffuser.

good searching capacity of the implemented routine. Moreover, the optimization results are coherent and consistent with the reality of the modeled system.

Chapter 6

Conclusion

This work presented a mathematical model for the sugar extraction process in moving-bed diffusers along with an user-friendly simulation framework. The proposed phenomenological abstraction and the mathematical formulation of the model provide an original and formal theoretical foundation to describe sugar extraction in sugarcane beds. Both at steady and transient states, the results of the simulations indicate that the model equations in their discretized form is well-posed. The steady-state simulations show that accurate results may be simulated in few seconds, which makes the simulation framework a fast tool to assess the sucrose extraction via diffusers. In their turn, the dynamic simulations emerges as a cunning way to assess the features of the path took by the extraction environment between two successive steady-state conditions.

No matter at steady-state or dynamic conditions, the simulations outcomes are in good agreement with the expected behavior of a real moving-bed diffuser under operation as well as with the phenomenology of the sucrose withdrawing from the sugarcane fibers. This agreement testifies in favor of the validity of the proposed model. With the simulated °Brix distribution, extraction is no longer a “black-box” process in which °Brix curve and sugar extraction degree are the only indicatives of the diffuser performance. Indeed, analyzing the °Brix distribution in the bed is a suitable new approach to asses the operation of moving-bed diffusers.

The optimization analyses performed in this thesis established the potential of the Simulation Framework to seek improvements in the extraction process via diffusers. The optimum results are achieved in few iterations, which evidences the quality of the searching procedure of the proposed optimization routine. The simulations considering cost assumptions

demonstrate the capacity of the Simulation framework to handle multi-objective functions in which the terms have divergent targets (i.e., maximization or minimization). As a whole, the optimization procedures lead to results that are coherent/consistent with the reality of the modeled system.

All things considered, the developed computer-aided Simulation Framework has the potential to assist diffuser design, operation, and optimization as a reliable predictive tool, which would make the operation of diffusers a less subjective procedure.

Chapter 7

Recommendations for future work

An enormous groundbreaking to the mathematical modeling of moving-bed diffusers would be the rigorous description of water-air distribution inside the sugarcane bed. With this description at hand, the extraction process may be simulated considering more realistic scenarios, in which unsaturated conditions are present along the diffuser's bed. By coupling a future water-air balance with the extraction model proposed in this thesis, it would be possible to assess the influence of unsaturated regions on the extraction performance. Moreover, the inclusion of these new balances in the model allows for the possibility to simulated start-up conditions as well as to predicted flooding during the extraction process.

In its essence, the mathematical modeling of this unsaturated conditions is a formal description of a multi-phase flow (*i.e.*, water and air) within a porous media. In order to explore some important features of such multi-phase flow, Figure 7.1 presents a schematic representation of the water and air distribution within an illustrative porous medium. At the beginning of the liquid aspersion in the medium (Figure 7.1-(a)), the porous system is filled with air, presenting only a thin layer of liquid on the surface of the fibers. This thin layer of liquid interacts with the fibers' surface by capillary and adsorption binding forces. As the amount of liquid increases in the system (Figure 7.1-(b)), this binding forces decrease up to a point in which water starts to flow within the porous medium (Figure 7.1-(c)). Even in flow conditions, there are regions of the porous structure with trapped air (Figure 7.1-(d)). As water penetrates thoroughly the porous system, these air pockets collapse, thus leading to full-saturated condition (Figure 7.1-(e))

The momentum balance of both water and air phase may be describe by Darcy's law (Eq 7.1). In Eq 7.1, the subscript φ represents a generic fluid phase (water or air), and v_φ

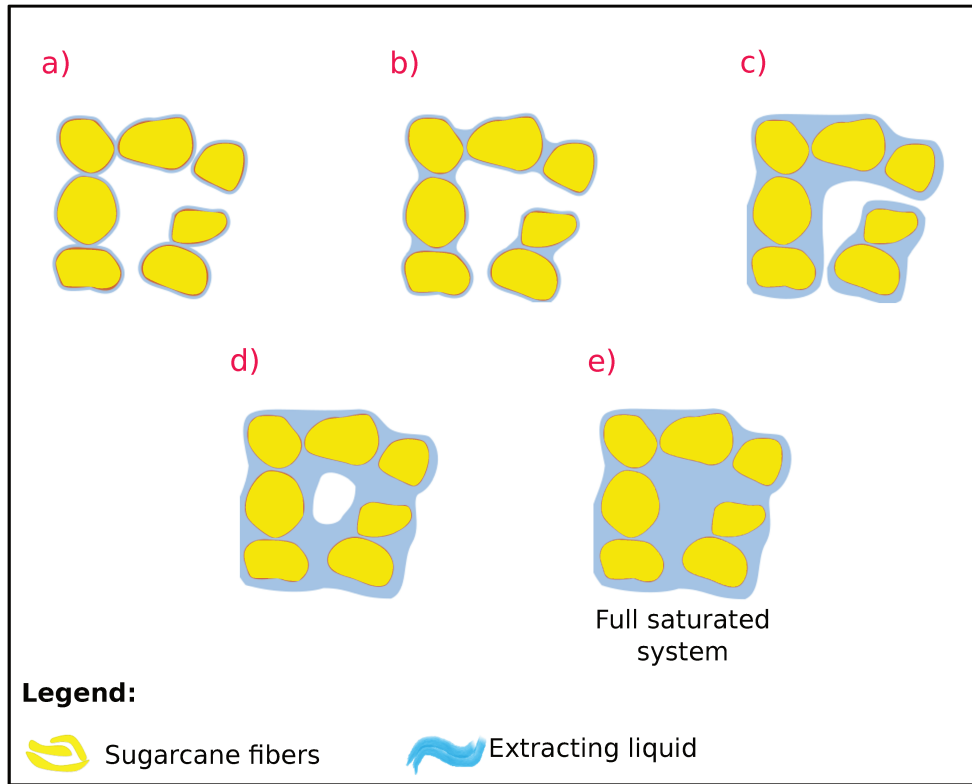


Figure 7.1: Spatial configurations of water and air in an unsaturated porous medium. Adapted from SZYMKIEWICZ, 2013 .

stands for the velocity of the phase φ . As presented in chapter 3, K_p is the permeability of the medium. Viscosity, pressure, and density of phase φ is accounted in the this equation for the terms μ_φ , P_φ , and ρ_φ , respectively. Under unsaturated conditions, K_p is not constant, but changes its value as function of the water saturation in the medium (SZYMKIEWICZ, 2013). It is necessary, therefore, to propose a model or even an empirical correlation to describe the relation between K_p and water saturation. Concerning the water-air-sugarcane system, however, such model or empirical correlation do not exist in the available literature.

$$v_\varphi = -\frac{K_p}{\mu_\varphi} (\nabla P_\varphi - \rho_\varphi g) \quad (7.1)$$

Concerning the studies of water-flow inside porous rocks, there are many equations available in literature to describe the relation between K_p and water saturation in the medium. The majority of these equations are functions of the aforementioned binding forces (*i.e.*, capillary and adsorption). In this sense, K_p value over the course of the saturation process is influenced by the strength in which water and air interact with the solid structure.

Another important point is that the strength of these interactions also influences the water pressure (P_{water}) when the system is under unsaturated conditions. Assuming that these facts are valid for the diffuser's bed, therefore, future works need to better understand the phenomenology of these binding forces in relation to the system water-air-sugarcane fibers.

The most traditional approach to perform these future works will include direct experimentation, collection of real data, and the fitting of a model/correlation. In this scenario, I would like to propose a new approach to be integrated with the traditional one. This new approach uses the Lattice Boltzmann methodology (LBM). LBM is a class of computational fluid dynamics methods that simulates the flow of Newtonian fluids with collision models (for further information about LBM see KRUGER *et al.*, 2017; MOHAMAD, 2011; and SUKOP and THORNE, 2006). In comparison with the Navier-Stokes equations, one of the most remarkable advantages of LBM is its ability to effortlessly handle scenarios with complex geometries (*e.g.*, sugarcane bed). Moreover, SUKOP and THORNE, (2006) report the use of LBM as a cunning tool to study capillary and adsorption binding forces of liquids on solid surfaces.

In parallel with the development of the Simulation Framework, this thesis also applied the LBM with the intention to simulate the water movement inside a diffuser's bed. For this sake, it was developed a computational routine in Python to implement the Lattice Boltzmann method. Figure 7.2 shows an example of a simulation performed using the developed LBM routine. The initial step of this routine is the conversion of a 2-D picture of a sugarcane bed (Figure 7.2-(a)) into a binary image, in which "0" means void space and "1" represents fiber. This binary image is used as the representation of the real medium during the application of the Lattice Boltzmann method. The second step of the routine is the Lattice Boltzmann method itself, in which LBM computes the velocity profile inside a section of a sugarcane bed. Figure 7.2-(b) shows the velocity profile at steady-state condition within the region of the picture surrounded by the red rectangle (in the "a" panel of Figure 7.2).

In its current version, the developed LBM routine provides interesting qualitative insights about the features of the water flow inside a sugarcane bed. For instance, Figure 7.2-(b) shows the existence of stagnant regions, which may jeopardize the extraction process. However, the developed LBM routine only simulates steady-state conditions with a single fluid phase embedded in a solid matrix. In order to use Lattice Boltzmann method to explore the features of unsaturated flows, the LBM simulations must account for multi-phase flows occurring under dynamic conditions. Moreover, more representative simulations necessarily imply in the use of 3-D descriptions of the sugarcane bed. Therefore, a future LBM routine

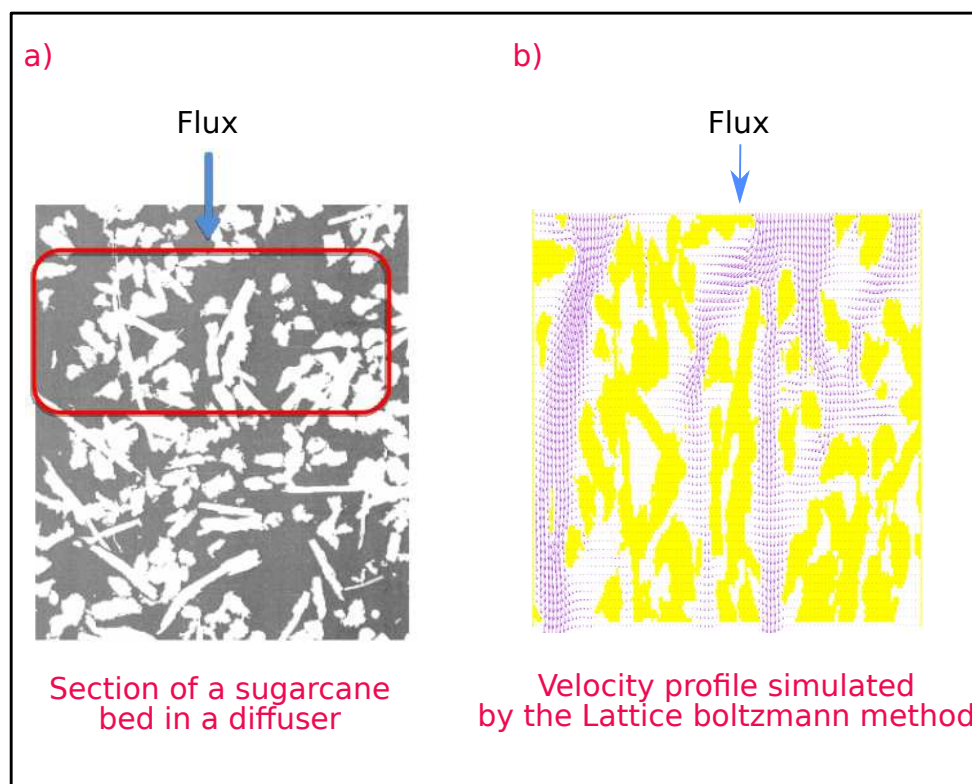


Figure 7.2: Simulated flux in a 2-D section of a sugarcane bed using the Lattice Boltzmann method. (a) Picture of a sugarcane bed used as base to perform the liquid flux simulation. (b) Velocity profile at steady-state condition within the region of the picture surrounded by the red rectangle (in the “a” panel).

designed with the intention to assess the evolution of K_p and P_φ value over the course of the saturation process must fulfill these requirements

Another huge contribution would be the energy balance of the extraction process via diffusers. Such balance may account for the steam balance required to keep the temperature inside a diffuser under satisfactorily operational conditions. By doing so, it would be possible to perform some optimization routines in order to decrease the energy consumption of diffusers.

Bibliography

- ARTSCHWAGER, E. Anatomy of the vegetative organs of the sugar beet. *Journal of Agricultural Research*, v. 33(2), 146–176, 1926.
- AURIAULT, J.-L., BOUTIN, C. and GEINDREAU, C. *Homogenization of Coupled Phenomena in Heterogenous Media*, chap. Incompressible Newtonian Fluid Flow Through a Rigid Porous Medium. 1^a ed., John Wiley and Sons, Inc, 2009.
- BEAR, J. *Dynamics of fluids in porous media*. 1^a ed., Dover Publications Inc., New York, 1972.
- BEAR, J. and BACHMAT, Y. *Introduction to Modeling of Transport Phenomena in Pourous Media*, v. 4 de *Theory and Applications of Transport in Porous Media*. Kluwer Academic Publishers, Dordrecht, The Netherlands, 1991.
- BEAR, J. and BUCHLIN, J. M. *Modelling and Applications of Transport Phenomena in Porous Media*. Kluwer Academic Publishers, 1987.
- BONOMI, A., CAVALETT, O., DA CUNHA, M. P. and LIMA, M. A. P., eds. *Virtual Biorefinery-An Optimization Strategy for Renewable Carbon Valorization*. Green Energy and Technology, 1^a ed., Springer International Publishing, Switzerland, 2016.
- BRUNICHE-OLSEN, H. and BUNDGAARD, A. G. Extraction Properties of Crushed or Shredded Cane. In *Proc. Int. Soc. Sugar Cane Technol.*, 1229–1236, 1971.
- BUONAFINA, M. M. O. and COSGROVE, D. J. *Sugarcane: Physiology, Biochemistry and Functional Biology*, chap. Cell Walls : Structure and Biogenesis, 307–329. 1^a ed., John Wiley and Sons, Inc., 2014.
- CAVALETT, O., CHAGAS, M., SEABRA, J. and BONOMI, A. Comparative lca of ethanol versus gasoline in brazil using different lcia methods. *Int. J. Life Cycle Assess*, v. 18(3), 647–658, 2013.

- CAVALETT, O., JUNQUEIRA, T. L., DIAS, M. O. S., JESUS, C. D. F., MANTELATTO, P. E., CUNHA, M. P., FRANCO, H. C. J., CARDOSO, T. F., FILHO, R. M., ROSSELL, C. E. V. and BONOMI, A. Environmental and economic assessment of sugarcane first generation biorefineries in brazil. *Clean Technol. Environ. Policy*, v. 14, 399–410, 2012.
- CERQUEIRA LEITE, R. and LEAL, M. R. L. V. O biocombustível no brasil. *Novos Estud. CEBRAP*, 15–21, 2007.
- CERQUEIRA LEITE, R. C., VERDE LEAL, M. R. L., BARBOSA CORTEZ, L. A., GRIFFIN, W. M. and GAYA SCANDIFFIO, M. I. Can Brazil replace 5% of the 2025 gasoline world demand with ethanol? *Energy*, v. 34(5), 655–661, 2009.
- CHAPRA, S. C. and CANALE, R. P. *Metodos Numericos para Engenharia*. 5^a ed., McGraw-Hill, São Paulo, SP, 2008.
- CLARKE, M. A. and SINGH, R. P. Beet Sugar. Encyclopedia Britannica, inc., 2017, Available in: www.britannica.com/science/sugar-chemical-compound/Beet-sugar. Accessed: 2018-06-22.
- DALE, B. Biofuels: Thinking clearly about the issues. *Journal of Agricultural and Food Chemistry*, v. 56(11), 3885–3891, 2008.
- DELAVIER, H. J. and SHOKRANI, R. Micro-Structure of Sugarcane Tissue for Solid-Liquid Extraction. In *Proc. Int. Soc. Sugar Cane Technol.*, 1475–1485, 1974.
- DEMIRBAS, A., ed. *Biorefineries: For Biomass Upgrading Facilities*. Green Energy and Technology, 1^a ed., Springer-Verlag, London, 2010.
- DEMMELE, J. W., EISENSTAT, S. C., GILBERT, J. R., LI, X. S. and LIU, J. W. H. A Supernodal Approach to Sparse Partial Pivoting. *Siam J. Matrix Anal. Appl.*, v. 20(3), 720–755, 1999.
- DIAS, M. O. S., JUNQUEIRA, T. L., CAVALETT, O., CUNHA, M. P., JESUS, C. D. F., ROSSELL, C. E. V., FILHO, R. M. and BONOMI, A. Integrated versus stand-alone second generation ethanol production from sugarcane bagasse and trash. *Bioresour. Technol.*, v. 103, 152–161, 2012.
- DIAS, M. O. S., MACIEL FILHO, R., MANTELATTO, P. E., CAVALETT, O., ROSSELL, C. E. V., BONOMI, A. and LEAL, M. R. L. V. Sugarcane processing for ethanol and sugar in brazil. *Environmental Development*, v. 15, 35–51, 2015.

- ELLABBAN, O., ABU-RUB, H. and BLAABJERG, F. Renewable energy resources: Current status, future prospects and their enabling technology. *Renewable Sustainable Energy Rev.*, v. 39, 748–764, 2014.
- ELLIOTT, M. C. and WESTON, G. D. *The Sugar Beet Crop*, chap. Biology and Physiology of Sugar-beet Plant, 37–66. 1^a ed., Chapman and Hall, London, United Kindom, 1993.
- FORTIN, F.-A., DE RAINVILLE, F.-M., GARDNER, M.-A., PARIZEAU, M. and GAGNÉ, C. Deap: Evolutionary algorithms made easy. *journal of Machine Learning Research*, v. 13, 2171–2175, 2012.
- GERALDO, C. V., TOLEDO, E. C. V., MACIEL FILHO, R., BONOMI, A. and MORAIS, E. R. Sugar extraction via moving-bed diffusers in ethanol production industry: Phenomenological modeling and finite-volumes simulation. *Industrial & Engineering Chemistry Research*, v. 57(41), 13769–13782, 2018.
- GERALDO, V. C., MORAIS, E. R., TOLEDO, E. C. V., JESUS, C. D. F., BONOMI, A. and MACIEL FILHO, R. Sugar extraction by moving-bed diffusers in ethanol production: development of a simulation tool. In Z. Kravanja and M. Bogataj, eds., *26th European Symposium on Computer Aided Process Engineering*, v. 38 de *Computer Aided Chemical Engineering*, 1425 – 1430, Elsevier, 2016.
- GOLDEMBERG, J. Ethanol For a Sustainable Energy Future. *Science*, v. 315(September), 808–810, 2007.
- GRINFELD, P. *Introduction to Tensor Analysis and the Calculus of Moving Surfaces*. 1^a ed., Springer-Verlag, New York, 2013.
- HAIRER, E., NORSETT, S. P. and WANNER, G. *Solving Ordinary Differential Equations I: Nonstiff Problems*, v. 8 de *Springer Series in Computational Mathematics*. 2^a ed., Springer-Verlag Berlin Heidelberg, 1993.
- HAMDI, S., SCHIESSER, W. and GRIFFITHS, G. Method of lines. *Scholarpedia*, v. 2(7), 2859, 2007.
- HASTIE, T., TIBSHIRANI, R. and FRIEDMAN, J. *The Elements of Statistical Learning-Data Mining, Inference, and Prediction*. Springer Series in Statistics, 2^a ed., Springer-Verlag New York, New York, New York, 2009.

- HEMAIDA, S. A. A., EL SAWAH, M. and SAYED, G. E. Egyptian bagasse diffuser versus mill. In *Proc. Int. Soc. Sugar-Cane Technol.*, 20, 8–14, 1989.
- HOEKSTRA, R. G. Energy consequences of diffusion versus milling. In *Proc. Annu. Congr. S. Afr. Sugar Technol. Assoc.*, v. 69, 205–207, 1995.
- HUGOT, E. *Handbook of Cane Sugar Engineering*. 3rd ed., Elsevier Science Publishers B. V., Amsterdam, The Netherlands, 1986.
- IEA. Resources to reserves 2013. *International Energy Agency*, 2013.
- IEA. Global energy CO₂ status report. *International Energy Agency*, 2017.
- JAMES, G., WITTEN, D., HASTIE, T. and TIBSHIRANI, R. *An Introduction to Statistical Learning-With Applications in R*, v. 7 de *Springer Texts in Statistics*. Springer-Verlag New York, New York, New York, 2013.
- JONES, E., OLIPHANT, T., PETERSON, P. and *et al.*, SciPy: Open source scientific tools for Python, 2001, URL <http://www.scipy.org/>, [Online; accessed 23/03/2018].
- KENT, G. and LEWINSKI, J. Milling and Diffusion Extraction - Theory and Practice. v. 26, 1404–1411, 2007.
- KOSTER, K. Some downstream effects resulting from diffusion compared with milling as published by the south african sugar industry. In *Proc. Annu. Congr. S. Afr. Sugar Technol. Assoc.*, v. 69, 201–204, 1995.
- KRUGER, T., KUSUMAATMAJA, H., KUZMIN, A., SHARDT, O. and VIGGEN, E. M. *The Lattice Boltzmann Method: Principles and Practice*. Graduate Texts in Physics, 1st ed., Springer International Publishing, Switzerland, 2017.
- KYAN, C. P., WASAN, D. T., KINTNER, R. C. and WASAN, D. T. Flow of single-phase fluids through fibrous beds. *Ind. Eng. Chem. Fundam.*, v. 9, 596–603, 1970.
- LEE, K. J., MARCUS, S. E. and KNOX, J. P. Cell wall biology: Perspectives from cell wall imaging. *Molecular Plant*, v. 4(2), 212–219, 2011.
- LI, L., WANG, C., SONG, B., MI, L. and HU, J. Kinetic parameters estimation in the polymerase chain reaction process using the genetic algorithm. *Ind. Eng. Chem. Res.*, v. 51, 13268–13273, 2012.

- LIONNET, G. R. E., PILLAY, M. and THIBELA, B. The effect of selected factors on percolation in pilot diffusion columns. In *Proc. S. Afr. Sug. Technol. Ass.*, 79, 249–257, 2005.
- LOUBSER, R. and JENSEN, P. Modelling juice flow in a shredded cane bed. In *Proc. Annu. Congr. S. Afr. Sugar Technol. Assoc.*, v. 85, 211–222, 2015.
- LOUBSER, R. C. and BARKER, B. Cane Characterisation : The Percolation Test. In *Proc. S. Afr. Sug. Technol. Ass.*, 413–422, 2011.
- LOVE, D. J. and REIN, P. W. Percolation behaviour of cane diffuser. In *Proc. Int. Soc. Sugar-Cane Technol.*, 17, 1900–1924, 1980.
- MALISKA, C. R. *Transferência de Calor e Mecânica dos Fluídos Computacional*. 2^a ed., LTC editora, Rio de Janeiro, RJ, 2012.
- MARTINEZ VILLEGAS, R., BUDMAN, H. and ELKAMEL, A. Identification of dynamic metabolic flux balance models based on parametric sensitivity analysis. *Ind. Eng. Chem. Res.*, v. 56, 1911–1919, 2017.
- MCGINN, J., VIDLER, T., ZEMEK, R. and MACCARTHY, W. Performance measurements on the inkerman mill diffuser extraction train. In *Proc. Conf. Aust. Soc. Sugar Cane Technol.*, v. 3, 261–266, 1981.
- MILFORD, G. F. J. *Sugar Beet*, chap. Plant Structure and Crop Physiology, 30–49. Blackwell Publishing Ltd, Oxford, United Kindon, 2006.
- MOHAMAD, A. A. *Lattice Boltzmann Method: Fundamentals and Engineering Applications with Computer Codes*. 1^a ed., Springer-Verlag London, 2011.
- MOON, R. J., MARTINI, A., NAIRN, J., SIMONSEN, J. and YOUNGBLOOD, J. Cellulose nanomaterials review: Structure, properties and nanocomposites. *Chem. Soc. Rev.*, v. 40(7), 3941–3994, 2011.
- MOUKALLED, F., L., M. and DARWISH, M. *The Finite Volume Method in Computational Fluid Dynamics: An Advanced Introduction with OpenFOAM and Matlab*, v. 113 de *Fluid Mechanics and Its Applications*. 1^a ed., Springer International Publishing, Switzerland, 2016.
- MÜLLER, W. H. *An Expedition to Continuum Theory*, v. 210 de *Solid Mechanics and Its Applications*. 1^a ed., Springer Netherlands, 2014.

- MUNSAMY, S. S. and BACHAN, L. A Review of Cane Diffusion At Sezela and Umzimkulu Sugar Factories. In *Proc. S. Afr. Sug. Technol. Ass.*, v. 80, 311–319, 2006.
- NOBEL, P. S. *Physicochemical and Environmental: Plant Physiology*. 4th ed., Elsevier Academic Press, 2009.
- OLIVERIO, J. L., D'AVILA, A. C. R., FABER, A. N. and SOARES, P. A. Juice extraction systems: Mills and diffusers—the brazilian experience. In *Proc. Int. Soc. Sugar-Cane Technol.*, v. 28, 1658–1672, 2013.
- OTEIZA, P. P. and BRIGNOLE, N. B. An evolutionary algorithm applied to inventory control for natural gasoline. *Ind. Eng. Chem. Res.*, v. 55, 13062–13073, 2016.
- PALACIOS-BERECHÉ, R., ENSINAS, A. V., MODESTO, M. and NEBRA, S. A. Extraction process in the ethanol production from sugarcane – a comparison of milling and diffusion. *Chem. Eng. Transac.*, 1519–1524, 2014.
- PATANKAR, S. V. *Numerical Heat Transfer and Fluid flow*. Computational Methods in Mechanics and Thermal Sciences, 1st ed., McGraw-Hill Book Company, New York, New York, 1980.
- PAYNE, J. H. Cane diffusion - The Displacement Process in Principle and Practice. In *Proc. Int. Soc. Sugar-Cane Technol.*, 103–121, 1969.
- PELLEGRINI, L. F. and DE OLIVEIRA, S. J. Combined production of sugar, ethanol and electricity: Thermoeconomic and environmental analysis and optimization. *Energy*, v. 36(6), 3704–3715, 2011.
- PETERS, M. S. and TIMMERHAUS, K. D. *Plant Design and Economics for Chemical Engineers*. 4th ed., McGraw-Hill, Inc., 1991.
- PICARO, T. and WHITE, E. T. A preliminary study of the fluid mechanics of part-flooded bed. *Chem. Eng. Sci.*, v. 48, 1985–1994, 1993.
- PICARO, T., WHITE, E. T. and EDWARDS, B. P. A model for the juice flows through a moving bed cane diffuser. In *Proc. Conf. Aust. Soc. Sugar Cane Technol.*, 278–286, 1994.
- POL, C. V. Some notes on the extraction of sucrose from cane by diffusion. In *Proc. Annu. Congr. S. Afr. Sugar Technol. Assoc.*, v. 34, 86–91, South African Sugar Technologists' Association, 1957.

- RAE, A. L., MARTINELLI, A. P. and DORNELAS, M. C. *Sugarcane: Physiology, Biochemistry and Functional Biology*, chap. Anatomy and Morphology, 19–33. 1^a ed., John Wiley and Sons, Inc., 2014.
- RAVEN, P. H., EVERT, R. F. and EICHHORN, S. E. *Biologia Vegetal*. 5^a ed., Guanabara Koogan S.A., Rio de Janeiro, RJ, 1996.
- RAVNO, A. B. Microbial Degradation in Sugar Cane Diffusers. In *Proc. Int. Soc. Sugar Cane Technol.*, 384–385, 2001.
- REIN, P. W. The mechanism of extraction in cane sugar diffusion process. In *Proc. Int. Soc. Sugar-Cane Technol.*, 14, 1254–1266, 1971.
- REIN, P. W. *A Study of The Cane Sugar Diffusion Process*. Ph.d. dissertation, University of Natal, South Africa, 1972.
- REIN, P. W. Prediction of the extraction performance of a diffuser using a mathematical model. In *Proc. Int. Soc. Sugar-Cane Technol.*, 15, 1523–1536, 1974.
- REIN, P. W. A comparison of cane diffusion and milling. In *Proc. Annu. Congr. S. Afr. Sugar Technol. Assoc.*, v. 69, 196–200, 1995.
- REIN, P. W. *Cane Sugar Engineering*. 2^a ed., Verlag Dr. Albert Bartens K G, Berlin, Germany, 2013.
- REIN, P. W. and INGHAM, P. J. S. Difuser performance optimization through control of liquid flow patterns. In *Proc. Int. Soc. Sugar-Cane Technol.*, 21, 779–796, 1992.
- REIN, P. W. and WOODBURN, E. T. Extraction of sugar from cane in the diffusion process. *Chem. Eng. J. (Amsterdam, Neth.)*, v. 7, 41–51, 1974.
- RFA. Industry statistics. Rel. téc., Renewable Fuels Association, Washington, DC., USA., 2017.
- RIVIERE, M. Washing sugar out of cane: A proposed new hydrodynamic extraction process. In *Proc. Int. Soc. Sugar Cane Technol.*, 225–232, 1989.
- RODRIGUEZ, E. O. *Desenvolvimento de um difusor para mini-usinas de alcool*. Tese de Doutorado, Faculdade de Engenharia de Alimentos-Unicamp, Campinas-SP, 1990.

- RYTIOJA, J., HILDÉN, K., YUZON, J., HATAKKA, A., DE VRIES, R. P. and MÄKELÄ, M. R. Plant-Polysaccharide-Degrading Enzymes from Basidiomycetes. *Microbiology and Molecular Biology Reviews*, v. 78(4), 614–649, 2014.
- SALLES-FILHO, S. L. M., DE CASTRO, P. F. D., BIN, A., EDQUIST, C., FERRO, A. F. P. and CORDER, S. Perspectives for the Brazilian bioethanol sector: The innovation driver. *Energy Policy*, v. 108(June 2016), 70–77, 2017.
- SANCHEZ FILHO, E. S. *Tensor Calculus for Engineers and Physicists*. 1^a ed., Springer International Publishing, Switzerland, 2016.
- SANT’ANNA, C., COSTA, L. T., ABUD, Y., BIANCATTO, L., MIGUENS, F. C. and DE SOUZA, W. Sugarcane cell wall structure and lignin distribution investigated by confocal and electron microscopy. *Microscopy Research and Technique*, v. 76(8), 829–834, 2013.
- SASTRY, K., GOLDBERG, D. E. and KENDALL, G. *Search Methodologies: Introductory Tutorials in Optimization and Decision Support Techniques*. 2^a ed., Springer US, New York, New York, 2014.
- SCHIESSER, W. E. *The numerical method of lines : integration of partial differential equations*. 1^a ed., Academic Press, Sandiego, USA, 1991.
- SCHMID, A. What is the Truth of Simulation ? *Journal of Artificial Societies and Social Simulation*, v. 8(4), 8–13, 2005.
- SCHRODER, K. E., VOIGT, I. and MOOR, B. S. C. The Conversion of a BMA Diffuser to a Bosch Projects Chainless Diffuser— The First Season’s Experience. In *Proc. Int. Soc. Sugar Cane Technol.*, v. 26, 1294–1304, 2007.
- SENDICH, E. D. and DALE, B. E. Environmental and economic analysis of the fully integrated biorefinery. *GCB Bioenergy*, v. 1(5), 331–345, 2009.
- SINGELS, A., MCFARLANE, S. A., NICHOLSON, R., WAY, M. and SITHOLE, P. Review of south african sugarcane production in the 2016/2017 season: Light at the end of the tunnel? In *Proc. Annu. Congr. S. Afr. Sugar Technol. Assoc.*, 1–19, 2017.
- SIVANANDAM, S. N. and DEEPA, S. N. *Introduction to Genetic Algorithms*. 1^a ed., Springer-Verlag Berlin Heidelberg, 2008.

- STANMORE, B. R. Generation of energy from sugarcane bagasse by thermal treatment. *Waste and Biomass Valorization*, v. 1, 77–89, 2010.
- SUKOP, M. C. and THORNE, D. T. *Lattice Boltzmann Modeling: An Introduction for Geoscientists and Engineers*. 1^a ed., Springer-Verlag Berlin Heidelberg, 2006.
- SZYMKIEWICZ, A. *Modelling Water Flow in Unsaturated Porous Media: Accounting for Non-linear Permeability and Material Heterogeneity*. GeoPlanet: Earth and Planetary Sciences, 1^a ed., Springer-Verlag Berlin Heidelberg, Berlin, 2013.
- TANNEHILL, J. C., ANDERSON, D. A. and PLETCHER, R. H. *Computational Fluid Mechanics and Heat Transfer*. Computational and physical processes in mechanics and thermal sciences, 2^a ed., Taylor and Francis, Washington, DC, 1997.
- TOLK, A. *Ontology, Epistemology, and Teleology of Modeling and Simulation : Philosophical Foundations for Intelligent MS Applications*, chap. 1, 1–26. 1^a ed., Springer-Verlag, Berlin, Heidelberg, 2013.
- TREYBAL, R. E. *Mass-transfer operations*. 3^a ed., McGraw-Hill Book Company, 1981.
- VERSTEEG, H. K. and MALALASEKRA, W. *An Introduction to Computational Fluid Dynamics: The Finite Volume Method Approach*. 1^a ed., Longman Scientific and Technical, Harlow, England, 1995.
- VOIGT, I. The implementation of south african sugar technology: The world's largest sugarcane diffusers. In *Proc. Int. Soc. Sugar-Cane Technol.*, v. 27, 1–10, 2010.
- VOIGT, I. and HULLEY, S. M. The return of bagasse diffusers. In *Proc. Annu. Congr. S. Afr. Sugar Technol. Assoc.*, v. 87, 128–139, 2014.
- ZABED, H., SAHU, J. N., SUELY, A., BOYCE, A. N. and FARUQ, G. Bioethanol production from renewable sources: Current perspectives and technological progress. *Renewable Sustainable Energy Rev.*, v. 71(October 2015), 475–501, 2017.
- ZAMBONI, A., SHAH, N. and BEZZO, F. Spatially explicit static model for the strategic design of future bioethanol production systems. 1. cost minimization. *Energy and Fuels*, v. 23(10), 5121–5133, 2009.
- ZHANG, J. A reliable neural network model based optimal control strategy for a batch polymerization reactor. *Ind. Eng. Chem. Res.*, v. 43, 1030–1038, 2004.

Appendix A

Averaging rules

This supporting information presents the averaging rules applied in this study. Sugar concentration C is used as an example to demonstrate such rules.

Average of a sum:

The average of the sum between C_1 and C_2 :

$$\overline{C_1 + C_2} = \overline{C_1} + \overline{C_2} \quad (\text{A.1})$$

Average of a product:

The average of the product between C_1 and C_2 :

$$\overline{C_1 \cdot C_2} = \overline{C_1} \cdot \overline{C_2} + \overline{\dot{C}_1 \cdot \dot{C}_2} \quad (\text{A.2})$$

The second term at the right side of the expression is a dispersive element.

Average of a spatial derivative:

The surface separating two distinct domains γ and ξ , $S_{\gamma,\xi}$, can be represented by normal unit vectors ν , pointing outwards this surface. Concerning a convective flux, the rule for spatial derivatives assumes the following form:

$$\overline{\nabla C V} = \nabla \overline{C V} + \langle C \cdot (V - u) \cdot \nu \rangle^{\gamma,\xi} \cdot \Lambda_{\gamma,\xi} \quad (\text{A.3})$$

The velocity of the ξ bed portion is represented by u . The difference between the velocities

accounts for the relative velocity between the two domains. The second term at the right side of the expression is detailed in Eq. A.4. In this equation, S stands for the whole surface of the continuous volume G_o . The surface integral computes the net convective flux across the separating surface.

$$\langle C \cdot (V - u) \cdot \nu \rangle^{\gamma, \xi} \cdot \Lambda_{\gamma, \xi} \equiv \frac{1}{G_o} \int_{S_{\gamma, \xi}} C \cdot (V - u) \cdot \nu \, dS \quad (\text{A.4})$$

The same rule is applied for a diffusive flux (Eq. A.5). The second term at the right side of the equation is also a surface integral (Eq. A.6), representing the net diffusive flux across $S_{\gamma, \xi}$.

$$\overline{\nabla j} = \nabla \bar{j} + \langle j \cdot \nu \rangle^{\gamma, \xi} \cdot \Lambda_{\gamma, \xi} \quad (\text{A.5})$$

$$\langle j \cdot \nu \rangle^{\gamma, \xi} \cdot \Lambda_{\gamma, \xi} \equiv \frac{1}{G_o} \int_{S_{\gamma, \xi}} j \cdot \nu \, dS \quad (\text{A.6})$$